Uniwersytet Śląski w Katowicach

Instytut Fizyki

Zakład Fizyki Teoretycznej

Dawid Wiesław Crivelli

Particle and energy transport in strongly driven one-dimensional quantum systems

Rozprawa doktorska

Promotor:

Prof. dr hab.
Marcin Mierzejewski

Promotor pomocniczy:

Dr Andrzej Ptok

Katowice 2016

Acknowledgments

My endless thanks to my advisor Prof. Mierzejewski, to whom I am greatly indebted for the support over the past few years, for showing me the fascinating new world of real–time quantum physics, for the compelling conversations, for the never ending stream of brilliant ideas and insights that were passed on.

I am also thankful for the young scientists watching over me during the years in Katowice, my supporting advisor Dr. Ptok mostly in the rôle of prolific coauthor, and Dr. Gardas with whom I could passionately discuss physics and life, that forced me to expand my horizons and be more active in research.

My thanks to the lovely Gosia from Stryszów, my wonderful colleagues and friends in Katowice, for making the journey worthwhile.

Dedicato a mia madre, per l'enorme supporto e conforto durante questi anni, che non vede l'ora di avere un dottore per casa, senza l'incoraggiamento della quale non avrei sicuramente continuato la mia carriera scientifica in Polonia e avrei probabilmente smarrito la strada.

Funding

My PhD has been supported by the TWING project in the years 2012-2014, by the FORSZT PhD Scholarship in the years 2014-2015, both funded by the European Social Fund. Funding by the project DEC-2013/09/B/ST3/01659 financed by the Polish National Science Center (NCN) is gratefully acknowledged.

Abstract

This Dissertation concerns the transport properties of a strongly–correlated one–dimensional system of spinless fermions, driven by an external electric field which induces the flow of charges and energy through the system. Since the system does not exchange information with the environment, the evolution can be accurately followed to arbitrarily long times by solving numerically the time–dependent Schrödinger equation, going beyond Kubo's linear response theory.

The thermoelectric response of the system is here characterized, using the ratio of the induced energy and particle currents, in the nonequilibrium state under the steady applied electric field. Even though the equilibrium response can be reached for vanishingly small driving, strong fields produce quantum–mechanical Bloch oscillations in the currents, which disrupt the proportionality of the currents.

The effects of the driving on the local state of the ring are analyzed via the reduced density matrix of small subsystems. The local entropy density can be defined and shown to be consistent with the laws of thermodynamics for quasistationary evolution. Even integrable systems are shown to thermalize under driving, with heat being produced via the Joule effect by the flow of currents. The spectrum of the reduced density matrix is shown to be distributed according the Gaussian unitary ensemble predicted by random–matrix theory, both during driving and a subsequent relaxation.

The first fully–quantum model of a thermoelectric couple is realized by connecting two correlated quantum wires. The field is shown to produce heating and cooling at the junctions according to the Peltier effect, by mapping the changes in the local entropy density. In the quasiequilibrium regime, a local temperature can be defined, at the same time verifying that the subsystems are in a Gibbs thermal state. The gradient of temperatures, established by the external field, is shown to counterbalance the flow of energy in the system, terminating the operation of the thermocouple. Strong applied fields lead to new nonequilibrium phenomena. At the junctions, observable Bloch oscillations of the density of charge and energy develop at the junctions. Moreover, in a thermocouple built out of Mott insulators, a sufficiently strong field leads to a dynamical transition reversing the sign of the charge carriers and the Peltier effect.

Keywords: Nonequilibrium transport, many–body fermionic system, thermalization, thermoelectrical effect, quantum thermodynamics, Bloch oscillations, integrable systems, computational methods, random matrix theory, entropy density, time–dependent Schrödinger equation, linear response theory, thermocouple, local temperature.

Streszczenie

Rozprawa doktorska poświęcona jest teoretycznym badaniom własności transportowych jednowymiarowego układu złożonego z silnie oddziałujących bezspinowych fermionów. Układ wzbudzany jest zmieniającym się w czasie polem magnetycznym, które indukuje przepływ ładunku i energii. Ponieważ układ nie wymienia informacji z otoczeniem, jego ewolucja może być śledzona dla dowolnie długich czasów poprzez numeryczne rozwiązanie równania Schrödingera. Pozawala to badać odpowiedź układu poza teorią Kubo liniowej reakcji.

Odpowiedź termoelektryczna została scharakteryzowana dla stanów kwazistacjonarnych oraz dalekich od równowagi, poprzez wyznaczenie stosunku prądów energii i ładunku indukowanych przez stałe pole elektryczne. Wyniki numeryczne uzyskane dla słabych pól są zgodne z teorią liniowej reakcji układu, jednak dla silniejszych pól pokazujemy, że zarówno prąd cząstek jak i prąd energii podlegają oscylacjom Blocha, co zaburza proporcjonalność pomiędzy obiema wielkościami.

Wpływ zewnętrznego pola na lokalne własności układu, analizowany jest przy pomocy zredukowanej macierzy gęstości wyznaczonej dla niewielkiego podukładu. Wielkość ta pozwala także zdefiniować gęstość entropii, która dla procesów kwazistacjonarnych jest spójna z zasadami termodynamiki. Pokażemy, że w obecności pola elektrycznego także układy całkowalne podlegają kwazirównowagowej ewolucji, a ich energia stopniowo rośnie w czasie na skutek wydzielania ciepła Joule'a. Pokazujemy także, że w obecności zewnętrznego pola oraz po jego wyłączeniu, widmo zredukowanej macierzy gęstości odpowiada unitarnemu rozkładowi gaussowskiemu dla macierzy przypadkowych.

Zasadnicza część rozprawy poświęcona jest sformułowaniu i analizie pierwszego w pełni kwantowego modelu termopary, zbudowanej z dwóch jednowymiarowych układów kwantowych. Model uwzględnia obecność oddziaływań wielociałowych. Śledząc ewolucję czasową gęstości entropii w różnych punktach układu, analizujemy działanie termopary w obecności pól elektrycznych o dowolnym natężeniu. W reżimie kwazistacjonarnym, małe podukłady termopary są w stanie termicznym Gibbsa, można więc zdefiniować lokalną temperaturę. Pokazujemy, że po włączeniu pola temperatura silnie rośnie w otoczeniu jednego ze złącz a maleje w otoczeniu drugiego, co odtwarza efekt standardowy Peltiera. W obecności silniejszych pól obserwujemy efekty nowe nierównowagowe. W szczególności w otoczeniu złącz, gęstość nośników oraz gęstość energii podlegają oscylacjom Blocha. Ponadto w przypadku termopary zbudowanej z domieszkowanych izolatorów Motta, dostatecznie silne pole może prowadzić do zmiany znaku nośników prądu i odwrócenie efektu Peltiera.

Słowa kluczowe: Transport nierównowagowy, wielociałowe układy fermionów, termalizacja, efekt termoelektryczny, termodynamika kwantowa, oscylacje Blocha, układy całkowalne, teoria macierzy losowych, gęstość entropii, równanie Schrödingera zależne od czasu, teoria liniowej reakcji, termopara, lokalna definicja temperatury.

Contents

Part I

Introduction

Chapter 1

Introduction

The system we are going to study is introduced through its Hamiltonian and Hilbert space. The basic theoretical frameworks needed to state the scientific problems and the results are presented, following the bibliography. The consequences of integrability for a quantum system are explained. The introduction to thermoelectrical effects and linear response motivates novel results in later chapters.

The problem of a one–dimensional quantum system driven arbitrarily by an external field requires an approach based on the real–time evolution of the system from its initial state. We study a ring of strongly interacting fermions, dependent on the external magnetic field piercing the ring, generating a flow of current by *induction*, which drives the system towards higher energies. The contact with external thermostats is thus avoided and only the system state needs to be specified.

The system is closed, meaning that it exchanges no *information* (heat or particles) with the environment. Since there is no flow of information, the evolution of a closed system is *unitary*, so pure states remain pure at arbitrary times. The evolution of the systems follows the Schrödinger equation, and does not necessitate the description in terms of a density matrix following the von Neumann equation.

We prepare the ring in an initial high–temperature state $|\psi(0)\rangle$, corresponding to a finite average energy $\bar{E}$ much higher than its ground state. As counterintuitive as it may sound, high–temperature states are as easily computed as the ground state, but are less sensitive to the microscopical details of the system, allowing us to establish a contact with the laws of *thermodynamics in the quantum regime*. Even if the system is prepared in low–energy configuration, driving it with an arbitrary protocol involves all states of the spectrum, so the classical renormalization-group picture of the relevant degrees of freedom does not apply, as the system will be driven towards high energies.

The strength of this approach comes from representing the quantum state of the closed system at all times as a pure wavefunction (or an average over a small number <10 of vectors), which can be propagated forward in time with minimal effort, using the Time–Dependent Schrödinger Equation (TDSE). The approach is depicted in Fig. 1.1, and is the following:

1. Prepare the initial state in a narrow window of energy corresponding to the set temperature

$$|\psi(0)\rangle = |\psi_E\rangle, \tag{1.1}$$

   using the computational ensembles of Section 3.2.

2. Evolve the system solving the Schrödinger equation to numerical precision, with the Hamiltonian $H[\phi(t)]$ depending on time through the external magnetic field $\phi(t)$

$$i\,\frac{d}{dt}|\psi(t)\rangle = H[\phi(t)]\,|\psi(t)\rangle, \tag{1.2}$$

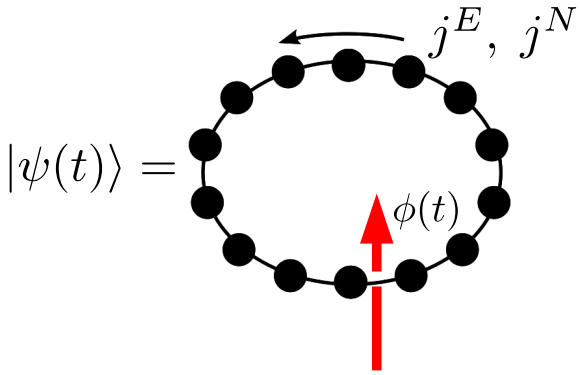

Figure 1.1: The state of the system is represented by a pure wavefunction, evolved in time according to the time-depending Schrödinger equation. Observables, such as the energy and particle currents are measured as expectation values on $|\psi(t)\rangle$.

using the methods of Section 2.2 and 3.2.3.

3. Compute any observable $\hat{A}[\phi(t)]$ at time t in the time-evolved state

$$\langle \hat{A} \rangle(t) = \langle \psi(t) \left| \hat{A}[\phi(t)] \right| \psi(t) \rangle \tag{1.3}$$

4. Obtain exact dynamics of any small subsystem by projecting its reduced density matrix $\rho_S(t)$ from the wavefunction of the whole ring. Thermodynamical quantities such as the *entropy density* can be extracted from the knowledge of $\rho_S(t)$, as shown in Chapter 6.

The evolution for a time δt generates a map in Hilbert space, represented by the unitary operator $\hat{U}(t) = \mathrm{e}^{-iH(t)\delta t}$. Under the evolution with a time-independent Hamiltonian, the energy eigenstates are stationary states. The evolution can be thus characterized by analyzing the projections of the initial state on the energy eigenbasis, reducing the problem to the study of the equilibrium states. Driven systems, on the other hand, at every instant generate different maps $\hat{U}(t)$ between the Hilbert spaces at t and $t + \delta t$. They can not be reasoned about in a fixed basis and require the machinery of explicit time evolution.

The advantages of highly energetic states can be visualized in Fig. 1.2: driving a gapped system with a slow variation of the phase ϕ from the ground-state manifold (the states visible at the bottom) only generates transitions between the two lowest-lying states. Starting from a "hot" state where the energy density is finite, i.e. there is almost a continuum of states, the transitions can be smooth and the behavior of the system close to the thermodynamic limit where the single energy levels are not resolved.

Changing the phase of the system from $\phi = 0$ to finite values changes the symmetries (see Section 1.1.1.1), and drives the system through a series of avoided and allowed crossings of the energy levels. Thus symmetries of the stationary system can be softly broken by driving, as seen in the appearance of *currents* that are time–reversal antisymmetric, and in Chapter 6 with the thermalization of driven integrable systems.

1.1 Spinless fermion model

The model that will be studied throughout this dissertation, is the $t - V - W$ spinless fermion model with a complex phase, the (extended) fermionic equivalent of the celebrated Heisenberg model.

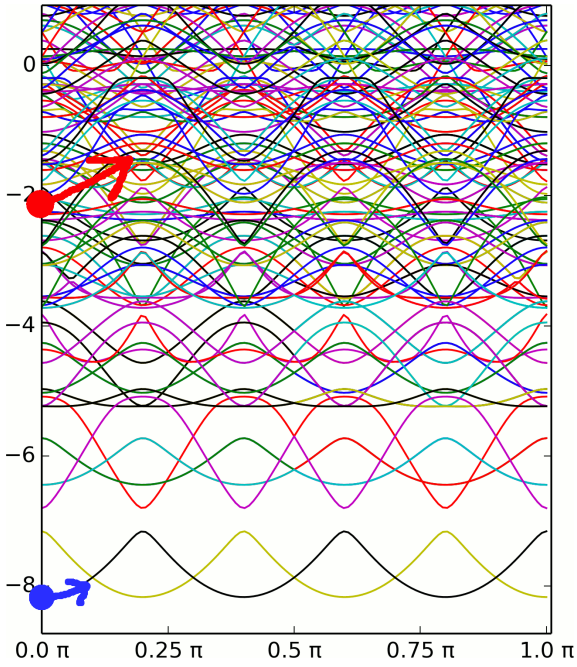

Figure 1.2: Energy levels of a very small $t-V$ Hamiltonian $H(\phi)$, at half-filling in an insulating phase ($V=3$), depending on the phase ϕ. The ground-state is marked by a blue arrow (lower one), a generic high-temperature state by a red arrow (upper one). The evolution of every eigenvalue along the change in the field was continuously tracked, identifying every state with a color, with a minor number of errors.

It is a model of coupled spin 1/2 particles, which in spite of its extreme simplicity, is a source of mathematical and physical insights through the interplay of its interactions. It provides an excellent description of the so-called spin-chain materials [SGO^+00, SGO^+01, TMEU96]: the transport properties of the Heisenberg model have been probed in depth in order to explain the anomalously large heat conductivity in $SrCuO_2$, Sr_2CuO_3, $KCuF_3$, $CuGeO_3$ spin chains. The root of the effect is considered to be the integrability of the model, which allows for the ballistic flow of energy through the system [HMHCB03, AG02, JHR06, KF13, KM01, Pro11, NMA98, OCC03, JR07].

The thermodynamical properties of the $t-V-W$ model mirror exactly those of the Heisenberg model, with a 1-to-1 correspondence of the spectrum and eigenstates. The mapping of states and operators can be explicitly performed and it is called the Jordan-Wigner transformation in the literature. Differences arise at the level of plain 2-point correlation functions, since fermionic operators such as $\left\langle c_i^\dagger c_{i+m} \right\rangle$ acquire a sign depending on the number of fermions between the sites i and $i+m$, corresponding to the expectation value of a string of spin operators such as $\left\langle S_i^+ S_{i+1}^z \dots S_{i+m-1}^z S_{i+m}^- \right\rangle$.

The $t-V-W$ Hamiltonian can be rewritten as the sum over all sites of the lattice of

$$H_{t-V-W}(\phi) = \sum_{l=1}^{L} H_l(\phi), \tag{1.4}$$

where the local Hamiltonian $H_l(\phi)$ is the sum of 3 competing interactions

1. $H_l^{\text{kin}}(\phi) = -t_h \, e^{i\phi} \, c_{l+1}^\dagger c_l - t_h \, e^{-i\phi} \, c_l^\dagger c_{l+1}$, the kinetic energy terms which represents the action of hopping between first neighbors, with the additional phase acquired in presence of a magnetic field in the ring

2. $H_l^{\text{V}} = V\left(n_l - \frac{1}{2}\right)\left(n_{l+1} - \frac{1}{2}\right)$, potential energy term giving repulsion (resp. attraction) between nearest neighbors with the same (resp. inverse) occupation

3. $H_l^{\mathrm{W}} = W\left(n_l - \frac{1}{2}\right)\left(n_{l+2} - \frac{1}{2}\right)$, potential energy due to the repulsion between second neighbors

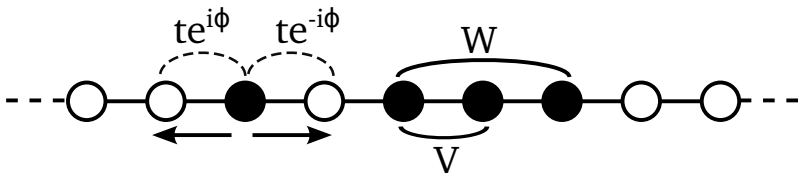

Figure 1.3: Schematic representation of the interactions of the $t-V-W$ Hamiltonian: fermions can hop to non-occupied neighboring sites, while experiencing repulsion between fermions on nearest (with strength V) and second (with strength W) occupied neighbors

To consider a closed ring of fermions, periodic boundary conditions equivalent to a one-dimensional torus are imposed. However, when $\phi > 0$, fermions acquire a phase while traversing the boundary. This periodic setup with finite constant phase is also called *twisted boundary conditions* [MR98, JŽ11a, SW04, LG03, SWZ93].

The phase ϕ in the kinetic energy is known as Peierls' gauge phase [HFG+05, GBM08, Gla66]. It represents a finite magnetic flux piercing the ring surface, which modifies the matrix elements between nearby orbitals, as simply captured by the minimal substitution of the hopping parameter in the tight-binding approximation. For special values, integer multiples of $\phi_0 = 2\pi/L$, the phase can be eliminated by suitable unitary transformations. The introduction of time dependence through the phase is the only way to correctly introduce an effective electric field in the ring topology of the system without breaking translational symmetry. A varying phase $\phi(t)$ induces time-dependent changes in the Hamiltonian $H[\phi(t)]$, in turn driving the system in real time.

A different notation $t-V-V'$ [MCR11] is also employed in the literature, with $V' = W$. More substantial variations of the model are known as well:

- $t-t'-V$ model with hopping on second neighbors with strength t' [Sha09].
- Staggered magnetization term $B\sum_l (-1)^l n_l$ [KIM13, OCC03, SGB15]

The reason of the introduction of second neighbor couplings is to avoid integrability, which causes anomalous transport properties and the possible failure of methods based on quantum typicality (see Section 3.1.5). The staggered magnetization serves a similar purpose, while remaining strictly local so easier to treat both analytically and numerically.

1.1.1 Hilbert space and symmetries

The use of symmetries is fundamental in numerical quantum mechanics to constrain the dimension of the Hilbert space, decomposing it into smaller subspaces not connected by matrix elements of the Hamiltonian. In the basis in which the symmetry operators are diagonal, the Hamiltonian is reduced into block-diagonal form. Four basic symmetries of the Hamiltonian will be explored, all but the first requiring spatial homogeneity of the system:

1. Particle number conservation, which is valid regardless of boundary conditions and additional local interactions
2. Particle-Hole transformation
3. Translational symmetry

4. Inversion parity

The exposition is meant to give a quick reference, more details regarding the equivalent Heisenberg model can be obtained in Ref. [San10], but necessitating reworking due to the absent fermionic signs.

We impose Periodic Boundary Conditions (PBC)[1], equivalent to considering a ring of L sites, with the symmetry enforced at the level of operators $c_{L+1} = c_1$. Every site j has a local Hilbert space $\mathscr{H}_j$ isometric to $\mathbb{C}^2$, so the total space is

$$\mathscr{H} = \otimes_{j=1}^{L} \mathscr{H}_j \tag{1.5}$$

$$\dim(\mathscr{H}) = \dim(\mathscr{H}_j)^L = 2^L. \tag{1.6}$$

The Hamiltonian conserves the total number of fermions N, which is the eigenvalue of the diagonal operator $\hat{N} = \sum_j \hat{n}_j$. Every state in $\mathscr{H}$ can be assigned a number of fermions, and a basis with a predetermined average occupation number N/L can be formed by choosing states $|i\rangle$ such that $\left\langle i \left| \hat{N} \right| i \right\rangle = N$. The dimension of a spinless fermion system, due to the Pauli exclusion principle, is the number of combinations of N indistinguishable hard-core particles on L positions:

$$\dim(\mathscr{H}^L_N) = \binom{L}{N}. \tag{1.7}$$

By the binomial theorem, the total Hilbert space decomposes into the N particle subspaces exactly

$$\dim(\mathscr{H}) = \dim(\mathscr{H}^L_0) + \dim(\mathscr{H}^L_1) + \ldots + \dim(\mathscr{H}^L_{L/2}) + \ldots + \dim(\mathscr{H}^L_L) = \sum_{m=0}^{L} \binom{L}{m} = 2^L. \tag{1.8}$$

A chemical potential can be added, but since it is a diagonal term constant in the N particle subspace, it can be seamlessly reabsorbed into the definition of the Hamiltonian

$$H + \mu\hat{N} \longrightarrow H. \tag{1.9}$$

Each basis state with N fermions out of L can be represented by an ordered string of L binary numbers where the ones correspond to the presence of a fermion creation operator on the zero-particle vacuum $|0\rangle$, for example

$$c_1^\dagger c_5^\dagger |0\rangle = |10001\ldots\rangle \quad \text{and } c_5^\dagger c_1^\dagger |0\rangle = -|10001\ldots\rangle. \tag{1.10}$$

The diagonal operators can be implemented by simple bit counting on each basis state, e.g. the first neighbors counting operator is the number of ones after a circular bitshift and a AND operation:

state of the system	`11001`
circular bithift	`11100`
bitwise AND	`11000`
count of ones	`2`

The hopping operators need to set a bitmask with a `1` corresponding to the initial and a `0` in final hopping site, checking that the former is filled and the latter empty, by AND bitwise comparisons. The occupation can be then reversed by a XOR operator with the two-bit mask. The fermionic parity is determined by calculating the sum of `1` bits between the two sites.

[1] Due to the better converge to the thermodynamic limit

1.1.1.1 Particle-Hole symmetry

The *Particle-Hole* (PH) transformation maps fermions to holes, and vice versa. To be a symmetry of the Hamiltonian, the following criteria must be satisfied:

- Zero external field $\phi = 0$. Allowing a more complicated transformation, $\phi = 2k\pi/L$ with $k \in \mathbb{Z}$.
- The chemical potential for $N = L/2$ particles is zero.

In that case, any energy eigenstate with N particles corresponds to an eigenstate with $L-N$ particles with the same energy.

The PH transformation corresponds to

$$c_l \xrightarrow{\text{PH}} (-1)^l c_l^\dagger, \qquad c_l^\dagger \xrightarrow{\text{PH}} (-1)^l c_l \qquad \phi \xrightarrow{\text{PH}} -\phi, \tag{1.11}$$

where the flip of the magnetic flux explains why it is not a symmetry of the Hamiltonian in a arbitrarily set external field. The PH operator $\hat{P}$ is realized (see [HFG+05]) by the set of local transformations $P_i = (c_i^\dagger + c_i)$, ordered [2] into

$$\hat{P} = P_L P_{L-1} \dots P_2 P_1. \tag{1.12}$$

Let us give a concrete example on a 5-sites system:

$$\hat{P}|01001\rangle = -|10110\rangle. \tag{1.13}$$

The kinetic energy is transformed into itself

$$c_{l+1}^\dagger c_l + c_l^\dagger c_{l+1} \xrightarrow{\text{PH}} -c_{l+1} c_l^\dagger - c_l c_{l+1}^\dagger = c_l^\dagger c_{l+1} + c_{l+1}^\dagger c_l, \tag{1.14}$$

whereas a typical nearest neighbor[3] interaction term is mapped to

$$n_l n_{l+1} \xrightarrow{\text{PH}} (-1)^{2l}(-1)^{2(l+1)}(1-n_l)(1-n_{l+1}) = (1-n_l)(1-n_{l+1}). \tag{1.15}$$

The interaction counts the number of pairs of consecutive occupied sites, which is zero for the empty lattice, and L for the maximum filling. The form used in Eq. (1.4) has been chosen to be PH symmetric

$$h_{\text{V},l} = \left(n_l - \frac{1}{2}\right)\left(n_{l+1} - \frac{1}{2}\right) \xrightarrow{\text{PH}} \left(\frac{1}{2} - n_l\right)\left(\frac{1}{2} - n_{l+1}\right) = h_{\text{V},l}. \tag{1.16}$$

The case for the W interaction term is analogous. In order to obtain a PH symmetric Hamiltonian is thus sufficient to replace any diagonal term n_l by $\tilde{n}_l = n_l - \frac{1}{2}$, a convention used in the remainder of this manuscript. The shift in the number operators

$$V \sum_l \tilde{n}_l \tilde{n}_{l+1} = V \sum_l n_l n_{l+1} - V \sum_l n_l + V \frac{1}{4} \sum_l \mathbb{1} = V \sum_l n_l n_{l+1} + V \underbrace{\left(\frac{L}{4} - N\right)}_{\mu(N)} \tag{1.17}$$

adds a constant term depending on N and thus corresponds to a shift of the chemical potential.

The *half-filled* case is the largest subspace with $N = L/2$, which is symmetric with respect to the PH transformation if the lattice has an even number of sites. The subspace can be further decomposed into even and odd subspaces with the projectors $\hat{P}_\pm = \frac{1 \pm \hat{P}}{2}$ if degeneracy must be avoided. It is very useful in practice to break the PH symmetry by applying a small finite phase (of the order of $\phi = 10^{-4}$ is enough in practice), in order to avoid degeneration of the spectrum. Moreover, the dynamical breaking due to the time variation of ϕ is at the root of the induction of currents.

[2] The order is essential to avoid ambiguities with the fermion signs

[3] Longer ranged interactions transform in the same way

1.1.1.2 Translational symmetry

The Hamiltonian is constructed as the sum of L shifted identical terms, and thus symmetric by construction. The translation operator is built using a set of swap operators

$$S_{j,l} = 1 - (c_j^\dagger - c_l^\dagger)(c_j - c_l). \tag{1.18}$$

The operator performing a *shift*, i.e. the translation by 1 site to the right can be written as

$$\hat{T} = S_{1,2} S_{2,3} \dots S_{L-1,L}. \tag{1.19}$$

The operator formulation is useful to prove identities, however it is best to give a representation on the computation binary basis. The translation operator acts as a signed permutation on the fermionic creation operators

$$\hat{T} c_{i_1}^\dagger c_{i_2}^\dagger \dots |0\rangle = \text{sign}(\sigma)\, c_{\sigma_{i_1}}^\dagger c_{\sigma_{i_2}}^\dagger \dots |0\rangle. \tag{1.20}$$

The set of indexes corresponding to filled sites is collected and successively permuted into a different position[4]

$$i \longrightarrow \sigma_i = [(i - 1 + K) \mod L] + 1 \quad \text{for translations by } K \text{ sites.} \tag{1.21}$$

The sign of the transformation corresponding to

$$\sigma = \begin{pmatrix} i_1 & i_2 & \dots \\ \sigma_1 & \sigma_2 & \dots \end{pmatrix} \tag{1.22}$$

is the canonical parity of the permutation. The empty sites cannot be included as to form a full permutation, but compiling the ordered N-vector $\sigma = (\sigma_1, \dots)$, the parity is given by the following formula:

$$\begin{aligned} P_\sigma &= \sum_{i=1, j=i+1}^{L} (\sigma_i > \sigma_j) \\ \text{sign}(\sigma) &= (-1)^{P_\sigma}, \end{aligned} \tag{1.23}$$

where the true or false values in the inequality correspond to arithmetic ones and zeros.

1.1.1.3 Momentum states

Using the transformation given above, each N-particle subspace can be decomposed into equivalence classes, where the different vectors are equivalent up to translations with momentum q. In each class, a representative vector is chosen, corresponding to the lowest ranking basis vector of the set, e.g.

$$\text{class}[|0,1,1,0,0\rangle] = [|0,1,1,0,0\rangle,\ |0,0,1,1,0\rangle,\ \underline{|0,0,0,1,1\rangle},\ |1,0,0,0,1\rangle,\ |1,1,0,0,0\rangle], \tag{1.24}$$

where the representative has been underlined. The momentum states

$$|a(q)\rangle = |a\rangle + e^{iq}\hat{T}|a\rangle + \dots + e^{iq(L-1)}\hat{T}^{L-1}|a\rangle \qquad \forall |a\rangle \tag{1.25}$$

form an orthogonal basis of the subspace with momentum q, constructed on a set of representative vectors $|a\rangle$. The normalization $N(a,q)$ has to be carefully determined numerically, as the appearance

[4] Using the convention that the sites are numbered from 1

of the fermionic signs in the translation operators renders the formulas provided in the literature for the momentum states of spin Hamiltonians unusable. Every basis vector $|i\rangle$ can be projected back to its representative by m translations

$$|a\rangle = \hat{T}^{-m}|i\rangle, \tag{1.26}$$

from which the momentum state $|a(q)\rangle$ can be identified. States with different momentum are orthogonal by construction with $\langle b(q')\,|\,a(q)\rangle = 0$ unless $q = q'$.

The momentum subspaces $\mathscr{H}^L_{N,q}$, with $q = \left\{\frac{2\pi}{L}q', q' = 0, \ldots, L-1\right\}$, have approximately the same dimension, reducing the Hamiltonian into L separate blocks. $\mathscr{H}^L_{N,q}$ has thus approximate dimension

$$\dim(\mathscr{H}^L_{N,q}) \approx \binom{L}{N}/L. \tag{1.27}$$

Only the representative states of each class need to be written down, if the momentum state has a nonzero norm $N(a,q) > 0$[5]. The matrix elements of the Hamiltonian in $\mathscr{H}_{N,q}$ between two momentum states $\langle b(q)\,|H|\,a(q)\rangle$ can be given in terms of the matrix element between the representatives. Acting with the Hamiltonian on $|a\rangle$ gives in general another state $|\tilde{b}\rangle = H|a\rangle$, which does need not to be the representative of its class. It is however true that $|b\rangle = \hat{T}^{-n}|\tilde{b}\rangle$ for some n, giving a phase factor $\phi = \left\langle b(q)\,|\,\tilde{b}\right\rangle$. The matrix element is

$$\langle b(q)\,|H|\,a(q)\rangle = \phi\sqrt{\frac{N(b,q)}{N(a,q)}}\left\langle \tilde{b}\,|H|\,a\right\rangle. \tag{1.28}$$

The momentum-basis Hamiltonian has an L times smaller dimension, but it is more dense and unavoidably complex. The use of the momentum basis allows the simulation of bigger systems, about 4 or 5 sites more, but complicates matters if the reduced density matrix of a subsystem is required, so it has been avoided in the course of this thesis. Another additional caveat is that if Chebyshev expansions are employed (see Section 3.2.2), different momentum subspaces have different spectral bounds. It is necessary to select the largest bounds in order to sample the density of states uniformly across all momentum subspaces.

1.1.1.4 Inversion parity

The inversion transformation $\hat{Z}$ is a parity operator ($\hat{Z}^2 = \mathbb{1}$) that maps opposing sites of the system into each other. It is a symmetry of the Hamiltonian even if open boundary conditions are used. Applying $\hat{Z}$ yields

$$c_l \xrightarrow{Z} c_{L-l+1}. \tag{1.29}$$

The inversion commutes with PH, but does not in general commute with the translation operator. In fact, applying it to a momentum state yields

$$\hat{Z}|a(q)\rangle = |a(-q)\rangle, \tag{1.30}$$

which is a symmetry only in the $q = 0$ and $q = \pi/L$ sectors. The symmetry is useful for studies of the spectrum, since it allows the remaining degeneracy to be lifted after PH is broken by a finite field $\phi > 0$.

[5]The states for which the norm is zero are dubbed *incompatible states*. The destructive interference of the phase shifts together with the translations may result in zero norm for some of the momentum values. No state is incompatible in all momentum subspaces.

1.1.2 Equivalent Heisenberg model

The $t-V-W$ model was chosen due to its simplicity and the ample information available, with many questions still unanswered, such as the nature of all of its conserved quantities and their effect on the Ballistic transport. However, the literature is available regarding the spin version almost exclusively, so a conversion is needed.

The extended XXZ model is a Heisenberg-type system with additional interactions across second nearest neighbors:

$$H = J\sum_l \left(S_l^x S_{l+1}^x + S_l^y S_{l+1}^y + \Delta_1 S_l^z S_{l+1}^z + \Delta_2 S_l^z S_{l+2}^z\right). \tag{1.31}$$

The spin operators commute between different sites $[S_i^{x,y,z}, S_j^{x,y,z}] = 0$ if $i \neq j$. This is different from fermions, which anticommute over disjoint sites $\{c_i^\dagger, c_j\} = 0$ if $i \neq j$.

The local representation of the operators $S^\pm = \frac{S^x \pm iS^y}{2}$ is identical to those of $c^\dagger$ and c respectively, however the global commutation properties differ. Introducing the Jordan-Wigner transformation, the spin operators are supplanted with nonlocal strings in order to correct the global commutation relations:

$$\begin{aligned} S_l^+ &= (-1)^{\sum_{i=1}^{k-1} n_i} c_l^+ \\ S_l^- &= c_l (-1)^{\sum_{i=1}^{k-1} n_i} \\ S_l^z &= n_l - \frac{1}{2} \end{aligned}$$

Using the transformation above, the extended XXZ Hamiltonian can be rewritten as

$$H = \frac{J}{2}\sum_l (c_{l+1}^+ c_l + h.c.) + J\Delta_1 \sum_l \left(n_l - \frac{1}{2}\right)\left(n_{l+1} - \frac{1}{2}\right) + J\Delta_2 \sum_l \left(n_l - \frac{1}{2}\right)\left(n_{l+2} - \frac{1}{2}\right). \tag{1.32}$$

This allows the identification

$$t_h = \frac{J}{2} \qquad V = 2t_h\Delta_1 \qquad W = 2t_h\Delta_2. \tag{1.33}$$

Since we have conventionally chosen $t_h = 1$ in the forthcoming chapters, this is equivalent to setting $V = 2\Delta_1$ and $W = 2\Delta_2$.

The half-filling condition $N = L/2$ corresponds to the subspace with $S_z = 0$, or an equal number of spins up and down. Finite doping of the system maps to the choice of a subspace of average nonzero magnetization.

1.1.3 Phase diagram

The half-filled Heisenberg XXZ model at $T = 0$, without any additional interactions, is gapless for $|\Delta_1| < 1$, and magnetically ordered otherwise. For $\Delta_1 > 1$ the model displays an antiferromagnetic phase, whereas for $\Delta_1 < -1$ it is ferromagnetic.

This corresponds to an insulating CDW (Charge-Density wave) phase in the fermionic language for $V > 2$ (the case of negative V is not investigated here), and a Luttinger liquid (metallic) phase for $V < 2$, with a quantum phase transition in between.

More is known about the phase diagram when the additional W interaction is switched on at zero temperature [MCR11]: for the small values of $W < V/2$ chosen in our work, we remain in the thermodynamical phase set by the value of V.

Working with a slight doping of the system, the additional charges available always lead to the formation of a metallic, conductive phase, with a visible peak in the conductivity $\sigma(\omega)$ for $\omega = 0$, as seen in Fig. 1.7 on page 21. On the other hand, at half-filling, an ideal insulating or ideal metal behavior can be found whenever the system is integrable, for $W = 0$ [MBP11]. The typical criteria for the metal–insulator classification apply to $T = 0$ only [SWZ93], whereas for the ideal integrable case, the criteria hold at all temperatures $T \leq \infty$. The *dc* conductivity of a conductor, i.e. the low frequency component, is characterized by a broadened delta peak, with dissipation rate $\Gamma \geq 0$

$$\sigma(\omega) = \frac{2iD^N}{\omega + i\Gamma} \qquad \text{for } \omega \to 0. \tag{1.34}$$

When $D^N > 0$, the system is metallic. At $T = 0$ for clean metals without disorder, the dissipation rate $\Gamma = 0$ and the conduction is delta-valued. At higher temperatures, the conductivity is usually broadened, unless the system is integrable. In the latter case, $D^N > 0$, $\Gamma = 0 \quad \forall T > 0$. Integrable (ideal) insulators have $\sigma(0) \to 0 \quad \forall T > 0$, while presenting a nonzero conductivity peak at $\omega = \Delta_{\text{gap}} > 0$.

In Chapter 5, we deal with a doped insulator and metal, with $V = 3$ and $V = 1.5$ respectively, both below half-filling. The type of the phase in both cases is metallic, with a *dc* conductivity peak, although the doped insulator is a case of bad metal [ZBF14, ZF12], with the largest conduction component for $\omega > 0$.

1.1.4 Current operators

The natural observables concerning the transport in a system are currents. Currents are Hermitian imaginary (i.e. there exists a basis on which their representative matrix is antisymmetric with imaginary entries) operators. We give their definition below, referring the full derivation to Section 5.1. The operators depend on the Peierls' phase nontrivially.
The particle current operator J_i^N counts the flux of particles moving from the site $i-1$ onto i,

$$J_i^N(\phi) = it_h \exp(i\phi)\, c_{i+1}^\dagger c_i - it_h \exp(-i\phi)\, c_i^\dagger c_{i+1}. \tag{1.35}$$

The energy current operator J_i^E measures the energy inflowing on the site i from the neighbors

$$J_i^E(\phi) = \underbrace{-\frac{t_h^2}{L}\left[i\,\mathrm{e}^{2i\phi}\, c_{i+1}^\dagger c_{i-1} + \text{H. c.}\right]}_{J_i^{E_1}} + \underbrace{\frac{J_i^N}{2L}\left[3W(\tilde{n}_{i+3} + \tilde{n}_{i-2}) + (2V - W)(\tilde{n}_{i+2} + \tilde{n}_{i-1})\right]}_{J_i^{E_2}}. \tag{1.36}$$

Under the PH symmetry, J_i^N is odd, as

$$J_i^N = it_h\, \mathrm{e}^{i\phi}\, c_{i+1}^\dagger c_i + \text{H. c.} \xrightarrow{\text{PH}} -it_h\, \mathrm{e}^{-i\phi}\, c_{i+1} c_i^\dagger + \text{H. c.} = it_h\, \mathrm{e}^{-i\phi}\, c_i^\dagger c_{i+1} + \text{H. c.} = -J_i^N. \tag{1.37}$$

The first sign changes due to the factors $(-1)^i(-1)^{i+1}$, which must equal -1 for all i. Conversely, J_i^E is even, as it can be seen by analyzing the components $J_i^{E_1}$ and $J_i^{E_2}$ separately. The first component, a two-site hopping term always acquires a positive sign, so $J_i^{E_1} \xrightarrow{\text{PH}} J_i^{E_1}$. The second term also changes sign twice, since for all k

$$J_i^N\, \tilde{\mathrm{n}}_{i+k} \xrightarrow{\text{PH}} (-J_i^N)(-\tilde{\mathrm{n}}_{i+k}) = J_i^N\, \tilde{\mathrm{n}}_{i+k}\,. \tag{1.38}$$

Thus, J_i^E is even under the PH transformation.

1.2 Integrability and Random Matrix Theory

Integrable systems comprise a remarkable class of models. The most widely known examples are the classical separable systems, characterized by periodic orbits and lack of correlations in the eigenvalues. In quantum integrable systems, the role of separability is born by solvability, the existence of an infinite set of local conserved operators, which can be used to block-diagonalize the Hamiltonian, leading the statistical independence of the separate spectrum sectors.

The Heisenberg model (equivalent to the model studied here) was the first quantum integrable system to be solved analytically by Bethe Ansatz in 1931. Such a solution guarantees the existence of an infinite set of local conserved operators, which can be mapped to the Hamiltonian through a continuous flow of a parameter λ [6] [YS13, Sha86, CM11]. For integrable systems, a transfer matrix operator $\hat{T}(\lambda)$ of the corresponding classical spin model is the generator of all local conservation laws, starting with the Hamiltonian

$$H = -\frac{d}{d\lambda} \log \hat{T}(\lambda)|_{\lambda=0}, \tag{1.39}$$

and all other local operators $\hat{Q}_n$ by the expansion

$$\log\left(\hat{T}(\lambda)\,\hat{T}(0)^{-1}\right) = \sum_{n=1}^{\infty} \frac{\lambda^n}{n!} \hat{Q}_{n+1}. \tag{1.40}$$

The use of the transfer matrix is the basis of most of the modern methods based on the Algebraic Bethe Ansatz [ND03, Deg04, MR98, PPSA14, ECJ12, CE13, NMA98, Sta93, Poz13, Pro15].

Since there is no algorithm capable of conclusively deciding whether a given quantum system is solvable, the eigenvalue statistics has become an empirical indicator of integrability [PZB$^+$93, PŽ13]. Random Matrix Theory (RMT) provides a parameter-free criterion, applicable to the Hamiltonian or to other operators representing the system, such as the (reduced) density matrix. RMT threads successfully apparently disconnected areas of physics [Bee15, Mir00, BFF$^+$81], from the spectra of atomic nuclei, to quantum chromodynamics and classical chaotic systems. It provides a characterization of universal classes of behaviors, abstracting the correlations in the eigenvalues of the matrix describing the problem, into terms of probabilistic ensembles of random Hermitian matrices. The statistically independent character of the constituent blocks of integrable systems is reflected by the Poissonian statistics of their spectrum.

Chaotic systems, on the other hand, have intrinsically nonseparable dynamics at the classical level, with given boundary conditions. In the quantum case, the so called *quantum chaos conjecture* connects the inextricable correlations to the spectrum to chaotic behavior, causing strong time decay of initial correlations and an evolution towards an equilibrium state weakly dependent on the initial state. Generic integrable systems with two or more degrees of freedom have energy levels that tend to cluster and are not forbidden from crossing when a parameter in the Hamiltonian is varied. The typical distribution of the spacings of neighboring levels is exponential, $P(S) = \mathrm{e}^{-s}$, as if the energies were uncorrelated points in a Poissonian time series. On the other hand, chaotic nonintegrable systems display correlations in their spectra, which strongly resist crossing, with a varying level of repulsion depending on the universality class the Hamiltonian only: $P(S) \sim S^{\beta}$ for $S \to 0$, with $\beta = \{1, 2, 4\}$.

The strength of the repulsion β does not depend on the microscopic details of the Hamiltonian, but on the type of time invariance, which uniquely determines the ensemble of random matrices sharing the same spectral characteristics. Time reversal is always a symmetry for real-valued spinless Hamiltonians,

[6] The spectral parameter λ depends here on the interaction strength Δ only

with the possible addition of a homogeneous electromagnetic field. Time reversal symmetric operators always have many real representations, since both the symmetry and the reality are preserved by the whole orthogonal group SO(n), and their properties are thus connected to real Gaussian Orthogonal Ensemble (GOE) with $\beta = 1$.

Hamiltonians for which a (generalized) time-reversal symmetry is absent correspond essentially to complex matrices. The only real representation is the eigenbasis, but it is not preserved by the most general group of transformations allowed by symmetry, the unitary group U(n). Their universality class for integer-spin particles it is the Gaussian Unitary Ensemble (GUE) with $\beta = 2$. We mention for sake of completeness, that for half-integer spins with time reversal symmetry, the Gaussian Symplectic Ensemble (GSE) and $\beta = 4$ is respectively found.

The strength of the repulsion can be understood as the unlikelihood of two energy levels being the same: a 2×2 representative of the ensembles needs up to $\beta + 1$ random real parameters to delicately match for a crossing to happen. The factor of s^β intuitively stems from the Jacobian of the parametrization, to spherical coordinates in that many dimensions, of the probability density.

The exact distribution probability for eigenvalues taken from one of the canonical matrix ensembles is hard to derive. The distribution of level spacings, the differences between adjacent energy levels $s = E_{n+1} - E_n$, is fortunately captured by *Wigner's surmise*, a formula valid for 2×2 matrices, which gives an asymptotically valid ansatz for all sizes. It is the generalized Wigner-Dyson distribution [GMW98]

$$P(s) = a_\beta s^\beta \mathrm{e}^{-b_\beta s^2}, \tag{1.41}$$

with the constants a_β and b_β defined uniquely (and continuously) by β. In the particular cases mentioned earlier, the distribution equals

$$P(s) = \begin{cases} \dfrac{\pi}{2} s \, \mathrm{e}^{-\frac{\pi}{4}s^2} & \text{GOE} \quad \beta = 1 \\ \dfrac{32}{\pi^2} s^2 \, \mathrm{e}^{-\frac{4}{\pi}s^2} & \text{GUE} \quad \beta = 2 \\ \dfrac{262144}{729\pi^3} s^4 \, \mathrm{e}^{-\frac{64}{9\pi}s^2} & \text{GSE} \quad \beta = 4 \end{cases} \tag{1.42}$$

The case of integrable systems lacking level repulsion is captured by the Poissonian distribution, which favors a finite density of crossings:

$$P(s) = \mathrm{e}^{-s} \quad \text{Integrable.} \tag{1.43}$$

1.2.1 Unfolding

RMT predictions accurately describe universal classes of matrices. How can it be possibly apply to a concrete Hamiltonian? If a generic quantum system carried no more information than a random Gaussian matrix, no space would be left for the intricacies of geometry, interactions and interplays of different particles.

As it turns out, RMT can be successfully applied to the deviations of the energy levels from their average distribution. The information in the spectrum is split into two: the fine, microscopic level structure has a universal random distribution captured by RMT, while the remaining smooth density of states is the one responsible for the thermodynamical behavior of the system (see Section 2.3.4).

Given a sequence of measured eigenvalues $\{E_1, E_2, \ldots, E_i\}$, obtained through Fourier analysis of a real-time experiment, or by exact diagonalization of a matrix, it is necessary to subtract the slowly varying continuous density $\rho(E)$ to extract the fluctuating part η_i

$$\eta_i = E_i - \rho(E). \tag{1.44}$$

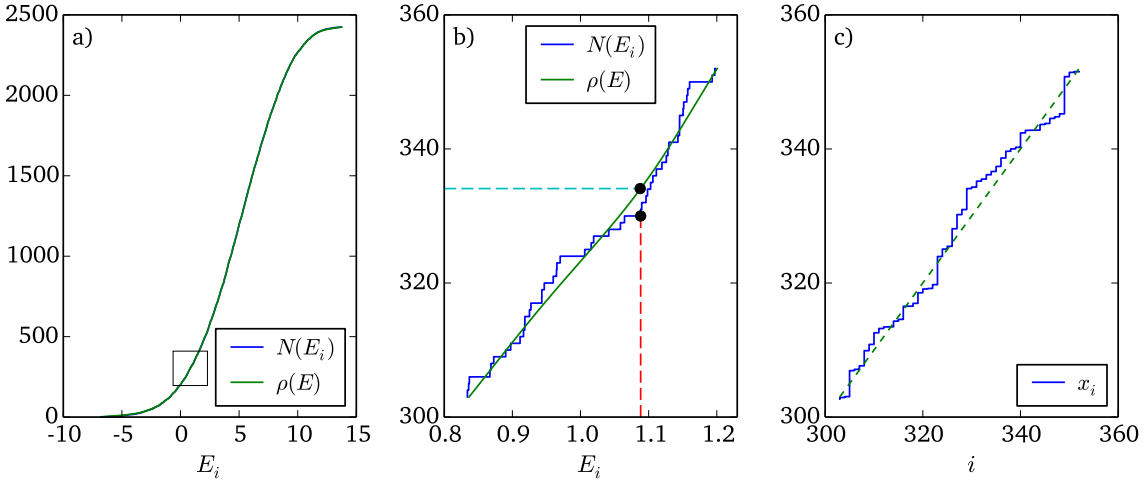

Figure 1.4: Unfolding procedure illustrated for the spectrum of a $t-V-W$ Hamiltonian, with $L=18, N=10, V=1.5, W=0.0$, zero external magnetic field, in the momentum subspace $q=0$. The system is integrable, although that plays no role here, with about 2400 energy levels in the symmetry subsector. (a) The integrated number of states as a function of the energy. Superimposed are both the smooth density $\rho(E)$ as well as the discontinuous $N(E)$. The square points out to the area of the spectrum which is zoomed in the next panel. (b) Detail of an area of the spectrum with 50 levels. The smooth and total density are plotted. The unfolding procedure assigns the value $\rho(E_i)$ (horizontal dotted line) to each energy level indexed E_i (vertical dotted line). (c) The same area of the spectrum is showed after the unfolding. The sequence x_i is plotted as a function of i (solid line), with the dotted line providing the ideal uniform distribution as a guide to the eye.

The set of $\{\eta_i\}$ needs to be normalized to be dimensionless. The overall procedure is called *unfolding*, and produces a set of values $\{x_1 \leq x_2 \leq \ldots \leq x_i\}$ with unit mean spacing and a distribution prescribed by one of the ensembles of RMT.

Unfolding can be performed at once, with a process shown in Fig. (1.4), starting with the total integrated number of states (panel a), as a function of the energy

$$N(E) = \sum_i \theta(E-E_i) = \sum_i \int^E \delta(e-E_i)\,de. \tag{1.45}$$

Calculating the points corresponding to E_i using the smooth integrated number of states $\bar{N}(E)$, as a function of the index i, straightens the values into a sequence with unit average density. This is shown for a single point in Fig. 1.4(b), where to the level $i=330$ is assigned $x_{330}=334.09$. This is the converse to the use of the inverse cumulative distribution function (CDF) in probability theory, to map uniformly distributed random numbers from the unit interval $[0,1]$ into the distribution given by ρ. Here we map numbers distributed according to $\rho(E)$ onto a more uniform sequence.

Precisely, the map is given by

$$[E_i, N(E_i)] \mapsto [i, x_i = \bar{N}(E_i)], \tag{1.46}$$

obtaining the ordered set $\{x_i\}$ with a uniform distribution, which preserves all the fluctuations on closer inspection [see Fig. 1.4(c)].

1.2.2 Details and examples

Let us describe in more detail the procedure, with concrete examples. For lattice Hamiltonians, the spectrum has typically finite density at the middle, with only a countable number of states at the edges.

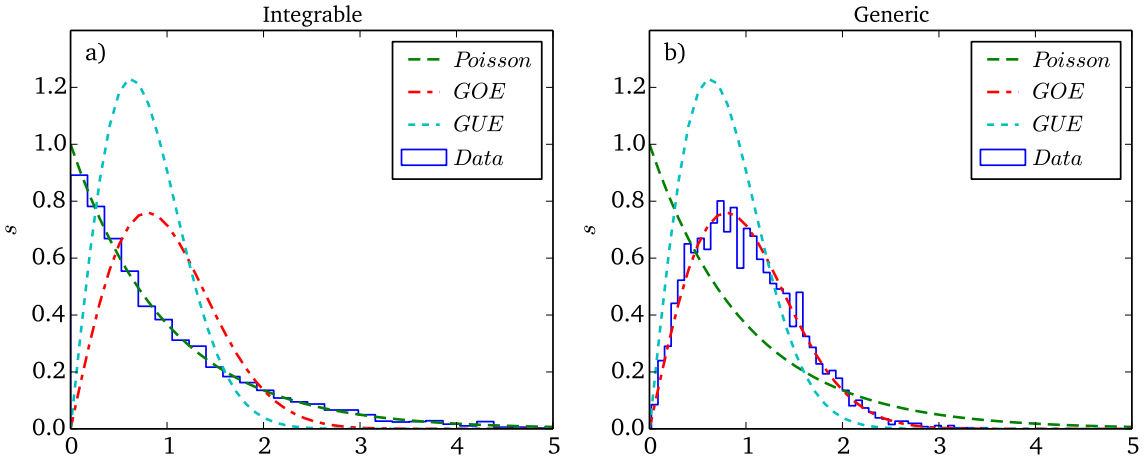

Figure 1.5: Spacing statistics, with energy levels taken from a $t-V-W$ Hamiltonian, with $L = 20, N = 12, V = 1.5$, zero external magnetic field, in the momentum subspace $q = 0$. Of the original 6300 levels, 15% has been discarded at either end of the spectrum. The spacing distribution (solid blue line) is plotted against the level distributions of equations (1.42) and (1.43). (a) The integrable system with $W = 0$. (b) The generic system with $W = 1.0$.

$N(E)$ has then a sigmoid shape when plotted as in Fig. 1.4(a) , which needs to be smoothed to obtain $\bar{N}(E)$. Since the density of the spectrum needs to be nonzero, the lowest and highest lying states need to be removed. The ends of the spectrum always satisfy *entanglement area-laws* [ECP10], meaning the number of states is countable even in the thermodynamical limit, and $\rho(E)$ is zero in measure and discontinuous.

Many recipes are available, but it is possible to simply convolve the sequence of energies $\{E_i\}$ with a window function of approximate Gaussian shape and width over 50-100 levels. The integrated density over the convolved spectrum gives an equivalently smooth $\rho(E)$, with reduced effort.

1. Take the sequence of levels $\{E_i\}$
2. Convolve it with a window function to obtain the smoothened sequence $\{S_i\}$
3. Calculate a spline interpolant to the points (S_i, i), which are the (x, y) coordinates of the smooth integrated density $\bar{N}$
4. Use the interpolant to calculate the values of $\bar{N}$ at the points E_i

Once the unfolding is completed, calculating simple quantities, such as the spacing distribution is trivial. Already for a small system such as the one in Fig. 1.5 the agreement with the predicted distribution is remarkable. A set of sorted random Gaussian numbers in place of the eigenvalues would have produced just as accurate an example of a noninteracting spectrum as the system in panel (a).

The greatest hurdle to the widespread application of RMT analysis is the requirement for the spectrum to come from an *irreducible* matrix, where all unnecessary degeneracies have been removed. The system parameters in the figure have been chosen to minimize the number of kinematic symmetries present: only translational symmetry and time-reversal invariance are left. Choosing a number of particles N greater than half of the number of sites $L/2$ breaks the particle-hole (PH) symmetry, so the parity under PH is not a conserved quantum number. Adding an external static magnetic field, threading the one-dimensional ring of fermions, would not have broken time reversal symmetry, just changed the corresponding generator of the symmetry. Finally, the momentum sector $q = 0$ has been chosen arbitrarily to remove all degeneracy.

The effect of turning on an additional interaction such as W is clearly seen. The statistics transition from those of a noninteracting system, to the chaotic GOE ensemble, confirming that the additional repulsive interaction between second neighbors breaks integrability. It is possible to observe a mix of distributions and the transition between the two as a parameter is varied in finite-size systems [RNM04], although in the thermodynamical limit only one remains.

Had we not reduced the matrix, the independent levels from the different sectors would not display any repulsion. Many levels would overlap due to degeneracies, and the spacing distribution would always resemble a Poissonian, with an additional $s = 0$ component.

1.3 Equilibrium linear response

Linear Response (LR) describes the result of applying an external perturbation to an equilibrium system. It is the framework used to *define* physical susceptibilities at the classical level. A typical example is the application of a frequency dependent electrical field, inducing a current in the system that defines a response called *optical conductivity* $\sigma^N(\omega)$.

In the classical LR formalism, a system with the unperturbed Hamiltonian H_0 is considered at equilibrium at t_0 (we will take $t_0 = 0$), then adiabatically perturbed by a time-dependent source operator $P(t)$[7] added to the total Hamiltonian

$$H(t) = H_0 + P(t). \tag{1.47}$$

The exact expectation value of an observable $\langle O(t)\rangle_{H(t)}$ evolved in time from t_0 with the full $H(t)$ may be impervious to computation, however the resulting variation $\delta\langle O(t)\rangle$ in first-order of $P(t)$ can be written using Kubo's formalism as an *equilibrium expectation value* of a more complicated operator.

As a notational remark, we switch to the quantum mechanical language for the description of LR. The natural setting of the perturbative formalism is the Interaction Picture (IP), where the unperturbed Hamiltonian H_0 is used to evolve a constant operator $O_I(t)$ according to the Heisenberg equations

$$O_I(t) = \mathrm{e}^{iH_0t}\, O\, \mathrm{e}^{-iH_0t}, \tag{1.48}$$

and the operator $P_I(t)$ generates the additional evolution on the states, with the operator

$$U(t,t_0) = \mathscr{T}\exp\left(-i\int_{t_0}^{t} P(t')\,dt'\right) \approx \mathbb{1} - i\int_{t_0}^{t} P_I(t')\,dt'. \tag{1.49}$$

The evolution of the state $\rho_I(t)$ in the interaction picture is given by (1.49) alone

$$\rho_I(t) = U(t,t_0)\,\rho_0\,U(t,t_0)^\dagger \tag{1.50}$$

where the additional hypothesis that the initial state ρ_0 in invariant under the evolution by H_0. It should be noted that the direction of the evolution in the equation above is opposite to the usual for the state.

The expectation value of any observable is given by combining equations (1.48) and (1.50)

$$\begin{aligned}\langle O_I(t)\rangle(t) &= \mathrm{Tr}\left[\rho_I(t)\,O_I(t)\right]\\ &= \mathrm{Tr}\left[\rho_0\,U^\dagger(t)\,O_I(t)\,U(t)\right]\\ &\approx \left\langle\left(1 + i\int_{t_0}^{t} P_I(t')\,dt'\right) O_I(t)\left(1 - i\int_{t_0}^{t} P_I(t')\,dt'\right)\right\rangle_0\end{aligned}$$

[7] The perturbation operator is denoted by the letter P to avoid later ambiguities

$$= \langle O(t)\rangle - i\int_{t_0}^{t} dt' \left\langle [O_{0I}(t), P_I(t')]\right\rangle_0 \tag{1.51}$$

where all averages $\langle\cdot\rangle_0$ are taken with respect to the unperturbed state ρ_0, e.g. $\langle O(t)\rangle_0 = \mathrm{Tr}[O(t)\rho_0]$ displays only the explicit time dependence of the operator, whereas the operators in the commutator have their constant term evolved from t_0.

In the case of the Hamiltonian (1.4), we take as $H_0 = H(\phi = 0)$, where the dependence of $H(\phi) \approx H(0) + (\partial_\phi H)\,\phi$ defines the perturbation

$$P(\phi(t)) = (\partial_\phi H)\,\phi(t) = -\phi(t)\,L\,J^N(0). \tag{1.52}$$

We will focus on the observables of interest, the J^N and J^E currents. Their expectation values will be denoted by j^N and j^E respectively, to keep the notation manageable. The shorthand $N(E)$ implies that the expression applies to j^N and j^E alike.
Suppose the currents depend explicitly on the phase with $\tau^{N(E)} = -\partial_\phi J^{N(E)}$ (see page 74), then

$$J^{N(E)}(t) = J^{N(E)}(0) - \tau^{N(E)}\,\phi(t). \tag{1.53}$$

The evolution in the interaction picture is given by the substitution $J^{N(E)} \longrightarrow J_I^{N(E)}$.

The expectation value for the current depends on the evolution of the state through equation (1.51), with the additional dependence through $\langle O(t)\rangle$ on the explicit phase of the current operators given by (1.53). The total current, knowing that $j^{N(E)}(0) = 0$, is

$$j_{\mathrm{LR}}^{N(E)}(t) = -\tau^{N(E)}\phi(t) + iL\int_{t_0}^{t} \left\langle [J^{N(E)}(t), J^N(t')]\right\rangle_0 \phi(t')\,dt', \tag{1.54}$$

where only the terms linear in $\phi(t)$ were retained. The first term on the r.h.s. depending explicitly on $\phi(t)$ is absent from the canonical derivations [Mah00, Kub57], which do not consider observables depending on the time. The formula is partially asymmetric between j^N and j^E, due to the fact that the source of the perturbation for both (see Eq. 1.52) is the rescaled particle current operator $P(t) = -L\,J^N\,\phi(t)$.

The LR of a system to an external perturbation is thus linear in the time-dependent expectation value of an equilibrium correlation function, which we further analyze in the next subsection.

1.3.1 LR in the spectral representation

Fourier analysis is most useful for the long-time response of a system perturbed by a superposition of periodic signals. The Fourier component of the response $j^{N(E)}(\omega)$ is the reaction of the equilibrium system to a perturbation in the form of a pure sinusoidal driving

$$\phi(t) = \phi(\omega)\,\exp(-i\,\omega^+ t) \tag{1.55}$$

with a small imaginary component $\eta > 0$ added to $\omega^+ = \omega + i\eta$ in order to ensure convergence of the following integrals. The field $F(t) = -\frac{d}{dt}\phi(t)$ in momentum space is given by $F(\omega) = -i\,\omega^+\phi(\omega)$, so the linearity of the response extends also to the derivative of the perturbation: if $j^{N(E)} \propto \phi(\omega)$, then $j^{N(E)} \propto -i\,\omega\,F(\omega)$.
Passing to momentum space, fixing without loss of generality $t_0 = 0$,

$$j^{N(E)}(\omega) = \int_0^\infty dt\,\mathrm{e}^{i\omega t}\,j_{\mathrm{LR}}^{N(E)}, \tag{1.56}$$

the famous Kubo linear relation

$$j^{N(E)}(\omega) \approx \sigma^{N(E)}(\omega)\, F(\omega) = -i\omega\sigma^{N(E)}\, \phi(\omega) \tag{1.57}$$

derives from Eq. 1.54, defining the generic conductivity[8]

$$\sigma^{N(E)}(\omega) = \frac{i}{\omega^+}\left[\tau^{N(E)} - iL\int_0^\infty dt e^{i\omega^+ t}\left\langle [J^{N(E)}(t), J^N(0)]\right\rangle_0\right], \tag{1.58}$$

where all the operators evolve in the Heisenberg picture and the average is still in the initial unperturbed state. Causality is properly taken into account, with the perturbation starting at $t_0 = 0$ and the observable being probed only at later times. The integral is the retarded Green function

$$\chi^{N(E)}(\omega) = -iL\int_0^\infty dt\ e^{i\omega^+ t}\left\langle [J^{N(E)}(t), J^N(0)]\right\rangle_0. \tag{1.59}$$

Using the Plemelj formula $\frac{1}{\omega^+} = \mathbf{P}\frac{1}{\omega} - i\pi\delta(\omega)$ it is possible to recover the real part of the conductivity

$$\sigma^{N(E)}_{\text{real}}(\omega) = \pi\delta(\omega)\left(\tau^{N(E)} + \text{Re}\,\chi(\omega)\right) - \mathbf{P}\left(\frac{1}{\omega}\right)\text{Im}\,\chi(\omega), \tag{1.60}$$

which shows the structure of a regular (the analytical function Im χ) and a singular (delta-valued) part

$$\sigma^{N(E)}(\omega) = 2\pi D^{N(E)}\delta(\omega) + \sigma^{N(E)}_{\text{reg}}(\omega). \tag{1.61}$$

Integrating the conductivity over all real frequencies, and applying the Kramers-Kronig relation

$$\int_\infty^\infty \mathbf{P}\left(\frac{1}{\omega}\right)\text{Im}\,\chi(\omega)\, d\omega = \pi\,\text{Re}\,\chi(0), \tag{1.62}$$

valid for the Green analytical functions, each conductivity is shown to obey the *sum-rule*:

$$\begin{aligned}\int_\infty^\infty \sigma^{N(E)}_{\text{real}}(\omega)\, d\omega &= \pi\underbrace{\left(\tau^{N(E)} + \text{Re}\,\chi(0)\right)}_{1/2\, D^{N(E)}} - \int_\infty^\infty \mathbf{P}\left(\frac{1}{\omega}\right)\text{Im}\,\chi(\omega)\, d\omega \\ &= \pi\,\tau^{N(E)}\end{aligned} \tag{1.63}$$

In the case of the electrical conductivity, this is simply

$$\int_\infty^\infty \sigma^N_{\text{real}}(\omega)\, d\omega = \frac{\pi}{L}|H_{kin}|. \tag{1.64}$$

When the Hamiltonian is generic (non-integrable), the singular part of the conductivity vanishes at $T > 0$, giving $D = 0$. In that case, $\sigma(\omega) = \sigma_{\text{reg}}(\omega)$ and the integral over the Green function alone is sufficient to test the sum rule. Keeping the sum rule with a positive sign was the reason for introducing the counterintuitive minus sign in Eq. (1.53).

1.3.2 Green functions in the canonical formalism

To obtain estimates of the regular and singular parts of the conductivity, the Green function (1.59) must be calculated, starting from the state at $t_0 = 0$. It should be now mentioned that the formalism so far is quite general, with slight modifications allowing for an initial state ρ_0 which is not an equilibrium

[8] $\sigma^E(\omega)$ is called a transport coefficient.

one, but for example obtained in a procedure of driving the system up to the time t_0, before the probe corresponding to the conductivity measurement at $t > t_0$ [LGBP14].

The expectation value of the commutator

$$\langle [J(t), J(0)] \rangle_0 = \langle J(t)J(0) \rangle_0 - \langle J(0)J(t) \rangle_0 = iC^>(t) - iC^<(t) \tag{1.65}$$

can be separated into the lesser $C^>(t)$ and greater $C^<(t)$ correlation functions. The retarded Green function is given by the Fourier transform of the real–time correlators, the first of which has been explicitly given in the canonical ensemble using typicality methods in Section 3.2.3. The greater correlation function can be similarly computed, but it does not need to be.

The *KMS condition* [HHW67, MS59, Kub57], equivalent to the fluctuation-dissipation theorem and valid for systems in thermal equilibrium, states that

$$\langle B(0)A(t) \rangle_\beta = \langle A(t - i\beta)B(0) \rangle_\beta \,. \tag{1.66}$$

It can be used to express one correlation function in terms of the other in Fourier space

$$C^>(-\omega) = e^{-\beta\omega} C^<(\omega). \tag{1.67}$$

The Green function simplifies to

$$\chi^R(\omega) = \left(1 - e^{-\beta\omega}\right) L \int_0^\infty dt \; \mathrm{e}^{i\omega^+ t} \, C^>(t) = \left(1 - \mathrm{e}^{-\beta\omega}\right) L \, C^>(\omega^+), \tag{1.68}$$

and the regular part of the conductivity at high temperatures follows from $(1 - \mathrm{e}^{-\beta\omega})/\omega \approx \beta$

$$\sigma_{\mathrm{reg}}(\omega) = \beta \, L \, C^>(\omega^+). \tag{1.69}$$

In the canonical ensemble there is no further simplification to be made, $C^>(\omega^+)$ must be obtained from real-time evolution, as already pioneered by [JP94], and recently with recent works emphasizing the typicality argument [SG09, EF13, FM13, SKN$^+$14, SGB14, SGB15].

1.4 Integrability and Dissipationless Transport

Small metallic rings in the quantum regime have been long known to allow for currents to flow indefinitely, without showing any dissipative losses [BIL83]. The system can be left in a current-carrying state by a small variation of the phase ϕ, and as long as the temperature and density of states are low enough, the conduction band structure prevents decay into a state with different momentum, irrespective of the interactions present.

Integrable systems on the other hand, allow finite amount of currents to flow without friction at all temperatures, as long as the system is isolated[9]. The set of conserved operators from Eq. (1.40), among which are an infinite number of currents[10], exists independently of the temperature. The expectation values of this set are algebraically precluded from decaying in time due to Umklapp or any other effects, since the interacting quasi-particles of the model only scatter elastically.

In the integrable model we consider with $W = 0$, the most important conserved operator is the energy current J^E. If the system is *phase quenched*, i.e. the phase is changed abruptly at $t = 0$ and

[9] Driving the system breaks the isolation and the currents decay. For the moment only the quench protocol is considered.

[10] Imaginary Hermitian operators

allowed next to evolve under a constant integrable Hamiltonian $H(t) = H(0^+)$, the observed current has a constant value. The quench protocol corresponds to the use of a time-dependent phase

$$\phi(t) = \Delta\phi\ \theta(t), \tag{1.70}$$

and since $[J^E, H] = 0$ for $t > 0$,

$$j^E(t) = \left\langle J^E(0^+) \right\rangle(t) = \mathrm{Tr}[e^{iH(0^+)t}\, J^E(0^+)\, e^{-iH(0^+)t}\, \rho_0] = \mathrm{Tr}[J^E(0^+)\rho_0] = j^E(0^+), \tag{1.71}$$

where all operators for $t \geq 0^+$ (the moment just after the quench) require to be evaluated with a finite phase $\Delta\phi$, and the initial state ρ_0 is arbitrary.

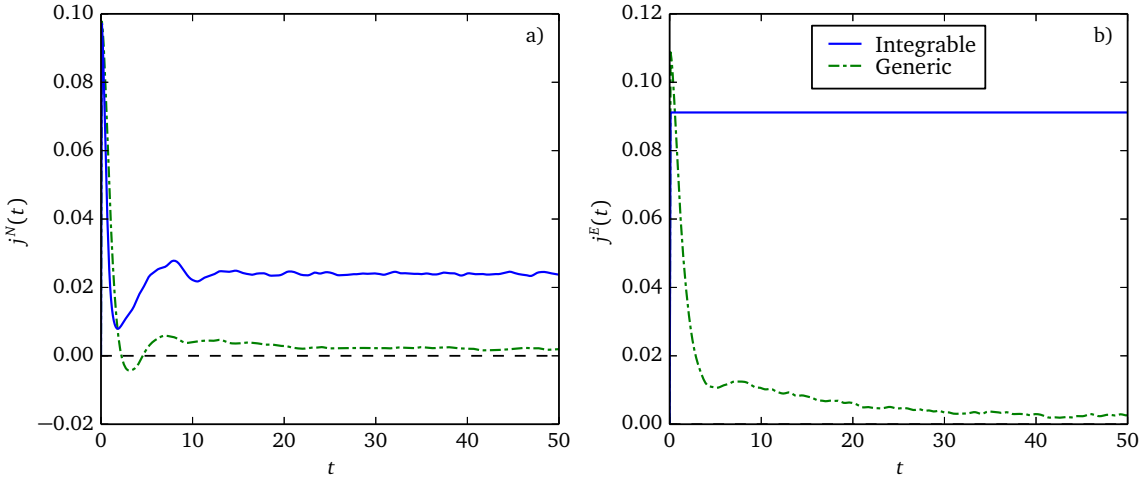

Figure 1.6: Expectation value of the currents in an integrable (solid) and generic (dot-dashed) insulator, with $L = 24, N = 10, V = 3$ and $W = 0$ or $W = 1$ for the integrable and generic system respectively. A dashed zero reference line has been added to guide the eye. (a) The nonvanishing particle current $j^N(t)$ (b) The exactly conserved energy current $j^E(t)$.

In Fig. 1.6 the result of a quench is shown, confirming that the energy current is exactly conserved. However, the particle current J^N does not vanish either, although it decays from its initial value, since it is not conserved in the strict sense as $[J^N, H] \neq 0$.

The non-decaying component of the currents after a quench leads to a singularly defined conductivity. If $j^E(t) = j^E(0^+)$, then the regular part of the conductivity Eq. (1.59) vanishes as the commutator is zero, leaving only the *energy–current stiffness* D^E:

$$\sigma^E(\omega) = 2\pi D^E \delta(\omega) = \pi\tau^E \delta(\omega), \tag{1.72}$$

meaning that the full transport is determined only by the sum-rule. This is clearly reflected in the conductivity (see Eq. 1.60), which shows only a delta-valued singular part. The analysis of the particle current conductivity $\sigma^N(\omega)$ is not as simple, due to only partial conservation. The current decays to a stationary value j_∞ after some time, and this value directly measures the *charge current stiffness* D^N. The measure of the current after a sufficient time has passed is often used to measure D^N [SGB14, KKM14, KMHM14], which we also employ in Chapter 5. The ratio of the zero-frequency singular component to the whole sum rule also gives a direct measure of the degree of conservation. A finite current stiffness is a hallmark of *ballistic transport*, as opposed to the usual diffusive behavior, the former encounters no dissipation [MS08, RS08, Zot99].

In order to measure the stiffness component D^N, it is useful to fit a broadened delta function of the correct functional form (Lorentzian or Gaussian) to the conductivity. In systems with strong ballistic transport, the ratio of D^N to the total sum-rule is close to 1, due to the constraint

$$2\,\pi D^N + \int_{-\infty}^{\infty} \sigma^{\rm reg}_{\rm real}(\omega)\,d\omega = \pi\tau^N, \tag{1.73}$$

which provides a way to calculate D^N if $\sigma^{\rm reg}_{\rm real}(\omega)$ is known to sufficient precision, a method employed historically in Ref. [HPZ11, BCW13, Sha09, SWZ93]. The required separation of the delta contribution from the regular part can significantly contribute to a loss of precision.

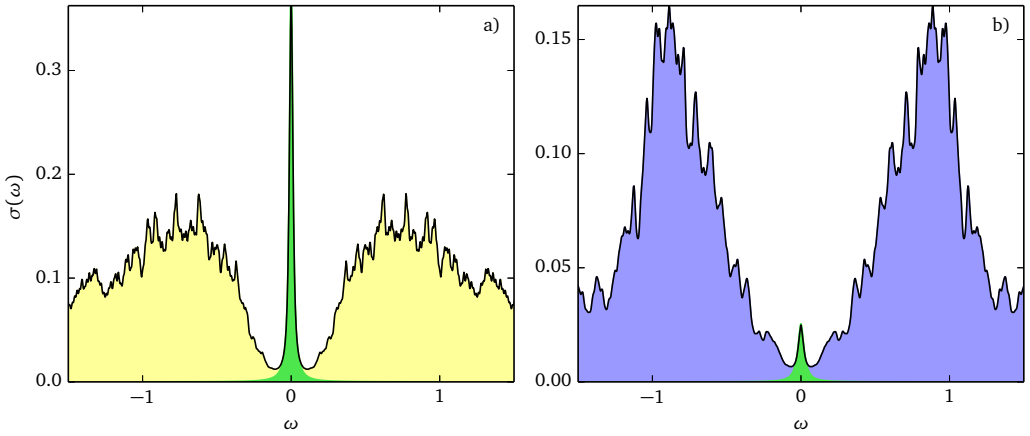

Figure 1.7: Singular (shaded in green) and regular (in yellow and blue) part of the real conductivity $\sigma^N(\omega)$, calculated according to the methods from Section 2.4 and a Lorentzian fit of the $\delta(\omega)$ peak broadened with a Lorentzian of width η, system size $L = 24, N = 10$. (a) Integrable doped insulator with $V = 3$, with a strong stiffness and finite-frequency conductance. (b) Integrable doped high-insulator with $V = 5$, nearly a perfect insulator with minimal residual stiffness.

The LR conductivity is defined through the current response of the system to an infinitely small quench in the magnetic phase. The $F \to 0$ limit is however singular [RSS13], not allowing to extend the results to a system *driven by a finite electric field*. The ratio of two currents characterized by a singular response might still be finite in an appropriate limit, so we investigated how the ballistic transport is modified when a finite field is switched on in Chapter 5.

1.4.1 Mazur bound on the Drude weight

The model we consider is the spinless-fermion version of the Heisenberg model, which in the integrable $W = \Delta_2 = 0$ case, has a macroscopic set of even (under particle-hole transformation) local conserved operators Q_n, leading to integrability. The even operators are real Hermitian, and they start with the Hamiltonian $Q_2 = H$. The odd-numbered conservation laws are imaginary Hermitian operators, which can be interpreted as *currents*, the first of which is the energy current $Q_3 = J^E$. The higher-order operators with $n \geq 4$ are beyond the scope of this dissertation, but can be generated algebraically by application of a suitable *ladder operator* [CET01, GM94, Haw09, LZMG01]. As stated above and inferred from Fig. 1.7, the particle current J^N is not a strictly conserved operator, although it has a ballistic conserved component

$$\bar{J}^N = \lim_{T\to\infty} \frac{1}{T} \int_0^T \mathrm{e}^{iHt}\, J^N e^{-iHt}\, dt, \tag{1.74}$$

which is the *diagonal* part of the current operator, in the eigenbasis of the Hamiltonian.

Mazur's bound, originally derived in Ref. [Maz69] and popularized by Zotos [ZNP97, CZP95, ZP03], used also in Ref. [DS03, JŽ11a, BCMM14, SKAS14, KBM12, BCW13, Žni11, KKM14, JŽ11b, KKHM15, HMHCB03], is the formalization of the following hypothesis:

> The ballistic component of J^N is the result of its non-zero projections onto the set of conserved quantities $\{Q_n\}$.

The validity of the hypothesis was long proven for the doped system with $N \neq L/2$. In the particle-hole symmetric case, D^N was already known to be nonzero from Bethe ansatz methods [Zot99], but there is no conserved local operator to satisfy the bound, as they are all even under PH symmetry. It was found that $D^N > 0$ in the metallic regime, i.e. when $V < 2$ (with a strict inequality); the Mott-insulator phase for $V > 2$ naturally does not allow the flow of dissipationless current. Recently, the Mazur bound was finally saturated by showing the existence of a set of quasi-local conserved operators, providing the needed projections for the particle current in the odd sector [MPP15a, MPP14, PPSA14, Pro15].

We analyze the case of a *doped Mott insulator*, with $L = 24$ and $N = 10$ or $L = 26$ and $N = 11$, where the additional charges break the particle-hole symmetry. In the *Ising regime* with $V > 2$, the finite Drude weight $D^N > 0$ is well taken into account by the projection on J^E alone, since their Hilbert-Schmidt scalar product [11] in non-zero. In the $V < 2$ regime, the bound is nonzero but it is not saturated using J^E alone.

The charge stiffness can be bound from below using the Mazur bound, a projection on every Q_n as fully derived in Ref. [MPP14]:

$$D^N = \frac{\beta L}{2} \left\langle \bar{J}^N J^N \right\rangle \geq D^N_{\text{Mazur}} = \frac{\beta L}{2} \sum_n \frac{\langle Q_n J \rangle^2}{\langle Q_n Q_n \rangle} \geq \frac{\beta L}{2} \frac{\left\langle J^E J^N \right\rangle^2_\beta}{\langle J^E J^E \rangle_\beta}. \tag{1.75}$$

In the case of doped Mott insulators, Ref. [HPZ11] shows that Eq. (1.75) saturates the Drude weight, meaning that $D^N \simeq D^N_{\text{Mazur}}$. The Mazur bound is calculated in an arbitrary equilibrium thermal state, as the ratio of the expectation value of the operators. To numerically evaluate the numerator and denominator separately, it is convenient to use the canonical-ensemble Chebyshev expansions at temperature β shown in Section 3.2.2.

The nonvanishing Drude weight is the most striking manifestation of the nonthermal behavior of integrable systems. At long times, their state does not relax to a thermal state, where all observables can be determined by the knowledge of the temperature β through the canonical density matrix of the system $\rho_\beta = Z^{-1} \exp[-\beta H]$. All the conserved quantities retain their initial values at indefinitely long times, requiring additional separate terms in the construction of the equilibrium density matrix. Generally, the temperature is set by the constraint that the average energy at equilibrium is the same as in the initial state of the quench: $\langle H \rangle_\beta = \langle \psi(0) \,|H|\, \psi(0) \rangle$. In integrable systems all the conserved quantities have their own Lagrange multipliers $\{\beta_i\}$. The equilibrium state is called the *Generalized Gibbs Ensemble* (GGE), and it is given by

$$\rho_{\text{GGE}}(\beta_1, \beta_2, \ldots) = \frac{1}{Z(\{\beta_i\})} \exp\Big[-\sum \beta_i Q_i\Big] \tag{1.76}$$

with the set β_i determined by the set of nonlinear integral equations

$$\text{Tr}\left[Q_i \, \rho_{\text{GGE}}(\{\beta_i\})\right] = \langle \psi(0) \,|Q_i|\, \psi(0) \rangle \qquad \forall \beta_i \tag{1.77}$$

[11] The scalar product in the space of operators on $\mathscr{H}$ [Ols15]. Equivalent to an expectation value at infinite temperature.

In the Extended GGE, the set of operators Q_i is augmented by quasi-local operators. It was shown in Ref. [MPP15a] that the Drude weight is saturated iff the state of the system relaxes to the (Extended) GGE.

The existence of a Drude weight in integrable systems can be reconciled with RMT at a very intuitive level, by noting that integrable systems have large degeneracies (the most probable spectral spacings tend to zero). The large degenerate subsectors of the Hamiltonian allow for large diagonal elements of the averaged operator $\bar{J}^N$. Conversely, generic systems have strong level repulsion with a vanishing density of degenerate elements, thus the conserved part vanishes as well in the thermodynamic limit.

1.5 Thermoelectrical effects

Electrons are charged fermions, which under the effect of an external applied electric field generate a current, due to the induced motion of the charges. Since the system possesses a well-defined energy, given by the expectation value of the Hamiltonian, the motion also generates a flow of energy between the sites of the system, which is measured by the *energy current* j^E (see Section 5.1.1 for a derivation). To each state of the system, a measured current can be unambiguously assigned.

In the framework of *linear irreversible thermodynamics*, where the thermodynamical *forces*[12] that bring the system out of equilibrium can be treated perturbatively, the notion of equilibrium is extended [VR01, LJV08, SL78] to the one of *local quasi equilibrium* (LQE). In LQE, every small portion of the system has still well-defined values of the intensive potentials (such as the temperature, or pressure), while the system as a whole is out of equilibrium. In this case, the first law of thermodynamics

$$\delta E = \delta Q + \underbrace{\mu_e \delta N}_{\delta W} \tag{1.78}$$

can be extended to the time-dependent case by considering fluxes of the quantities: the flow of the energy in time[13] is $j^E = \frac{\delta E}{dt}$ in this approach, and $j^N = \frac{\delta N}{dt}$. In the relation above, the first law of thermodynamics allows the identification of heat Q. We defined the electrochemical potential $\mu_e = \mu_c + eV$, where μ_c is the chemical potential, and V an applied external electric field. The performed work δW is effected only by changes in the particle number N. The corresponding relation for the fluxes is

$$j^E = j^Q + \mu_e j^N \tag{1.79}$$

where the *heat current* (or flow) j^Q has been identified. Very close to thermal equilibrium, this means that we could define $j^Q = j^E - \mu_e j^N$, although an operator for Q is missing.

Continuing this train of thought, any change from the equilibrium value of the external potentials (forces F_i) generates fluxes (currents j^i). The fundamental quantity to consider is the *entropy production*

$$\dot{S} = \frac{dS}{dt} = \sum_i \underbrace{\frac{\partial S}{\partial X_i}}_{F_i} \underbrace{\frac{dX_i}{dt}}_{j^i} = \sum_i F_i j^i, \tag{1.80}$$

which for any natural process occurring close to equilibrium is maximal. The *principle of maximum entropy production* is sometimes confusingly stated as "minimum entropy production" [Mar13, Cal57, Dom54] by using an alternative choice of thermodynamical potentials. The thermodynamical *forces* F_i are defined as derivatives of the entropy with respect to a variation of an extensive thermodynamical potential from

[12] Intensive quantities, such as a mechanical force, an electrical field or a chemical potential.

[13] This is not a formal definition of the quantum current operator.

equilibrium. Any flux generated by a nonzero force brings the system back towards equilibrium, due to the concavity of the entropy, so the entropy production according to the second law of thermodynamics is always positive $\dot{S} \geq 0$. Anticipating our results, this is seen in Fig. 1.8, where the production in a nonequilibrium state is very strong at the beginning (and nonthermodynamically convex), but vanishes ($\dot{S} \to 0$) when the system finally reaches the thermodynamical equilibrium. This is achieved by raising the effective temperature of the system so much that no flow of current is possible, which is effectively what we observe in the later chapters.

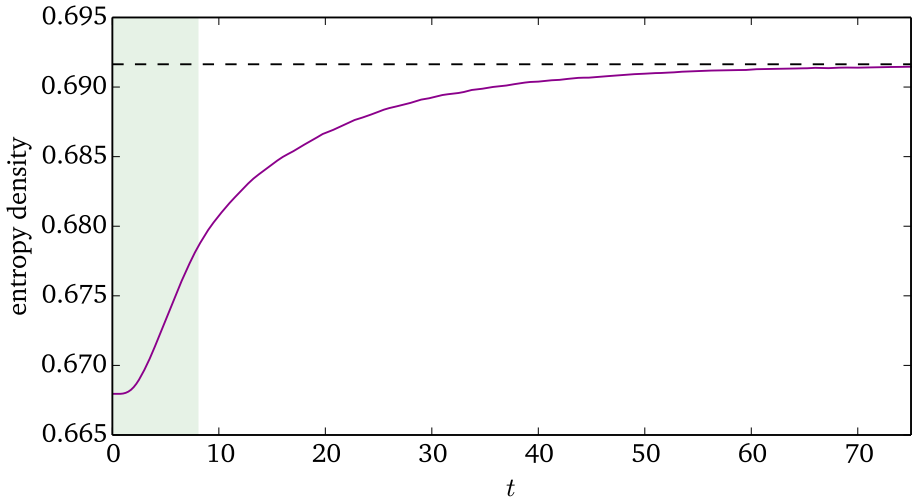

Figure 1.8: Entropy density $s(t)$ (solid line) as function of time in a driven system, with $V = 1.5$, $W = 1.0$, $L = 24$, $N = 12$. The entropy was measured on a $M = 4$ sites subsystem, with the procedure outlined in Section 6.1.1. The data is taken from the same simulation as the ones in Fig. 6.8. The entropy grows with a non-thermodynamical convexity at the beginning (shaded) in order to maximize the rate of growth, later to settle and vanish when the system reaches an effective equilibrium state, set by the infinite-temperature entropy density s_∞ (dotted line), calculated by Eq. (6.35)

For the energy and particle current the quantum operators are rigorously defined as observables in Hilbert space. Their *heat* counterpart j^Q has no corresponding expression, so a *heat conductivity* cannot be defined as done for the others in Section 1.3.2, apart from semiclassical estimates on the phonon conductivity.

This leads to many equivocal statements in the literature, where the energy current conductivity is taken as the heat conductivity [KIM13, EOG15, MSLL12, PSH07]. The lack of applicable definitions is the reason why the derivation of Fourier's law

$$j^Q(t,x) = \kappa_{\text{therm}} \nabla \left(\frac{1}{T(x)} \right) \tag{1.81}$$

in the quantum regime has proven impossible so far [BCMMP15, MAAACJ13, SG09, MH14, Tsc00, SL78], and even attempts using the energy-current conductivity have been fraught with difficulties. A derivation of Ohm's law for closed system, given the precise nature of the particle current, will be outlined in Chapter 5.

1.5.1 Thermoelectrical response

The thermodynamical response of a system to an external perturbation in general implies that all possible fluxes become nonzero to maximize the associated entropy production. In the case of charged

fermions, where the energy and charge transport are coupled, both types of currents can be stimulated by the application of an external electrical potential. Symmetrically, a thermal gradient (e.g. heating one piece of the system in order to push it away from the equilibrium temperature T_{eq}) induces a flow of particles, at the same time locally providing a movement of charges.

Following the notation of the great review [GSZ+11], the forces are given in a continuum description by the gradient of temperature and the gradient of the electrochemical potential

$$F_Q = \nabla\left(\frac{1}{T}\right) = -T^{-2}\nabla T, \quad F_N = -\frac{1}{T}\nabla\mu_e = \frac{F}{T}, \tag{1.82}$$

which differ from the usual definition of forces (F stands for the induced electric field) in order to be derivatives of the entropy function. They induce the currents through a matrix of transport coefficients

$$\begin{bmatrix} j^N \\ j^Q \end{bmatrix} = \begin{bmatrix} L_{11} & L_{12} \\ L_{21} & L_{22} \end{bmatrix} \begin{bmatrix} F_N \\ F_Q \end{bmatrix}. \tag{1.83}$$

Onsanger's theorem [Ons31], of great applicability [Cal48], states that sufficiently close to equilibrium, if the dynamics are microscopically reversible [Cas45], the response matrix is *symmetric* ($L_{12} = L_{21}$), and positive definite to satisfy $\dot{S} > 0$.

The four coefficients, in general nonzero, lead to four known effects by a proper configuration of boundary conditions:

1. $F_Q = 0$: when the whole system is kept at uniform temperature, *Ohm's law* corresponds to the diagonal component L_{11} via

$$j^N = \frac{L_{11}}{T}F = \beta \underbrace{L_{11}}_{LC>} F \tag{1.84}$$

   which captures the high-temperature character of the conductivity, as in Eq. (1.69).

2. $F_N = 0$: when there is no applied field, the temperature gradient induces the flow of heat via *Fourier's law*, Eq. (1.81)

3. $\nabla T \neq 0$, $j^N = 0$: by keeping the system in an open circuit configuration, we prevent the flow of current. Then, the first equation of (1.83) is equal to zero

$$L_{11}\frac{F}{T} + L_{12}\nabla\frac{1}{T} = 0. \tag{1.85}$$

   This defines the open circuit voltage, when a temperature gradient is applied to the system,

$$F|_{j^N=0} = \frac{1}{T}\frac{L_{12}}{L_{11}}\nabla T \tag{1.86}$$

$$= \alpha\nabla T, \tag{1.87}$$

   known as the *Seebeck effect*, characterized by the coefficient α. The offdiagonal terms are known as thermoelectric terms for this reason.

4. $F > 0$, $T = const$ and $F_Q = 0$: the *Peltier effect* is seen when a flow of current, induced by a nonzero field at uniform temperature, produces a flow of heat. From the second equation of (1.83),

$$j^N = L_{11}\frac{F}{T}, \quad j^Q = L_{21}\frac{F}{T}, \tag{1.88}$$

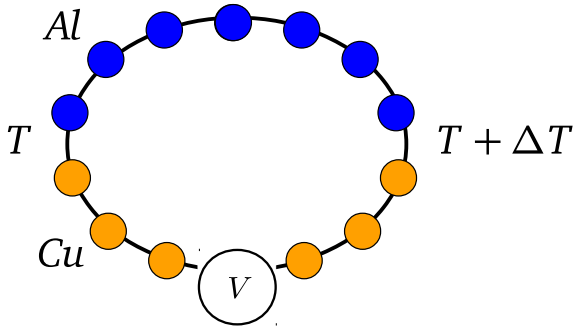

Figure 1.9: The *thermocouple* is the device where the Seebeck effect is best seen: two materials with different electronegativity are connected together and the junctions are set at different temperatures. The circuit is interrupted by a voltmeter to read the voltage produced by the accumulation of charges moved by thermal effects. Two materials typically used are aluminum and copper.

the currents are actually proportional with $j^Q = \frac{L_{21}}{L_{11}} j^N$, defining the Peltier coefficient Π

$$j^Q = \Pi j^N. \tag{1.89}$$

Using Onsager's relations $L_{21} = L_{12}$, the Peltier and the Seebeck coefficients are proportional,

$$\Pi = \frac{L_{21}}{L_{11}} = T\alpha, \tag{1.90}$$

being manifestations of the same phenomenon of coupled transport.

In Chapter 5, we analyze the situation of the Peltier effect induced in a homogeneous system, driven by a finite field. Not having access to the heat current j^Q, we study the similarly defined ratio $R = j^E/j^N$. It differs from the definition of the Peltier coefficient by a term proportional to μ

$$\Pi = \frac{j^Q}{j^N} = \frac{j^E - \mu j^N}{j^N} = \frac{j^E}{j^N} - \mu = R - \mu. \tag{1.91}$$

Whereas the first term is the ratio of the expected values of two observables, the third is only defined in thermal equilibrium.

In Chapter 7, we provide the first fully quantum description of a thermocouple, a device similar to the one in Fig. 1.9, where the system is formed by a junction of two different metals, where a current is driven by a field, generating a visible heating and cooling effect due to the induced transport of energy (and heat) from one junction to the other.

Chapter 2

Numerical methods for quantum thermal dynamics

We review in this standalone chapter all computational methods employed throughout the thesis, summarized from an extensive bibliography, with the addition of a novel method in the last section. The interested reader will learn all the basics and some implementation details needed to reproduce all the results later presented.

The operators in quantum mechanics are by definition Hermitian. On the other hand, all systems that can be simulated on a computer are necessarily finite. The models used in the thesis are short-ranged, with local interactions. In the intersection of the requirements above, all the operators are represented by *finite, Hermitian, sparse* matrices. These constraints pave the way for enormous simplifications, where exact dense linear algebra is supplanted by iterative methods on sparse matrices, which require the user just to implement an efficient multiplication operation between the sparse matrices and vectors.

The sparsity patterns are evident in Fig. 2.1. Only $3.6 \cdot 10^5$ entries are nonzero, out of $9 \cdot 10^8$, a fill factor of 0.04%. Using sparse methods, a speedup equivalent to the inverse of the fill factor is expected.

In Section 2.4 we introduce a method, originally developed by the author of the Dissertation, to greatly improve the computation of transport coefficients in the spectral representation, based on the Lanczős method.

2.1 Lanczős method

In gapped quantum systems there is a surprisingly effective way to determine the ground-state eigenpair (energy and vector) of a sparse Hamiltonian[1] H: the Lanczős iteration, beautifully described in Ref. [TB97, Saa03]. It is an iterative randomized method [HMT11], where the starting point is a random vector in the full Hilbert space, from which the normalized ground state component is projected out, at the same time providing approximated values for the extrema of the spectrum.

The method requires only a certain number of matrix-vector multiplications and the diagonalization of a dense $M \times M$ matrix, where $M \ll N$ is the number of iterative steps taken. Here and throughout the rest of the chapter $N = \dim \mathscr{H}$. Since most of the tight-binding Hamiltonians are sparse, the method allows to use optimized Sparse Matrix Vector Multiplications (SpMV, commonly provided by sparse linear algebra implementations [GKK+13], such as Intel MKL), instead of costly dense linear algebra

[1] Any Hermitian operator will do, so quantum observables all fall in the applicability range.

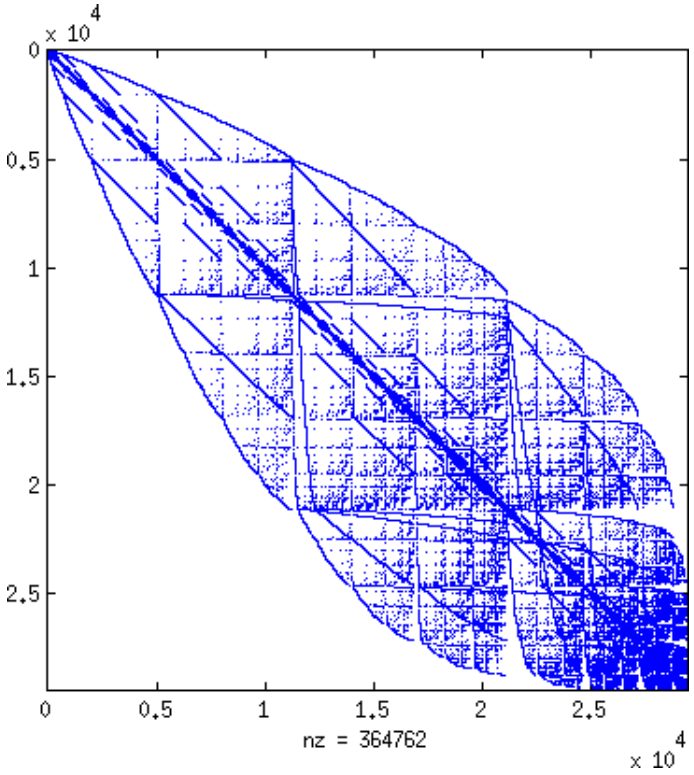

Figure 2.1: Sparsity pattern of a small $t-V-W$ Hamiltonian with $L=10$ sites, in the $q=0$ momentum sector.

routines. The time cost of the method is then $O(M\cdot \mathrm{NNZ})$, where NNZ is the number of nonzero entries in the matrix H. This is contrasted with full diagonalization which requires $O(N^3)$ operations, where N is the dimension of the matrix. Since for typical sparse Hamiltonians[2] NNZ $\propto N$, the method is exponentially faster for larger matrices, as long as only the ground state is required. In case the ground state is degenerate, the convergence will take place to a random superposition of the vectors.

The biggest downside of the plain Lanczős method is the inability to get any reliable information about the spectrum away from the extrema. This can be overcome by applying the original Lanczős method to the matrix resolvent $(H-\lambda I)^{-1}$ at every step of the iteration, with orders of magnitude higher computational requirements, although due to the obvious interest there exist many methods targeting explicitly the interior of the spectrum [FS12, Pol09, Dol06, Wya95, Sim13, WN95, CBPS13, LDZ12], including the ubiquitous Arpack package (see [BDD+00] for a description). We have avoided this difficulty by using Chebyshev expansions for thermodynamical applications requiring the spectrum interior.

Typical precisions available for ground state calculations is $\|H\|_2\epsilon_{\mathrm{machine}}\approx 10^{-14}$ for Hamiltonians such as the one in Fig. 2.1, usually requiring $M\sim 100-200$ steps.

2.1.1 Implementation

We give here a complete recipe for the implementation of the Lanczős method, which can be found also in the introductory materials [Koc11, San10], following closely [TB97]. The Lanczős method is equivalent to choosing a proper subspace V of the Hilbert space and diagonalizing the Hamiltonian projected in V. By choosing carefully V, it ensures that the extremal eigenvectors are well represented.

[2]The proportionality constant is the bandwidth of the matrix H, which is usually twice the number of fermions in the system.

According to the Arnoldi approximation problem [TB97, Eq. (34.3)], V must be the Krylov subspace of a random normalized vector q with nonzero overlap with the ground state, i.e. the orthonormalized set[3] of the powers of H applied to q

$$\text{span}(V) = \text{span}\left\{q, Hq, H^2q, H^3q, \ldots, H^{M-1}q\right\}. \tag{2.1}$$

Collecting the vectors $\left\{q, Hq, H^2q, H^3q, \ldots, H^{M-1}q\right\}$ as columns of a $M \times N$ matrix K, one can obtain the orthonormalized basis for the set by means of a Gram-Schmidt procedure, in practice implemented using a QR-decomposition. Decomposing $K = QR$, the (truncated) unitary matrix $V = Q$ has an orthonormal span of columns. Since $V\,V^\dagger = P_{\text{Krylov}} \neq \mathbb{1}$, the matrix is clearly not unitary, but acts as a projection into a much smaller, M-dimensional Krylov subspace. Projecting H, one obtains the $M \times M$ dimensional matrix T, or equivalently

$$H \approx V\,T\,V^\dagger. \tag{2.2}$$

The much smaller matrix T can be diagonalized without effort to

$$T = X\,D\,X^\dagger. \tag{2.3}$$

The eigenvalues of H restricted to the subspace V are the diagonal elements D. The Hermitianity condition $H = H^\dagger$ immediately gives $T = T^\dagger$, but allows further simplifications. It can be proven that T is tridiagonal real symmetric, so the storage and diagonalization of T has negligible computational cost.

Algorithm 1 Lanczős eigenvalue method

1: **Input**: The number of steps M, the operator H
2: Allocate vectors $|q_{n-1}\rangle$, $|q_n\rangle$, $|v\rangle$ of size N with zeros
3: Set $|q_n\rangle$ to a normalized random vector with zero mean (random signs)
4: Allocate the vectors **a** and **b** of size M filled with zeros
5: **for** $n = 1, 2, \ldots, M$ **do**
6: *Use $|q_n\rangle$ as the n-th column of V (optionally)*
7: $|v\rangle = H\,|q_n\rangle$ Generate next vector
8: $a_n = \langle q_n \,|\, v\rangle$ Projection on previous vector
9: $|v\rangle = |v\rangle - a_n|q_n\rangle - b_{n-1}|q_{n-1}\rangle$ Orthogonalization on-the-fly with previous vectors
10: $b_n = \langle v \,|\, v\rangle$ Normalization of next vector
11: $|q_{n-1}\rangle = |q_n\rangle$
12: $|q_n\rangle = |v\rangle / b_n$
13: **end for**

Storing the full matrix V can be too costly when $N > 10^5$, so the full version of the Lanczős algorithm consists in the orthogonalization on-the-fly of V, manipulating only 3 vectors at a time and building the matrix T directly. The memory requirements are thus reduced to $3N$ if the vectors are updated in-place.

The algorithm is listed in pseudocode in Alg.(1), and returns the diagonal elements **a** and offdiagonal **b** of T. All other elements are zero

$$T = \begin{bmatrix} a_1 & b_1 & & & \\ b_1 & a_2 & b_2 & & \\ & b_2 & a_3 & \ddots & \\ & & \ddots & \ddots & b_{M-1} \\ & & & b_{M-1} & a_M \end{bmatrix}. \tag{2.4}$$

[3] The span is the linear algebraic subspace generated by a set of vectors.

The algorithm as listed is sufficient to obtain the eigenvalues of H approximated as the eigenvalues of T, but what about the eigenvectors of H? They are the eigenvectors of T rewritten in the computation basis of the full Hilbert space

$$H \approx V\,T\,V^\dagger = V\,X\,D\,X^\dagger\,V^\dagger = (V\,X)\,D\,(V\,X)^\dagger = UDU^\dagger. \tag{2.5}$$

The equation gives the approximate eigenvectors U of H, $U = VX$. The first eigenvector is then the approximate ground state, so $|U_1\rangle = V\,|X_1\rangle$[4]. After the diagonalization of T, the matrix X is known and its components give the coefficients of the expansion over the column vectors of V. However, the full matrix V has not been built, as the vectors were determined successively: it is necessary to run the algorithm a second time, generating the vectors again. To get an approximate eigenvector $|\psi_1\rangle$ of the ground state, it suffices to modify line (6) of Alg.(1), as shown in Alg.(2).

Algorithm 2 Lanczős eigenvector algorithm for 1st vector

5: **for** $n = 1, 2, \ldots, M$ **do**
6: $\quad |\psi_1\rangle = |\psi_1\rangle + X_{n,1}\,|q_n\rangle$
7: $\quad \ldots$
8: **end for**
9: **return** $|\psi_1\rangle$

There is one parameter left free in the procedure, i.e. the number of steps M. It can be determined by calculating the matrix T at every iteration and checking convergence of the approximate ground state value $E = D_{1,1}$ across iterations. When the convergence criterion

$$\frac{|E_{new} - E_{old}|}{E_{new}} < 10^{-15} \tag{2.6}$$

is met, the procedure must be stopped and the eigenvectors X are determined[5]. The procedure is then run a second time if the corresponding eigenvector is required.

Caveat: The Lanczős algorithm is intrinsecally unstable, since the spectral radius ρ of H

$$\rho_H = \max_{\|\psi\|=1} \|H\psi\| \tag{2.7}$$

is usually $\rho_H \gg 1$, and the inner iteration at line (7) of Alg.(1) corresponds to taking successive powers of H. Since at every iteration the norm $\langle v\,|\,v\rangle^{1/2}$ usually grows as large as ρ_H, truncation errors grow at the geometrical rate ρ_H^n, causing a loss of orthogonalization between the columns of V and leading to *ghosts* and other artifacts in the middle of the spectrum. As long as the ground state is unique, the algorithm usually converges to it quickly[6], but it has to be stopped as soon as Eq.(2.6) is fulfilled. The instability can only be cured by running the algorithm in integer arithmetics, which is disastrous for the performance, or by keeping the whole of V in memory and performing reorthogonalizations, which requires too much memory. Possible solutions are mentioned in Ref. [SBR06, Saa03].

Note: The upper eigenvalue can be determined just as accurately and quickly, as $D_{M,M}$. This allows the spectral bounds E_0 and E_{max} to be calculated at once, which is necessary for the Chebyshev algorithm.

[4] By a single lower index we denote the column vector of the matrix
[5] The subroutine DSTEVR from LAPACK can be used
[6] At least as fast as the geometrical rate set by the spectral gap $|(E_1 - E_0)/E_0|$

2.1.2 Lanczős based function evaluation

Besides from the original purpose as spectral approximation and the solution of linear systems of equations [Sim13, She94], the Lanczős method can be applied to functions of Hermitian operators. Since $H \approx V\,T\,V^\dagger$, then $f(H) \approx V\,f(T)\,V^\dagger$ for analytical functions.

The most commonly needed application is the case of an operator function applied to a vector $|v\rangle$, using a similar factorization to Eq. (2.5)

$$f(H)\,|v\rangle \approx (V\,X)\,f(D)\,(V\,X)^\dagger\,|v\rangle. \tag{2.8}$$

Keeping in mind the caveat at the end of the previous section, the global approximation of any $f(H)$ is pointless. The application on a vector $f(H)|v\rangle$ can be very accurate, however. If the vectors of the Krylov space will generated started from $|v\rangle$ instead of a random vector, the space K will accurately predict the action of $f(H)$ if the function does not differ too greatly from the identity.

Since the vectors in V are approximately orthogonal, if $|V_1\rangle = |v\rangle/\|v\|$, then all other columns will be orthogonal to $|v\rangle$. In this case $V|v\rangle = [\|v\|, 0, 0, \ldots] = \|v\|\,|\,\mathrm{e}_1\rangle$, the first elementary basis vectors with all zeros for components other than the first. The algebra then simplifies,

$$f(H)\,|v\rangle \approx (V\,X)\,f(D)\,X^\dagger\,V\,|v\rangle = V\,X\,f(D)\,X^\dagger|\,\mathrm{e}_1\rangle = V\,f(T)|\,\mathrm{e}_1\rangle. \tag{2.9}$$

This can be further simplified, since $f(T)|\,\mathrm{e}_1\rangle$ is the first column of the matrix $f(T)$, which does not need to be completely computed. Calling this vector $\mathbf{C} = f(T)|\,\mathrm{e}_1\rangle$, its components can be shown to be

$$\mathbf{C}_i = \left(X\,f(D)\,X^\dagger\right)_{i,1} = \sum_j X_{i,j} f(D)_j X^\dagger_{j,1} = \sum_j X_{i,j}\,X^*_{1,j}\,f(D)_j. \tag{2.10}$$

The determination of the i-th component $\mathbf{C}_i$ is then mostly equivalent to a single scalar product, once the whole vector $f(D)$[7] has been precomputed.

Artifacts such as the appearance of *ghosts* in the truncated eigen-expansion are here inconsequential, since the weight $\mathbf{C}_i$ associated with spurious eigenvalues is nearly zero. In fact it is a common technique to monitor the weights over a carefully chosen $f(H)$ to recognize and remove the ghosts [DWH+12].

2.1.3 Krylov based propagator

The most commonly encountered functions of the Hamiltonian, and the only one needed in this manuscript, are:

1. The time propagator on a state: $\mathrm{e}^{-iH\Delta t}\,|v\rangle$
2. Finite temperature reweighting, or imaginary time propagator: $\mathrm{e}^{-\beta H}\,|v\rangle$
3. Pure state Green function for the operator O: $\left\langle v \left| O\,\frac{1}{\omega + H - E_0 I}\,O \right| v \right\rangle$

To calculate the time evolution propagator, it is enough to substitute the e^{-iHt} for $f(H)$ in the previous section. The resulting approximation is called *Krylov Time Propagator* [MV03] in the literature, originally publicized by [PL86]. It is accurate to numerical precision (10^{-16}) if a sufficient of iterations M is taken for the given time interval Δt. For any number of steps, the propagator is unitary and the Hamiltonian does not need to be bounded, so the applicability is perfectly general, even for systems treated within the DMRG numerical scheme, where the spectral radius of the Hamiltonian exceeds $\rho_H > 10^{300}$ for

[7] The matrix D is treated as vector

reachable[8] values of the system length L. In this case only the Krylov based time propagator is applicable with great success [WC12] (see also [Sch04, SRU13, ZMK+15, DWH+12, GR06]), whereas the Chebyshev based scheme becomes too demanding [WMPS14, HWM+11, BS14].

The time evolution in an interval Δt on a pure state, with a constant Hermitian generator of the time translation such as a time independent Hamiltonian, is given by the propagator $e^{-iH\Delta t}$, which is the solution of the Schrödinger equation in the interval $(t, t+\Delta t)$. We apply Eq.(2.9) to $|\psi(t)\rangle$, the state at time t,

$$|\psi(t+\Delta t)\rangle = e^{-iH\Delta t}\,|\psi(t)\rangle = V\, e^{-iT\Delta t}\, V^{\dagger}|\psi(t)\rangle = V\; e^{-iT\Delta t}\,|\,e_1\rangle = \sum_{k=1}^{M} \mathbf{C}_k |V_k\rangle. \tag{2.11}$$

The equation is the expansion with coefficients $\mathbf{C}_k$ (see Eq. 2.10) over the subspace of orthonormal Krylov vectors $|V_k\rangle$, starting with $|V_1\rangle = |\psi(t)\rangle$. As such, the precision of the truncation to M terms can be estimated *a posteriori* by

$$\| |\psi(t+\Delta t)\rangle_{\text{approx}} - |\psi(t+\Delta t)\rangle_{\text{exact}} \| \leq |\mathbf{C}_M| \||\psi(t)\|, \tag{2.12}$$

i.e. bounded by the norm of the last coefficient of the expansion. While this does not allow to predict the number of steps to be taken, it is useful to monitor if the expansion was sufficient. A sufficient number of steps to be taken is [MA06]

$$M \gtrsim 1.5\,\rho_H\,\Delta t > 10, \tag{2.13}$$

v which shows that the algorithm has a *linear complexity in time*, superior to the Runge-Kutta type of integrators commonly used for nonlinear ordinary differential equations.

The algorithm for the Krylov based time evolution can be summarized in three steps, and it is a minimal (5 lines of code) extension of the algorithm for the ground state:

1. Starting with $|\psi(t)\rangle$, perform M steps of the Alg. (1) (cost: M SpMV)
2. Compute $\mathbf{C}$ from Eq. (2.10) with $f(x) = e^{-ix\Delta t}$, checking that M is sufficient
3. Run again the iteration in Alg. (2) using $\mathbf{C}$ instead of X_1 (cost: M SpMV)

At least $M = 10$ is required for the algorithm to start and be effective, so the time step is to be adjusted accordingly. Precisions down to 10^{-16}, defined as in Eq. (2.12), can be achieved in about 30 SpMV for $t = 0.5$.

2.2 Time–Dependent Schrödinger equation

The previous section detailed how to compute a unitary approximation to the solution of the Time–Independent Schrödinger equation (TISE), in which the time translation and energy operator H is constant in time. We now review how to apply the techniques already known to allow for explicit time dependence of the H operator.

The Time–Dependent Schrödinger Equation (TDSE) is given by

$$i\hbar\partial_t |\psi(t)\rangle = H(t)\,|\psi(t)\rangle \tag{2.14}$$

[8] The norm of even a simple spin Hamiltonian $\sum_i \sigma_i^z \sigma_{i+1}^z$ can be seen to grow as $O(4^L)$

where ∂_t stands for the partial time derivative, and $\hbar$ will be set to 1 for the remainder of the manuscript. In general, the solution of this equation is given in terms of the time propagator $U(t_0,t)$ from time t_0 to t, which satisfies $|\psi(t) = U(t_0,t)|\psi(t_0)\rangle\rangle$ and $U(t,t) = \mathbb{1}$.

Formally the propagator can be computed as $U(t_0,t) = \mathscr{T}\, \mathrm{e}^{-i\int_{t_0}^{t} d\tau H(\tau)}$, which requires the time ordering operator $\mathscr{T}$ due to the noncommutativity $[H(t),H(t')] \neq 0$ for $t \neq t'$. A practical and readily implementable form is found by partitioning the time interval $[0,t]$ over which the evolution is required. The simplest choice is to use N segments δt long, such that $N\,\delta t = t$, in the limit $\delta t \to 0$. Combining the pieces the propagator is decomposed as

$$U(0,t) = \lim_{N\to\infty} \prod_{k=1}^{N} U(t_k, t_k+\delta t) = U(0,\delta t)\,U(\delta t, 2\delta t), \ldots, U(t-\delta t, t), \tag{2.15}$$

where every piece $U(t_k, t_k+\delta t)$ can be replaced by a the time-independent propagator, such as the one given in Eq. (2.11). Using the *midpoint rule*, i.e. approximating the time dependent Hamiltonian by its value in the middle of the interval

$$U(t_k, t_k+\delta t) = \exp\left[-iH\left(t_k + \frac{\delta t}{2}\right)\delta t\right], \tag{2.16}$$

leads to an error proportional to $O(\delta t^3)$ for every time step. However, since the number of time steps is proportional to N, the total error is bounded by $O(N\delta t^3) = O(T\delta t^2)$.

In case of nearly constant Hamiltonians, the midpoint rule is sufficient. However, the error depends on the rate of change of the Hamiltonian over time. The parallel with integration theory, from which the midpoint approximation takes its name, points to the need of a better rule in case the Hamiltonian is varying rapidly over each time step δt, to prevent an unnecessary and costly increase in the number of steps N. It is possible to find an operator Ω such that $U(0,t) = \mathrm{e}^{-i\Omega t}$ for whole interval, requiring thus only one propagator. This technique bears the name of Magnus expansion [PT07], which is a cumulant expansion for the time ordered exponential. Using Ω in one propagator seemingly reduces the complexity, however the expansion involves an exponentially growing number of commutators of operators, which in turn increases the density of the sparse matrix exponentially, turning the perceived advantage into an obstacle.

The solution is to apply Commutator Free Exponential-Time propagators (CFET), the equivalent of Suzuki-Trotter formulas of higher order [HS05], instead of the linear subdivision scheme of Eq. (2.15). The full derivation is found in Ref. [AF11, WC12, AFL12] so we report only the formulas needed for the implementation. We employ the most popular 4th order CFET, in which the total error scales as $O(\delta t^4)$.

In all the cases treated in the thesis, the Hamiltonian decomposes in its time dependence as

$$H(t) = D + f(t)\,G. \tag{2.17}$$

Here D and G are full quantum operators, respectively the potential and hopping parts of the Hamiltonian, whereas $f(t) = \mathrm{e}^{iFt}$ is a scalar function defining the time dependence. In this case, the full propagator over the interval $(t, t+\delta t)$ is given by:

$$U_{\mathrm{CFET}}(t, t+\delta t) = \exp[\delta t_1 (B + f_1 C)]\exp[\delta t_2 (B + f_2 C)]\exp[\delta t_1 (B + f_3 C)], \tag{2.18}$$

with the time steps

$$\delta t_1 = \frac{11}{40}\delta t, \qquad \delta t_2 = \frac{9}{20}\delta t, \tag{2.19}$$

and the coefficients f_1, f_2, f_3 in each time step are given by the linear combination

$$\begin{pmatrix} f_1 \\ f_2 \\ f_3 \end{pmatrix} = \begin{pmatrix} h_1 & h_2 & h_3 \\ h_4 & h_5 & h_4 \\ h_6 & h_2 & h_1 \end{pmatrix} \begin{pmatrix} f(t + x_1 \delta t) \\ f(t + x_2 \delta t) \\ f(t + x_3 \delta t) \end{pmatrix} \tag{2.20}$$

using

$$\begin{aligned} h_1 &= \frac{37}{66} - \frac{400}{957}\sqrt{\frac{5}{3}}, \quad h_2 = -\frac{4}{33} \quad h_3 = \frac{37}{66} + \frac{400}{957}\sqrt{\frac{5}{3}}, \\ h_4 &= -\frac{11}{162}, \quad h_5 = \frac{92}{81} \end{aligned} \tag{2.21}$$

and

$$x_1 = \frac{1}{2} - \sqrt{\frac{3}{20}}, \quad x_2 = \frac{1}{2} \quad x_3 = \frac{1}{2} + \sqrt{\frac{3}{20}}. \tag{2.22}$$

The total propagation over $(t, t + \delta t)$ is split into three parts, during each of which the time evolution is computed using the value of $H(t)$ through $f(t)$, at 3 internal points. The coefficients are the result of matching the more complicated Magnus expansion up to the 5th order with the ansatz from Eq. (2.18). The use of three exponentials is offset by greater time step δt allowed with the higher order expansion. Every operator exponential should be calculated using a numerically exact unitary propagator such as the Chebyshev based expansion, the Krylov space propagator (see Section 2.1.3), or other spectral approximations [CP10]. They display linear performance in the time step δt, so the time cost is bound by the number of steps taken, which scales as $O(T^{5/4})$ at fixed precision, just as the Runge-Kutta (RK45) algorithm, although with a lower proportionality constant. If the variation of $f(t)$ from Eq. (2.17) is slow, longer intervals δt are possible. The step size is the same as required for the accurate integration of $f(t)$ with a 4th order method: since 3 points are computed for every δt, it can be comparable to a half-period for a sinusoidal $f(t)$.

Global interpolation methods can construct an optimal time evolution operator in the interval δt, by approximating the time dependent part $f(t)$ with exponential precision in the number of steps [NTEKK10, TEKS12, ST07]. This goes beyond the scope of the thesis, since we required steps small enough to plot observables along the evolution.

Note: The CFET algorithm as shown here can handle identically cases in which the time evolution generator is not Hermitian. Lindblad operators $\mathscr{L}$, usually non-Hermitian with a complex spectrum, are commonly used to model dissipative interactions of quantum systems with an environment. In that case, only the constant-time propagator $e^{\mathscr{L}t}$ needs to be modeled differently.

For the TDSE the maximum precision is lower than for time independent problems. Using the definition in Eq. (2.12), 10^{-6} for times $t = 100$ and $F = 1.0$ is reachable with about 2500 SpMV.

2.3 Thermodynamical averages

This thesis deals with high temperature dynamics of quantum systems. Static averages based on the Density Of States (DOS) are however needed in abundance, for initialization, e.g. the average energy at given temperature for the microcanonical ensemble, or for comparison, such as linear response high temperature coefficients.

All states in the spectrum contribute to the averages at high temperatures, leading to the necessary used of mixed density matrices. This can be however offset by judicious use of Monte Carlo averaging

techniques which we detail in the following. Quantities involving the whole spectrum, and the interior in greater measure, require a completely different technology than Lanczős expansions, which target only the extremes and skew severely the DOS distribution.

The need for global approximations leads immediately to the use of orthogonal polynomials for the expansions. Functions of operators are interpreted as functions of the spectra, which are real valued intervals. The simplification allows approximation theory to be applied. For bounded spectra, as in the present case of finite tight-binding systems, the task is analogous to the optimal approximations of functions in a bounded and closed interval $[-1,1]$, for which the natural basis is expressed in Chebyshev or Legendre polynomials. Fourier methods require nonpolynomial function evaluations, and are thus too expensive for operator valued functions. For unbounded spectra, Laguerre or Hermite expansions are also available [VWB99], but they lack properties of absolute stability provided by bound intervals.

2.3.1 Chebyshev expansions

Chebyshev polynomials are the nearly optimal basis for all possible applications in bounded intervals, with a flourishing literature and hundreds of applications. They are fundamental for solving PDEs [Boy00, CHQZ06, Tre00] and are instrumental in bringing commonly needed algorithms to numerical precision with reduced effort [HT12, MH03, AKT14, BT04]. A comprehensive and thought provoking review is [Tre13].

The Chebyshev expansion can be thought to be the result of the application of Fourier series methods to nonperiodic functions in the interval $[-1,1]$. The function is first made periodic by a change of variables,

$$x = \cos(\theta) \quad \text{with } \theta \in [-\pi, \pi]. \tag{2.23}$$

When θ varies, x traces a closed loop in $[-1,1]$. With this parametrization, any function $f\,(x(\theta))$ can be expanded in the even Fourier (cosine) series. The natural basis is thus provided by the Chebyshev polynomials of the 1st type

$$T_n(x) = \cos(n\,\theta) = \cos(n\,\arccos(x)) \qquad \text{for } x \in [-1,1]. \tag{2.24}$$

The basis functions fill the defining interval uniformly, with increased precision near the ends. A recursion relation allows simple calculation:

$$\begin{aligned} T_0(x) = 1, \quad T_1(x) = T_{-1}(x) = x \\ T_{m+1}(x) = 2\,x\,T_m(x) - T_{m-1}(x). \end{aligned} \tag{2.25}$$

In order to approximate any function, start with the ansatz

$$f(x) = \alpha_0 + 2\sum_{n=0} \alpha_n T_n(x). \tag{2.26}$$

The coefficients α_n are recovered using the standard scalar product $\alpha_n = \langle f \mid T_n \rangle$. Chebyshev polynomials are orthogonal under the scalar product $\langle f \mid g \rangle = \int_{-1}^{1} w(x) f(x)\, g(x)\, dx$ with the weight

$$w(x) = \frac{1}{\pi} \frac{1}{\sqrt{1-x^2}}. \tag{2.27}$$

Keeping in mind the application requiring the scalar product to be used between matrix functions in Hilbert space, the square root needs to be avoided. In the physics literature, it is common to use a

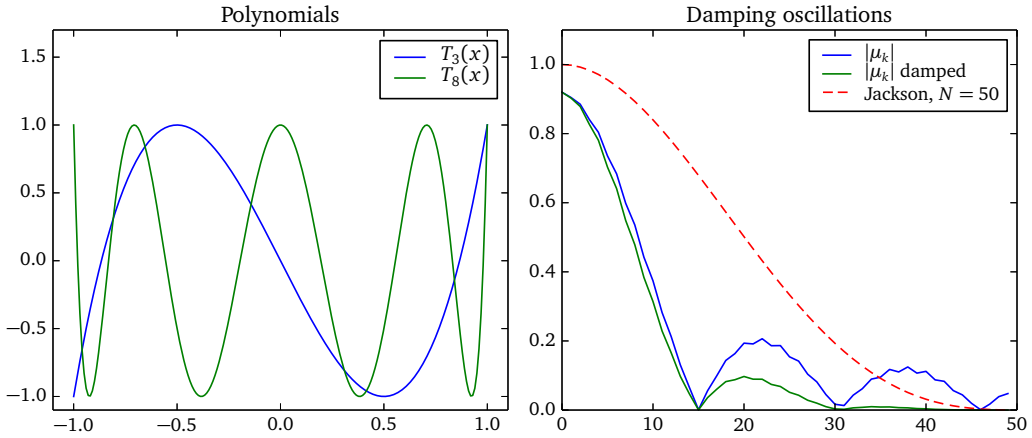

Figure 2.2: (left) Chebyshev polynomials of order 3 and 7. They fill the interval $[-1,1]$ uniformly and provide an excellent basis. (right) Poor convergence for the moments of a discontinuous function, which can lead to aliasing as known from Fourier theory. The situation can be improved by a choice of a kernel (see Eq. 2.54).

different moment expansion than in numerical analysis. Instead of expanding $f(x)$, the approximation of $w(x)f(x) = \pi\sqrt{1-x^2}f(x)$ is sought:

$$f(x) = \frac{1}{\pi}\frac{1}{\sqrt{1-x^2}}\left[\mu_0 + 2\sum_{n=0}\mu_n T_n(x)\right]. \tag{2.28}$$

In this case, the moment defining scalar product simplifies to $\mu_n = \langle f \mid T_n\rangle = \int_{-1}^{1} f(x)\,T_n(x)\,dx$.

Innocuous as it may seem, if $f(x)$ is analytic, then $w(x)f(x)$ is not. This implies that numerical precision can never be achieved with the expansion in the modified momenta Eq. (2.28), since the convergence of spectral methods is dictated by the radius of analyticity[9]. The functions to be approximated depend on the discrete (thus completely discontinuous) spectrum, so poor convergence was already to be expected.

2.3.2 Operator valued expansions

We follow now the physics' literature [WWAF06] to apply the expansions to concrete matrix problems, the most important of which is the approximation of various DOS distributions [SRVK96].

The Hamiltonian needs to rescaled for the spectrum $[E_0, E_{\max}]$ to fit into $(-1,1)$ (notice the excluded end points to avoid overflows), otherwise the previous formulas are meaningless. The spectral bounds are easily found using the Lanczős method, Section 2.1. Using a safety margin of $\alpha = 1\%$, we define

$$a = \frac{E_{\max} - E_0}{2-\alpha}, \quad b = \frac{E_{\max} + E_0}{2}, \tag{2.29}$$

so

$$\bar{H} = \frac{H-b}{a} \text{ fits into } (-1,1). \tag{2.30}$$

The shift factor b centers the spectrum around 0, while a rescales it in the needed range and it is similar in value to the spectral radius ρ_H.

To calculate the matrix elements of a function of the Hamiltonian of the type $\langle L \mid f(H) \mid R\rangle$, the function is expanded in Chebyshev polynomials of the matrix H according to Eq. (2.28)

$$\left\langle L \,\middle|\, f(\bar{H}) \,\middle|\, R\right\rangle = \frac{1}{\pi}\frac{1}{\sqrt{1-x^2}}\sum_{n=0}\mu'_n \left\langle L \,\middle|\, T_n(\bar{H}) \,\middle|\, R\right\rangle \quad \text{by linearity} \tag{2.31}$$

[9] In case of Chebyshev expansions, by the distance of the nonanalyticity to Bernstein's ellipse.

where $\mu'_0 = \mu_0$, $\mu'_n = 2\mu_n$ for brevity. The Chebyshev polynomials in H are generated by the recursion relation (2.25)

$$\begin{aligned} T_0(\bar{H}) &= \mathbb{1} \\ T_1(\bar{H}) &= H \\ T_{m+1}(\bar{H}) &= 2\bar{H}T_m(\bar{H}) - T_{m-1}(\bar{H}). \end{aligned} \tag{2.32}$$

If the recursion is seen as a sequence of SpMV operations on the right-hand side $|R\rangle$, then starting with

$$\begin{aligned} |v_0\rangle &= T_0(\bar{H})|R\rangle = |R\rangle, \\ |v_1\rangle &= T_1(\bar{H})|R\rangle = \bar{H}|v_0\rangle, \\ |v_m+1\rangle &= 2\bar{H}|v_m\rangle - |v_m-1\rangle. \end{aligned} \tag{2.33}$$

To obtain a scalar matrix element:

1. Start the iteration with $|R\rangle$
2. Generate at every step a new vector $|v_{m+1}\rangle$ with one SpMV (expensive)
3. Calculate the scalar product $\langle L \,|\, v_m\rangle$ (cheap)
4. At the end, sum up all scalar products and rescale in Eq. (2.31)

If multiple left-hand side vectors $|L_1\rangle, |L_2\rangle, \ldots$ are present, only additional cheap scalar products are required at step 3. to generate the corresponding moments $\mu_n^{L_1}, \mu_n^{L_2}, \ldots$.

2.3.3 Chebyshev time evolution

If the function to be computed is $f(x) = \mathrm{e}^{-ixt}$, the coefficients for the original expansion Eq. (2.26) can be calculated analytically

$$\alpha_m(t) = \int_{-1}^{1} \frac{T_m(x)\,\mathrm{e}^{-ixt}}{\pi\sqrt{1-x^2}}\,dx = (-i)^m J_m(t), \tag{2.34}$$

where $J_m(t)$ denotes the Bessel function of order m. The coefficients decay exponentially for $m \geq m_0 = 1.5t$, leading to extremely fast convergence.
Expanding $|\psi(t)\rangle = \mathrm{e}^{-i\bar{H}t}\,|\psi(0)\rangle$ with the recursion defined in Eq. 2.32, starting with $|v_0\rangle = |\psi(0)\rangle$

$$|\psi(t)\rangle = \mathrm{e}^{-i\bar{H}t}\,|\psi(0)\rangle = \sum_{m=0} \alpha'_m\, T_m(\bar{H})\,|\psi(0)\rangle = |v_0\rangle + 2\sum_{m=1}(-i)^m J_m(t)\,|v_m\rangle \tag{2.35}$$

The Chebyshev expansion has numerous advantages:

- Stable to arbitrary order, i.e. arbitrarily long time t
- Known order of the expansion in advance
- Does not require a second pass, unlike Eq. (2.11), since the coefficients are known already during the iteration. The performance is double!

Using the unnormalized Hamiltonian H for the time evolution requires rescaling time and an additional phase, while the vectors $|v_m\rangle$ still need to be generated using the normalized $\bar{H}$ for stability:

$$\mathrm{e}^{-iHt}\,|\psi(0)\rangle = \mathrm{e}^{-i\bar{H}at+ibt}\,|\psi(0)\rangle = \mathrm{e}^{ibt}\left[|v_0\rangle + 2\sum_{m=1}(-i)^m J_m(at)\,|v_m\rangle\right] \tag{2.36}$$

Note: As mentioned at the end of section 2.2, sometimes it is necessary to evolve the system using a dissipative, non-Hermitian operator. By stretching the analyticity limits, the Chebyshev expansion can work with operators having a slightly complex spectrum without breaking down. If the eigenvalues are located inside the analyticity ellipse having its foci at -1 and 1, imaginary values are small compared to the spectral radius and the expansion Eq. (2.32) is (precariously) stable and used in the literature [Maz10, ZKAHD07], whereas Krylov based methods [Gut92] lose in popularity.

2.3.4 Density of States

The DOS is a scalar function of the energy, defined as

$$\rho(E) = \langle\, \delta(H-E)\,\rangle_{T=\infty} = \frac{1}{N}\sum_{k=1}^{N}\delta(E-E_k). \tag{2.37}$$

By sampling its moments μ_n it can be reconstructed to arbitrary precision. The truncation to a finite number of moments corresponds to a smoothing of the distribution, which is a necessary step to obtain results meaningful in the thermodynamic limit [HWM+11]. By necessity, the sampling procedure acquires the moments of $\bar{\rho}(\bar{E})$, the distribution function in the rescaled energy range $[-1,1]$, which can be later converted to the proper $\rho(E)$. The moments are defined by the scalar product

$$\begin{aligned}\mu_n &= \int_{-1}^{1}\bar{\rho}(\bar{E})T_n\left(\bar{E}\right)dx = \frac{1}{N}\sum_{k=1}^{N}T_n(\bar{E}_k)\\ &= \frac{1}{N}\sum_{k=1}^{N}\left\langle k\,\middle|\,T_n(\bar{H})\,\middle|\,k\right\rangle = \frac{1}{N}\operatorname{Tr}\left(T_n(\bar{H})\right).\end{aligned} \tag{2.38}$$

The central insight of the matrix valued expansion theory is evident: the interplay between functions defined on the spectrum and their operator valued version. Sampling a function turns into an expansion corresponding to Eq. (2.32).

The trace in Eq. (2.38) needs to be evaluated for the moments to be available. This is possible by performing a *stochastic trace sampling*. The trace of an arbitrary operator A can be approximated via Monte Carlo sampling, using a sequence of R random vectors $|r\rangle$

$$\operatorname{Tr}[A] = \frac{1}{N}\sum_{k=1}^{N}\langle k\,|A|\,k\rangle \approx \frac{1}{R}\sum_{r=1}^{R}\langle r\,|A|\,r\rangle\,. \tag{2.39}$$

Converge is typical of Monte Carlo methods, where the error decreases as $O(R^{-1/2})$ when the number of random vectors is increased. The dimensionality N of the Hilbert space also dramatically influences the converge, since for *typical systems* (see Section 3.1.2) the error scales as $O\left(N^{-1}R^{-1/2}\right)$, i.e. geometrically in the number of sites L of the system, since N is usually exponential in the volume.
To sample stochastically the moments:

1. Generate a normal vector $|r\rangle$ with random zero-mean entries
2. Run the recursion in Eq. (2.32) with $|v_0\rangle = |r\rangle$, saving the moments μ_n
3. Average the moments μ_n over R different starting vectors

2.3.5 Thermal expectation values

Scalar expectation values of the Hamiltonian are easily computed if the DOS is available, via

$$\langle H\rangle = \frac{1}{Z}\operatorname{Tr}\left[H\,\mathrm{e}^{-\beta H}\right] = \frac{1}{Z}\int_{E_0}^{E_{\max}} E\,\rho(E)\,\mathrm{e}^{-\beta E}\,dE = \frac{1}{Z}\int_{-1}^{1}(a\bar{E}+b)\,\bar{\rho}(\bar{E})\,\mathrm{e}^{-\beta(a\bar{E}+b)}\,d\bar{E} \tag{2.40}$$

$$Z = \operatorname{Tr}\left[\mathrm{e}^{-\beta H}\right] = \int_{E_0}^{E_{\max}} \rho(E)\,\mathrm{e}^{-\beta E}\,dE \quad = \quad \int_{-1}^{1}\bar{\rho}(\bar{E})\,\mathrm{e}^{-\beta(a\bar{E}+b)}\,d\bar{E}. \tag{2.41}$$

It is easier to use the reconstructed rescaled density $\bar{\rho}(\bar{E})$, which requires scaling also the exponential factors. Function averages such as $\langle f(H)\rangle$ can be obtained by substituting $f(a\bar{E}+b)$ in Eq. (2.40).

What about the expectation values of other functions? What is the average of the observable A at inverse temperature β? It is the average of the expectation value of $A(E)$, the density of A at average energy E, divided by Z obtained from Eq. (2.41)[10],

$$\begin{aligned}\langle A\rangle = \frac{1}{Z}\operatorname{Tr}\left[A\mathrm{e}^{-\beta H}\right] = \frac{1}{Z}\sum_k \langle k\,|A|\,k\rangle\,\mathrm{e}^{-\beta E_k} &= \frac{1}{Z}\int_{E_0}^{E_{\max}}\left(\sum_k \langle k\,|A|\,k\rangle\;\delta(E-E_k)\right)\mathrm{e}^{-\beta H}\,dE \\ &= \frac{1}{Z}\int_{E_0}^{E_{\max}} a(E)\,\mathrm{e}^{-\beta H}\,dE\end{aligned} \tag{2.42}$$

where the density of an operator at finite energy

$$a(E) = \left(\sum_k \langle k\,|A|\,k\rangle\;\delta(E-E_k)\right) \tag{2.43}$$

can be sampled via its moments

$$\mu_n^A = \operatorname{Tr}\left[A\,T_n(H)\right] \tag{2.44}$$

using the random sampling of the trace together with Eq. (2.31), where $|L\rangle = A|r\rangle$ and $|R\rangle = |r\rangle$

$$\mu_n^A = \operatorname{Tr}\left[A\,T_n(H)\right] = \frac{1}{R}\sum_{r=1}^{R}\langle r|A\,T_n(H)|r\rangle. \tag{2.45}$$

Computing M moments using R random vectors requires $O(M\,R)$ sparse SpMV, plus additional scalar products if more left hand sides (for expansions of the density of multiple operators $A_1, A_2, \ldots$) are needed.

Often the average value of a function at a certain energy is sought, since $a(E)$ equals the *micro-canonical expectation value*. The expansion (2.45) provides a means for the approximation, if certain conditions are met. Consider the $a(E)$ as a set of random variables indexed by the energy. The scaling of the point-wise variance of $a(E)$, as a function of M and R, provides a quantitative condition: if $a(E)$ uniformly approaches a well defined distribution in the thermodynamic limit, the system satisfies the ETH (Eigenvalue Thermalization Hypothesis) [SKN+14, SHP13]. The density $\rho(E)\,\delta E$ on the other hand provides a rough count of the eigenvalues in an interval $(E, E+\delta E)$ [DPS13]. Even if (point-wise) variance of $a(E)$ does not reach zero in the thermodynamical limit, the distribution for a *finite matrix* can be approximated if the number of steps M and random vectors R are taken high enough.

The thermodynamical meaning of the normalization Z is connected to the count of states, since the available phase space (or rather Hilbert space, in this case) grows as the result of heating. The *thermodynamical free energy* F is just

$$F_\beta = -\beta^{-1}\log Z_\beta, \tag{2.46}$$

[10] Z is also an average quantity defined over the density of energy states

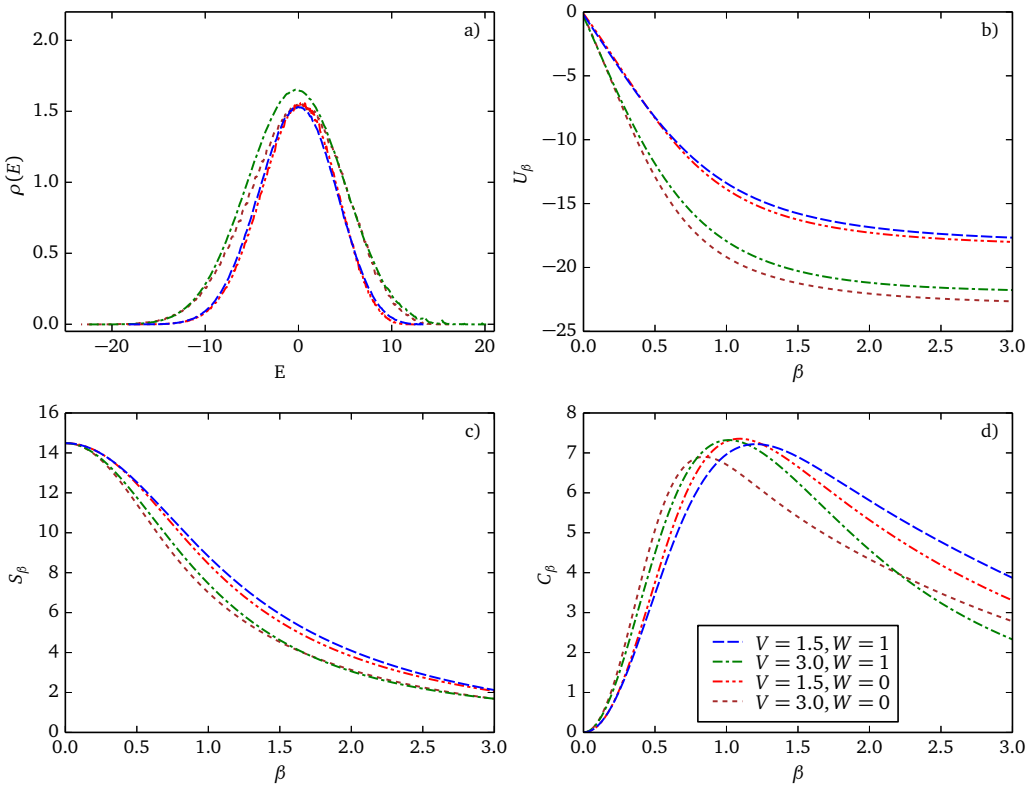

Figure 2.3: Thermal expectation values, for 4 different parameter sets of the $t-V-W$ model with (L=24, N=10, $\dim \mathscr{H} \approx 2 \cdot 10^6$), obtained using only the thermal expectation values based on the density of states of the energy $\rho(E)$. (a) DOS appearing smooth at this resolution, (b) average internal energy as a function of β (c) thermodynamic entropy (d) heat capacity at constant volume. The energy in panel (b) is seen converging to the different ground state energies of the systems.

which allows easy calculation of the *thermodynamical entropy* S_β using the internal energy $U_\beta = \langle H \rangle_\beta$,

$$S_\beta = \beta[U_\beta - F_\beta]. \tag{2.47}$$

Another important function is the *thermal capacity* C_v[11], proportional to the variance of the energy

$$C_\beta = \beta^2 \left(\langle H^2 \rangle_\beta - \langle H \rangle_\beta^2 \right). \tag{2.48}$$

The DOS of the Hamiltonian, the internal energy and the last two thermodynamical functions, are plotted in Fig. 2.3. For the thermodynamical entropy to be consistent with the third law of thermodynamics, the normalization constant Z_β for $\beta = 0$ must be normalized to $Z_{\beta=0} = \dim \mathscr{H}$, so in the trivial limit of infinite temperature we can set the entropy explicitly

$$S_{\beta=0} = \log Z_{\beta=0} = \ln(\dim \mathscr{H}), \tag{2.49}$$

which on the other hand is equivalent to supplying an absolute scale for the entropy, $S(T=0) = 0$. The DOS in the figure has been obtained by sampling $M = 1000$ Chebyshev moments, averaged $R = 10$ times; it appears nearly smooth, due to the fact that the resolution (see Eq. (2.55) below) is three orders of magnitude too small to resolve the individual states. The difference between integrable ($W = 0$) and nonintegrable ($W = 1$) systems is negligible in the average values of the DOS and observables, affecting

[11] At constant volume

mostly the point-wise variance (not shown in the figure). The most visible differences here are due to the difference in the energy between weaker ($V = 1.5$) and stronger ($V = 3$) interactions.

2.3.6 Reconstruction from the moments

For the scheme to be useful, the reconstruction of all aforementioned functions must be possible from a limited number of moments. The partial sum

$$f_M(x) = \frac{1}{\pi\sqrt{1-x^2}}\left[\sum_{n=0}^{M} \mu_n' T_n(x)\right], \tag{2.50}$$

converges uniformly

$$\lim_{M\to\infty} |f(x) - f_M(x)| \to 0 \qquad \forall x \in [-1,1] \tag{2.51}$$

if a *smoothing kernel* is properly chosen. The choice of a good kernel is necessary in order to avoid the Gibbs phenomenon, unwanted and unavoidable (even for $M \to \infty$ limit) finite oscillations in $f_M(x)$ if $f(x)$ is not continuous. All densities sampled (equations 2.37 and 2.43) fall into this category. Discontinuous functions have weakly decaying moments, $|\mu_n| = O(1/n)$ or worse, so a finite density of

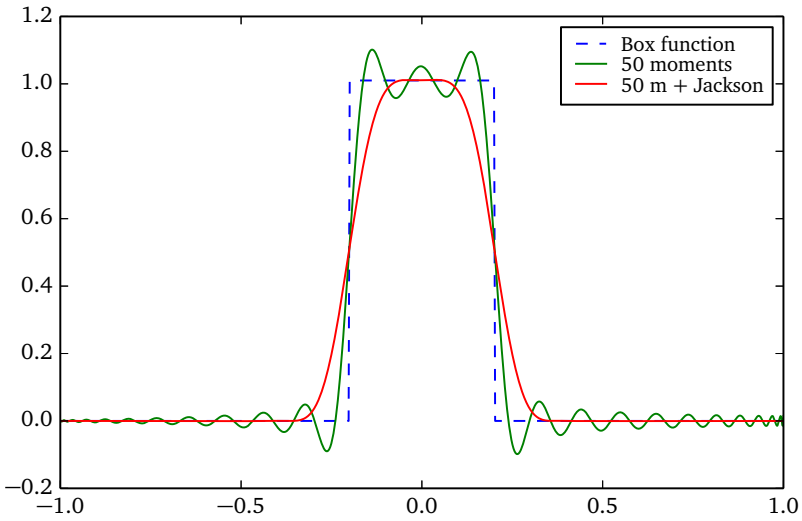

Figure 2.4: The effects of choosing a good smoothing kernel. The original discontinuous box function (dashed blue line) is approximated by a truncated expansion with 50 moments (equivalent to equation (2.50)), showing wild Gibbs oscillations and lack of positivity. Once smoothened by the Jackson kernel (2.54) (red line), the reconstructed function is completely positive, does not oscillate and retains optimal resolution, measured by the maximum distance on the x-axis from the step.

moments is always left when truncating the series to M. A complete truncation in momentum space corresponds to the multiplication with the box function $1-\theta(x-n)$. In real space, this is a convolution with the rapidly oscillating, non-positive sinc function. The result is uncontrolled oscillations which can lead to the reconstructed distribution being nonpositive, which is extremely detrimental to numerical averages. The solution is provided by [WWAF06], defining the optimal Jackson kernel, a function similar to a Gaussian smoothing kernel but defined over finite support M:

$$g_n^J = \frac{(M-n+1)\cos\frac{\pi n}{M+1} + \sin\frac{\pi n}{M+1}\cot\frac{\pi}{M+1}}{M+1}. \tag{2.52}$$

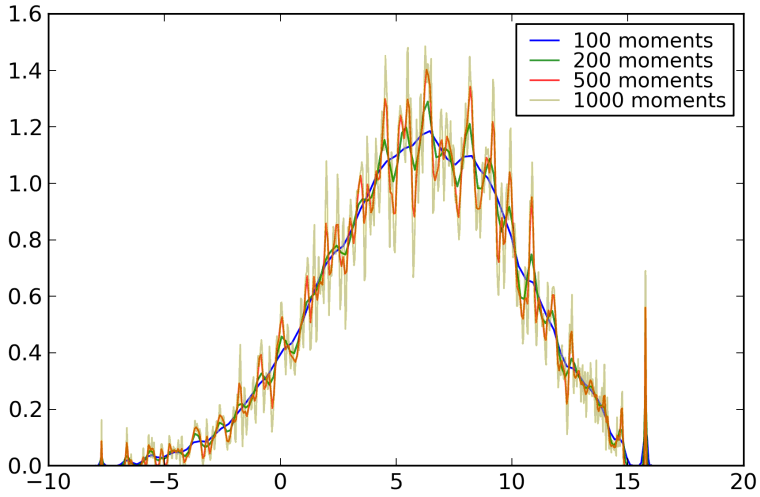

Figure 2.5: The resolution for a typical reconstructed density of states $\rho(E)$ dramatically increases with the number of moments sampled. The Hamiltonian is that of the $t-V-W$ model, with $L=12$ and a total number of states $N=8008$.

The Jackson-smoothed moments $\mu_n \longrightarrow \mu_n^J = g_n^J \mu_n$ lead to uniform converge of f_M^J.

The reconstruction of $f(x)$ proceeds using the regularized moments μ^J, summing the functions $T_n(x)$ obtained recursively from Eq. (2.25). The function $f_M(x)$ is best reconstructed from M available moments, if computed at the points

$$x_k = \cos\frac{\pi + 1/2}{M+1} \qquad \text{for } k \in \{1,2,\ldots,M\}, \tag{2.53}$$

which are the roots of $T_M(x)$ [MH03], or Chebyshev points of the first type[12]. Their advantage is they avoid the points $\{1,-1\}$, poles of Eq. (2.50). Using the functions reconstructed at $f(x_k)$, the integrals become also exact for Chebyshev polynomials (Gauss-Lobatto formulas), so the functional evaluations in equations (2.40)-(2.42) have the least error. The precise sum with all the normalization factors is

$$\int_{E_0}^{E_{\max}} E\,\rho(E)\,\mathrm{e}^{-\beta E}\,dE \mapsto \frac{1}{\pi M}\sum_{x_k}(ax_k+b)\,\rho(x_k)\,\mathrm{e}^{-\beta(ax_k+b)}. \tag{2.54}$$

The density function reconstructed this way has an integral rigorously equal 1.0 and is always positive, which does not happen if a proper kernel is not chosen.
The high order Jackson kernel guarantees a relative resolution

$$\sigma_{\text{rel}} = \frac{\pi}{M} \tag{2.55}$$

steadily improving with the order of the expansion. Whereas a bare series can attain perfect resolution if the function is completely interpolated in M moments, the use of a kernel smooths the partial series, leading to loss of resolution but providing a safety net against worst behavior, an indispensable trade-off if the expansion has to be truncated.

The maximum precision is limited by the notoriously poor Monte Carlo convergence in the number of samples R. Together with the impossible convergence of the moments of $a(E)$ or $\rho(E)$, the maximum precision is very far away from the machine limit, and about 1% in our calculations.

[12]The choice made in numerical analysis are points of the first type, which are the extrema

2.3.7 Zero temperature spectral functions

Briefly mentioned in subsection 2.1.3, the zero temperature spectral functions of an operator A are a staple of condensed matter theory, deserving another cursory mention here, for sake of comparison. They are defined as

$$A(\omega) = -\mathrm{Im}\left\langle 0 \left| A \frac{1}{\omega + i0^+ - (H - E_0)} A \right| 0 \right\rangle = \left\langle 0 \left| A \left(\sum_n \delta(\omega - E_n - E_0) \right) A \right| 0 \right\rangle \tag{2.56}$$

Following a similar derivation to Eq. (2.42), the spectral function $A(\omega)$ can be expanded after a rescaling $\omega \to \bar{\omega}$, into a series of the type Eq. (2.28). The moments are simply as

$$\mu_n = \left\langle 0 \left| A\, T_n(\bar{H}) A \right| 0 \right\rangle = \left\langle \psi_A \left| T_n(\bar{H}) \right| \psi_A \right\rangle, \tag{2.57}$$

where the recursion starts with $|v_1\rangle = |\psi_A\rangle$ and does not require a stochastic trace, giving it accuracy down to the resolution π/M. The guaranteed converge and speed are the reason for its wild popularity [AF08, BS14, HWM$^+$11, WMPS14], to mention a few.

Lanczős based methods however outperform this type of expansion for a pure state, and a generalization (with applications) by the author will be now presented.

2.4 Numerical Equilibrium Linear Response

In this section we present *previously unpublished* numerical methods employed to calculate the finite-temperature conductivity $\sigma^N(\omega)$ for the particle current J^N, or the transport coefficient $\sigma^E(\omega)$ for the operator J^E when the system is driven by an electric field. The conductivity of a system is defined by its linear response, which was briefly reviewed in Section 1.3.

The most expedite way to calculate the conductivities in the system under consideration, is to use the LR formalism introduced in Section 1.3.1, but formulated in a pure state instead of the canonical ensemble. The equilibrium microcanonical state is analyzed detail in Section 3.2.4, and it is used as a starting point for the TDSE but provides numerous advantages also for this kind of calculation.

The regular part of the (generalized) conductivity is related via Eq. (1.60) to the imaginary part of the retarded Green function $\mathrm{Im}\,\chi_{AB}(\omega)$ between two operators $A \equiv J^N$, and $B \equiv J^N$ or J^E. The spectral Green function is related to the correlator $C^{>}_{AB}(\omega)$ via Eq. (1.68), and the latter will be calculated using Lanczős expansions for a function of the Hamiltonian, introduced in Section 2.1.2. We distinguish two cases:

- Diagonal Green function: when $A = B = J^N$, it serves to calculate the optical conductivity $\sigma^N(\omega)$, for which efficient expansions were developed already in the 1970.
- Offdiagonal Green function: they are needed to calculate the ratio j^E/j^N, which depends on $\sigma^E(\omega)$. We develop the method to treat efficiently the case with arbitrary operators $A \neq B$, using the microcanonical ensemble.

2.4.1 Correlation functions in the microcanonical ensemble

The microcanonical state $|\psi_E\rangle$ corresponding to the temperature β satisfies the approximate eigenvalue equation $H|\psi_E\rangle = \bar{E}|\psi_E\rangle$, where $\bar{E} = \langle H \rangle_\beta$. The time-evolved state $|\psi_E(t)\rangle = \mathrm{e}^{-iHt}|\psi_E\rangle$ is an

excellent approximation to the time-evolved thermal state initially prepared at the temperature β, as shown in Chapter 3. Moreover, the definition of the microcanonical state allows the great simplification

$$\mathrm{e}^{-iHt}\,|\psi_E\rangle = \mathrm{e}^{-iEt}\,|\psi_E\rangle. \tag{2.58}$$

The correlation function in a pure state ensemble is a scalar product between two time-evolved states, acted on by the observable and perturbation in a different order

$$C^{>}(t) = -i\,\langle B_I(t)A(0)\rangle = -i\left\langle \psi_E \,\middle|\, \mathrm{e}^{iHt}\,B^\dagger\,\mathrm{e}^{-iHt}\,A \,\middle|\, \psi_E\right\rangle = -i\left\langle B\,\mathrm{e}^{-iHt}\,\psi_E \,\middle|\, \mathrm{e}^{-iHt}\,A\psi_E\right\rangle. \tag{2.59}$$

The expression can be simplified using Eq. (2.58)

$$\begin{aligned} C^{>}(t) &= -i\left\langle B\,\mathrm{e}^{-iHt}\,\psi_E \,\middle|\, \mathrm{e}^{-iHt}\,A\psi_E\right\rangle && (2.60)\\ &= -i\,\mathrm{e}^{iEt}\left\langle B\,\psi_E \,\middle|\, \mathrm{e}^{-iHt}\,A\psi_E\right\rangle \\ &= -i\left\langle \psi_E \,\middle|\, B^\dagger\,\mathrm{e}^{i(E-H)\,t}\,A\,\middle|\, \psi_E\right\rangle, && (2.61)\end{aligned}$$

with the time appearing only *once*, as opposed to twice as in Eq. (3.42). The Fourier transform is

$$C(\omega^+) = \int_0^\infty dt\;\mathrm{e}^{i\omega^+ t}\,C(t) = \left\langle \psi_E \,\middle|\, B^\dagger \frac{1}{\omega^+ + E - H} A\,\middle|\, \psi_E\right\rangle, \tag{2.62}$$

where $\omega^+ = \omega + i\eta, \eta > 0$. This is formally identical to the value of the correlator at zero temperature, with the ground state substituted by the microcanonical finite-temperature state.

The traditional solution, due to Haydock [HHK72, HHK75] and nicely summarized in Ref. [Dag94], used exclusively throughout the literature [JP00], is to expand the diagonal elements of the correlator $C(\omega) = \left\langle \psi_E \,\middle|\, A(\omega^+ + E - H)^{-1} A\,\middle|\, \psi_E\right\rangle$ in the Krylov basis, requiring that $B = A = A^\dagger$, limiting the scope of the approximation. The value $C(\omega)$ is interpreted as the first component of the solution of a linear system. By rewriting $|\phi_A\rangle = A|\psi_E\rangle$, it is found that $C(\omega) = \left\langle \phi_A \,\middle|\, (\omega^+ + E - H)^{-1}\phi_A\right\rangle$. If the Lanczős recursion with M steps for the function $f(H) = (\omega^+ + E - H)^{-1}$ is started from the vector $|v_1\rangle = |\phi_A\rangle / \sqrt{\langle \phi_A \,|\, \phi_A\rangle}$. Inserting the approximate projection into the Krylov space $V^\dagger V$, one obtains according to the methods and notation outlined in Section 2.1.2

$$C(\omega) \approx \|\phi_A\|^2 \left\langle v_1 \,\middle|\, V^\dagger V f(H) V^\dagger V\,\middle|\, v_1\right\rangle = \|\phi_A\|^2\,\langle \mathrm{e}_1 \,|\, f(T) \,|\, \mathrm{e}_1\rangle = \|\phi_A\|^2 (\omega^+ + E - T)^{-1}_{1,1}, \tag{2.63}$$

where $T = V\,H\,V^\dagger$ is the tridiagonal $M \times M$ matrix corresponding to the projected Hamiltonian in the Krylov space V, and only the first element of the resolvent of T is needed, since $V|v_1\rangle = |\,\mathrm{e}_1\rangle$ which is the first basis vector. This scalar quantity is then computed as a continued fraction in the Lanczős expansion coefficients a_n and b_n obtained from the matrix Eq. (2.4). While not without advantages, such as the possibility to extrapolate the expansion beyond M terms, the resolution provided is limited, being equivalent to the expansion in Lorentzians, mentioned below.

2.4.2 Novel off-diagonal method

The difficulty in obtaining the *off-diagonal matrix elements* of the correlation function such as Eq. (2.62), is that the right-hand and left-hand state are different in

$$C^{>}(t) = -i\left\langle \psi_E \,\middle|\, B^\dagger\,\mathrm{e}^{i(E-H)\,t}\,A\,\middle|\, \psi_E\right\rangle = -i\left\langle \phi_B \,\middle|\, \mathrm{e}^{i(E-H)t}\,\middle|\, \phi_A\right\rangle, \tag{2.64}$$

with $|\phi_A\rangle = A|\psi_E\rangle$ and $|\phi_B\rangle = B|\psi_E\rangle$, whereas the Lanczős expansion of $\mathrm{e}^{i(E-H)t}$ works best if the final and initial state are the same. Nonetheless, departing completely from the resolvent-based approach, we

use *spectral representation*, expanding the exponential using the approximate eigenvalues ϵ_n and eigenstates $|U_n\rangle$ of the Hamiltonian, from an M step Lanczős expansion from the state $|v_1\rangle = \phi_A/\sqrt{\langle\phi_A|\phi_A\rangle}$. *Reminder:* The approximate eigenvalues and states are obtained by Eq. (2.5)

$$H \approx V\,T\,V^\dagger = V\,X\,D\,X^\dagger\,V^\dagger = (V\,X)\,D\,(V\,X)^\dagger = UDU^\dagger. \tag{2.65}$$

The approximate eigenvalues ϵ_n are the elements of the diagonal matrix D

$$\epsilon_n = D_{n,n}, \tag{2.66}$$

whereas the corresponding approximate eigenstates $|U_n\rangle$ are the columns of the matrix U

$$|U_n\rangle = V\,X_n = \sum_k V_k X_{k,n} = \sum_k X_{k,n}|v_k\rangle, \tag{2.67}$$

which is a sum over all Krylov vectors $|v_k\rangle$ with the coefficients $X_{k,n}$.

This is equivalent to substituting $e^{i(E-H)t} \approx V^\dagger\, e^{i(E-H)t}\, V = \sum_n |U_n\rangle\langle U_n|\, e^{i(E-\epsilon_n)t}$ in (2.64):

$$C^>(t) = -i\sum_{j=0}^{M}\langle\phi_B|U_n\rangle\, e^{-i(\epsilon_n-E)t}\,\langle U_n|\phi_A\rangle\,. \tag{2.68}$$

The Fourier space version $C(\omega^+)$ is just the transform of the approximation (2.68)

$$\begin{aligned} C(\omega^+) &= \left\langle \psi_E \left| B^\dagger \frac{1}{\omega^+ + E - H} A \right| \psi_E \right\rangle \\ &= \sum_{n=1}^{M}\langle\phi_B|U_n\rangle \frac{1}{\omega^+ + E - \epsilon_n}\langle U_n|\phi_A\rangle \\ &= \sum_{n=1}^{M}\overline{\langle U_n|\phi_B\rangle}\,\langle U_n|\phi_A\rangle \frac{1}{\omega^+ + E - \epsilon_n} \end{aligned} \tag{2.69}$$

for any desired frequency ω^+.

The only nontrivial quantity to calculate is one of the vectors of scalar products. Without loss of generality, let us choose $\langle\phi_B|U_n\rangle$ with $B \neq A$ as the nontrivial case, matching the interesting case of $B = J^E$ and $A = J^N$. The other scalar products $\langle U_n|\phi_A\rangle$ are already known in the literature, since

$$\langle U_n|\phi_A\rangle = \|\phi_A\|\,\langle VX_n|v_1\rangle = \|\phi_A\|\,\langle X_n|e_1\rangle = \|\phi_A\|\,X_{1,n}, \tag{2.70}$$

the scalar products are just the rescaled components of the eigenvectors in Krylov space. The other scalar products do not benefit from this trick, since $|\phi_B\rangle$ does not correspond to a vector of the Krylov basis, and would require the construction of all the Hilbert space vectors $|U_n\rangle$, in turn requiring access to the matrix V row-wise. Since the columns are generated on-the-fly, the matrix would be needed in its entirety to perform the scalar products. But V is useless to store for $M = 1000$ and a Hilbert space dimension of $D = 10^7$, since it would require accessing

$$16MD \text{ bytes} = 1.6\cdot 10^{11} \text{ bytes} = 149 \text{ GB of hard-drive space} \tag{2.71}$$

in the wrong order, i.e. without the chance to cache any result in memory.

Many solutions have been proposed, from using double Lanczős expansions[13], limiting each to about $M \sim 100$, or to use the less stable and accurate biorthogonal expansion [CBPS13][14]. Let us now

[13] One on each side of $|\phi\rangle$

[14] Private communication at a conference

show the optimal solution, which can be used also for ground-state Green function, and allows the simultaneous computation of as many different observables (represented by different $\langle \phi_{B1}|, \langle \phi_{B2}|, \ldots$) on the left-hand side of the correlator as needed at negligible cost.

The approximate eigenvectors can be seen as either $|U_n\rangle$ in $\mathscr{H}$ (Hilbert space), or as X_n in K (Krylov space), connected by the linear projections

$$H \underset{V}{\overset{V^\dagger}{\rightleftharpoons}} K, \tag{2.72}$$

meaning that a vector could be converted either way

$$|\phi\rangle_{\mathscr{H}} \mapsto |\phi\rangle_K = V^\dagger |\phi\rangle_{\mathscr{H}} \quad \text{and} \quad |\phi\rangle_K \mapsto |\phi\rangle_{\mathscr{H}} = V|\phi\rangle_K, \tag{2.73}$$

so the scalar products can be computed in either space

$${}_{\mathscr{H}}\langle U_n \,|\, \phi_B\rangle_{\mathscr{H}} = {}_{\mathscr{H}}\langle VX_n \,|\, \phi_B\rangle_{\mathscr{H}} = {}_K\left\langle X_n \,|\, V^\dagger \phi_B\right\rangle_K. \tag{2.74}$$

The vectors in K are entities described by M scalars, as opposed to the $D \gg M$ entries in the full Hilbert space. Whereas it is inconvenient to up-project X_n into the Hilbert space, it is straightforward to project any vector into Krylov space and perform the scalar product in the dimensionally-reduced space. It is simple to perform the projection on-the-fly, while generating the Krylov space vectors $|v_k\rangle$: the n-th component $(|\phi_B\rangle_K)_n = \langle v_n \,|\, \phi_B\rangle_{\mathscr{H}}$ demands a relatively cheap scalar product operator.

Summary To compute the generic correlation function between two current operators J^N and J^E:

1. Start the Lanczős procedure on $|\phi_A\rangle = J^N|\psi_E\rangle$, on the microcanonical state with energy E
2. Generate the orthonormal vectors $|v_k\rangle$
3. Tabulate the M-dimensional projected vectors $V^\dagger|\phi_A\rangle = \sqrt{\langle \phi_A \,|\, \phi_A\rangle}|\mathrm{e}_1\rangle$ and $V^\dagger|\phi_B\rangle_{\mathscr{H}} = |\phi_B\rangle_K$
4. Diagonalize T
5. Obtain the eigenvalues ϵ_n from the matrix D and the eigenvalues $|U_n\rangle$ from the columns of X
6. The scalar products $\langle U_n \,|\, \phi\rangle$ are just the components of the matrix-vector product in Krylov space
$$\langle U_n \,|\, \phi\rangle = (X^\dagger|\phi\rangle_K)_n \tag{2.75}$$
7. Save the M eigenvalues ϵ_j and $2M$ scalar products $\langle U_n \,|\, \phi\rangle$
8. Calculate Eq. (2.69)

So far the formalism has been quite general, not limited to the real or imaginary part of $C(\omega^+)$, which is another shortcoming of the resolvent approach. However, only the imaginary part of the correlation function is needed for the real conductivity in Eq. (1.60). Using again Plemelj's identity,

$$\operatorname{Im} C(\omega) = \sum_{n=1}^{M} \overline{\left\langle U_j \,|\, \phi_B\right\rangle} \left\langle U_j \,|\, \phi_A\right\rangle \delta(\omega^+ + E - \epsilon_j). \tag{2.76}$$

The sum of weighted delta peaks is unphysical, since the function must be continuous in ω in the thermodynamic limit. The delta functions must be smoothened to leave only frequencies which do not resolve the individual energy states [JF07, BSW09, PWA09, BSS12]. The prescription given in Eq. (2.55),

$\sigma_{\rm rel} = \pi/M$ is reasonable also in this case, simultaneously defining the resolution for the smoothened delta functions and an upper limit on $M \sim 1000$.

Traditionally, the Lorentzian smoothening $\delta(\omega - E) \longrightarrow \frac{\eta}{(\omega-E)^2+\eta^2}$ with a small $\eta > 0$ is taken for granted, being equivalent to taking the imaginary part of Eq. (2.69), and it is the basis for the resolvent expansion of Haydock. However, there is freedom to choose any other representation of the delta function. The choice

$$\delta(\omega - E) \longrightarrow \frac{1}{\sigma\sqrt{2\pi}} \exp\left(\frac{(\omega-E)^2}{2\sigma^2}\right) \tag{2.77}$$

leads to a significantly improved resolution, without the power-law tails of the Lorentzian. The Chebyshev-based methods are often touted as having an exponentially better resolution, but the advantage is completely leveled with the prescription in Eq. (2.77). The Lorentzian smoothing however has important additional analytical properties, not required here. If only the imaginary part is needed, the prescription above together with a sufficiently large $\sigma = E_{\max}\pi/M$ leads to an overall improved correlator resolution.

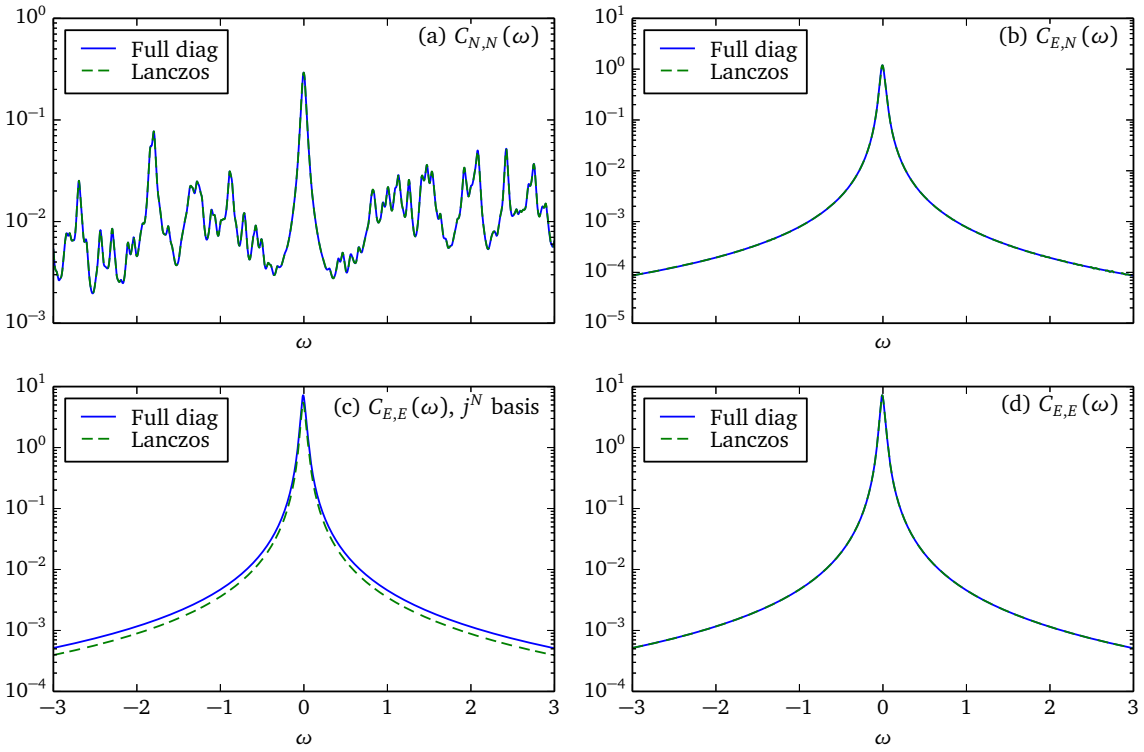

Figure 2.6: Correlation functions (2.62) in the spectral representation, calculated on the same state $|\psi_E\rangle$, with two methods for the resolvent: exact diagonalization of the Hamiltonian and Lanczős based expansion (2.79) with few moments $M/D = 0.01$ and Lorentzian smoothing. The system is integrable, with $V = 1.5$ and $W = 0.0$, of very small size $L = 16, N = 7, D = 11440$ to allow the diagonalization of the Hamiltonian. Due to integrability, all the correlators involving J^E are delta shaped: it requires perfect cancellation of all spurious peaks, which is achieved well by the Lanczős expansion. (a) Correlator contributing to the electrical conductivity, starting the Lanczős expansion with $J^N|\psi_E\rangle$ (b) Mixed correlator, used in the calculation of the Peltier coefficient, started with $J^N|\psi_E\rangle$ (c) Thermal conductivity correlator, using the scalar products $\langle U_n \,|\, \phi_E\rangle$ obtained from an improper starting vector $J^N|\psi_E\rangle$: with minimal 1% loss of precision due to the improper basis (d) Thermal conductivity in the proper basis starting with $J^E|\psi_E\rangle$

We are now able to quote the final form for the regular real conductivity, for both the J^E and J^N

observables:

$$\sigma_{\text{reg}}^{N(E)}(\omega) = L\frac{1-\mathrm{e}^{-\beta\omega}}{\omega}\ \mathrm{Im}\, C^{>}_{N(E)}(\omega), \tag{2.78}$$

$$\mathrm{Im}\, C^{>}_{N(E)}(\omega) = \sum_{n=1}^{M} \overline{\left\langle U_j \,|\, J^{N(E)}\, \psi_E \right\rangle} \left\langle U_j \,|\, J^N\, \phi_E \right\rangle (\sigma\sqrt{2\pi})^{-1} \exp\left[(\omega - E)^2/(2\sigma^2)\right] \tag{2.79}$$

2.4.3 Validity

The quality of the approximation still needs to be discussed. We have made explicit the connection between the real time (2.68) and spectral (2.79) version. They would be completely equivalent, if the correlator were to be extrapolated to infinite real time before taking the Fourier transform, and the Lorentzian smoothing[15] was used in (2.69). If the time evolution is discrete and time-limited up to a maximum time T, the signal $C(t)$ needs to be windowed properly [SS11] for the Fast Fourier Transform to give meaningful results, unless T is so big that $C(t > T) \approx 0$. The alternative is Linear Extrapolation [RGSB08, BHVC09, MWH$^+$10a, BSW09], where the series $C(t)$ is nonlinearly fitted with a sum of decaying complex exponentials, so the components of $C(\omega_n)$ can be extracted more precisely than allowed by a linear FFT with windowing.[16].

The spectral version (2.79) is equivalent to a perfect analytical extrapolation of the time signal, without any artifact, and can have much higher resolution thanks to the Gaussian, as opposed to Lorentzian, smoothing. Thus it is at least *as reliable as the microcanonical approximation* used for the initial value $C(0) = \left\langle \psi_E \left| J^{N(E)} J^N \right| \psi_E \right\rangle$, since the Krylov time propagation procedure is numerically exact.

[15] Corresponding to adding a regularizing factor $\mathrm{e}^{-\eta t}$ in Eq. (2.68)

[16] The "missing" information is provided by smoothness and analyticity assumptions built-in in the extrapolation

Chapter 3

Pure state thermodynamics

In this chapter the theoretical basis for efficient high-temperature quantum computations is introduced, showing how pure states are sufficient for a numerically accurate description of arbitrary observables, in equilibrium and during time evolution.

Many–body quantum mechanics is fraught with an exponential amount of parameters needed for a complete description. Dirac in 1929 prophesied that since the equations are impossible to solve exactly in most cases, the effort will be concentrated on better approximate methods. History teaches that macroscopic numbers of degrees of freedom have not made classical physics impossible, just ushered the era of statistical mechanics, in which the accuracy of the prediction scales as the inverse of the dimensionality of the problem.

In this section we deal with generic quantum systems, not restricted to one model in particular, but with examples taken in the Heisenberg model. The number of real parameters needed to describe a pure quantum state is twice the dimensionality of the complex vector space of the wavefunctions. It is the Hilbert space $\mathscr{H}$ of L spins (see Section 1.1.1), which we consider for simplicity as qubits with two degrees of freedom with no additional constraints, with complex dimension $D = \dim \mathscr{H} = 2^L$. Computations on a single server realistically support up to 10^7 real parameters, which limits the available size to $L \simeq 23$. Generic quantum states are represented by density operators ρ on the Hilbert space, needed for the description of mixed states characterized by a (classical) probabilistic superposition of quantum pure states,

$$\rho_{mixed} = \sum_{k=1}^{D} p_k \rho_k = |\psi_k\rangle\langle\psi_k| \tag{3.1}$$

with p_k the probability of each pure state $\rho_k = |\psi_k\rangle\langle\psi_k|$. Such a sum leads to dense, semi-positive definite, normalized Hermitian operators of rank N, with $\dim(\rho) = 4^L - 1$ real parameters. Writing a full thermal state is possible only for $L \simeq 12$, drastically limiting the available system size.

Additional use of symmetries shown in Section 1.1.1, such as restricting the magnetization M_z to take a particular value, the use of invariance under translations or spacial reflections, can bring the number of available sites to $L \simeq 32$ for calculations involving pure states. Is that enough to extract relevant thermodynamical quantities? We show how the question has been answered affirmatively by us in **[MPCP13]** and in the literature listed throughout this section.

First, we overview how non-equilibrium pure quantum systems under the action of *typical Hamiltonians*, for long observation times, can lead to the emergence of thermal equilibrium behavior

[GE15, DKPR15, EFG15], suggesting that pure states can lead to the physics of equilibration.

3.1 Thermalization

The topic of thermalization in closed quantum systems is riddled with paradoxes, perhaps even more than the problem of entropy increase in classical statistical physics. A quantum equilibrium thermal state ρ_β has a *thermodynamical entropy S* equal to von Neumann entropy of its density matrix

$$S[\rho_\beta] = \mathrm{Tr}[\rho_\beta \log \rho_\beta]. \tag{3.2}$$

It should be reminded that the time evolution for a closed quantum system is unitary. For a pure state it is determined by $|\psi_t\rangle = U(0,t)|\psi_0\rangle$ (see Section 2.2), with $U(0,t)$ the unitary propagator from time 0 to t. The density matrix evolves according to

$$\rho_t = U(0,t)\,\rho_0\,U^\dagger(0,t). \tag{3.3}$$

Once a quantum state is prepared, the following happens

1. The *von Neumann entropy* never increases if the evolution is unitary

$$S_t = \mathrm{Tr}[\rho_t \log(\rho_t)] = \mathrm{Tr}[(U\,\rho_0\,U^\dagger)(U\,\log\rho_0\,U^\dagger)] = \mathrm{Tr}[\rho_0 \log \rho_0] = S_0. \tag{3.4}$$

2. Pure states never turn into mixed states.

3. Since the von Neumann entropy is constant, it is thought that the temperature cannot increase in closed systems.

The paradox is immediate: if it were possible to write the Hamiltonian for a pot of water and a stove, initially at a temperature T_0, then no matter what happens the total entropy of the system does not increase, even when the water starts boiling [Gra08]. The solution of the paradox is to note that the entanglement entropy (which is the only quantity measured by the von Neumann entropy) is not equal to a proper thermodynamic entropy, especially in non-equilibrium situations where the latter is altogether not defined. Alternative definitions exist [Pol08, Pol11], and we also define an entropy-like quantity in Chapter 6, in the spirit of Ref. [Deu10, DLS13], namely the *entropy density*.

So how can the thermal behavior emerge from the evolution of a pure quantum system initially *out of equilibrium*? The predictions of classical statistical physics are overwhelmingly confirmed by everyday experience, meaning that many systems behave as possessing a well-defined temperature.

Conditions necessary for a system to reach thermal equilibrium from an initial non-equilibrium state, are at least [LPSW10]:

1. Equilibration: all relevant expectation values must be observed to be almost constant after an initial evolution time

2. Independence of initial state: the microscopical details of the global initial state do not matter in the equilibrium expectation values of local observables, only a few macroscopic parameters emerge, e.g. the energy density (or temperature)

3. Thermalization: the expectation values in the equilibrium state equal the predictions of a thermal ensemble

We shall discuss them after defining the state that exactly describes the long time behavior of quantum systems.

3.1.1 Time-averaged ensemble

Let us prepare a pure quantum state $|\psi_0\rangle$ at time $t = 0$, and evolve it unitarily in time under the system Hamiltonian H. This protocol, where the system is driven out of equilibrium via a Hamiltonian with parameters depending on time through a theta function, it is called a *quantum quench*. Time evolution is diagonal in the energy eigenbasis, so it is best expressed in terms of the eigenstates $|n\rangle$ and energies E_n

$$|\psi(t)\rangle = \mathrm{e}^{-iHt}\,|\psi_0\rangle = \sum_n \mathrm{e}^{-iE_n t}\,c_n|n\rangle. \tag{3.5}$$

Each component acquires a complex phase, weighted by $c_n = \langle n\,|\,\psi_0\rangle$. The infinite-time limit $|\psi_\infty\rangle$ does not exist as a wave function: in $\lim_{t\to\infty}|\psi(t)\rangle$ the phase of each component keeps oscillating. However, the *time-averaged ensemble* can be defined

$$\rho_\infty = \lim_{T\to\infty}\frac{1}{T}\int_0^T |\psi_t\rangle\langle\psi_t|\,dt \tag{3.6}$$

which can be calculated exactly. For any finite time t, the instantaneous density matrix decomposes in

$$|\psi_t\rangle\langle\psi_t| = \sum_{E_n=E_m} c_n c_m^*|n\rangle\langle m| + \sum_{E_n\neq E_m} c_n c_m^*|n\rangle\langle m|\,\mathrm{e}^{-i(E_n-E_m)t}, \tag{3.7}$$

where the first sum is over all sets of degenerate eigenvalues (including singletons), and the second is over all combinations of different energies. The latter part $\int_0^\infty dt\,\mathrm{e}^{-i(E_m-E_m)t} \to 0$ when $E_n \neq E_m$ under the time average due to dephasing. The time independent part is equal to the *diagonal ensemble*

$$\rho_\infty = \overline{|\psi_t\rangle\langle\psi_t|} = \lim_{T\to\infty}\frac{1}{T}\int_0^T |\psi_t\rangle\langle\psi_t|\,dt = \sum_{E_n=E_m} c_n c_m^*|n\rangle\langle m| = \rho_d. \tag{3.8}$$

If there is no degeneracy, $E_n = E_m \Longrightarrow n = m$, the diagonal ensemble is simply the projector over the eigenstates of the Hamiltonian weighted with the original weight at time $t = 0$:

$$\rho_d = \sum_n |c_n|^2\,|n\rangle\langle n|. \tag{3.9}$$

This ensemble retains a macroscopic amount of information about the initial conditions, in D real numbers $|c_n|^2$. However, the information is classical since the quantum off-diagonal terms in Eq. (3.9) have been averaged out. The time-averaged ensemble has a well–defined nonzero entropy, despite that the state $|\psi(t)\rangle$ is pure. This is the so called *diagonal entropy*, $S_d = -k_B\sum_n |c_n|^2\log|c_n|^2$. Another very useful measure of the thermalization is the *Inverse Participation Ratio* (IPR), which is the *linear entropy* of the diagonal ensemble, or an effective dimensionality of the problem

$$D_{\text{eff}}(\rho_d) = \frac{1}{\mathrm{Tr}\,\rho_d^2} = \frac{1}{\sum|c_n|^4}. \tag{3.10}$$

Since the projectors on the single energy states are conserved, as $P_n = |n\rangle\langle n|$ commute with the Hamiltonian $H = \sum_{n=1}^D E_n P_n$, it is expected that this exponentially large set of operators must retain its initial expectation values: $\langle P_n(t)\rangle = |c_n(t)|^2 = |c_n(0)|^2$. Under the Principle of Maximum Entropy, the *diagonal ensemble* is the least constrained quantum state that conserves all these conserved quantities, raising the additional question of how can a quantum system thermalize under all these constraints.

3.1.2 Equilibration

Can the expectation value of an operator A, for all times after an initial waiting period, equal its time averaged value? The question is answered by the probability of observing any fluctuation

$$P(|\operatorname{Tr}(A\rho(t)) - \operatorname{Tr}(A\rho_D)|^2 > \epsilon). \tag{3.11}$$

Equilibration holds only for the expectation values of a set of allowable observables. It is easy to construct a counterexample [Rei08], a quantum operator whose expectation value never reaches a stationary value: the offdiagonal value of the density matrix in the energy eigenbasis, with $\omega = E_m - E_n > 0$:

$$\hat{K} = \frac{|m\rangle\langle n|}{\rho_{m,n}(0)} + H.c., \tag{3.12}$$

has an expectation value

$$\operatorname{Tr}(\hat{K}\,\rho(t)) = 2\cos(\omega t). \tag{3.13}$$

The operator so constructed is necessarily extremely nonlocal [SKAS14]. For local operators spanning a system of a few sites, the state of the whole system with L sites can be partitioned over a small subsystem S with L_S sites, and a remaining bath B, with L_B such that $L_S + L_B = L$. If $|N_S| < |N_B|$, the relative size of the Hilbert spaces is exponentially smaller,

$$\frac{D_S}{D_B} \sim \exp(L_S - L_B) \ll 1. \tag{3.14}$$

The disparity in the dimensionality mirrors the situation considered in the foundations of statistical physics [Rei07]: a small system is coupled to a much larger bath, and the dimensional ratio can be used to rigorously bound predictions.

The physical reason for this phenomenon has been related to the second law of thermodynamics: at growing temperatures, the increasing entanglement between the system and the bath is the source of the many, nearly thermal and random, contributions to the expectation values in small subsystems [PSW06, RDYO07a].

The density matrix of the reduced system ρ^S can be shown to almost never differ from its time average [LPSW10, Sho11, Rei08, Rei10], meaning that the subsystem does equilibrate:

$$\operatorname{dist}(\rho^S(t),\ \rho^S_\infty) < \frac{1}{2}\sqrt{\frac{D_S}{D_{\text{eff}}}}, \tag{3.15}$$

which is exponential in the size difference. The distance used for the density matrices is the trace distance, measuring the maximum deviation of any normalized observable between the two states. Since the bound is tight for the density matrix of the subsystem S, all expectation values of observables that can be defined on a subsystem S also equilibrate. Thus *local observables* equilibrate, which means that it is exponentially (in the system size) unlikely to observe fluctuations from their equilibrium (time–averaged) values. in Ref. [Rei15b], the fluctuation probability is given as

$$P(\,|\operatorname{Tr}(A\,\rho(t)) - \operatorname{Tr}(A\,\rho_d)|^2 > \epsilon) < \exp[-k\epsilon D_{\text{eff}}], \tag{3.16}$$

where k is a collection of constants of order $O(1)$. Smaller systems, such as few-level quantum systems, are never observed to equilibrate, whereas in mesoscopic quantum systems with $D \sim 10^7$ states, equilibrium is *apparent*. The lack of an *observable* recurrence time is due to the enormous amount of degrees of freedom, and requires an exponentially complicated set of measurements to be distinguished from true equilibration [UWE13]. The time necessary to attain equilibration is difficult to bound analytically, but some progress has been made [SF12, GHT13].

3.1.3 Independence from initial state

The only conditions to impose on the observables are locality and boundedness. Much stronger are the bounds on the Hamiltonian and the initial state $|\psi_0\rangle$. If the system is prepared in a clean superposition of very different energy eigenstates, e.g. $\frac{1}{\sqrt{2}}|0\rangle + |D\rangle$, the interference pattern in the observables can be visible at any time.

The bound in Eq. (3.15) requires the effective dimensionality of the initial state D_{eff} to be as large as possible [RS12]. This implies an overlap with almost all the eigenstates of the Hamiltonian used in the time evolution. If the states $|\psi_0\rangle$ are *typical*, i.e. selected according to a uniform probability measure in a subspace $\mathscr{H}_R$ of the full Hilbert space with dimension D_R, the probability [LPSW10] of having a small effective dimension is bounded by

$$P_{\psi_0}\left[D_{\text{eff}}(\psi_0) < \frac{D_R}{4}\right] \leq 2\exp\left(-c\sqrt{D_R}\right), \tag{3.17}$$

i.e. almost all initial states lead to a time averaged density matrix with very uniform overlap in the energy eigenbasis, with a constant $c \sim 10^{-4}$.

A gedanken counterexample is the following: if an experimentalist prepares the initial state in an energy eigenstate, then $D_{\text{eff}} = 1$ and the equilibration is impossible. As argued by Reimann [Rei07], a mole of atoms is described by $D_S = O(10^{10^{23}})$ parameters; even if the experimentalist could determine the energy with a precision of $10^{-10^{22}}$, thus collapsing the wavefunction to a narrow window of energies, there would still be $D_{\text{eff}} \sim D_R = O(10^{10^{23}-10^{22}}) = O(10^{0.9\cdot 10^{23}})$ energy levels in the distribution, greatly satisfying the requirement $D_{\text{eff}} \gg 1$.

Since all relevant quantum observables are *local*, the precise initial state of the global system $|\psi_0\rangle$ should not matter, as only the information available in the local *reduced density matrix* ρ_S is relevant, and that operator has contributions averaged over all combinations of states in the total system. The only observables that govern the expected values after thermalization can be densities defined over the subsystem: energy density, magnetization density, or other expectation values of local observables (although the latter are relevant only in the extreme case of *integrable systems*). The parallel with classical thermodynamics is evident, as all uncontrolled microscopic degrees of freedom are irrelevant in the macroscopic description and visible only as constituents of heat and entropy. Only a handful of macroscopic observables set the behavior of the system.

The reason why the conserved quantities appearing in Eq. (3.9), the projectors $P_n = |n\rangle\langle n|$ on the eigenstates, do not prevent the equilibration of *local* observables is that the P_n are *nonlocal*. As we argued, their effect on the reduced density matrix of an arbitrary subsystem should be limited. Local fluctuations would need to be offset exactly by corresponding changes on the whole system. This would violate *locality*, an emergent property characterized by a finite maximum speed of propagation of information in a system with short-ranged interactions, called Lieb-Robinson velocity [BEL14,ES12,LR72,KGE14,Kas15]. The emergent locality is a property of not only 1D quantum systems, leading to a general argument for the relevance of only the *local* conserved operators.

The constraints on the Hamiltonian are essentially requirements for the energy operator to be strongly nondegenerate and *irreducible*[1] over the whole Hilbert space. Technically, this is the *nondegenerate gap condition*, known also as the *non-resonance condition* [SF12]:

$$E_m > E_n > E_l > E_k \tag{3.18}$$

[1] This excludes the case of integrable systems, whose Hamiltonian can be put in block-diagonal form with respect to local conserved operators.

$$\text{implies} \quad E_m - E_n \neq E_l - E_k, \tag{3.19}$$

which is a stronger generalization of the non-degeneracy condition, preventing also equal excitation gaps in the energies, and excludes integrable systems from the rigorous results. It is argued that every *typical* Hamiltonian satisfies these requirements: if it does not, it is sufficient to add a Hermitian perturbation operator ϵ to the initial H_0

$$H_{\text{pert}} = H_0 + \epsilon + \epsilon^T, \tag{3.20}$$

where the matrix elements of ϵ are small, e.g. $|\epsilon_{i,j}| \sim 10^{-8}$, to satisfy Eq. (3.18). Such a small perturbation should not influence the observed physics, but it is enough to guarantee equilibration in the long time limit.

The conditions necessary in practice are somewhat more intricate, requiring that the initial states have sufficient thermal features, such as extensivity of the entropy [GME11] and wide overlaps in the energy window [SPR12, BCH11]. Counter-examples have been also provided by [BKL10], making the often overlooked point that even though relations such as Eq. (3.17) state that the probability of non-typical (leading to nonequilibrium) states is zero, peculiar initial conditions persisting in finite-size systems are observable.

3.1.4 Thermalization

The expected value of all observables need not necessarily match those of a thermal ensemble, unless

$$\langle A \rangle (t \to \infty) = \sum_n |c_n|^2 \langle n | A | n \rangle = \sum_{E_n \in [\bar{E}-\delta/2, \bar{E}+\delta/2]} A(E_n) = \text{Tr}(\rho_{\text{MC}} A). \tag{3.21}$$

where

$$\rho_{\text{MC}} = \frac{1}{Z} \sum_{E_n \in [\bar{E}-\delta/2, \bar{E}+\delta/2]} |n\rangle\langle n| \tag{3.22}$$

is the *microcanonical ensemble* corresponding to the mean energy $\bar{E}$, which is the maximum entropy ensemble for a system with fixed energy in a window of microscopic width δ.

The statement is the essence of the *Eigenvalue Thermalization Hypothesis* (ETH):

1. The distribution $|c_n|^2$ is centered around some average energy $\bar{E}$, where the width of the distribution δE is negligible compared to the mean, $\delta E/\bar{E} \to 0$ in the thermodynamic limit.

2. The expectation values of any relevant observable across excited eigenstates in the same energy window $[\bar{E} - \delta/2, \bar{E} + \delta/2]$ is more or less constant, depending smoothly only on the energy, $A(E_n) \approx A(E)$. The expected values of highly–excited energy eigenstates are thus already *thermal*, earning ETH its name.

In short, most distributions of energy weights c_n resemble a microcanonical distribution, and all reasonable observables have the expectation values equal to the ones from the microcanonical ensemble. The statement seems stronger than the preceding sections, invoking only arguments based on typicality, but the two viewpoints can be smoothly interpolated, by the concept of typicality not only in Hilbert space, but in the space of operators using Random Matrix Theory (RMT). The perturbation argument used in Eq. (3.20) is an example of RMT in action, pointing to properties of typical operators.

The statement (1.) is usually justified by supposing that the predictions are performed on an ensemble (in the sense of Gibbs) of many replicas of the system, experimentally prepared by letting

them interact weakly with a reservoir to achieve a repeatable initial state, then driven to nonequilibrium if needed. This is equivalent to the coefficients c_n being drawn from a random distribution, which can be flat in some window $[\bar{E}-\delta/2, \bar{E}+\delta/2]$. In an extensive system, density of states in any energy window is exponentially proportional to the volume [Deu10]. This guarantees that the smoothed distribution $c(\bar{E})$ has a support over an exponential number of states, i.e. its fluctuations compared to the mean vanish, leading to a well defined microcanonical state. Different initial temperatures, if needed, can be represented by a different average energy density.

The ETH approach using RMT was first developed by Deutsch [Deu10], summarized in Ref. [Rei15a]. Essentially equivalent is the approach of Ref. [GLTZ10], which is a modern statement of the *Quantum Ergodic Theorem* by von Neumann from 1929. A generalization making contact with the theory of *quantum typicality*, can be found in Ref. [DKPR15], which we follow.

Let us write $\sigma^2(\bar{A}) = \left\langle |\mathrm{Tr}(A\rho(t)) - \mathrm{Tr}(A\rho_D)|^2 \right\rangle$ for the variance of any expectation value. If the fluctuations of the average energy $\bar{E}$ in the initial state $|\psi_0\rangle$ are well behaved, i.e. $\sigma^2(\bar{E}) \simeq \bar{E}$, then the predictions of RMT are fulfilled in the thermodynamical limit, and

$$\bar{A} = \mathrm{Tr}[\overline{\rho_t} A] = \mathrm{Tr}(\rho_d A) = \mathrm{Tr}(\rho_{\mathrm{MC}} A). \tag{3.23}$$

Since the coefficients c_n are random and uncorrelated, the expectation values for the offdiagonal elements $\left\langle A_{n,m} \right\rangle = \left\langle c_m^* c_n \langle n|A|m\rangle \right\rangle$ which are supposed to vanish in the diagonal ensemble, satisfy [Per84]

$$\left\langle A_{n,m} \right\rangle \propto \frac{\mathrm{Tr}A^2}{D_{\mathrm{eff}}}. \tag{3.24}$$

The fluctuations $\sigma^2(\bar{A})$ of the expectation value $\bar{A}$ after the thermalization are bounded (see Eq. 3.16) by the offdiagonal elements expectation

$$\sigma^2(\bar{A}) \leq \max_{n\neq m} \left\langle A_{n,m} \right\rangle \leq \frac{\mathrm{Tr}A^2}{D_{\mathrm{eff}}} \tag{3.25}$$

so the equilibration can also be proven at the level of ETH.
The equality for the expectation value follows from

$$\bar{A} = \mathrm{Tr}[\rho_d A] = \sum_n |c_n|^2 A_{n,n} = A(\bar{E}) + \frac{1}{2}(\delta E)^2 A''(\bar{E}) + \ldots \tag{3.26}$$

where the second term depends on the energy fluctuations in the initial state. If the energy distribution is narrow, which is the only requirement, $\delta E \to 0$ and the prediction is fulfilled, as the contributions of the offdiagonal elements $A''(\bar{E})$ are negligible.

3.1.5 Lack of thermalization

Thermalization is a statistical effect, just as in classical physics. Out of equilibrium states evolve according to the internal microscopical dynamics set by the Hamiltonian. If those states, according to the fully time-reversible dynamics, enter the High Probability Manifold (HPM) – the equilibrium subspace [Gra08] of the Hilbert space with measure 1, they will not become nonequilibrium states again with high probability. The effect is purely entropic, owing to the enormous disparity between the volume of states in the HPM and the rest. This equilibration, and subsequent thermalization, mechanism can break down in many cases, some of which we overview below.

1. Integrable systems. The thermalization to a canonical ensemble is impossible due to the macroscopic number of local conserved operators, proportional to the volume of the system L. They however can equilibrate in certain cases to the Generalized Gibbs Ensemble [RDYO07a, GME11, Poz13]

shown in Eq. (1.76), which is a maximum entropy ensemble conserving all local operators. The thermalization of driven integrable systems is investigated in Chapter 6.

2. Breaking of ergodicity in Many Body Localized (MBL) systems [Mir00, PKCS15, HNO14, SSB$^+$10, AES14]. MBL is typical of systems with strong disorder or defects, such as the prototypical result of Anderson, leading to a weakly-growing (as the logarithm of time, instead of linearly) entanglement entropy and vanishing Lieb-Robinson velocity. These systems fail to act as their own heat baths and *dc* transport becomes impossible. The system has a number, exponential in the volume of the system, of conserved quantities that are all local, acting only on the typical length scale of the disorder, breaking the ergodicity and preventing the HPM from existing.

3. Periodically driven systems with MBL in energy space [PPHA15, DP13, DR14]. If the system is driven by switching the Hamiltonian periodically, the state can be approximated using the time-averaged evolution operator. Its logarithm can be obtained by a singular Magnus expansion, giving an effective Hamiltonian that can lead to localization in energy space. The driving protocol used in this thesis does not belong in this category, as the time-averaged Hamiltonian equals a chaotic (i.e. ergodic) operator, the Hamiltonian at time $t = 0$.

4. Pre-thermalization [BBW04, LGK$^+$13, EKW09, KWE11, GKL$^+$12, MK10]. It is a phenomenon that characterizes perturbed integrable systems, relaxing to a meta-stable state of the GGE type. The state indistinguishable from a thermal one is only reached after long times. In many cold-atoms experiments, after what was believed to be a sufficient time, they observed a state differing from the predictions of the relevant quantum thermal ensemble. Only continuing the experiment (after suitable upgrades) for longer times lead to the solution of the discrepancy. When a perturbation is added as per Eq. (3.20), the time needed to observe the effects of the perturbation are inverse to its strength, leading to a problematic separation of time scales.

3.2 Computational ensembles

We have shown in this Chapter how pure states can be indistinguishable from thermal states. This allows calculations to be performed on a (set of) wave-function, instead of the density matrix of the whole system, which for mesoscopic systems has an exceedingly large dimensionality. The convergence of the expected values to their equilibrium value, often as fast as the exponential size of the Hilbert space (see Eq. 3.15), allows in some cases the use of a single pure state. High-temperature expectation values can be computed as efficiently as averages on the ground state, which we first review.

The previous section dealt with the case of a state initially out of equilibrium, reaching an apparent thermal state that matches the ensemble expectation values, showing that almost any pure state, after waiting long enough, can be used to calculate otherwise inaccessible thermal predictions. This raises the question of the optimal choice of states, in order to estimate expectation values in a quantum ensemble, without having to wait any dephasing time.

We show how instead of using nonequilibrium states, carefully chosen random states can optimally give equilibrium expectation values already at $t = 0$; moreover, their time evolved set is useful to calculate any time-dependent observable at times $t > 0$.

3.2.1 Zero temperature methods

Quantum systems at a finite temperature [AFP09] are characterized by a density matrix with monotonically nonincreasing diagonal elements

$$\rho_\beta = \frac{1}{Z}\,\mathrm{e}^{-\beta H} = \frac{1}{Z}\sum_{n=1}^{\dim\mathscr{H}} \mathrm{e}^{-\beta E_n}\,|n\rangle\langle n| \tag{3.27}$$

where the sum is over the eigenvalues E_n and eigenvectors $|n\rangle$ of the Hamiltonian in increasing order, with the partition function $Z = \sum_n \mathrm{e}^{-\beta E_n}$ normalizing the trace of the matrix. The *ground state* of the system is attained by cooling to zero temperature or equivalently in the $\beta \to \infty$ limit. Supposing the existence of a unique ground state, which is usually the case away from critical points and in non-glassy systems, it can be seen that the density matrix selects the ground state. Shifting the energy levels by $-E_0$ leaves the density matrix invariant, since it changes the weights and the normalization constant, but allows to take a proper limit since all weights $\mathrm{e}^{-\beta(E_n-E_0)}$ for $n > 0$ vanish. In this case

$$\lim_{\beta\to\infty}\rho_\beta = \lim_{\beta\to\infty}\frac{1}{Z'}\left[|0\rangle\langle 0| + \sum_{n=2}^{\dim\mathscr{H}} \mathrm{e}^{-\beta(E_n-E_0)}\,|n\rangle\langle n|\right] = |0\rangle\langle 0|, \tag{3.28}$$

the matrix decomposes into the projection onto the pure $|0\rangle$ which is the unique ground state of the system. All thermodynamical averages at zero temperature are just expectation values in the ground state, considerably simplifying the algebra. The ground state eigenvector can be determined by variational methods involving constraints relaxation [BH12, Arb12, BV04], or directly from a concrete representation of the Hamiltonian as a matrix using e.g. the Lanczős method as described in Section 2.1.

Any relevant observable can be obtained as simply as

$$\lim_{\beta\to\infty}\langle A\rangle_\beta = \langle 0\,|A|\,0\rangle\,. \tag{3.29}$$

3.2.2 Canonical ensemble

More often than at zero temperature, classical statistical physics deals with systems being able to exchange energy with an environment, which acts as a bath with a well defined temperature. The system is weakly coupled with a bath that allows only the exchange of energy, left to thermalize, then the coupling is adiabatically turned off until at time $t = 0$, the system remains in the equilibrium state parametrized by the density matrix from Eq. (3.27).

The simplest nonzero temperature to analyze is the infinite temperature limit, $\beta \to 0$. In this case

$$\lim_{\beta\to 0}\rho_\beta = \frac{1}{D}\sum_{n=1}^{D}|n\rangle\langle n| = \frac{1}{D}\,\mathbb{1}, \tag{3.30}$$

the identity matrix normalized so that $\mathrm{Tr}\left(\rho_{\beta=0}\right) = 1$. The normalization constant can also be obtained as the expectation value of the operator $\mathbb{1}$, at any temperature. The sum over the projectors of all possible states of $\mathscr{H}$ can be replaced by an expectation value over random states $|r\rangle$, a so called *Hilbert space average*

$$\frac{1}{D}\mathbb{1} = \mathbb{E}_{|r\rangle}\left[\frac{1}{R}\sum_{r=1}^{R}|r\rangle\langle r|\right] \qquad \text{with } |r\rangle \in \mathscr{H}, \tag{3.31}$$

where the expectation $\mathbb{E}_{|r\rangle}$ is taken over a subset of R random vectors $\{|r\rangle\}$ in $\mathscr{H}$. Since the average is over complex subspace of D normalized parameters, it is equivalent to averaging over a $2D-1$ dimensional

real sphere[2]. Averages over a huge number of dimensions lead to the phenomenon called *concentration of measure*, already encountered in Eq. (3.15): it is a theorem due to Polya [LPSW09, appendix B], stating that almost all values of functions $f(x)$ defined on such spheres, lie close to their mean $\bar{f}$:

$$P_x\left(f(x) > \bar{f} + \epsilon\right) \leq 2\exp\left[-\frac{2D-1}{9\pi^3\lambda_f^2}\epsilon^2\right]. \tag{3.32}$$

This implies that any expectation value in the infinite-temperature limit is effectively sampled by an average over random states

$$\langle A\rangle_{\beta=0} = \frac{1}{D}\operatorname{Tr}(A\,\mathbb{1}) = \frac{1}{R}\sum_r \langle r\,|A|\,r\rangle \tag{3.33}$$

with the usual Monte Carlo scaling in the number of tries $O(R^{-1/2})$, as shown in Section 2.3.4. The variance is $O(D)$, so the relative error scales as $O(D^{-1/2})$, which is almost exponential in the number of sites of the system.

Any finite temperature can be obtained by a re-weighting of the probability shown in Eq. (3.33), by using the normalized expectation value of the operator $\mathrm{e}^{-\beta H}A$, instead of A

$$\langle A\rangle_\beta = \operatorname{Tr}(A\,\rho_\beta) = \frac{\operatorname{Tr}(A\,\mathrm{e}^{-\beta H})}{\operatorname{Tr}(\mathbb{1}\,\mathrm{e}^{-\beta H})} = \frac{\operatorname{Tr}(A\,\mathrm{e}^{-\beta H}\,\mathbb{1})}{\operatorname{Tr}(\mathrm{e}^{-\beta H}\,\mathbb{1})} = \frac{\left\langle A\,\mathrm{e}^{-\beta H}\right\rangle_{\beta=0}}{\left\langle \mathrm{e}^{-\beta H}\right\rangle_{\beta=0}}. \tag{3.34}$$

The symmetric version is even more useful and numerically accurate, by using the cyclical property of the trace $\operatorname{Tr}(A\,\mathrm{e}^{-\beta H}) = \operatorname{Tr}(A\,\mathrm{e}^{-\beta H/2}\,\mathrm{e}^{-\beta H/2}) = \operatorname{Tr}(\mathrm{e}^{-\beta H/2}\,A\,\mathrm{e}^{-\beta H/2})$. The numerator becomes

$$\operatorname{Tr}(A\,\mathrm{e}^{-\beta H}) = \operatorname{Tr}(\mathrm{e}^{-\beta H/2}\,A\,\mathrm{e}^{-\beta H/2}) = \frac{1}{R}\sum_{i=1}^{R}\left\langle r_i\,\middle|\,\mathrm{e}^{-\beta H/2}A\mathrm{e}^{-\beta H/2}\,\middle|\,r_i\right\rangle = \frac{1}{R}\sum_{i=1}^{R}\left\langle \phi_i^\beta\,|A|\,\phi_i^\beta\right\rangle, \tag{3.35}$$

whereas the normalization constant in the denominator of Eq. (3.34) is

$$Z = \operatorname{Tr}\left(\mathrm{e}^{-\beta H}\,\mathbb{1}\right) = \frac{1}{R}\sum_{i=1}^{R}\left\langle \phi_i^\beta\,|\,\phi_i^\beta\right\rangle. \tag{3.36}$$

We have chosen to index the random states $|r_i\rangle$, since each of them enters only after a re-weighting with $|\phi_i^\beta\rangle = \mathrm{e}^{-\beta H/2}|r_i\rangle$. The set of vectors $\{|\phi_i^\beta\rangle, i = 1,\ldots,R\}$ span a rank-R approximation to the unnormalized density matrix $\mathrm{e}^{-\beta H} \approx \sum_{i=1}^R |\phi_i^\beta\rangle\langle\,\phi_i^\beta|$. It is numerically equivalent ensemble of vectors, reaching easily a precision of 1% with $R = 10$ for *generic* systems.

Since the error scales as $O(D^{-1/2}R^{-1/2})$, for $D \gg 1$, already $R = 1$ might be sufficient. In this case, a single random vector $|r\rangle$ (or equivalently $|\phi\rangle$), can be enough to approximately represent physical results. It is a *pure state approximation to the canonical ensemble*.

The first uses of this approximation date to the works of Jaklič and Prelošek [JP94, JP96, JP00], where it was dubbed the Finite Temperature Lanczős Method (FTLM), as opposed to the ground state method mentioned in Section 3.2.1. The name stems from the method[3] used to calculate $\mathrm{e}^{-\beta H}|r\rangle$, which was the Lanczős based imaginary-time propagator, discussed in Section 2.1.3. Unfortunately, the method fell out of fashion in the early 2000s outside the condensed-matter community (Ref. [SSZT12] is an example of the latter), to be rediscovered in the DMRG community under the name of METTS (Minimally Entangled Typical Thermal States) in Ref. [SW10], where the vectors ϕ_i were instead calculated by a Suzuki-Trotter approximation, with some notable applications [BEL14]. Independently,

[2]The real and imaginary parts of the components of any $|r\rangle$ are to be taken as independent

[3]The unsymmetric version Eq. (3.34) was used

quantum typicality approaches [GMM04] also arrived at the expression (3.34), with later independent publications [SS13], but for the first time rigorous error bounds in $O(D^{-1/2})$ were derived and the idea of approximating a whole ensemble, not only the expectation values, was born.

The dimensionless normalization constant Z_β, also serves as a measure of the effective dimension $D_{\text{eff}} = Z$ of states entering the average. in Ref. [BP03], it is stated that good convergence is only expected when the number of states as function of the temperature satisfies $Z_\beta \gg 1$. This is in line with the conclusions of Section 3.1.3, since for purely random states the effective temperature is infinite, and the canonical expectation value for $Z_{\beta=0}$ is the dimensionality of the subspace $\mathscr{H}_R \subseteq \mathscr{H}$ from where the random vectors are generated from, giving $D_{\text{eff}} = D_R$. Whenever $Z_\beta \to 1$, the system is effectively at zero temperature.

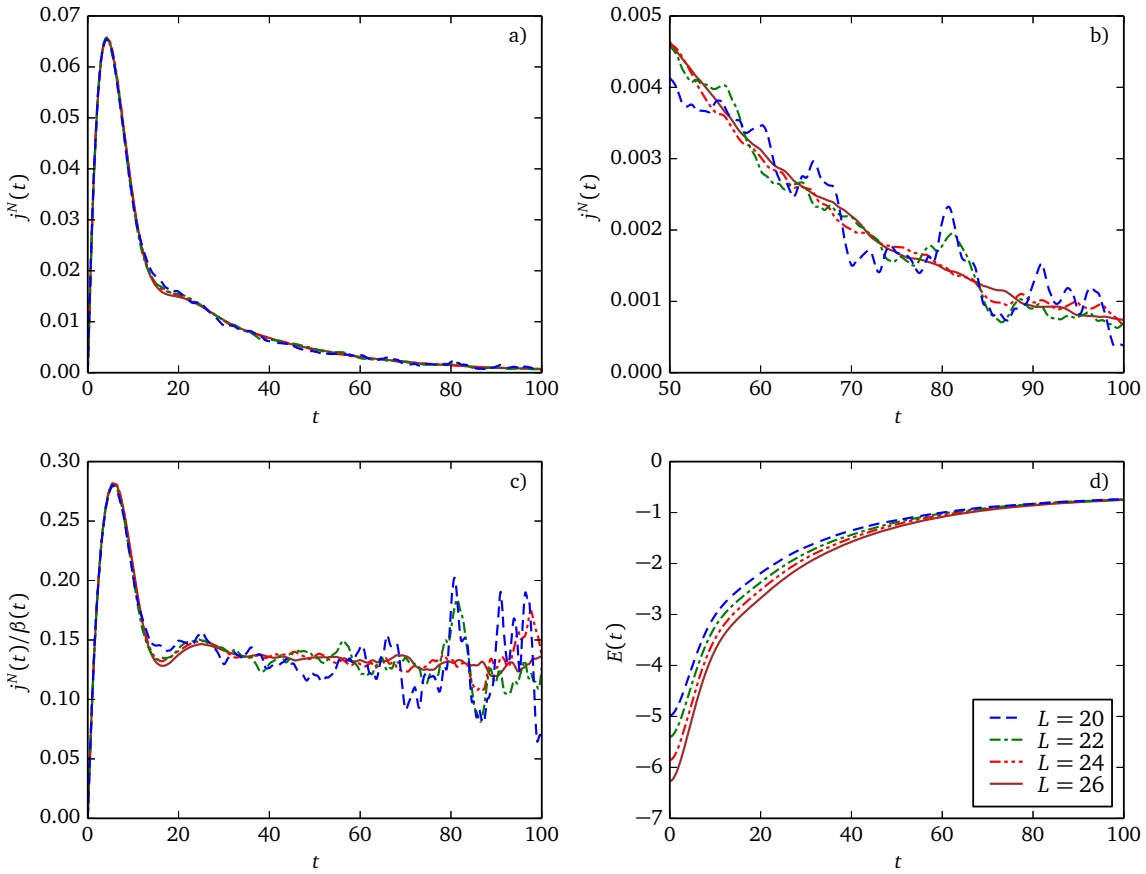

Figure 3.1: Comparison of observables under a single realization $|\phi^\beta\rangle$ ($R = 1$) of the approximate canonical ensemble, for different system sizes. The system Hamiltonian is typical, i.e. it fulfills the requirements for thermalization to work. It is a fermionic $t-V-W$ model at half-filling, $V = 1.5$ and $W = 1.0$, started at equilibrium with $\beta = 0.3$ and driven with an electrical field $F = 0.2$. In each panel a different observable is shown: (a) particle current, (b) zoom of the later times, to show the oscillations of the decaying current, (c) ratio of the particle current to β, which is expected to be constant for $\beta \to 0$. The ratio allows the oscillations of the current to be clearly seen, (d) the instantaneous energy.

All the quantities defined above are easily calculated using the set of vectors $|\phi_i^\beta\rangle$. However, a much more efficient version, allowing the expectation values to be computed at any temperature, is given by using the scalar density of states averages obtained by Chebyshev expansions, shown in Section 2.3.5. We summarize the results using the vectors now, since they are most useful beyond equilibrium.

1. For all $i \in \{1,\dots,R\}$
   (a) Extract a random vector $|r_i\rangle$, representing a state at infinite temperature, $|\phi_i^{\beta=0}\rangle = |r_i\rangle$
   (b) Re-weight to obtain finite temperature $|\phi_i^{\beta}\rangle = \mathrm{e}^{-\beta H/2}|\phi_i^{\beta=0}\rangle$, by Chebyshev or Lanczős imaginary-time propagators
   (c) Compute the expectation value for any set of operators $A_1, A_2, \dots, A_k$ as $A_k = \left\langle \phi_i^{\beta} \,|A_k|\, \phi_i^{\beta} \right\rangle$
   (d) If higher moments are needed, use e.g. $\left\langle H^2 \right\rangle = \| H|\phi_i^{\beta}\rangle \|^2$
   (e) Compute the normalization $Z = \| \,|\phi_i^{\beta}\rangle \|^2 = \left\langle \phi_i^{\beta} \,|\, \phi_i^{\beta} \right\rangle$
2. Average all contributions to the observables A_k and Z, $\langle A_k \rangle_\beta = A_k/Z$

Step (d) is a necessary *variance reduction* technique, to make sure that moments of the energy such as $\sigma_H^2(\beta) = \left\langle H^2 \right\rangle_\beta - \langle H \rangle_\beta^2$, do not require R^2 terms instead of R to achieve reasonable accuracy. In short, the variance needs to be calculated over the same set of vectors [Bra06].

We are now able to cite the reason why the approximation is so effective at equilibrium and beyond, following [BG09]. It is required that all physical observables of the system, as stated in Section 3.1.4, have fluctuations compatible with their mean $\sigma^2(A) \sim \bar{A}$, moreover moments with order higher than 2 also stay bounded. Then, the *Hilbert space average* of any observable A, or infinite-temperature average over random vectors $|r\rangle$, leads to an expectation value

$$\bar{A} = \mathbb{E}_{|r\rangle}[\langle r \,|A|\, r\rangle] = \frac{\mathrm{Tr}(A)}{D}, \tag{3.37}$$

with variance[4]

$$\begin{aligned}\sigma^2(\bar{A}) &= \mathbb{E}_{|r\rangle}\left[\left\langle r \,\middle|A-\bar{A}\middle|\, r\right\rangle^2\right] \\ &= \frac{1}{D+1}\left(\frac{\mathrm{Tr}A^2}{D} - \left(\frac{\mathrm{Tr}A}{D}\right)^2\right) \\ &= \frac{1}{D+1}(m_2 - m_1^2),\end{aligned} \tag{3.38}$$

if we denoted by m_1 and m_2 the first and second moment of A at infinite temperature, respectively. The variance of the expected values over the Hilbert space thus decreases linearly with the dimension of $\mathscr{H}$, or exponentially in the number of sites. To obtain finite temperature results, the reasoning is applied to the modified observable $A \mapsto A\mathrm{e}^{-\beta H}$. The reader is reminded that this is the variance of an expectation value, which tends to an extremely peaked distribution already for small-sized quantum systems, not the variance of a measurement, which has the requested scaling properties of any thermal quantity, as noted in Ref. [DKPR15].

3.2.3 Time evolution

The same subset of vectors $|r_i\rangle$, can be propagated forward in time with any unitary evolution operator $U(0,t)$, obtaining an expectation value of $A(t)$

$$\langle A(t)\rangle_\beta = Z^{-1}\frac{1}{R}\sum_{i=1}^{R}\left\langle \phi_i^{\beta} \,\middle|\, U(0,t)^\dagger A\, U(0,t)\middle|\, \phi_i^{\beta}\right\rangle = \frac{1}{R}\sum_{i=1}^{R}\left\langle \phi_i^{\beta}(t) \,|A|\, \phi_i^{\beta}(t)\right\rangle, \tag{3.39}$$

[4]Let us remind the reader that $\sigma^2(\bar{A})$ measures the fluctuations of the expectation value $\bar{A}$, not of single measurements of A.

where we have switched to the Schrödinger picture, including the explicit time dependence in the random state vectors

$$|\phi_i^\beta(t)\rangle = U(0,t)\,|\phi_i^\beta\rangle = U(0,t)\,\mathrm{e}^{-\beta/2H}\,|r_i\rangle. \tag{3.40}$$

The last expression reduces to $|\phi_i^\beta(t)\rangle = \mathrm{e}^{-(it+\beta/2)H}\,|r_i\rangle$ for the time-independent Schrödinger equation. The normalization Z is constant for any kind of unitary real-time evolution, no adjustment is necessary for $t > 0$.

Unitary operators conserve distances and angles in Hilbert space. In particular, the spread of $\langle A(t)\rangle_\beta$ from the true value stays bounded

$$\sigma^2[\bar{A}(t)] = O\left(\frac{1}{D}\right) \tag{3.41}$$

according to [BG09, Eq.(9)], analogously to Eq. (3.38). If the initial states are chosen to approximate equilibrium values at $t = 0$ well, they will do so at later times $t > 0$. The computational cost consists in having to evolve every vector $|r_i\rangle$ in both imaginary and real time, and averaging all necessary quantities over the whole set of vectors and times.

Sites	$\dim\mathscr{H}$ **(millions)**	**SpMV**	**Time**	**Time /** $\dim\mathscr{H}$
20	0.184756	11748	77	416
22	0.705432	11950	365	518
24	2.704156	12351	1500	554
26	10.400600	12554	5750	552

Table 3.1: Scaling of the timings (in seconds) necessary to obtain the data from Fig. 3.1. The times scale proportionally to the Hilbert space dimension, whereas the number of sparse matrix vector products is weakly dependent on the system size through the spectral radius.

The setup is necessary to calculate correlation functions in real time, and was already pioneered in Ref. [JP94]. Correlation functions measure the overlap between a state initially in thermal equilibrium at time $t = 0$ and later times $t > 0$:

$$\begin{aligned} C(t) = \langle A(t)\,A(0)\rangle_\beta &= Z^{-1}\,\mathrm{Tr}\left(\mathrm{e}^{-\beta H/2}\,U(0,t)^\dagger A\,U(0,t)A\,\mathrm{e}^{-\beta H/2}\right) \\ &= \frac{\sum_{i=1}^R \left\langle \phi_i^\beta \,\middle|\, U(0,t)^\dagger A\,U(0,t)A \,\middle|\, \phi_i^\beta \right\rangle}{\sum_{i=1}^R \left\langle \phi_i^\beta \,\middle|\, U(0,t)^\dagger U(0,t) \,\middle|\, \phi_i^\beta \right\rangle} \\ &= \frac{\sum_{i=1}^R \left\langle \phi_i^\beta(t)\,|A|\,\varphi_i^{A,\beta}(t)\right\rangle}{\sum_{i=1}^R \left\langle \phi_i^\beta \,|\, \phi_i^\beta \right\rangle}. \end{aligned} \tag{3.42}$$

We have defined $|\varphi_i^{A,\beta}(t)\rangle = U(0,t)|\varphi_i^{A,\beta}(0)\rangle = U(0,t)A|\phi_i^\beta\rangle$, noted that $\langle\,\phi_i^\beta|U(0,t)^\dagger = \langle\,\phi_i^\beta(t)|$, and simplified the denominator. The correlation function is then the normalized expectation value of A between the two time-evolved states $|\phi\rangle$ and $|\varphi\rangle$. This method has been the basis for most of the studies of high-temperature correlation functions [DWH$^+$12, MWH$^+$10b, MWH$^+$10a, SJ09, KK14, BHVC09, ZMK$^+$15, KBM12, vSG14, MHWG08, Sch04, PVM13, KBM12, EK08].

3.2.4 Microcanonical ensemble

Statistical physics textbooks tend to present first the microcanonical ensemble, which is the relevant ensemble for an isolated system at equilibrium, where the energy is fixed at an average value $\bar{E}$. The more

general canonical ensemble, in which the energy can fluctuate, is usually derived in the configuration of a subsystem connected to a bath, where the whole system is described by a microcanonical state. The predictions of the two ensembles are usually equivalent in the thermodynamical limit, since the energy distribution in the canonical ensemble becomes infinitely narrow. There are several studies on the necessary conditions for the equivalence [LL69, Geo95], or on counterexamples [Kas10]. A most recent and detailed paper for the quantum case [BC15], states that the equivalence always holds for large enough volumes if the interactions are strictly local, i.e. for lattice Hamiltonians as treated in this thesis, and the correlation lengths are finite, excluding critical systems.

The microcanonical state is a diagonal, mixed state, represented by the mixture of all energy states around $\bar{E}$ with a certain width δE

$$\rho_{\mathrm{MC}} = \frac{1}{D_{\mathrm{MC}}} \sum_{E_n \in [E-\delta/2, E+\delta/2]} |n\rangle\langle n|. \tag{3.43}$$

The maximum entropy principle requires all microstates $|n\rangle$ to have an equal probability D_{MC}^{-1}, which is the inverse of the number of the states in the selected energy window. As argued in Section 3.1.4, for practical purposes the weights need not be exactly equal, but if the state ρ_{MC} is itself averaged over different realizations, the weights can just have the same statistical distribution.

The ETH requires that all generic states have a well defined, narrow distribution of energies for thermalization to happen, and that such a distribution is typical for random states in Hilbert space. Recalling the statement of the ETH, all excited states of the Hamiltonian give approximately similar predictions for local observables

$$\langle n \,|A|\, n\rangle \approx A(\bar{E}) \qquad \forall n : E_n \in [\bar{E} - \delta/2, \bar{E} + \delta/2]. \tag{3.44}$$

Choosing any initial state $|\psi_E\rangle$, with a distribution $c_n = \langle n \,|\, \psi_E\rangle$ centered around $\bar{E}$, will give a satisfactory approximation the microcanonical distribution $\rho_{\mathrm{MC}} \approx |\psi_E\rangle\langle\psi_E|$. For improved accuracy, the average can be taken over several realizations of the state $|\psi_E\rangle$, although it was unnecessary in our experience.

Selecting carefully only one pure state to perform averages for $t \geq 0$ is motivated by the success of ETH to describe the thermalization of generic quantum systems. Paraphrasing Landau [LL77], the density matrix formalism combines the averaging over the initial mixture of pure states with the quantum mechanical average over superpositions of energy eigenstates; by carefully choosing the latter, a mixture with only one state can be chosen. Such approximation to the microcanonical ensemble is better motivated than the canonical case, due to the very broad spread of energy for relatively small systems in the latter formulation. Choosing a state with a well defined initial energy, with $\delta E/\bar{E} < 1\%$, is possible only with a microcanonical formulation. However, if one does not need to have a narrow distribution of energies, averaging over a few canonical typical states $|\phi^\beta\rangle$ can give smoother and better behaved predictions, but the results are largely equivalent. A comparison is given in Fig. 3.3, where the time evolved observables an a single microcanonical pure state are compared with the predictions of the canonical ensemble with $R = 10$, giving a very reasonable agreement once the system has passed the initial nonequilibrium transient.

The first quantum microcanonical state approach known to the author was in Ref. [LPE+03], although later works derived from quantum typicality approaches also appeared [SS12]. The key is to find an optimal *pure microcanonical state*, satisfying the requirement that the energy variance is narrow:

$$\left[H - \bar{E}\hat{\mathbb{1}}\right]^2 |\psi_E\rangle = \sigma_E^2 |\psi_E\rangle \tag{3.45}$$

The equation above states that the variance σ_E^2 has a well defined value on the state $|\psi_E\rangle$ at average energy $\bar{E}$. The variance operator on the left-hand side of Eq. (3.45) is positive semidefinite on $\mathscr{H}$,

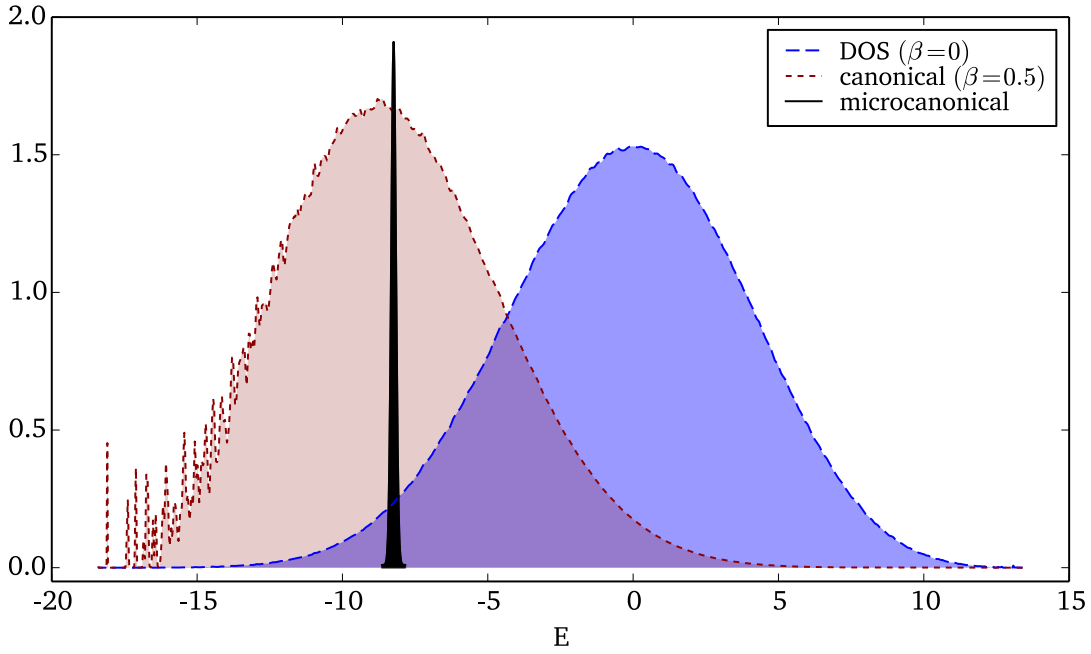

Figure 3.2: Distribution of energies in the different ensembles, with the DOS $\rho(E)$ from Eq. (2.37), the canonical distribution $\rho(E)\mathrm{e}^{-\beta H}$, and the microcanonical density $\rho_{\mathrm{MC}}(E)$ from Eq. (3.43). The data is the same as in Fig. 3.1 with $\beta = 0.5$ and $L = 24$. The density of states (dashed line) corresponds to a canonical distribution at infinite temperature, and the canonical distribution (dotted line) is very broad at any temperature but has noticeable contributions from the lower-lying energy states where the density is low. The microcanonical distribution (solid line, non-normalized) is peaked at the mean energy of the canonical ensemble, but its width is only $\sigma_E = 0.01\bar{E}$.

meaning that the search for a minimum of the variance is a well-posed problem. However, the actual minimum of the variance is not useful, since a wider spread in the energy is required to satisfy $D_{\mathrm{eff}} \gg 1$, where D_{eff} (see Eq. 3.10) counts the number of energy states overlapping with $|\psi_E\rangle$.

The operator equation (3.45) is an eigenequation with minimal eigenvalue σ_E^2, thus can be most effectively solved via the Lanczős ground-state method, Alg.(1) in Section 2.1. The convergence to the ground state of $\left[H - \bar{E}\hat{\mathbb{1}}\right]^2$ is quite slow, due to the vanishing gap of the operator: the states of the Hamiltonian are exponentially dense near the middle of the spectrum where the values of $\bar{E}$ are most common. The gap is exponentially small, so the convergence time inversely increases. Whereas 100 steps are common for excellent convergence to the ground state in gapped systems, after 5000 steps only a convergence to $\sigma_E^2/\bar{E} \sim 0.001$ is achieved. The energy window does not need to be smaller though, otherwise single energy states would be singled out, so a number of steps below 1000 may be sufficient. If an exact diagonalization mapping of the spectrum is available, which is only the case for operators too small for quantum typicality arguments to apply successfully, the microcanonical state can be constructed explicitly as

$$|\psi_E\rangle = C \sum_{n=1}^{D} \exp\left[-\frac{(E_n - \bar{E})^2}{2\sigma^2}\right] |n\rangle, \tag{3.46}$$

where C is just the normalization factor which depends on the multiplicity of the eigenstates in the energy window. This explicit construction has been used for benchmarking in Fig. Figure 2.6.

The Lanczős method is equivalent to an extrapolation at infinite imaginary time of the propagator

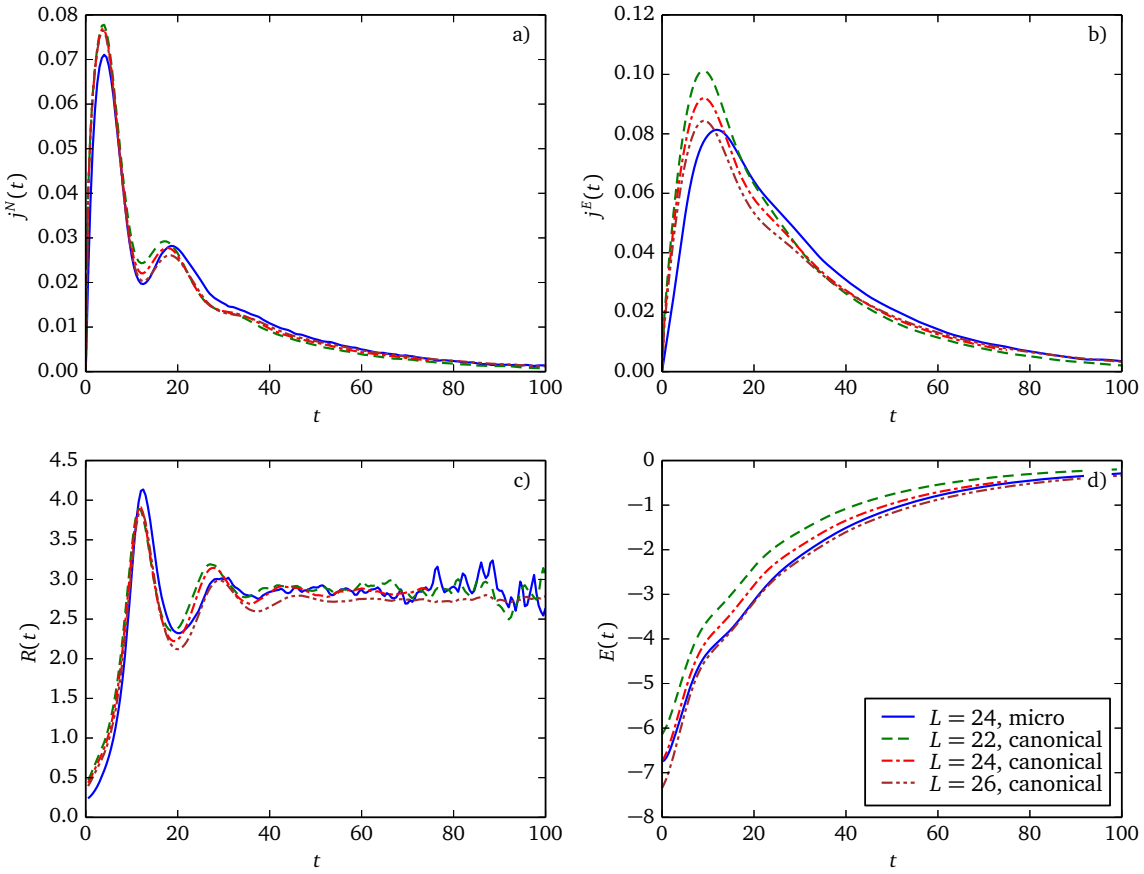

Figure 3.3: Comparison of observables under the approximate the canonical ensemble, averaged over $R = 10$ states, and the single realization microcanonical, marked as "micro", for different system sizes. The system is an integrable, metallic fermionic $t-V$ model, $V = 1.5$, started at an energy corresponding to $\beta = 0.4$ and driven with an electrical field $F = 0.2$. The integrability of the system serves as a worst-case scenario, to show that even when the typicality proofs break down, for a finite system the thermal behavior is properly modeled. In each panel a different observable is shown: (a) particle current, (b) energy current, (c) ratio of the two currents, (d) instantaneous energy

$e^{-\beta(H-\bar{E}\mathbb{1})^2}$ applied to a random state, so the distribution of the energy is actually Gaussian centered around $\bar{E}$ with variance σ_E^2. An alternative exists, iterating the operator $E_{\max}\mathbb{1} - H$ on a random state, which successively lowers the average energy, providing a tool to monitor the temperature of the microcanonical state, based on the relation $\partial S(E)/\partial E = \beta$, where $S(E)$ is the microcanonical entropy [Rei15a] defined as $S(E) = \ln \Omega(E)$, the logarithm of the number of states at energy equal or lower than E. The approach based on a target Gaussian distribution leads to much finer predictions close to the thermodynamical results, and it is also favored by the detailed analysis of the alternatives in Ref. [LPE+03], where the connection is made using Laplace transforms to generate the correct distributions [PHT85].

The only parameter left free is $\bar{E}$, which we have set to the average energy at the canonical inverse temperature β obtained from the thermodynamical equation of state

$$\bar{E} = \langle H \rangle_\beta \,. \tag{3.47}$$

The relation has been determined using the methods of Section 2.3.5 in the canonical ensemble, or using a High Temperature Expansion (HTE), explained in Section 6.2. The initial state $|\psi_E(0)\rangle$ thus

satisfies

$$\langle \psi_E \,|H|\, \psi_E \rangle = \bar{E}, \tag{3.48}$$

$$\left\langle \psi_E \,\middle|\, [H-\bar{E}\mathbb{1}]^2 \,\middle|\, \psi_E \right\rangle = \sigma_E^2. \tag{3.49}$$

Expectation values of operators closely related to the Hamiltonian, such as the kinetic or potential energy alone, agree generally closely with the canonical predictions

$$\langle A \rangle_{\mathrm{MC}} = \mathrm{Tr}(\,\rho_{\mathrm{MC}} A) \sim \langle \psi_E \,|A|\, \psi_E \rangle \approx \frac{1}{Z}\,\mathrm{Tr}(\,\mathrm{e}^{-\beta H}\, A) \tag{3.50}$$

if the temperature is chosen from Eq. (3.47) (or using other relations [Rug97, GOM01]), since the microcanonical state samples the most relevant energy configurations, whereas the contributions from further areas of the spectrum dephase in the canonical distribution. On the other hand, operators with wildly differing expectation values on close energy eigenstates have less accurate predictions in the microcanonical state than using the canonical formalism of Section 3.2.2. In that event, the averaging over different realizations of the state $|\psi_E\rangle$ must be employed.

The main reason for the use of the microcanonical pure-state ensemble is the simplicity in the time evolution. Observables at $t > 0$ need only be calculated with one time-evolved wavefunction

$$\langle A(t) \rangle = \left\langle \psi_E \,\middle|\, U(0,t)^\dagger\, A\, U(0,t) \,\middle|\, \psi_E \right\rangle = \langle \psi_E(t) \,|A|\, \psi_E(t) \rangle\,. \tag{3.51}$$

The microcanonical state is an approximate eigenvector of the initial Hamiltonian, so

$$\mathrm{e}^{-iHt}\,|\psi_E\rangle = \mathrm{e}^{-iEt}\,|\psi_E\rangle, \tag{3.52}$$

simplifying greatly the expressions for the correlation functions $C(t)$ from Eq. 3.42, if the evolution is with the time-independent Hamiltonian $U(0,t) = \mathrm{e}^{-iHt}$

$$\begin{aligned} C(t) = \langle A(t)\, A(0) \rangle_E &= \left\langle \psi_E \,\middle|\, \mathrm{e}^{iHt}\; A\; \mathrm{e}^{-iHt}\; A \,\middle|\, \psi_E \right\rangle \\ &= \mathrm{e}^{iEt} \left\langle \psi_E \,\middle|\, A\; \mathrm{e}^{-iHt}\; A \,\middle|\, \psi_E \right\rangle \\ &= \mathrm{e}^{iEt} \left\langle \psi^A \,\middle|\, \mathrm{e}^{-iHt} \,\middle|\, \psi^A \right\rangle \\ &= \mathrm{e}^{iEt} \left\langle \psi^A(0) \,|\, \psi^A(t) \right\rangle. \end{aligned} \tag{3.53}$$

We have used Eq. (3.52) in the second line, relabeled $|\psi^A\rangle = A|\psi_E\rangle$ in the third, applied the time evolution in the forth, to rewrite the correlator as a modulated scalar product (in the Loschmidt echo form [HPK13, SRH14, Zur03]).

Chapter 4

Motivation

The original work presented in this Dissertation concerns the nonequilibrium states of nanoring structures driven strongly with an electric field. The understanding of realistic thermoelectric devices is necessary for the improvement of the efficiency of modern energy-generating devices. Realistic regimes require them to operate at finite power, and thus under a finite field, where the approaches based on LR may not be sufficient to investigate the system. Those limitations can be overcome going beyond the equilibrium framework, using the tools of real–time evolution.

The energy-current response is tightly woven to the transport of heat, although the latter can be defined only in a quasi-equilibrium regime. We only make use of quantum observables that allow the expectation value to be computed in arbitrary states of the system. Furthermore, we develop a nonequilibrium analogues of thermodynamical quantities, such as the entropy density, from which the effects of heating can be deduced.

The effect of conservation laws is investigated in a driven integrable insulator or metal. The integrability of a system allows for ballistic transport of charge and energy as long as the system is completely isolated from its environment. On one hand, the existence of conserved quantities could highly improve the performance of thermoelectrical devices. On the other, an applied field induces dissipation in the system by breaking the symmetries in a controlled way. These effects cannot be treated perturbatively, as the limit of no field is singular. The real-time approach can give answers in this case, and we study both the transport of energy and the effects of the dissipated heat on the system in the long-time regime.

Chapter 5

The transport under finite field requires the extension of Ohm's law to the transport of charge and energy. What is sought here is the generalization of the Linear Response formulated for the energy current in a closed system, where the leading effect beyond LR is captured by the increase of the instantaneous energy density. The limits of this quasi-equilibrium approach are also determined.

The presence of a finite driving modifies the thermoelectrical response of a system, defined as the ratio of the energy and particle currents $R = j^E / j^N$. At the LR level, R is given by the ratio of the *dc* conductivities. The calculation of the transport coefficient $\sigma^E(\omega)$ in the LR regime for the large systems considered here required the development of a new algorithm. Corrections due to the additional presence of a field must be taken into account through broadening of the response.

In integrable systems the equilibrium transport coefficients develop singularities, making the prediction of the thermoelectric response an even more daunting task. Integrable systems oscillate at low fields, breaking the proportionality with F, but the (thermal) response can be surprisingly well characterized. An analytical bound is sought for integrable metals and integrable doped Mott insulators.

The results were presented in **[CMP14]** and **[CMP15]**.

Chapter 6

The understanding of the nonequilibrium thermodynamics of driven systems requires an alternative to the entropy, especially if the closed system is in a pure state. An entropy-like quantity can be defined using the subsystems density matrix, confirming the validity of the second law of thermodynamics for weakly driven (generic and integrable) strongly-interacting systems.

The effect of the driving on the thermalization of integrable systems and the details of their long-time local states were open problems. By the criteria exposed in Section 3.1 and 1.4, they should retain memory of the initial conditions and the different subsectors should be independent. Applying the tools of RMT to study the systems during driving and relaxation, we show that the spectrum of the reduced density matrix agrees with predictions of the Gaussian Unitary Ensemble.

The nature of the energy increase caused by the Joule effect on a closed system can be two-fold: as heat or as reversible work. We show the former is true, by the spectral analysis of the density matrix of subsystems. The time evolution is shown to lead to Gibbs local states with a well defined effective temperature, confirming again the thermalization even in integrable driven systems.

The results were first published in **[MPCP13]**.

Chapter 7

The quantum model of a thermoelectric couple is built using the concepts of quantum typicality, and the measured distributions are shown to match the high-temperature expressions for the heating rate and local observables.

We investigate the differences between a model with fully quantum evolution and its counterpart which relies on the concept of local quasiequilibrium and on the LR theory. We show genuine nonequilibrium phenomena that arise for longer times due to the heating, to the equilibration of the thermodynamical fluxes, and due to Bloch oscillations of the currents and densities.

We also show the dynamical inversion of the Peltier response in a thermocouple built out of two Mott insulators, which occurs only for sufficient strengths of the applied field.

The surprising result has been shown in **[MCP14]**.

Part II

Results

Chapter 5

Transport in strongly driven homogeneous quantum systems

We analyze the transport dynamics of a strongly correlated quantum nano-ring, under external finite-field inductive driving. The operator observables are carefully defined, their expectation values bounded by analytical and numerical predictions, even in the case of integrable systems.

In order to push the system out of equilibrium and induce the flow of currents, the ring is threaded by a time-dependent magnetic field flux $\phi(t)$. The dependence on the externally controlled parameter is incorporated through the Peierls' phase ϕ in the Hamiltonian $H(\phi)$ from Eq. (1.4), which is reported below for convenience:

$$\begin{aligned} H(\phi) &= \sum_l H_l(\phi) \\ H_l &= \underbrace{\left(-t_h\, \mathrm{e}^{i\phi}\, c^\dagger_{l+1} c_l \quad + \mathrm{H.c.}\right)}_{H_{\mathrm{kin}}} + \underbrace{V\, \tilde{n}_{l+1}\tilde{n}_l + \frac{1}{2} W\, (\tilde{n}_{l-1}\tilde{n}_{l+1} + \tilde{n}_l \tilde{n}_{l+2})}_{H_{\mathrm{pot}}}, \end{aligned} \tag{5.1}$$

where $\tilde{n}_l = n_l - \frac{1}{2}$, $n_l = c^\dagger_l c_l$, t_h is the hopping integral, whereas V and W are the repulsive interaction strengths for particles on the nearest and the next nearest sites, respectively. We have also defined the kinetic H_{kin} and potential H_{pot} parts of the energy.

5.1 Currents and other observables

The aim of studies discussed in the following section is a derivation of the continuity equations for the particle and energy density for the time–independent Hamiltonian, which in turn lead to the definition of the current density operators: J^N_l and J^E_l respectively [MPCP13, ZNP97, MS08]. In the absence of driving, i.e. for a constant magnetic flux ϕ, the particle number and the total energy are conserved, hence one derives the continuity equations which do not contain any source terms. The total current is defined as the zero-momentum component, or the average over the whole system, of the current densities

$$J^N = \frac{1}{L}\sum_l J^N_l \quad \text{and} \quad J^E = \frac{1}{L}\sum_l J^E_l. \tag{5.2}$$

In the Heisenberg picture the equation of motion for the particle density[1] operator $\tilde{\mathrm{n}}_l$

$$\frac{\mathrm{d}}{\mathrm{d}t}\,\tilde{\mathrm{n}}_l + i\,[\tilde{\mathrm{n}}_l, H] = 0 \tag{5.3}$$

can be compared with the continuity equation $\frac{\mathrm{d}}{\mathrm{d}t}\,\tilde{\mathrm{n}}_l + \nabla J_l^N = 0$, defining the corresponding current density J_l^N by

$$\nabla J_l^N \equiv J_{l+1}^N - J_l^N = i[\tilde{\mathrm{n}}_l, H]. \tag{5.4}$$

The solution of Eq. (5.4) for the Hamiltonian given above is

$$J_l^N = i t_h \exp(i\phi)\, c_{l+1}^\dagger c_l + \mathrm{H.c.}, \tag{5.5}$$

fulfilling also the relation $J_l^N = -\partial_\phi H/L$. In order to determine the energy current the energy density H_l must be defined. Since H can be split into H_l in many inequivalent ways, the energy current operator is not uniquely defined either. In Eq. (5.1) we take H_l which has support symmetric with respect to the bond between sites l and $l+1$. Then, similarly to Eq. (5.4), one defines the energy current through the continuity equation as

$$\frac{\mathrm{d}}{\mathrm{d}t}H_l + i[H_l, H] = \frac{\mathrm{d}}{\mathrm{d}t}H_l + J_{l+1}^E - J_l^E = 0 \tag{5.6}$$

The calculations are straightforward for the translationally invariant case which we will use for the driven homogeneous system in this chapter, so we reverse the derivation for the general case. The spatially–averaged current was already given in Eq. (1.36),

$$\begin{aligned} J^E = &\frac{1}{L}\sum_l (-t_h^2)[i\,\mathrm{e}^{2i\phi}\, c_{l+1}^\dagger c_{l-1} + \mathrm{H.}c.] \\ &+ \frac{1}{L}\sum_l J_l^N \left[\frac{3W}{2}(\tilde{n}_{l+3} + \tilde{n}_{l-2}) + \frac{2V-W}{2}(\tilde{n}_{l+2} + \tilde{n}_{l-1})\right]. \end{aligned} \tag{5.7}$$

In the LR regime the currents can be equivalently derived from the polarization operators [Sha09, LG03, PK03].

5.1.1 Derivation of the energy current for inhomogeneous systems

Let us now allow site–dependent interactions $V \to V_l$ $W \to W_l$ as well as on-site energies ϵ_l. This is the form needed for the thermocouple setup in Chapter 7. The energy density takes the form:

$$H_l = H_{l,l+1}^{tV} + \frac{1}{2}H_{l-1,l+1}^W + \frac{1}{2}H_{l,l+2}^W \tag{5.8}$$

$$\begin{aligned} H_{l,l+1}^{tV} &= \left(-t_h\,\mathrm{e}^{i\phi}\, c_{l+1}^\dagger c_l + \mathrm{H.c.}\right) + V_l\,\tilde{n}_l\,\tilde{n}_{l+1} + \frac{1}{2}\epsilon_l\,\tilde{n}_l + \frac{1}{2}\epsilon_{l+1}\,\tilde{n}_{l+1} \\ H_{l-1,l+1}^W &= W_{l-1}\,\tilde{n}_{l-1}\,\tilde{n}_{l+1} \end{aligned} \tag{5.9}$$

This form of the local energy density has a support on sites $l-1$ through $l+2$, as seen on Fig. 5.1. We look for the PH-symmetric form of J^E, using only the symmetrized number operators $\tilde{\mathrm{n}}$, motivated by requiring a property of J^E: in homogeneous integrable systems ($W = 0$), J^E in this form fulfills

$$[J^E, H] = 0, \tag{5.10}$$

i.e. it is a constant of motion and $\left\langle J^E \right\rangle(t) = \mathrm{const}$.

[1] The derivation is identical for the non PH-symmetrized operator $n_l = \tilde{\mathrm{n}}_l + \frac{1}{2}$

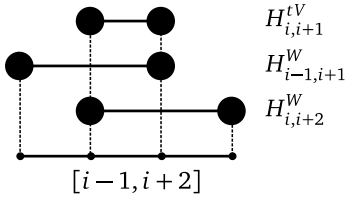

Figure 5.1: Symmetric support of the three parts of the Hamiltonian, compared to the total support.

The partition in 3 distinct terms has been made also to ease the calculation of the commutators. The case of local dependence of the hopping parameter t_h does not need to be separately considered, it is sufficient to perform a transformation $t_h \mapsto (t_h)_l$ in equations (5.5)-(5.7).

From Eq. (5.6) it is evident that we need to compute the commutator of H_l with H and break the term $J^E_{l+1} - J^E_l$ into distinct contributions to the energy current

$$\frac{d}{dt}H_l = i\,[H, H_l] = i\,[\textstyle\sum_j H_j, H_l] \tag{5.11}$$

$$= i\,[H_{l-3} + H_{l-2} + H_{l-1} + H_l + H_{l+1} + H_{l+2} + H_{l+3},\, H_l] \tag{5.12}$$

since all terms with $|l-j| \geq 4$ share no common operators and commute. The task is complicated by the interplay of the interaction beyond nearest neighbors and the locality of the definition of ∇J^E_l. Writing explicitly the values for all H_l,

$$\begin{aligned}\frac{d}{dt}H_l = -\,i\,[&H^{tV}_{l,l+1} + \frac{1}{2}H^{W}_{l-1,l+1} + \frac{1}{2}H^{W}_{l,l+2}\,,\\ &+ H^{tV}_{l-3,l-2} + H^{tV}_{l-2,l-1} + H^{tV}_{l-1,l} + H^{tV}_{l+1,l+2}\\ &+ H^{tV}_{l+2,l+3} + H^{tV}_{l+3,i+4} + \frac{1}{2}H^{W}_{l-4,l-2} + H^{W}_{l-3,l-1}\\ &+ \frac{1}{2}H^{W}_{l-2,l} + \frac{1}{2}H^{W}_{l-1,l+1} + \frac{1}{2}H^{W}_{l,l+2} + H^{W}_{l+1,l+3}]\end{aligned} \tag{5.13}$$

and expanding the big commutator, one obtains two nonzero terms involving only H^{tV}:

$$\left[H^{tV}_{l,l+1}, H^{tV}_{l-1,l}\right],\ \left[H^{tV}_{l,l+1}, H^{tV}_{l+1,l+2}\right]. \tag{5.14}$$

All terms involving only H^W commute, leaving 12 nonzero mixed terms:

$$\begin{aligned}&2\,\frac{1}{2}\left[H^{tV}_{l,l+1}, H^{W}_{l-2,l}\right], && 2\,\frac{1}{2}\left[H^{tV}_{l,l+1}, H^{W}_{l+1,l+3}\right],\\ &\frac{1}{2}\left[H^{tV}_{l,l+1}, H^{W}_{l-1,l+1}\right], && \frac{1}{2}\left[H^{tV}_{l,l+1}, H^{W}_{l,l+2}\right], \frac{1}{2}\left[H^{W}_{l-1,l+1}, H^{tV}_{l-2,l-1}\right],\\ &\frac{1}{2}\left[H^{W}_{l-1,l+1}, H^{tV}_{l-1,l}\right], && \frac{1}{2}\left[H^{W}_{l-1,l+1}, H^{tV}_{l+1,l+2}\right], \frac{1}{2}\left[H^{W}_{l,l+2}, H^{tV}_{l-1,l}\right],\\ &\frac{1}{2}\left[H^{W}_{l,l+2}, H^{tV}_{l+1,l+2}\right], && \frac{1}{2}\left[H^{W}_{l,l+2}, H^{tV}_{l+2,l+3}\right],\end{aligned}$$

where the first two terms are to be counted twice in order to pair each commutator uniquely. Before calculating the explicit values for the above operators, it is useful to separate the contributions to J^E_l in Eq. (5.6) from J^E_{l+1}, leaving only $14/7 = 2$ terms to expand.

The structure of Eq. (5.14) allows one to immediately recognize their sum as a difference between operators defined on two contiguous sites

$$i\left[H^{tV}_{l,l+1}, H^{tV}_{l+1,l+2}\right] + i\left[H^{tV}_{l,l+1}, H^{tV}_{l-1,l}\right] =$$

$$i\left[H^{tV}_{l,l+1},H^{tV}_{l+1,l+2}\right]-i\left[H^{tV}_{l-1,l},H^{tV}_{l,l+1}\right]= J^{E_a}_{l+1}-J^{E_a}_{l} \tag{5.15}$$

we thus define the first current $J^{E_a}_l$ and look for a similar pattern, which holds for 5 of the 7 pairs. The remaining ones encode a difference between second neighbors.

$$\begin{aligned} i\frac{1}{2}\left[H^{W}_{l,l+2},H^{tV}_{l+2,l+3}\right]+i\frac{1}{2}\left[H^{tV}_{l,l+1},H^{W}_{l-2,l}\right]= \\ i\frac{1}{2}\left[H^{W}_{l,l+2},H^{tV}_{l+2,l+3}\right]-i\frac{1}{2}\left[H^{W}_{l-2,l},H^{tV}_{l,l+1}\right]= \\ \bar{J}^{E}_{l+2}-\bar{J}^{E}_{l} \end{aligned}$$

The double difference needs to be interpreted as arising from a partial cancellation:

$$\bar{J}^{E}_{l+2}-\bar{J}^{E}_{l}=(\bar{J}^{E}_{l+2}+\bar{J}^{E}_{l+1})-(\bar{J}^{E}_{l+1}+\bar{J}^{E}_{l}),$$

and the contribution to the current for site l must be interpreted as

$$J^{E_f}_l=\bar{J}^{E}_{l+1}+\bar{J}^{E}_{l}=i\frac{1}{2}\left[H^{W}_{l-1,l+1},H^{tV}_{l+1,l+2}\right]+i\frac{1}{2}\left[H^{W}_{l-2,l},H^{tV}_{l,l+1}\right]$$

The full list of currents contributing to J^E_l is:

$$\begin{aligned} J^{E_a}_l &= i\left[H^{tV}_{l-1,l},H^{tV}_{l,l+1}\right] \\ J^{E_b}_l &= \frac{1}{2}i\left[H^{tV}_{l-1,l},H^{W}_{l-1,l+1}\right] \\ J^{E_c}_l &= \frac{1}{2}i\left[H^{tV}_{l-1,l},H^{W}_{l,l+2}\right] \\ J^{E_d}_l &= \frac{1}{2}i\left[H^{W}_{l-2,l},H^{tV}_{l,l+1}\right] \\ J^{E_e}_l &= \frac{1}{2}i\left[H^{W}_{l-1,l+1},H^{tV}_{l,l+1}\right] \\ J^{E_f}_l &= \frac{1}{2}i\left[H^{tV}_{l-2,l-1},H^{W}_{l-1,l+1}\right]+\frac{1}{2}i\left[H^{tV}_{l-1,l},H^{W}_{l,l+2}\right] \\ J^{E_g}_l &= \frac{1}{2}i\left[H^{W}_{l-2,l},H^{tV}_{l,l+1}\right]+\frac{1}{2}i\left[H^{W}_{l-1,l+1},H^{tV}_{l+1,l+2}\right] \end{aligned}$$

The operators thus defined are automatically Hermitian, since they are the commutator of two Hermitian operators multiplied by i. The commutators are straightforward to calculate, and follow the pattern of an expression involving the number operators $\tilde{n}_l$ and the particle current defined in Eq. (5.5). The current term from Eq. (5.15) deviates from the rule and includes a hopping term between second neighbors. We summarize all the contributions in their full functional form, since they cannot be further simplified:

$$\begin{aligned} J^{E_a}_l &= -t_h^2\left(ie^{2i\phi}{c^\dagger}_{l+1}c_{l-1}+H.c.\right) \\ &\quad +\left(\tilde{n}_{l+1}V_l+\frac{\epsilon_l}{2}\right)J^N_{l,l-1}+\left(\tilde{n}_{l-1}V_{l-1}+\frac{\epsilon_l}{2}\right)J^N_{l+1,l} \\ J^{E_b}_l &= -\frac{1}{2}\tilde{n}_{l+1}W_{l-1}J^N_{l,l-1} \\ J^{E_c}_l &= \frac{1}{2}\tilde{n}_{l+2}W_l J^N_{l,l-1} \\ J^{E_d}_l &= \frac{1}{2}\tilde{n}_{l-2}W_{l-2}J^N_{l+1,l} \\ J^{E_e}_l &= -\frac{1}{2}\tilde{n}_{l-1}W_{l-1}J^N_{l+1,l} \end{aligned}$$

$$J_l^{E_f} = \frac{1}{2}\left(\tilde{n}_{l+1} W_{l-1} J^N_{l-1,l-2} + \tilde{n}_{l+2} W_l J^N_{l,l-1}\right)$$
$$J_l^{E_g} = \frac{1}{2}\left(\tilde{n}_{l-2} W_{l-2} J^N_{l+1,l} + \tilde{n}_{l-1} W_{l-1} J^N_{l+2,l+1}\right)$$

$$J_l^E = J_l^{E_a} + J_l^{E_b} + \ldots + J_l^{E_g} \tag{5.16}$$

We have used the shorthand $J^N_{l,l+1} = i t_h \exp(i\phi)\ c^\dagger_{l+1} c_l + \text{H.c.}$ For a homogeneous, translationally invariant system, the average current $J^E = \frac{1}{L}\sum_{l,i} J_l^{E_i}$ reduces to Eq. (5.7), with an additional $(-\epsilon J^N_{l+1,l})$ contribution due to a shift of the energy by ϵ.

5.1.2 Continuity equation with driving

When the time-dependent magnetic field is varied, according to the linear law $\phi(t) = -Ft$, a constant EM force is induced in the closed loop

$$F_{\text{EM}}(t) = -\frac{\partial \phi(t)}{\partial t} = F. \tag{5.17}$$

All the operators previously defined depend explicitly on the time, through the Peierls' gauge phases in the hopping terms. The only strictly conserved operator is the number of particles N, so the continuity equation (5.4) defining the particle current J^N is invariant.

The Hamiltonian is not conserved in this case, its expectation value in the Schrödinger picture on an arbitrary state $E = \langle H \rangle = \text{Tr}[H(t)\rho(t)]$ varies in time according to

$$\dot{E} = \frac{d}{dt}\langle H(t)\rangle = i\langle [H(t), H(t)]\rangle + \frac{\partial}{\partial t}\langle H(t)\rangle = \left\langle \dot{H}(t)\right\rangle, \tag{5.18}$$

where the partial time derivative acts on $\phi(t)$ in the Hamiltonian definition Eq. (5.8). Remembering that $\partial_\phi H = -L J^N$ and $\dot{\phi} = -F$,

$$\frac{d}{dt}\langle H(t)\rangle = \left\langle \dot{H}(t)\right\rangle = \left\langle \frac{\partial H(\phi)}{\partial \phi}\dot{\phi}\right\rangle = FL\left\langle J^N\right\rangle. \tag{5.19}$$

This is the expression for the expected value of the *Joule heating* in which energy is produced according to the known formula $\dot{E} = JF^2$, derived in a purely quantum setting. Thus, the average energy increases due to frictional effects[3], which counter the flow of the current. This is an effect going beyond the Linear Response (LR) formalism, since the current response is roughly proportional to the applied field F at least at short times, leading to a heating $\dot{E} \propto F^2$.

The Joule effect is a local source of energy, under the form of heat, which provides a right-hand side to the operator continuity equation for the energy density

$$\frac{d}{dt}H_l(t) + \nabla J_l^E(t) = F J_l^N, \tag{5.20}$$

raising the question if the definition of the energy current must be modified in presence of driving to accommodate this part into a definition of $\bar{J}^E$ that restores the form of Eq. (5.6)

$$\frac{d}{dt}H_l(t) + \nabla \bar{J}_l^E(t) = 0.$$

[2]Power equals current times voltage difference, in words.

[3]They are present also in integrable systems driven with a finite field.

However, the equation above implies the conservation of energy

$$\frac{d}{dt}H(t) = \sum_l \frac{d}{dt}H_l(t) = -\sum_l \nabla \bar{J}_l^E(t) = 0, \tag{5.21}$$

since $\sum_l \bar{J}_{l+1}^E - \bar{J}_l^E = 0$ due to the translational symmetry of the system. Thus, the correct definition is given in Eq. (5.20).

Open systems: The continuity equation can be derived also for the evolution of the density matrix $\rho(t)$ of the driven system is modeled by a Lindblad-Liouville equation [Dal14, BP07, AL06] where the effect of the environment are included in the dissipators L_n acting on the system. The equation of motion for $\rho(t)$ reads

$$\dot{\rho}(t) = -i[H, \rho(t)] + \sum_n \big(2L_n\rho(t)L_n^\dagger - L^\dagger L\rho(t) - LL^\dagger\rho(t)\big). \tag{5.22}$$

The evolution of expectation of the local energy density $\langle H_l(t)\rangle(t) = \mathrm{Tr}(H_l(t)\rho(t))$ has an additional contribution due to the action of the dissipators L on the system, which potentially increase the local density of energy

$$\frac{d}{dt}\langle H_l(t)\rangle(t) + \nabla\left\langle J_l^E\right\rangle = F\left\langle J_l^N\right\rangle + \left\langle 2L^\dagger H_l L - H_l L^\dagger L - L^\dagger L H_l\right\rangle. \tag{5.23}$$

If $[L, H_l] = 0$, then the equation is formally the same as Eq. (5.20). The explicit time dependence of $\dot{H}_l = F J_l^N$ enters through the first source term. It should be noted that the dissipator term acts through the Hermitian conjugate on H_l, compared to Eq. (5.22).

5.1.3 Short-time behavior

To avoid redundancy, expressions symmetric in J^N and J^E are derived for both using the symbol $J^{N(E)}$. Moreover, we denote the expectation value of operators using the lower-case version $j^{N(E)} = \left\langle J^{N(E)}\right\rangle$.

The first LR result is the derivation of the expectation values of the currents for $t \to 0$. Their expectation value in an arbitrary equilibrium state at $t = 0$ is zero, due to the time invariance of the initial equilibrium state

$$\mathrm{Tr}\big[J^N(0)\,\rho(0)\big] = \mathrm{Tr}\big[J^E(0)\,\rho(0)\big] = 0. \tag{5.24}$$

In the following simulations, we have chosen the pure microcanonical ensemble explained in Section 3.2.4. The state $\rho(t) = |\psi_E(t)\rangle\langle\psi_E(t)|$ is evolved according to the Time Dependent Schrödinger equation (TDSE) using the algorithm from Section 2.2.

The derivatives of the current operators $\tau^N = -\langle\partial_\phi J^N\rangle$ and $\tau^E = -\langle\partial_\phi J^E\rangle$ are generalized stress coefficients (tensors in anisotropic systems, similar to kinetic energies in the case considered below) determining the short-time LR to the flux change

$$\tau^N = \frac{t_h}{L}\sum_l \big[\mathrm{e}^{i\phi}\, c_{l+1}^\dagger\, c_l + \mathrm{H.c.}\big] = -\frac{H_{\mathrm{kin}}}{L} \tag{5.25}$$

$$\tau^E = \frac{t_h^2}{L}\sum_l \Big\{\big[\mathrm{e}^{2i\phi}\, c_{l+1}^\dagger\, c_{l-1} + \mathrm{H.c.}\big] + \frac{\tau_l^N}{2}\big[3W(\tilde{n}_{l+3} + \tilde{n}_{l-2}) + (2V - W)(\tilde{n}_{l+2} + \tilde{n}_{l-1})\big]\Big\}. \tag{5.26}$$

The local stress coefficient τ_l^N has been introduced in analogy to the J_l^N term in Eq. (5.7).
Shortly after turning on the electric field, the expectation values $\left\langle J^{N(E)}\right\rangle$ can be easily determined from the equations of motion [MP10]

$$\frac{d}{dt}\mathrm{Tr}\big[J^N(t)\,\rho(t)\big]_{t=0} = \mathrm{Tr}\big[\dot{J}^N(0)\,\rho(0)\big] + \mathrm{Tr}\big[J^N(0)\dot{\rho}(0)\big]$$

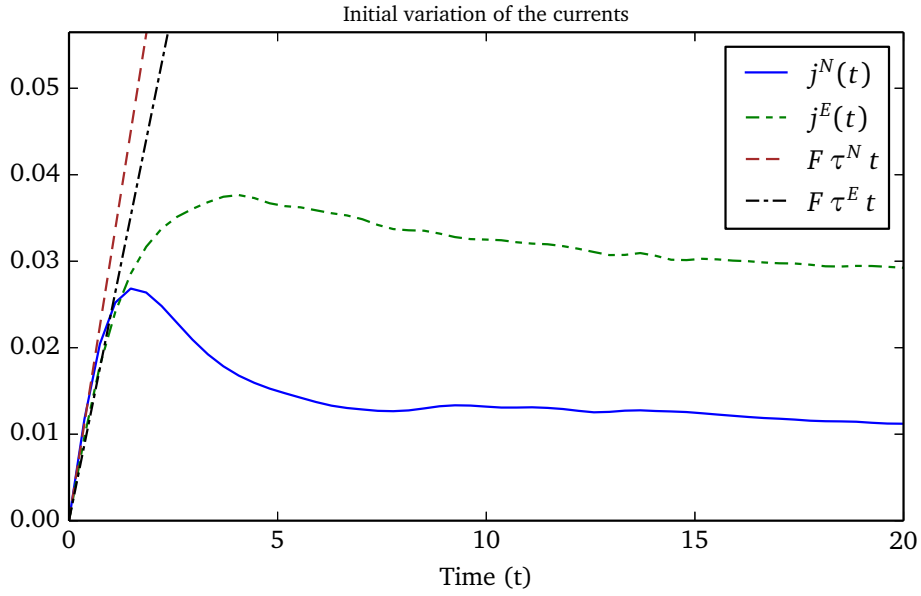

Figure 5.2: Initial slope of the currents, in a driven system with $V = 3, W = 1$, and field $F = 0.2$. The predictions are according to Eq. (5.29)

$$\begin{aligned}\frac{d}{dt}\,\mathrm{Tr}\left[J^N(t)\,\rho(t)\right]_{t=0} &= -\left\langle\,\tau^{N(E)}\,\right\rangle\dot{\phi} + i\,\mathrm{Tr}\left(J^{N(E)}(0)\,[H,\rho(0)]\right)\\ &= -\left\langle\,\tau^{N(E)}\,\right\rangle\dot{\phi} + i\left\langle[H,J^{N(E)}]\right\rangle. \end{aligned} \tag{5.27}$$

In order to obtain the slope, the averages are taken with respect to the initial state $\rho(0)$, which commutes with the Hamiltonian in all cases considered: in the canonical $\rho = \mathrm{e}^{-\beta H}$ and the microcanonical $(H-\mathbb{1}\bar{E})^2|\psi_E\rangle = \sigma_E^2|\psi_E\rangle$. Thus, in any equilibrium state the commutator in the last line vanishes

$$\mathrm{Tr}\left(H\,J^{N(E)}\,\rho(0) - J^{N(E)}\,H\,\rho(0)\right) = \mathrm{Tr}\left(J^{N(E)}\,\rho(0)\,H - J^{N(E)}\,H\,\rho(0)\right) = 0. \tag{5.28}$$

The short–time dependence

$$\frac{d}{dt}\,j^{N(E)}(t) = -\tau^{N(E)}\dot{\phi} = \tau^{N(E)}\,F \tag{5.29}$$

is shown in Fig. 5.2. These estimates fall short for longer times, since the current cannot grow arbitrarily large in a tight-binding system, where all operators are finite and thus bounded. The long–time, which includes contributions from the non-negligible second term of Eq. (5.27), will be the topic of the rest of the chapter.

5.2 Drude weight after a quench

In integrable systems, the conductivity $\sigma^N(\omega)$ is a complex quantity, formed by a regular and a singular component. As explained in Section 1.4, the singular part is delta-valued with strength D^N, called the Drude weight. The long-time expectation value of the current after a quench is thus proportional to D^N, calculated in the relevant initial state. The most reliable and simple way to obtain the Drude weight is to perform a quench and analyze the long-time behavior of the current. Conversely, the LR based approach of the previous section becomes less reliable when applied to integrable systems.

At $t = 0$ we quench the flux $\phi(t) = \Delta\phi\;\theta(t)$ inducing an electric field $F(t) = -\Delta\phi\;\delta(t)$. For this to be consistent with the LR regime, $\Delta\phi \ll 1$. To the first order in $\Delta\phi$ the time–dependent particle

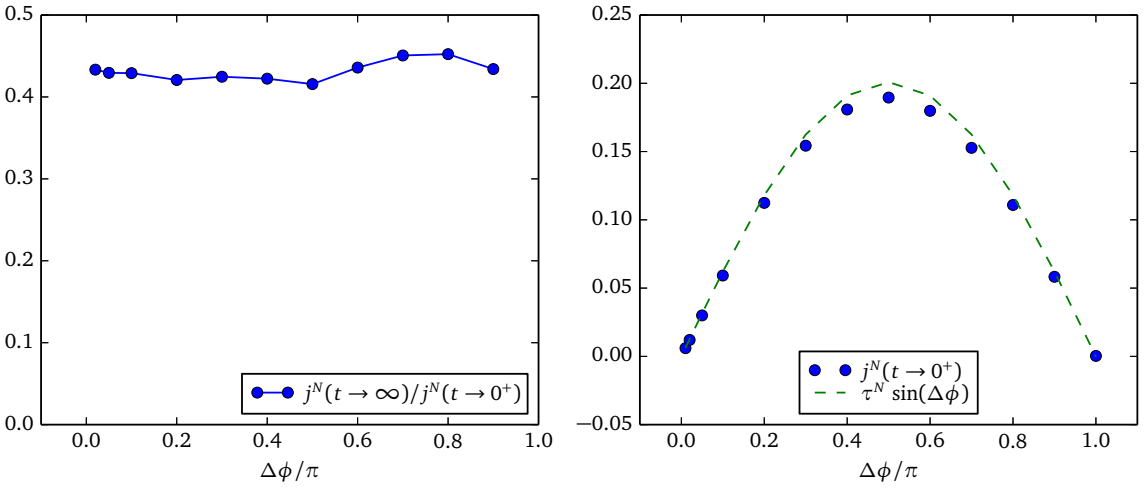

Figure 5.3: Results for quenches in a system with $V = 1.5$, $L = 24, N = 10$ in the microcanonical state corresponding to $\beta = 0.4$. The phase is changed by an amount $\Delta\phi$, as in Eq. (1.70), and the current monitored in time. (a) The ratio of the peak to long-time currents, described by Eq. (5.34). The ratio is found to be independent of the phase quench even for large values of $\Delta\phi$. (b) The initial current depending on the instantaneous phase change. The current expectation value differs from the LR value (5.29) for large values of $\Delta\phi$. The ansatz $t^N \sin(\Delta\phi)$ recovers the correct functional form, allowing a very accurate determination of t^N is required.

current reads

$$j^N(t) = -\tau^N \Delta\phi - iL \int_0^t \langle [J^N(t'), J^N(t)] \rangle \Delta\phi \; dt', \tag{5.30}$$

which gives the peak value $j^N(t \to 0^+) = -\tau^N \Delta\phi$ since the integrand is smooth. The real-time LR current is given by

$$j^N(t) = -\frac{1}{2\pi} \int_{-\infty}^{\infty} d\omega \, F(\omega) \, \sigma^N(\omega) \, \mathrm{e}^{-i\omega^+ t} \tag{5.31}$$

where $F(\omega) = -\Delta\phi$, and σ^N is the complex conductivity. The regular part of σ^N is smooth and gives no contribution to $j^N(t)$ for $t \to \infty$, as it averages to zero due to the Riemann-Lebesgue lemma

$$\lim_{t\to\infty} \int_{-\infty}^{\infty} \sigma^N_{\mathrm{reg}}(\omega) \, \mathrm{e}^{-i\omega t} \; d\omega = 0. \tag{5.32}$$

With the complex singular part $\boldsymbol{\sigma}^N_{\mathrm{sing}}(\omega) = \frac{2iD^N}{\omega + i0^+}$, the current after the quench stabilizes to

$$j^N(t\to\infty) = -\int_{-\infty}^{\infty} \frac{\Delta\phi}{2\pi} \frac{2iD^N}{\omega + i0^+} \, \mathrm{e}^{-i\omega t} \; d\omega \overset{Res}{=} -2D^N \Delta\phi. \tag{5.33}$$

We have calculated the ratio of the peak to long time currents also for finite $\Delta\phi$ and estimate the ratio of the Drude weight intervening in the quench to the sum-rule expectation value:

$$\frac{j^N(t\to\infty)}{j^N(t\to 0^+)} = \frac{2D^N_{\mathrm{quench}}}{\tau^N}, \tag{5.34}$$

which is needed later. The quench protocol provides the fastest way to numerically compute the Drude weight in an arbitrary, canonical or microcanonical, initial state, to high accuracy as shown in Fig. 5.3.

5.3 Generalized Linear Response in a driven quantum system

Once we switch on the electrical field $F(t) = \text{const} > 0$, the system goes into a nonequilibrium state. The effect of the field is the generation of currents continuously flowing through the ring. The naive expectation would be a steady flow of current through the system, set by the intrinsic conductance, in accordance to the LR formalism. A steady *dc current* naturally corresponds to the zero-frequency ($\omega \to 0$) component of the current response $j^{N(E)}(\omega)$, which is the long-time limit of the real-time response

$$\lim_{t\to\infty} j^{N(E)}(t) = \lim_{\omega\to 0} j^{N(E)}(\omega), \tag{5.35}$$

where the limit is understood to hold for properly averaged values, since the zero-frequency component is the integral average of the real-time signal. As we have shown, the steady-state response at zero frequency in the LR regime is connected to the real part of the relevant transport coefficient[4]

$$j^N(\omega = 0) = \sigma^N(\omega = 0)\, F \qquad \text{and} \qquad j^E(\omega = 0) = \sigma^E(\omega = 0)\, F, \tag{5.36}$$

proportionally to the external applied field. Plotting $j^N(t)/F$ and $j^E(t)/F$ in Fig. 5.4 shatters this expectation: there is no steady–state response for closed quantum systems. We will now proceed to show how to derive a generalized Linear Response in this setting.

The energy is not constant in a driven quantum system with finite $F > 0$. The instantaneous energy, given by the expectation value of the time-dependent Hamiltonian in the time-evolved state, is growing in time according to Eq. (5.19)

$$\dot{E}(t) = L\, F\, j^N(t), \tag{5.37}$$

where $E(t)$ and $j^N(t)$ denote the average value of the energy and particle current respectively, as explained before. In thermal equilibrium, the temperature and the energy are closely connected, by the thermodynamical equations (2.40) or the equivalent (3.34) of the form

$$E(\beta) = \langle H \rangle_\beta = f[\beta]. \tag{5.38}$$

If the rate of heating, set by the external field F, is not too high, there is a chance for a redistribution of the energy across all degrees of freedom of the system under the form of heat. We call this regime *Local Quasi Equilibrium* (LQE). We define an effective, time-dependent temperature β_{eff} set by the *instantaneous energy* of the system

$$\beta_{\text{eff}}(t) = f^{-1}[E(t)]. \tag{5.39}$$

We will prove in Chapter 6 that indeed the energy increase is due to heating, by showing that the reduced density matrix of any subsystem is thermal at the temperature $\beta_{\text{eff}}(t)$.

The effective temperature increase is due to the closeness of the system, which prevents a transfer of the excess heat to an external environment. The increase of the internal energy in a quasistatic process, lacking any work to be done by the system, goes into entropy production, according to the combined first two laws of thermodynamics

$$T\, dS = dE - \delta W = dE \quad \text{when } \delta W = 0. \tag{5.40}$$

In Section 2.4, we have carefully analyzed the equilibrium conductivity of a generic quantum system,

[4] Generalizing the conductivity also for the case of j^E

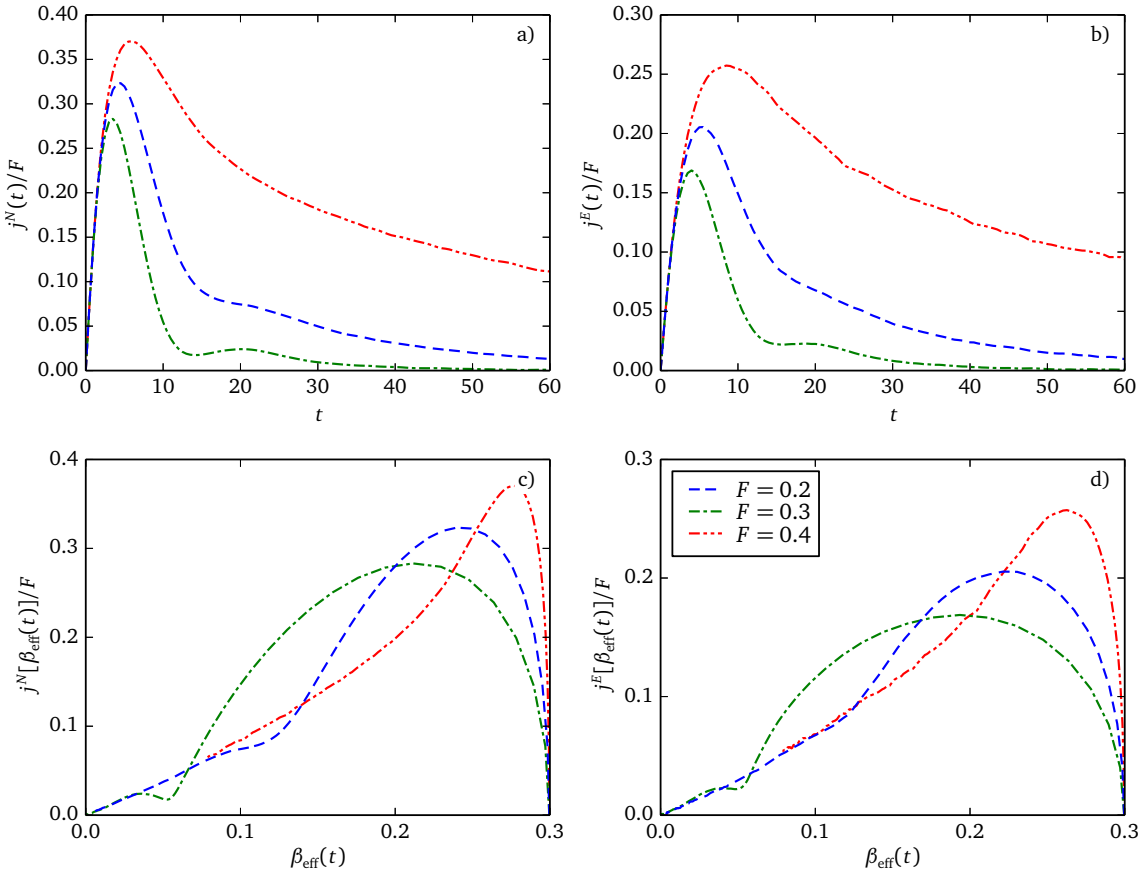

Figure 5.4: Expectation values of the time-dependent conductivities, i.e. the currents j^N and j^E in a $L = 26, N = 11, V = 1.5, W = 1.0$ system, divided by the inducing field F, for different values of the external driving field. (a) and (b) show the currents divided by the field as a function of time, which leads to an apparent wildly different value of the conductivities. (c) and (d) the same data is plotted as a function of the time-dependent inverse temperature $\beta_{\rm eff}(t)$. The evolution starts at $\beta = 0.3$ and proceeds towards $\beta = 0$, where the system response converges to a universal value of the conductivity, given by equation (5.41).

defined in the LR limit of the external field $F \to 0$. The transport coefficient $\sigma^{N(E)}$ depends strongly on the inverse temperature of the system, through the explicit β parameter in Eq. (2.78), and implicitly through the state $|\psi_{E(\beta)}\rangle$ in Eq. (2.79). The effective increase in the temperature is reflected by the conductivity σ^N and σ^E, which are not functions of the frequency alone, but also of the effective temperature. The correct generalized response depends on the time through the instantaneous energy

$$j^N(t) = \sigma^N\left(\beta_{\rm eff}(t)\right) F \qquad \text{and} \qquad j^E(t) = \sigma^E(\beta_{\rm eff}(t))\, F, \tag{5.41}$$

where we denote by $\sigma^{N(E)}(\beta)$ the *dc* (zero-frequency) component at the effective temperature. The proper functional form in the time domain involves a convolution in the form $j^{N(E)}(t) = \int_0^t \sigma^{N(E)}(t-t')F(t')\,dt'$ as done in Ref. [MP10], but we analyze only the long-time behavior. From Eq. (2.78) the main contribution to the temperature dependence can be isolated in the exponential, which can be expanded for small β in series

$$\frac{1-\mathrm{e}^{-\beta\omega}}{\omega} \approx \beta \Longrightarrow \sigma^{N(E)}_{\rm reg}(\omega) \approx L\,\beta\ \mathrm{Im}\, C^{>}_{N(E)}(\omega). \tag{5.42}$$

The correlation–function dependence on $|\psi_{E(\beta)}\rangle$ is much weaker for the *dc* component ($\omega = 0$), so the main contribution of the temperature is through the β factor in (5.42). Plotting the currents dependence

as a function of time, as in Fig. 5.4(a-b) does not show the clear existence of the linear relation (5.41), whereas a plot as a function of $\beta_{\text{eff}}(t)$ in Fig. 5.4(c-d) allows us to define a *generalized Linear Response* for weakly-driven generic quantum systems.

5.4 Current ratios in generic systems

We study the ratio of the expectation values of the currents

$$R(t) = \frac{j^E(t)}{j^N(t)}, \tag{5.43}$$

in systems that are generic, i.e. non-integrable. The ratio measures the coupling of the charge and energy transport in the ring, as explained in Section 1.5.1. When the system is driven, the currents initially increase at a rate set by the respective operator derivatives according to Eq. (5.29), hence the short–time ratio of the energy and particle currents

$$R(t \to 0^+) = \frac{\tau^E}{\tau^N}, \tag{5.44}$$

is field–independent and always consistent with the LR theory [LG03, ZP05]. In tight-binding model, where the system volume is finite and the energy levels are discrete and bounded, the expectation values of all operators are also bounded. If the current in a *dc response* were constant, the steady increase in the energy produced by the Joule effect (see Eq. 5.19) would imply a constant growth of the energy, which is impossible due to the upper bound of the energy spectrum. Furthermore, the infinite temperature state is a fixed point of an arbitrary unitary time evolution

$$\rho_{\beta=0,t} = U(t,0)\left(\frac{1}{D}\mathbb{1}\right)U(t,0)^\dagger = \rho_{\beta=0}, \tag{5.45}$$

thus it is not possible to raise the energy of a system by driving, once it reaches the local equilibrium temperature $\beta = 0$ at the corresponding infinite-temperature energy $E_\infty = D^{-1}\,\mathrm{Tr}[H]$.

We have shown how the long-time dependence can be reconciled with the LR expectation by taking into account heating effects in Section 5.3. The ratio of the currents provides a natural way to take into account the heating, since for $\beta \to 0$, the thermal effects cancel out, and $R(t \to \infty)$ is well-defined and finite

$$R(t \to \infty) = \frac{\sigma^E(\omega \to 0, \beta \to 0)}{\sigma^N(\omega \to 0, \beta \to 0)} = \frac{C_E^>(\omega \to 0, E \to E_\infty)}{C_N^>(\omega \to 0, E \to E_\infty)}, \tag{5.46}$$

with the effects of the external field F and the biggest temperature dependence, the β factor in σ, canceling exactly. A limiting procedure in necessary owing to the fact that each of the quantities is strictly zero in the $\beta = 0$ limit, which is attained by choosing the infinite-temperature energy E_∞ in the microcanonical ensemble in Eq. (2.79). Thus, the calculations are performed slightly below E_∞, or alternatively at the average instantaneous temperature $\beta(t)$ to predict a ratio curve.

In order to robustly estimate the time-dependent $R(t)$ in the long-time limit, we resort to least-squares fitting of j^E against j^N for long times $t > t_0 \simeq 50$, determined by

$$\frac{d}{dR}\sum_i \left[j^E(t_i) - R\, j^N(t_i)\right]^2 = 0, \tag{5.47}$$

which does not suffer from numerical instabilities in the regime where both the currents tend to zero, due to the temperature increase. It can be seen in Fig. 5.5(a) that in the limit of $F \to 0$ the LR expectation

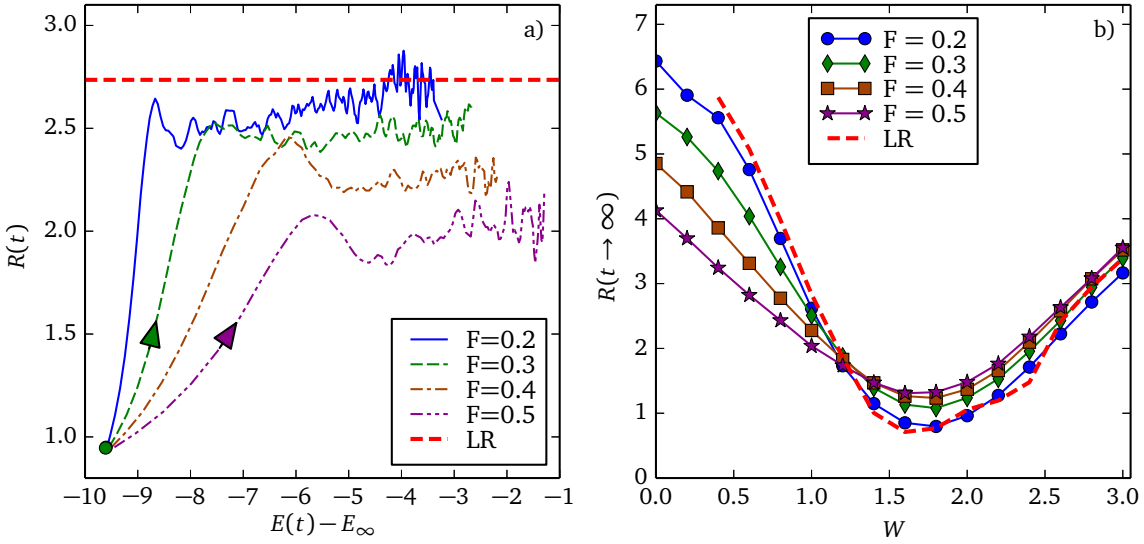

Figure 5.5: Ratio of currents for a generic driven system, with $L = 24, N = 10, V = 3$ and $W = 1$ in the first panel. (a) Time dependent ratio $R(t)$ as a function of the instantaneous energy $E(t) - E_\infty$, so the zero value corresponds to infinite temperature. The various curves correspond to different driving fields F. $R(0)$ is at the value τ^E/τ^N evaluated in the initial state. The LR line is the prediction of Eq. (5.46), calculated close to $\beta = 0$. (b) Estimated $R(t \to \infty)$ as a function of the integrability-breaking interaction W. The value $W = 0$ corresponds to an integrable system where the LR prediction breaks down. The LR value is calculated as before.

can be reliably recovered, proving that the extrapolation of the response of a finitely-driven quantum system is well-defined and convergent. The tiny oscillations of currents around their average values originate from the finiteness of the system simulated and the use of a single initial state. However small these oscillations are, they eventually dominate when the system approaches $\beta \to 0$ and the smooth components of the currents vanish. Then, the numerical results for $R(t)$ being the ratio of two vanishing quantities unavoidably becomes noisy (see Fig. 5.5(a)). These oscillations have no physical meaning and can be reduced by either increasing the system size or by averaging over many initial states.

On the other hand, in the case where $W \to 0$, the LR response is poorly defined due to the delta-like behavior of $\sigma^{N(E)}(\omega)$. At the same time, the independence of the expectation values from the microscopical initial state and the (local-)equilibration in time break down at the onset of integrability. Thus, even the time-dependent data and the fitting through Eq. (5.47) develops singularities, as we show in the remainder of the chapter.

5.5 Strong–field Bloch oscillations

Another source for the break-down of the time evolution method used to obtain $R(t)$ in driven quantum systems, is the appearance of Bloch oscillations for the strongly–driven case. This is a universal feature in lattice models, which has been proven in the real-time domain in a diverse set of microscopic Hamiltonians [BK03], in particular for the Falicov–Kimball model on infinite–dimensional lattice [Fre08], previously for this model of one–dimensional interacting spinless fermions [MP10], for the infinite–dimensional Hubbard model [EW11],the one–dimensional extended Hubbard model [ECP14]. They have been experimentally observed in a semiconductor superlattice [FLS$^+$92], cold atoms [BPR$^+$96], and kicked quantum rotor molecules [FKAB15, FA14]. All tight-binding quantum systems undergo the Bloch oscillations if the driving field is sufficiently strong, a phenomena which is due to the phase oscillation

in the phase–dependent part of the operators. We briefly review its origin and the consequences. Here we choose the arguments which apply not only to the particle currents but also to the energy currents.

As argued earlier in Section 5.1, the density of particle and energy currents can be found from continuity relations. While the explicit solution of these equations is clearly model dependent, the current operators consist of terms which share a common structure. In the case of one–dimensional systems, one expects the following general structure of the particle and the energy currents (in the Schrödinger picture):

$$\begin{aligned} J_k(t) &= \sum_\alpha J_k^\alpha(t), \\ J_k^\alpha(t) &= [i\, e^{i(b-a)Ft}\, c^\dagger_{k+a} c_{k-b} + \text{h.c.}]\, f(\tilde{n}_k, \tilde{n}_{k\pm1}, \tilde{n}_{k\pm2}, \ldots), \end{aligned} \tag{5.48}$$

where f is a certain function of the particle–number operators which is independent of the magnetic flux ϕ. Various contributions (labeled by α) may involve different functions f and hopping terms (described by a and b). It is convenient to introduce generalized auxiliary stress-tensor operators generalizing equations (5.25-5.26), which have the form of a correlated-hopping energy density

$$\tau_k^\alpha(t) = [e^{i(b-a)Ft}\, c^\dagger_{k+a} c_{k-b} + \text{h.c.}]\, f(\tilde{n}_k, \tilde{n}_{k\pm1}, \tilde{n}_{k\pm2}, \ldots). \tag{5.49}$$

In equilibrium $\langle J_k^\alpha \rangle$ vanishes, while its operator derivative $\langle \tau_k^\alpha \rangle$ is in general non-zero. Considering the evolution in the time–window (t_0, t) one finds the following identity

$$\begin{aligned} \left\langle \psi(t) \left| J_k^\alpha(t) \right| \psi(t) \right\rangle = &\cos[F(t-t_0)(b-a)] \left\langle \psi(t) \left| J_k^\alpha(t_0) \right| \psi(t) \right\rangle \\ &+ \sin[F(t-t_0)(b-a)] \left\langle \psi(t) \left| \tau_k^\alpha(t_0) \right| \psi(t) \right\rangle. \end{aligned} \tag{5.50}$$

The energy spectrum of the tight–binding models is bounded from above hence changes of the matrix elements on the RHS of Eq. (5.50) cannot be arbitrary fast. In particular one does not expect significant changes of these matrix elements on a time scale that is much shorter than the relaxation time after instantaneous quenches. It means that one can always find a sufficiently short time window (t_0, t) and sufficiently strong F that the time–dependence of $\left\langle \psi(t) \left| J_k^\alpha(t_0) \right| \psi(t) \right\rangle$ is governed by the oscillating functions $\cos[F(t-t_0)(b-a)]$ and $\sin[F(t-t_0)(b-a)]$.

To summarize this discussion we note that under external driving, the current operators explicitly depend on time also in the Schrödinger picture. For sufficiently strong driving this dependence prevails, leading to the Bloch oscillations of the particle and energy currents, which should be generally expected for tight–binding models. The extension of the above reasoning to the case of spinful fermions and multidimensional systems is straightforward.

In the context of our model, the generalized currents are the ones corresponding from J^N and from the two contributions (as shown in Eq. 1.36 and on the different lines in Eq. 5.7) of J^E, labeled J^{E_1} and J^{E_2} for clarity. The phase difference in J^{E_2} is the same as J^N, with $(b-a)=1$. On the other hand, the two-site hopping in J^{E_1} (and the corresponding τ^{E_1}) generates a term with a phase proportional to e^{2iFt}. The latter term cannot be in phase with J^N, precluding a coherent oscillation of the two currents. Due to an exact doubling of the frequency of their oscillations the currents form a damped Lissajous figures in the parametric plane (j^E, j^N) as shown in Fig. 5.6.

The strong–field BO are seen when the driving field F is much stronger than the interaction even for interacting insulators with $V \geq 3$. In general, the strong–field BO irreparably break the equivalence

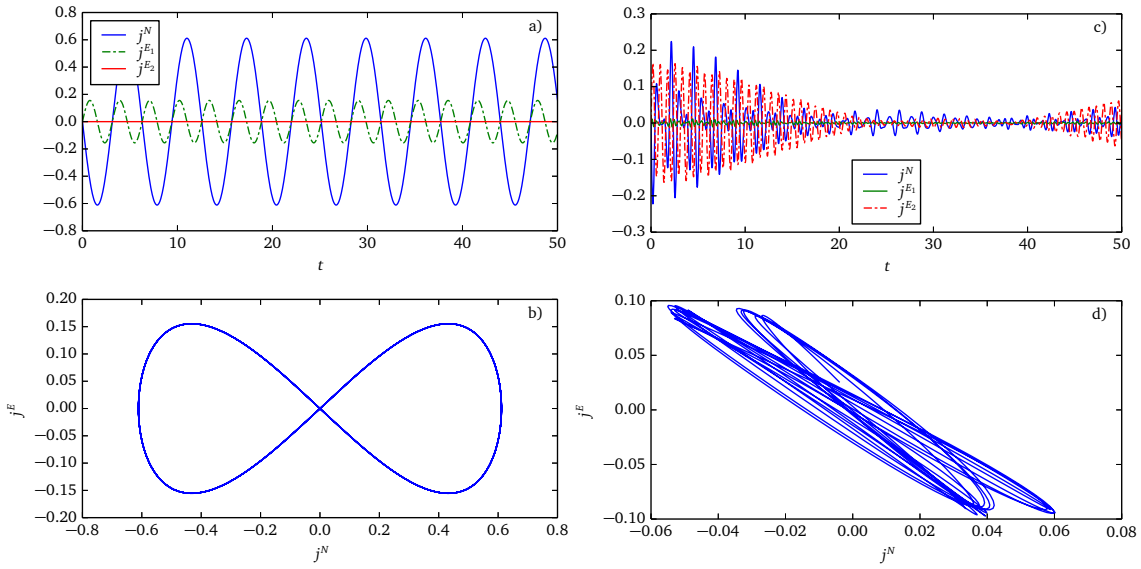

Figure 5.6: Plots of the currents for systems displaying strong Bloch oscillations. (a) Plot of the currents for a system of free fermions with $V = 0$. (b) Parametric plot of the currents for the free fermion system, showing the doubling of the frequency of j^{E_1} as a Lissajous figure. (c) Strongly-interacting doped insulator with $V = 3, W = 1$, under strong field $F = 8.0$. The beat pattern in the currents is the same as found in Ref. [Fre08] (d) Parametric plot of the data presented in (c), showing a deformed Lissajous figure analogous to the one in (b).

between the instantaneous energy and the effective temperature. When the currents oscillate, the system cannot be in the local equilibrium regime, since the energy becomes a non-monotonic function of time. The understanding of Eq. (5.19) as a source of heat due to Joule effect also needs to be abandoned, since heat cannot be properly understood in a non-equilibrium setting. Thus the limits of our approach are identified: as soon as the currents become nonmotononous and oscillate, the effective temperature $\beta_{\text{eff}}(t)$ and ratio of currents $R(t)$ cannot be determined.

In the non-interacting case, with $V = W = 0$, or its perturbations with $V \ll 1$, no proportionality can be expected between J^N and J^E: $R(t)$ is thus ill-defined. This is clearly demonstrated in free systems, where the Bloch oscillations are exactly described by Eq. (5.50). The continuous transition to the monotonous behavior of interacting systems can be seen in Fig. 5.7, where the proportionality is restored.

5.6 Driven integrable doped Mott insulators

After showing that our method to determine $R(t \to \infty)$ reliably applies to the driven generic case, we restrict the scope to driven integrable systems and set $W = 0$, with $V > 2$ in this chapter.

According to the LR theory, j^N and j^E should grow linearly in time for a *dc* driving. However, this linear growth cannot be unlimited in time under a finite driving as argued in the preceding sections. Then, the currents may develop either into BO or into a decreasing quasistatic current as observed for generic systems. The latter is also possible since finite F breaks the integrability. Figure 5.8(a) shows that the strength of the driving determines the scenario which prevails. We observe oscillatory response in the limits of very weak and very strong driving, and quasisteady currents for the intermediate F.

The relation between j^N and j^E can be inferred from Fig. 5.8 as well as from the parametric plots shown in Fig. 5.9. For a weak–to–moderate driving, both currents are roughly proportional to each

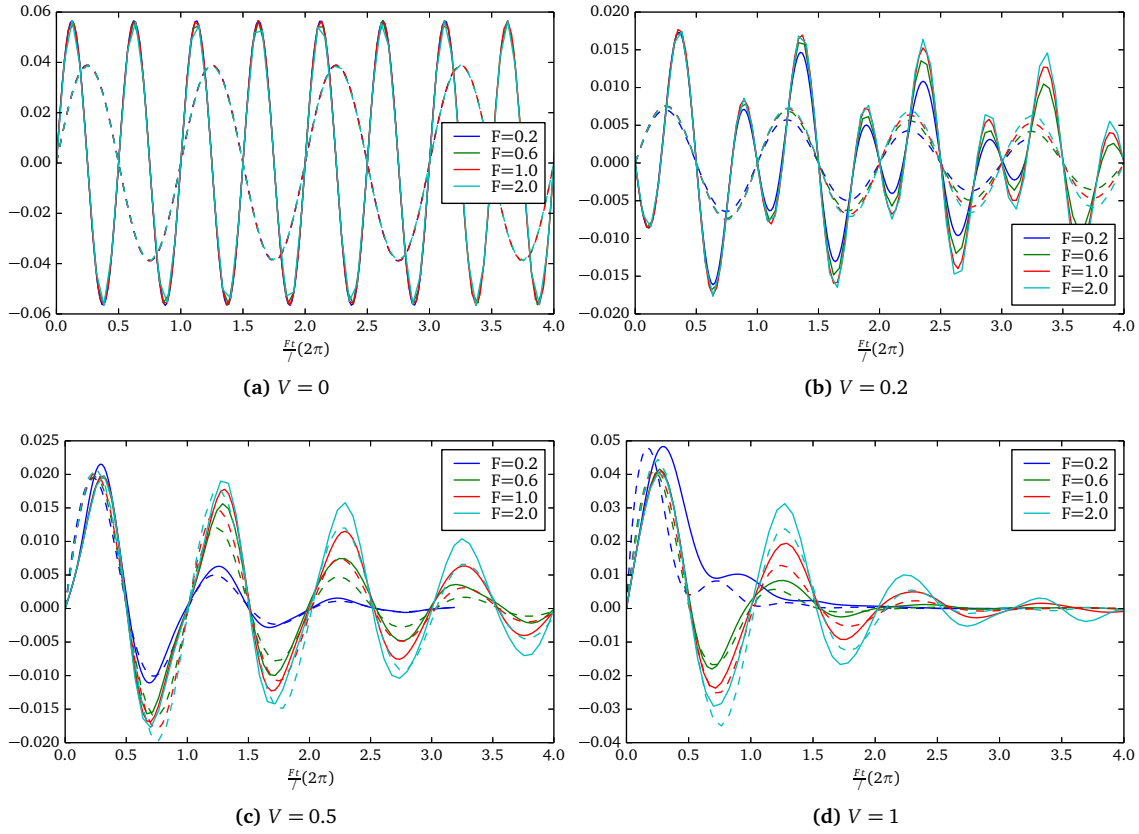

(a) $V = 0$ **(b)** $V = 0.2$

(c) $V = 0.5$ **(d)** $V = 1$

Figure 5.7: Expectation values for the currents j^E (solid) and j^N (dashed, same color) plotted together as a function of the rescaled phase for different values of the driving field F. The system is (nearly)-noninteracting with $L = 24, N10$. For weak interactions the currents have very different periods, since J^{E_1} is negligible. For $F \simeq V$, the oscillations are in phase.

other. It holds true independently of whether these currents are quasistatic as shown in figures 5.8(b) and 5.9(b) or undergo the Bloch oscillations (Fig. 5.6). Hence in this regime the ratio $R(t)$ is indeed well defined and meaningful despite the singular LR of the integrable system. The proportionality between oscillating currents j^N and j^E for $F \to 0$ is rather unexpected. Such proportionality is evidently broken for BO for very weak V (see Fig. 5.7) and/or large F (see Fig. 5.6).

In order to explain the numerical results we first focus on the regime of intermediate driving, when currents show the same steady behavior as in generic systems under quasiequilibrium evolution. Hence, we apply a similar phenomenological modification of LR which turned out to be successful in the case of generic systems [MP10, MBP11]. Since the driving itself is sufficient to damp oscillations of the energy current, the main effects must be the broadening of the singular response functions [AG02].

A phenomenological attempt would be to modify Eq. (1.72) using a Lorentzian ansatz with an effective scattering rate $\Gamma[F]$

$$\delta(\omega, F) \longrightarrow \frac{1}{\pi} \frac{\Gamma[F]}{(\omega^2 + \Gamma[F]^2)}. \tag{5.51}$$

It leads to an effective *dc* response $\sigma^E(\omega \to 0) = \tau^E/\Gamma$ and a quasistatic energy current

$$j^E = \frac{\tau^E}{\Gamma} F. \tag{5.52}$$

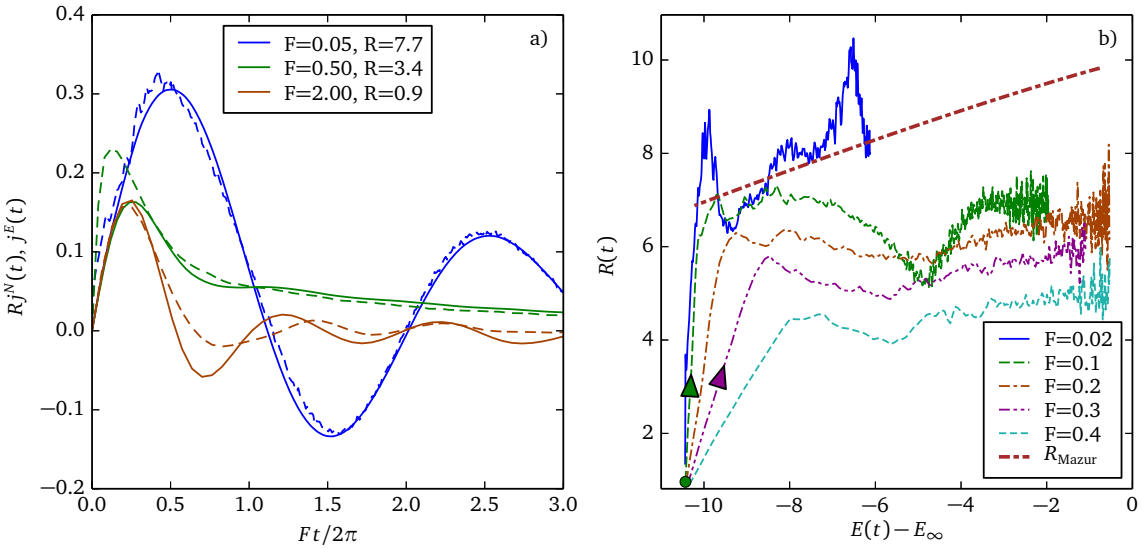

Figure 5.8: Currents for $L = 24, N = 10$, $V = 3$ and $W = 0$. (a) $j^E(t)$ (solid lines) together with $Rj^N(t)$ (dashed lines) for R shown in the legend. (b) $R(t)$ vs instantaneous energy compared to R_{Mazur} [see Eq. (5.54)].

We have used this formula together with the numerical data for $j^E(t)$ and determined the (phenomenological) effective scattering rate shown in Fig. 5.10(a). One may observe that Γ increases with F and after the initial transient it becomes independent of the instantaneous energy. Therefore the heating effect (dependence on the energy) is included entirely in the sum rule τ^E, while Γ describes solely the broadening of the response–function by external driving.

It is also interesting that the numerical values of Γ are very close to F, so the effective scattering (damping) rate is close to the frequency of the BO ($\omega_B = F$). Therefore, within this phenomenological picture the regime of the quasistatic current is just at the boundary of overdamped BO.

The same reasoning should also hold for the particle current, however the numerical analysis would be much more demanding since close to half-filling ($\langle n\rangle \sim 1/2$) the stiffness $D^N \ll \tau^N/2$ in contrast to $D^E = \tau^E/2$. However, with the strong assumption that a single scattering rate gives the broadening of both response functions, one may estimate the ratio $R(t\to\infty)$ in the quasi-equilibrium regime

$$R(t\to\infty) = \left.\frac{2\pi D^E \delta(\omega,F)}{2\pi D^N \delta(\omega,F)}\right|_{F\to 0}. \tag{5.53}$$

The finite scattering introduced in Eq. (5.51) provides a *regularization* of the singular response functions. In the limit of $F\to 0$ this allows to have a well-defined ratio.

The current ratio can be estimated using an alternative approach to the LR conductivities, using Mazur's inequality introduced in Section 1.4. The expectation value $j^N(t\to\infty)$ can be bounded from below by the projection of J^N on the most relevant local conserved operator $Q_3 = J^E$, using Eq. (1.75). Thus, $R = D^E/D^N$ is estimated via the Mazur's inequality

$$R_{\mathrm{Mazur}} = \frac{D^E}{D^N_{\mathrm{Mazur}}} = \frac{\tau^E}{\beta L}\frac{\langle J^E J^E\rangle}{\langle J^N J^E\rangle^2} > \frac{D^E}{D^N}. \tag{5.54}$$

The results in Fig. 5.8(b) and 5.10(b) in fact show that $R(t\to\infty)$ is reasonably close to R_{Mazur}, provided F is small enough. In the published article, the deviations between the results from the real–time dynamics and Eq. (5.54) in Fig. 5.10(b) were overestimated, since R_{Mazur} was determined at $E\to E_\infty$, instead of the highest reachable energy $E(t_{\mathrm{max}})$ as done here.

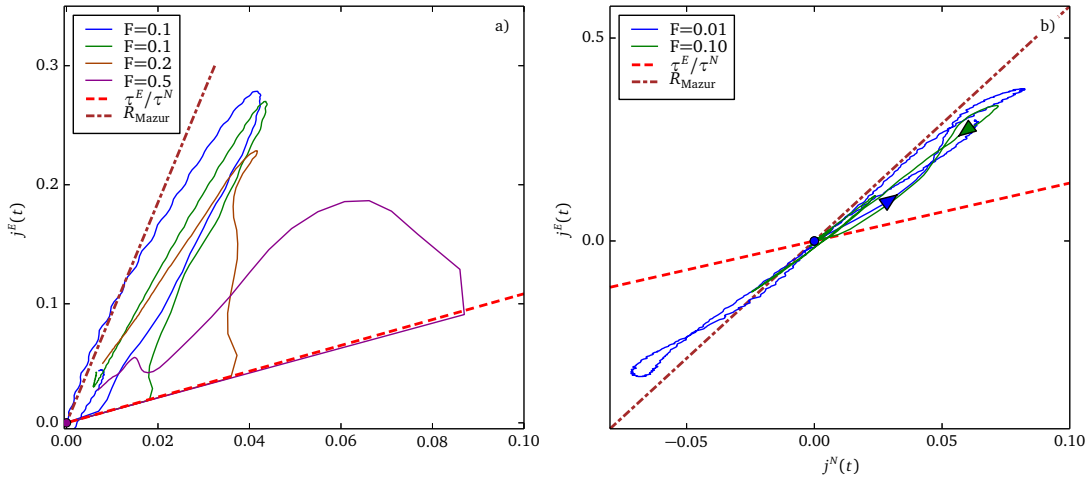

Figure 5.9: Parametric plots $j^E(t)$ vs. $j^N(t)$ for $V = 3, W = 0$. (a) Results for $L = 24, N = 10$ (b) $L = 26, N = 9$ In the two latter panels the straight lines show τ^E/τ^N for the initial β [see Eq. (5.44)] and $R_{\rm Mazur}$ for $\beta \to 0$ [see Eq. (5.54)].

Quite surprisingly, the prediction (5.54) is accurately fulfilled also for weaker driving when both currents oscillate. In Fig. 5.9(b) such behavior is shown for a different filling factor, providing an independent test. After a short transient, the currents oscillate perfectly in phase with a relative amplitude R satisfying the Mazur bound of Eq. 5.54, regardless of F. This agreement makes a clear connection between the BO under finite but weak F, and the stiffness within the LR theory. Note also that this relation is broken for large F, when BO are independent of integrability and occur also in generic systems.

5.7 Integrable metals close to half-filling

We now turn to the case $V < 2$ when the system is metallic at arbitrary filling factor. For moderate fields, currents again display only modest oscillations, so the ratio $R(t)$ can be determined directly, as shown in Fig. 5.11.

It has been shown for integrable metals at half–filling that the Mazur bound needs to be formulated in terms of quasi-local conserved operators, as mentioned in Section 1.4.1, otherwise $D^N_{\rm Mazur} = 0$ while D^N stays nonzero. For slightly smaller concentration of fermions [HPZ11] ($\langle n\rangle < 1/2$), D^N is still much larger than $D^N_{\rm Mazur}$, hence the ratio $R(t \to \infty)$ was expected to be consistently lower than $R_{\rm Mazur}$ formulated in terms of J^E alone (see Eq. 5.54).

However, the numerical data in Fig. 5.11 show that $R(t)$ departs from LR and approaches $R_{\rm Mazur}$, as if the energy current were the only relevant conserved quantity. Figure 5.12(a) shows $R(t \to \infty)$ calculated for small but nonzero W in comparison to the LR results obtained directly from the response functions as well as with $R_{\rm Mazur}(W = 0)$. Upon decreasing W, the response of a driven integrable system splits for different fields, departing from the predictions of LR theory towards $R(t \to \infty)$ for $W = 0$. When the dissipation induced by the electric field is minimal, the currents oscillate in phase with maximal amplitude, in analogy to the case of doped insulators.

We expect that breaking the integrability by finite F is responsible for the observed departure from LR regime. In order to verify this expectation we have compared the response of the system driven by $F > 0$ with its nonequilibrium relaxation at $F = 0$. In particular, we have calculated the value of the

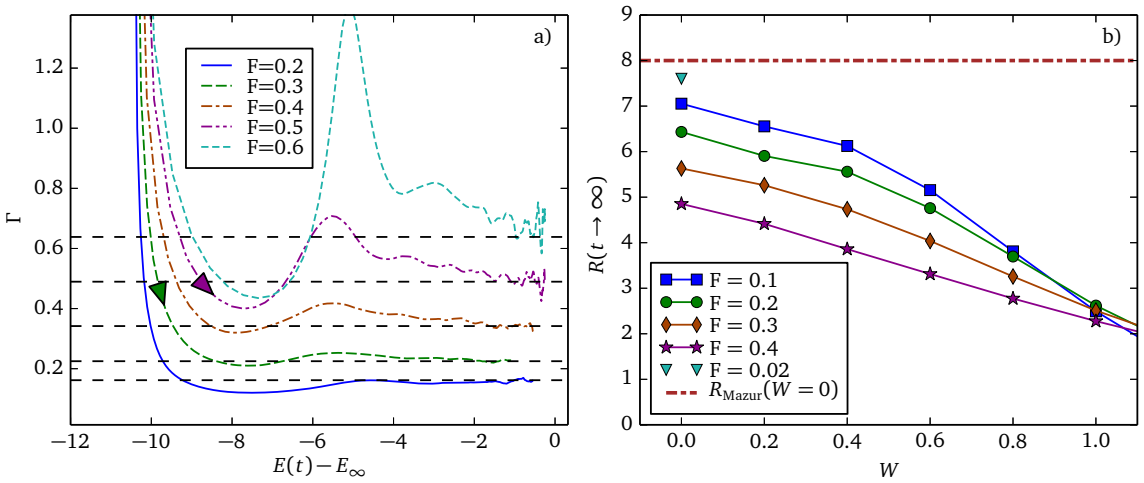

Figure 5.10: Results for $V = 3$, $L = 24$ and $N = 10$. (a) Phenomenological scattering rate Γ as a function of the instantaneous energy for $W = 0$. (b) $R(t \to \infty)$ for small but finite integrability-breaking interaction W The value of $R_{\rm Mazur}$ (at $\beta = 0.2$) for $W = 0$ is shown for comparison.

stiffness in 4 different ways, which we expected to merge when LR theory is applicable.

1. $D^N_{\rm Mazur}$ given by Eq. (1.75)

2. The proper charge stiffness calculated from the sum rule in Eq. (2.78), computing the regular conductivity in the initial microcanonical state

$$D^N_{\rm LR} = \frac{\tau^N}{2} - \frac{1}{2\pi}\int_{-\infty}^{\infty} \sigma^N_{\rm reg}(\omega)\, d\omega. \tag{5.55}$$

3. The stiffness under long-time driving. For a system evolving under finite F one can estimate the charge stiffness from $R(t \to \infty)$ assuming that $j^E/j^N \simeq D^E/D^N_{\rm driving}$ holds in long–time regime similarly to the case of doped insulators. Then,

$$D^N_{\rm driving} = \frac{\tau^E}{2R(t\to\infty)}. \tag{5.56}$$

4. The stiffness of a system undergoing an instantaneous change of the magnetic flux which should also be consisted with LR. This corresponds to the determination of D^N from the quench protocol shown in Fig. 5.3 and quantified by Eq. (5.34)

$$\frac{j^N(t\to\infty)}{j^N(t\to 0^+)} = \frac{2D^N_{\rm quench}}{\tau^N}. \tag{5.57}$$

All these estimates of the stiffness are compared in Fig. 5.12(b). For vanishing electric field $D^N_{\rm driving}$ approaches $D^N_{\rm Mazur} \ll D^N$, whereas $D^N_{\rm quench}$ nicely reproduces the LR result $D^N_{\rm LR}$. The latter agreements holds also for strong quenches $\Delta\phi$, i.e. for relaxation from far–from–equilibrium states. This leads to different expectations of R depending on the method used to estimate D^N, and different measured thermoelectrical responses: if the system is driven, the long–time value of the current j^N is lower than in the quench protocol, whereas the response for the energy current is proportionally the same, leading to differing values for the thermoelectrical response.

It remains to be checked whether $j^E(t)/j^N(t)$ approaches $R_{\rm Mazur}$ also for other driven integrable systems. Recent results [MPP15b] suggest that higher order conserved quantities, having a support

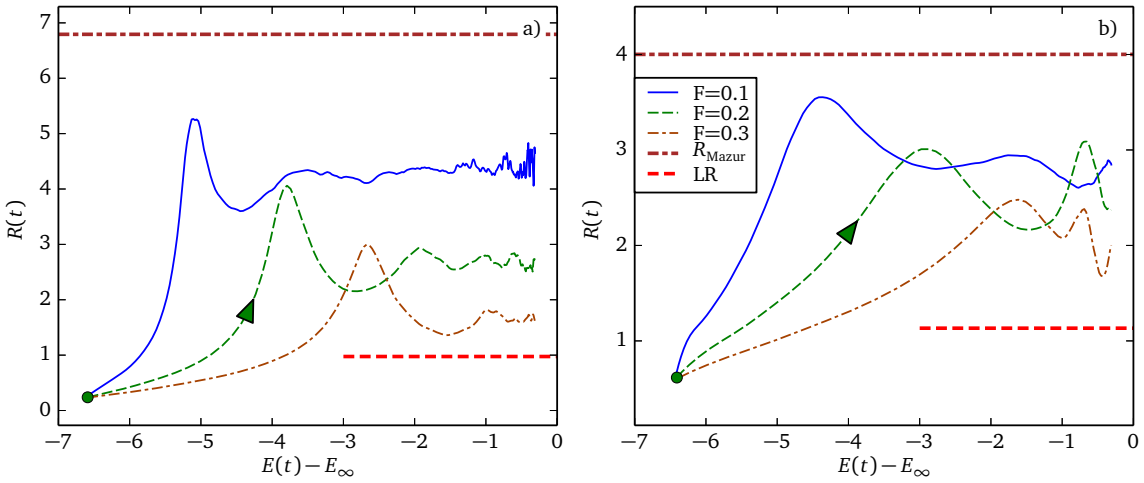

Figure 5.11: $R(t)$ as a function of instantaneous energy for $V = 1.5$, $W = 0$. (a) Results for $L = 24$ and $N = 10$. (b) $L = 26$ and $N = 9$. Dashed lines show R_{Mazur} based on Eq. (5.54) and the LR ratio $\frac{D^E}{D^N}$ from Eq. (5.46) both at $\beta = 0.1$.

over a larger number of sites than the fundamental conserved quantity J^E, are less robust with respect to integrability breaking perturbations. The tools available at the moment are perfectly suited for the analysis of integrability breaking in the quench protocol, which requires only two instantaneous operator bases: one before and one after the quench. On the other hand, the driven case requires the use of the Floquet formalism with an infinite-dimensional basis over a period of oscillation of the time dependent Hamiltonian. Thus, the deeper understanding of the contrasting result for driving and relaxation remains an open problem and requires further studies.

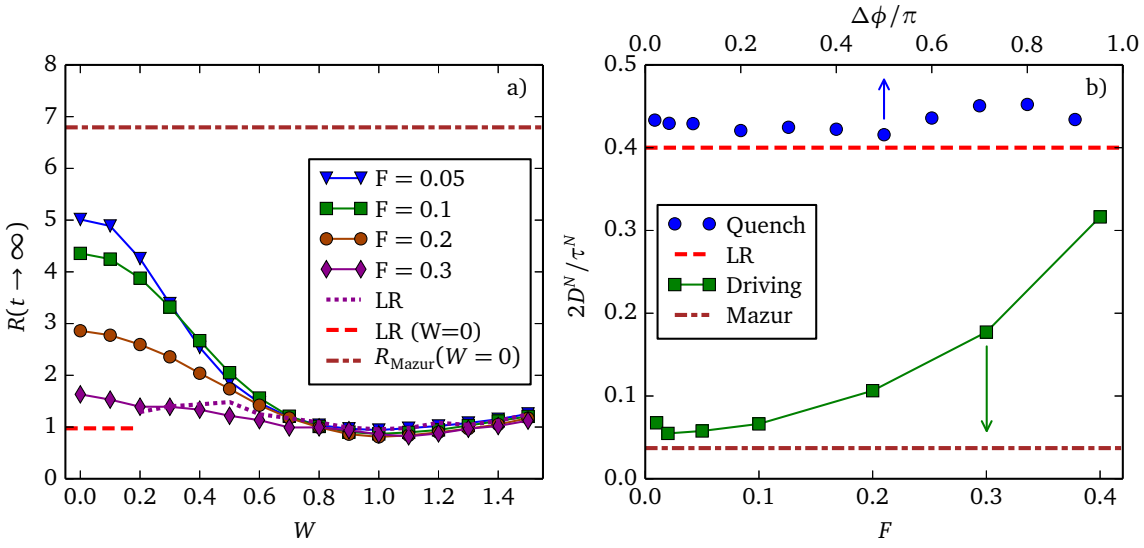

Figure 5.12: Results for $V = 1.5$, $L = 24, N = 10$. (a) $R(t \to \infty)$ for decreasing W compared with the LR result (see Eq. (5.46)). For the case $W = 0$ we also show R_{Mazur} (Eq. (5.54)) and LR ratio $\frac{D^E}{D^N}$ (see Eq. ((5.55)) both at $\beta \to 0$. (b) The stiffness D^N, D^N_{Mazur}, D^N_{driving} and D^N_{quench} normalized to $\tau^N/2$ for $W = 0$ as detailed in the text.

Chapter 6

Reduced dynamics and entropy density in strongly driven systems

In this chapter we set up the local analysis of thermodynamics of interacting quantum systems strongly driven in time, needed for subsequent analysis of inhomogeneous thermoelectrical devices, by studying the exact dynamics of any subsystem.

In Chapter 5, we used local observables to monitor the evolution of a driven quantum systems. We showed that in generic, nonintegrable systems, for slow enough driving F, the flow of the particle current produces an increase in the energy of the system due to the Joule effect.

All pointed to the direction that the work being done on the ring by the field is being dissipated into *heat*. The system act as a resistor, leading to an increase of the *temperature*, not storing energy reversibly as in a reactance [Lan87]. However, irreversible heating can not be demonstrated only by looking at the expectation values of a few local observables. In fact, the unitary evolution of the system can be in principle (and on the computer) reversed.

To settle this question, in this chapter we study the *exact dynamics* of the Reduced Density Matrix (RDM) of a subsystem, by evolving the wavefunction of the whole system in time with a numerically exact method. The approach opens a rare window into the local dynamics of strongly correlated quantum systems. The spectral statistics of the RDM are shown to be consistent with chaotic, thermal evolution. The local entropy, defined as the entanglement entropy of the RDM, increases according to the second law of thermodynamics. The subsystems are shown then to evolve in quasi-equilibrium according to a canonical *thermal* distribution dictated by a time-independent entanglement Hamiltonian, with the *temperature* set by the external driving.

6.1 Reduced Density Matrix

The wavefunction $|\psi(t)\rangle$ of a closed[1] system contains complete information about the values of all possible observables, captured by the density matrix

$$\rho_T(t) = |\psi(t)\rangle\langle\psi(t)|, \tag{6.1}$$

where the subscript T stands for total system. Its evolution in time follows the Time Dependent Schrödinger Equation, with Hamiltonian given by Eq. (5.1) and driven in the same way as in the

[1] Not exchanging particles or heat with the environment, but the environment can act on the system

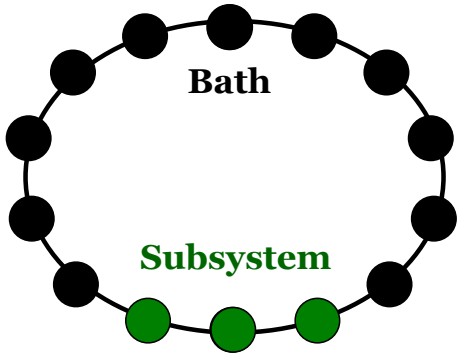

Figure 6.1: The whole strongly interacting system can be partitioned into two: a subsystem of interest on which the RDM will be calculated, and the (larger) remainder of the system which acts as a thermal bath.

previous chapter. The time propagation, following sections 2.2 and 3.2.3, is numerically exact and the description of the whole system by $|\psi(0)\rangle = |\psi_E\rangle$ in the microcanonical ensemble was demonstrated to be very effective at capturing the physics of the high–temperature $t-V-W$ model.

The interacting ring $T = S \otimes B$, can be decomposed as a subsystem of interest S on M sites, and a bath B comprising the remaining $L-M$ sites, as seen in Fig. 6.1. The information regarding the subsystem S alone can be obtained from its density matrix $\rho_S(t)$, which is a partial trace over the bath degrees of freedom, analogous to the integration over marginal variables in probability theory:

$$\rho_S(t) = \mathrm{Tr}_B\, \rho_T(t) = \mathrm{Tr}_B\, |\psi(t)\rangle\langle\psi(t)|. \tag{6.2}$$

Usually, the evolution of a small system is performed perturbatively, supposing a weak coupling to a much larger bath that is treated as macroscopic object (e.g. having infinitely short relaxation times). Perturbation theory cannot treat the case of a subsystem of a strongly interacting ring of fermions, where the coupling between the sites inside the subsystem and to the bath has equal strength. The setup we propose is able to capture very accurately the dynamics of the subsystem: as shown in Section 3.1.4, the description of local observables, such as a whole subsystem density matrix ρ_S is exponentially accurate in the size of the total Hilbert space, where the error is bounded by the ratio $\frac{D_S}{D}$. Even in the case of the largest subsystem we considered, with size equal to half of the ring $M = L/2$, the error ratio is of the order $\frac{D_S}{D_S^2} = \frac{1}{D_S} \ll 1$.

The dynamics of the whole system T, generates a map on the projected RDM of the subsystem. This map is given by

$$\rho_S(0) = \mathrm{Tr}_B\, |\psi_E\rangle\langle\psi_E| \xrightarrow{t} \rho_S(t) = \mathrm{Tr}_B\, |\psi(t)\rangle\langle\psi(t)|. \tag{6.3}$$

The partial trace, as explained below, is a sum over all matrix elements of the bath that are irrelevant for ρ_S: the larger B, the better Hilbert space average[2] is obtained for ρ_S.

Since the density matrix of the whole system is equivalent in terms of information to the D-dimensional complex wavefunction $|\psi\rangle$, where we momentarily omit the temporal dependence for convenience of notation, it is not necessary to construct the $D \times D$ density operator in order to perform a partial trace. Using the computational basis $\{|i\rangle,\ i = 1,\ldots,D\}$ to expand the wavefunction

$$c_i = \langle i\,|\,\psi\rangle\,, \tag{6.4}$$

[2] In the sense of a smaller variance of the expected value

the matrix elements of ρ_T are

$$\langle i \,|\, \rho_T \,|\, j \rangle = \langle i \,|\, \psi \rangle \langle \psi \,|\, j \rangle = c_j^* c_i. \tag{6.5}$$

The subsystem S also possesses a complete basis of dimension 2^M, where M is the volume (or number of sites) of the subsystem. The number of fermions $N_S = \{0, 1, \ldots, \min(N, M)\}$, can vary up to the smallest number between the volume and the total fermions in the system. The RDM of the subsystem can be organized from the beginning into a block-diagonal structure as seen in Fig. 6.2, with each block labeled by its fermion occupation number N_S. Each block has dimension $D_S = \binom{M}{N_S}$. In this chapter, the largest RDM has been determined for a chain with $L = 26, N = 13$, where we selected $M = 12$ sites for the subsystem, and used the largest subspace with $N_S = 6$ fermions.

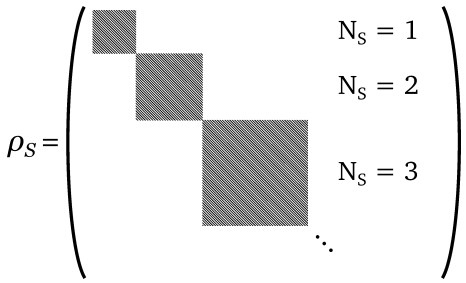

Figure 6.2: Block diagonal form of the reduced density matrix for the subsystem S. The blocks are ordered in growing size from $D_S = M$ for $N_S = 1$, to $D_S = M(M-1)/2$ for $N_S = 2$ and so forth.

We apply the analysis of the RDM to the largest irreducible component, thus we select usually $N_S = M/2 < N$, with maximum dimension $D_S \leq \frac{M!}{(M/2)!^2}$.

In order to compare directly subsystems of different sizes M, we will switch to *densities*. The energy density in a subsystem can be calculated by

$$\varepsilon = \frac{\mathrm{Tr}[H\rho_S]}{M}, \tag{6.6}$$

equal to the density of the whole system $\varepsilon(t) = \langle H(t) \rangle / L$, up to microscopical fluctuations. The subsystem also comes with a corresponding fermion density $n(t) = \langle N \rangle / M$, and the entropy density $s(t) = S/M$, displaying a weak nontrivial scaling with M.

6.1.1 Entropy density

The local generation of heat, accounting for the increase of temperature, needs to be accompanied by a corresponding increase in an entropy-like quantity. Since this is a nonequilibrium setting, the entropy is not formally defined. The entropy is not an observable in quantum mechanics, as no linear Hermitian operator can be found to have the entropy as its expected value. The thermodynamical entropy of a system S, prepared in a canonical ensemble ρ_β by weak coupling to a thermostat, is equal to the entanglement entropy of S with the thermal bath B. As argued in Chapter 3, the system S will be in a canonical state irrespective of the details of the coupling to B or to the exact state of $S \otimes B$. The equivalence leads to the definition of the von Neumann entropy of a quantum thermal state as

$$S_\beta = \mathrm{Tr}[\rho_\beta \log \rho_\beta].$$

The nonlinearity in ρ of the entropy functional is evident, precluding the existence of a state-independent operator $\hat{S}$ such that $\mathrm{Tr}[\rho_\beta \hat{S}] = S_\beta$.

Following the approach of Deutsch, for systems with local interactions, an approximate entropy measurable can be constructed, with a definition independent of the preparation of the thermal state. It is the *entropy density of the RDM*, which in the limit of small subsystem size $M/L \to 0$ must be close to the entropy density of the whole system, as the thermodynamical entropy is additive when the correlations are weak[3]. Considering a subsystem S of a larger system $S \otimes B$, its entanglement entropy S_E is

$$S_E = \mathrm{Tr}[\rho_S \log \rho_S] = \mathrm{Tr}[\rho_B \log \rho_B]. \tag{6.7}$$

The same entanglement entropy is shared by both S and B, which can be trivially proven using the Schmidt decomposition of the density matrix $\rho_{S\otimes B}$ before performing the partial trace. This is intuitively supported by the notion that the entanglement is holographic, i.e. depends only on the shared *surface* between the two parts of the system.
The entropy density s of the subsystem S is defined as

$$s \equiv \frac{S_E}{M} = \frac{\mathrm{Tr}[\rho_S \log \rho_S]}{M} \tag{6.8}$$

Clearly, since the system is finite and the dimension of the Hilbert space is bounded, the entanglement entropy density for the bath tends to zero at all temperatures, because in that case $M/L \to 1$, or the subsystem size grows macroscopically whereas its boundary surface remains microscopic. Thus the entropy density is a valid thermodynamical-entropy-like quantity under the constraint

$$M \ll L/2. \tag{6.9}$$

The main advantage of the entropy density is that it is nonzero for *arbitrary states* of the system $S \otimes B$, including highly excited pure states $|\psi(t)\rangle$. Even in the pure microcanonical ensemble, the density is nonzero and approaches the thermodynamical value. The notion that pure states have zero entropy comes from erroneous conflation (since there is no alternative definition) of the entanglement and thermodynamical entropy. Using the entropy density allows for the correction of this bias. Moreover, the entropy density $s(t)$ as a function of time serves as a useful measurable outside of equilibrium, where the usual von Neumann definition cannot be applied.

Now, we proceed to outline the computational tools for the entropy density, by providing an efficient algorithm to project the RDM in real time, from which the entanglement entropy can be readily calculated.

6.1.2 Summation algorithm

In order to determine the matrix elements of ρ_S, a basis needs to be selected: the vectors $|l\rangle$ are in one-to-one correspondence with the set of D_S combinations of N_S fermions on M sites, which can be represented as vectors with at most N_S ones and $M - N_S$ zeros. The order relation is given number the sites from the right to the left, i.e. the highest numbered site is the leftmost. The vectors are indexed starting with $|1\rangle$ having N_S ones on the right, and $|D_S\rangle$ having N_S ones on the left.[4] As an example, for $M = 5, N_S = 3$, the eight vector state has the following enumeration on its bits:

$$|8\rangle \quad = \quad |1_5 \quad 1_4 \quad 0_3 \quad 0_2 \quad 1_1\rangle \qquad \text{with the positions as subscripts.} \tag{6.10}$$

Any basis vector of the whole system can be seen as the tensor product of a vector from the system and one from the bath

$$|i\rangle_T = |m\rangle_S \otimes |b\rangle_B. \tag{6.11}$$

[3] It is the case between two disjoint subsystems

[4] The convention allows using machine bitwise comparisons if the state vectors are represented as integers on common Little Endian processors such as Intel's.

The matrix elements of the RDM of the subsystem S are calculated by summing over all bath vectors. This is equivalent to extending the sum over the whole-system vectors that share a particular configuration of the subsystem: given $|m\rangle_S$, the sum is performed over all $|b\rangle_B$, i.e. all $|i\rangle_T$ such that ${}_T\langle i\,|\,m\rangle_S \neq 0$:

$$\rho_S = \sum_{|b\rangle_B} {}_B\langle b\,|\,\rho_T\,|\,b\rangle_B = \sum_{i_T, j_T, k_B} c_j^* c_i \underbrace{{}_B\langle b\,|\,i\rangle_T}_{|m\rangle_S} \underbrace{{}_T\langle j\,|\,b\rangle_B}_{\langle n|_S} \tag{6.12}$$

$${}_S\langle m\,|\,\rho_S\,|\,n\rangle_S = \sum_{|b\rangle_B} c_j^* c_i \qquad \text{such that } {}_T\langle i\,|\,m\rangle_S \otimes |b\rangle_B \;\; {}_T\langle j\,|\,n\rangle_S \otimes |b\rangle_B \neq 0. \tag{6.13}$$

The result of the sum is a well defined matrix, due to Eq. (6.11) and the tensor identity $\langle b_B\,|\,i_T\rangle = |m\rangle_S$. The constraint in the sum of Eq. (6.13) does not allow for a simple recipe. The range of elements such that ${}_T\langle i\,|\,b\rangle_B \neq 0$ needs to be determined. The length of the range is the dimensionality of the Hilbert space of the bath, $D_B = \binom{L-M}{N-N_S}$. If the sites are ordered carefully, such a range is dense: only the index i_1 of the first and i_{D_B} of the last element require computation, whereas the other numbers lie in between:

$$|i\rangle_T \qquad \text{with } i \in [i_1, \ldots, i_{D_B}]. \tag{6.14}$$

The ordering properties given above serve this purpose. We need to generate all states $|b\rangle_B$ of the bath with the states of the subsystem $|m\rangle_S$ fixed. Putting the bits corresponding to the configuration $|m_S\rangle$ in the leftmost positions, and the states $|b\rangle_B$ on the right, i.e. determining the RDM of the sites $[L-M+1, L-M+2, \ldots, L]$, we obtain the ordering needed. Let us motivate it with an example, using 4 sites for S as well as for B, with 4 fermions in total. There are 6 possible states in S (and B) with $N_S = 2$:

$$\text{basis}(S) = \text{basis}(B) = |0011\rangle_1, |0101\rangle_2, |0110\rangle_3, |1001\rangle_4, |1010\rangle_5, |1100\rangle_6. \tag{6.15}$$

The order relation in S (and B) is given by their subscript. In $\mathrm{T} = \mathrm{S} \otimes \mathrm{B}$, the states are ordered first according to their index in S, then with respect to the index in B. Thus

$$\underbrace{|1010\rangle_5|1100\rangle_6}_{51} > \underbrace{|1010\rangle_5|0011\rangle_1}_{46} > \underbrace{|1001\rangle_4|1100\rangle_6}_{45} > \underbrace{|1001\rangle_4|0011\rangle_1}_{40}. \tag{6.16}$$

In S, there are $\binom{8}{4} = 70$ possible states, and the numbers below the braces refer to that numeration. The states of the form $|1010\rangle \otimes |b\rangle_B$ with $|b\rangle_B \in \text{basis}(B)$ take the contiguous range from $i_1 = 40$ to $i_{D_B} = 45$. In general, given any state $|m\rangle_S$, the range can be determined by looking up $|i_1\rangle_T = |m\rangle_S \otimes |i_1\rangle_B$ and $|i_{D_B}\rangle_T = |m\rangle_S \otimes |i_e\rangle_B$. The sum in Eq. (6.13), requires 4 state lookups for each matrix elements to determine the two ranges $[i_1, \ldots, i_{D_B}]$ and $[j_1, \ldots, j_{D_B}]$. The ranges are different in general. According to the example above, the matrix element corresponding to $|5\rangle_S$ and $\langle 4|_S$ is:

$$\langle 1010\,|\,\rho_S\,|\,1001\rangle = \sum_{k=0}^{5} c_{k+40}^* c_{k+45}, \tag{6.17}$$

with a single summation continuous range. The lookup is best performed by a binary search of the basis vectors list, in $O(\log D)$ steps, but the actual algorithm used[5] for the lookup is irrelevant, as long the ordering is the same. Of course, if the ordering is reversed, the optimal location for S on the chain needs to be rearranged.

[5]The combinatorial number system gives a way to map the combination of fermions to the combination index without the need for a table

Arbitrary positions

If the sites spanned by S are not the last M ones of the chain, the previous algorithm cannot be applied. Determining each index for a matrix element would need $2D_B$ lookups, which for a 924×924 sized matrix would amount to billions of lengthy[6] operations, taking hours on a modest desktop computer.

However, any contiguous range of M sites over which we defined S can be mapped unitarily into $[L-M+1,\ldots,L]$. The unitary mapping is a translation T, a permutation with sign information due to the fermionic nature of the system, as described in Section 1.1.1.2. Recalling the example above, if one were interested in the RDM of the first 4 sites, the range corresponding to the matrix element $|b\rangle_B \otimes |1001\rangle_S$ is $\{13, 23, 29, 43, 49, 59\}$, with no easily determined relation.

After the permutation T

$$|\psi\rangle \mapsto T|\psi\rangle$$
$$c_i \mapsto \mathrm{sign}(\sigma[i])\, c_{\sigma_i}$$

and the range is mapped the one given by Eq. (6.17), with modified coefficients c_i. The sign is different for each of the basis vectors, since the fermion operators were rearranged differently. If the RDM of subsequent sections of the ring is needed, one can rotate the system by one site at a time and project the RDM at each step. After L rotations, the wavefunction is mapped into its initial value.

6.2 High Temperature Expansion

In order to obtain analytical approximations to the thermodynamical parameters, we employ High Temperature Expansions (HTE). The system under study is started close to and brought near the infinite temperature fixed point at $T = \infty$ or $\beta = 0$, the small parameter around which we develop the series expansion. Most of the observables in the canonical ensemble, at fixed temperature and number of particles, can be calculated exactly close to the HT limit. Any observable can be expanded as

$$\langle A\rangle_\beta = \frac{\mathrm{Tr}[A\,\mathrm{e}^{-\beta H}]}{\mathrm{Tr}\,\mathrm{e}^{-\beta H}} = \frac{\mathrm{Tr}[A-\beta AH+O(\beta^2)]}{\mathrm{Tr}[\mathbb{1}-\beta H+O(\beta^2)]}. \tag{6.18}$$

The denominator contains the factor $\mathrm{Tr}[\mathbb{1}]$, equal to the infinite-temperature normalization factor $Z_\infty = \lim_{\beta\to 0}\mathrm{e}^{-\beta H} = D$ equal to the dimension of $\mathscr{H}$. By collecting the normalization term, the expansion can be organized in powers of β, where each term is of the form

$$\left\langle AH^k\right\rangle_\infty = \frac{\mathrm{Tr}[AH^k]}{\mathrm{Tr}[\mathbb{1}]}, \tag{6.19}$$

for some exponent k. The first order for any observable is

$$\langle A\rangle_\beta = \langle A\rangle_\infty - \beta\big[\,\langle AH\rangle_\infty - \langle A\rangle_\infty \langle H\rangle_\infty\,\big] + O(\beta^2). \tag{6.20}$$

The scheme relies on the ability to calculate the trace of any observable easily. Any off-diagonal operator such as the kinetic energy of the Hamiltonian has zero trace and thus expectation value in the HT limit, e.g. $\left\langle c^\dagger_{i+1}c_i\right\rangle_\infty = 0$. Diagonal observables, on the other hand, usually are nonzero. They can be written as strings of local operators $n_i\,n_j\,n_k,\ldots$, which have a simple expectation value if the sites are different $i \neq j \neq k$:

$$\langle n_1\rangle_\infty = \frac{N}{L}$$

[6] Not cache friendly

$$\langle n_1 n_2 \rangle_\infty = \frac{N(N-1)}{L(L-1)}$$
$$\langle n_1 \dots n_m \rangle_\infty = \frac{N(N-1)\dots(N-m+1)}{L(L-1)\dots(L-m+1)}$$

The expectation values are dictated by the constraint of having N available fermions on L sites, with Pauli exclusion. If the expectation value of two fermion operators is needed, the first fermion must be placed, then the number of positions for the second is reduced to $L-1$ and only $N-1$ fermions are available, and so on. At first order in L^{-1} for m operators, the expectation value is

$$\langle n_1 \dots n_m \rangle_\infty = \left(\frac{1}{2}\right)^{m+1}\left[1 - \frac{(1+m)M}{2L} + O(L^{-2})\right]. \tag{6.21}$$

Without the particle number constraint, in the grand canonical ensemble, the term in brackets would just equal 1.

Any expression involving a diagonal operator, coming from powers of H such as $H_V H_W$, can be computed using the table above. However, if the number operators appear on the same sites, due to the idempotency of fermionic number operators ($\langle n_1 n_1 \rangle = \langle n_1 \rangle$), they must be counted only once. As an example, the term $\left\langle \sum_{i=1}^{L}(n_i n_{i+1}) \sum_{j=1}^{L}(n_j n_{j+1}) \right\rangle_\infty$ requires counting the multiplicities of the tuple $(n_i, n_{i+1}, n_j, n_{j+1})$ over the double sum. We have explicitly not taken into account the particle-hole symmetrized interaction shown in Eq. (1.17) for sake of simplicity. The result is

$$L(L-3)\left\langle n_1 n_2 n_3 n_4 \right\rangle_\infty + 2L \langle n_1 n_2 n_3 \rangle_\infty + L \langle n_1 n_2 \rangle_\infty = \frac{L^2}{16}\left(1 - \frac{1}{L-1}\right). \tag{6.22}$$

The count of multiplicities must be a polynomial $p^k(L)$ of order at most k in L with integer coefficients, for each of the k terms in the sum representing the counts of non-overlapping indexes. The translational invariance always allows to fix the operator with the first free index $\sum_i n_i \dots$ to $L n_1$ and reduce the polynomials to order $p^{k-1}(L)$. To determine the coefficients, an explicit calculation on a finite-size ring with dimensions $L = [k+1, k+2, \dots, 2k]$ [7] can determine k coefficients of the polynomials through an integer-valued interpolation. The fitting trick is the most efficient implementation. For the example above, it is enough to calculate $p(L=5)$ and $p(L=6)$, respectively for 2,3 and 4 unique indexes, to fit 3 polynomials of the form $L^2 + a_1 L + a_0 = L^2$.

Offdiagonal operators have zero trace, such as H_{kin}, as well as mixed products with odd powers, e.g. $\langle H_{\text{kin}} H_V \rangle_\infty = 0$. Their even powers, starting from H_{kin}^2, have nonzero diagonal terms. They can be rearranged into sequences of diagonal operators and irrelevant offdiagonal terms by proper ordering. The result of the ordering can be shown to be equivalent to a modified fermionic Wick's expansion $\mathbb{W}$. Every sequence of creation and annihilation operators is Wick expanded, by matching every creation to a destruction operator. This is equivalent to throwing out all normal ordered operators, and setting the contraction value to being a number operator to be evaluated later in the HTE scheme. One step of the expansion could be

$$\mathbb{W}\left[\overbrace{c_i^\dagger f_1 f_2 \dots f_k \, c_j}\right] = \delta_{ij}\, n_i\, (-1)^k\, \mathbb{W}[f_1 f_2 \dots f_k] \tag{6.23}$$

where the group of operators $f_1 \dots f_k$, and any other pairwise combination will be further contracted. The fermionic sign has been taken into account by counting the number of operators in between. The result is a string of number operators and delta function of symbolic indexes, which need to be simplified. The matching produces a series of terms such as $\delta_{i,j}$ or $1-\delta_{i,j}$, which can be counted at the end of the

[7] The sizes given here are the smallest able to avoid artifacts due to accidental overlap

expansion to determine how many unique indexes are left. For the first nonzero power of the kinetic energy the expansion can be done by hand, yielding

$$\begin{aligned}\left\langle H_{\text{kin}}^2 \right\rangle_\infty &= t_h^2 \left\langle \sum_i \left(c_{i+1}^\dagger c_i + c_i^\dagger c_{i+1}\right) \sum_j \left(c_{j+1}^\dagger c_j + c_j^\dagger c_{j+1}\right) \right\rangle_\infty \\ &= 2t_h^2 \left\langle \sum_i (n_i - n_i n_{i+1}) \right\rangle_\infty = \frac{2t_h^2 N(N-L)}{L-1}. \end{aligned} \tag{6.24}$$

The Wick expansion is the most complicated step of the HTE, effectively limiting the maximum order reached in Eq. (6.20) to β^4 in our case. The results quoted here are however limited to first order for sake of brevity.

6.2.1 HTE for the energy

Given the Hamiltonian in Eq. (5.1) at zero phase, the term linear in β for the expectation of the energy from Eq. (6.20) reads

$$\langle H \rangle(\beta) = \langle H \rangle_\infty - \beta \left(\left\langle H^2 \right\rangle_\infty - \langle H \rangle_\infty^2 \right) = \langle H \rangle_\infty - \beta \sigma_\infty^2, \tag{6.25}$$

where we have recognized that the expression in the last brackets is the variance of the energy at infinite temperature σ_∞^2. All expressions referring to the expectation values at $T = \infty$ will be denoted by the symbol ∞. The temperature can be inferred from the instantaneous energy E to

$$\beta(E) = \frac{\langle H \rangle_\infty - E}{\sigma_\infty^2}. \tag{6.26}$$

Plugging the operators $H = H_{\text{kin}} + H_V + H_W$ from Eq. (1.4) into the equation above, knowing that $\langle H_{\text{kin}} \rangle_\infty = 0$, one obtains exactly

$$\langle H \rangle_\infty = \langle H_V \rangle_\infty + \langle H_W \rangle_\infty = \frac{V+W}{4} \frac{L(L-1) - 4N(L-N)}{L-1}. \tag{6.27}$$

The linear term in β is too long to be reported here, but the leading–order expression at half filling, as in the remainder of this chapter, is

$$\langle H \rangle_\beta = -\frac{1}{4}(V+W) - \frac{\beta}{16}\left[8t_h^2(L-1) + 4VW - L(V^2+W^2)\right] + O\left(\frac{1}{L}\right). \tag{6.28}$$

Another observable useful to estimate the temperature is the kinetic energy. Since the expectation value is zero at $T = \infty$, the value to linear order in β is just

$$\langle H_{\text{kin}} \rangle(\beta) = -\beta \left\langle H_{\text{kin}}^2 \right\rangle_\infty, \tag{6.29}$$

using the expression given above in Eq. (6.24). In thermodynamical equilibrium the temperature inferred from the kinetic energy $\beta_{\text{kin}}(t) = -H_{\text{kin}}(t) / \left\langle H_{\text{kin}}^2 \right\rangle_\infty$ is consistent with any other measure, however during the time evolution the instantaneous temperature thus measured can differ [LGBP14].

The HTE relations are useful also for thermodynamical quantities defined over the subsystem S. The energy density, due to its good scaling with the system size L, follows the same relation as the energy: $\varepsilon_\beta = \varepsilon_\infty - \beta \sigma_\infty^2$. We use the same symbol for the variance of the density, not to burden the notation further.

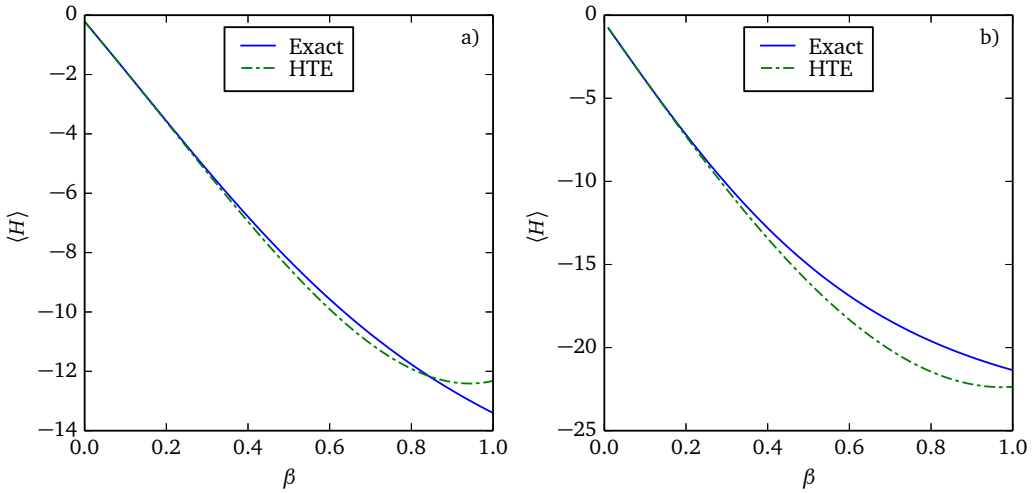

Figure 6.3: Comparison of the HTE results for expansion of the energy up to order β^4, with the numerically exact results from the Chebyshev sampling of the energy spectrum density. The system has size $L = 24, N = 10$. (a) Generic metal with $V = 1.5, W = 1$ (b) Insulator with $V = 4, W = 1$. The HTE in both cases is seen to hold well for the energy operator up until $\beta \simeq 0.4$.

6.2.2 Canonical entropy of the RDM

From the equation linking the energy and the temperature, more thermodynamical relations can be derived. We use the density notation, since we refer to quantities pertaining the subsystem. The definition of the temperature in the microcanonical ensemble is $\beta = \frac{\partial s}{\partial \varepsilon}$, which can be inverted to $ds = \beta\, d\varepsilon$. To obtain $s(\varepsilon)$ both sides are integrated

$$s(\varepsilon) = s_\infty + \int_{\varepsilon_\infty}^{\varepsilon_\beta} \beta(\varepsilon)\, d\varepsilon = s_\infty - \frac{(\varepsilon_\beta - \varepsilon_\infty)^2}{2\sigma_\infty^2} \tag{6.30}$$

For a system of L sites at infinite temperature, the thermodynamical entropy is just the entropy of a flat distribution over D states, $S_\infty = \log D$, with $D = \binom{L}{N}$. In the limit of infinite L and finite fermion density $n = N/L$, using Stirling's formula the entropy in that case is

$$S_\infty(n) = L[(n-1)\log(1-n) - n\log n], \qquad S_\infty\left(n = \frac{1}{2}\right) = L\log(2). \tag{6.31}$$

The entropy density at infinite temperature s_∞, for a subsystem with Hilbert space dimension $D_S = 2^M$ is **not** $\log(D_S)/M = \log(2)$. The canonical constraints for the number of particles in the full system play a role. Supposing that the energy density follows Eq. (6.20), identifying the correct value for s_∞ is the leading order correction. At infinite temperature, s_∞ weights the combinations of fermions in the subsystem. Given a ring with L sites and N fermions in total, what is the probability $P(N_S, M, N, L)$ of each state with N_S fermions enclosed in the M consecutive sites of the subsystem? Out of the $\binom{L}{N}$ states, the number of arrangement satisfying the criterion are the combination of $N - N_s$ fermions onto the remaining $L - M$ sites:

$$P(N_S, M, N, L) = \frac{\binom{L-M}{N-N_S}}{\binom{L}{N}}. \tag{6.32}$$

The thermodynamical entropy density equals the Shannon entropy density of the probability distribution: in each sector with $N_S \in [0, M]$, it equals the entropy of each state $P\log P$, multiplied by the number of

states $\binom{M}{N_S}$. The sum is performed at constant system size (L) and occupation (N):

$$s_\infty = -\frac{1}{M}\sum_{N_S=0}^{M}\binom{M}{N_S}P(N_S,M)\log P(N_S,M). \tag{6.33}$$

The expressions above can be calculated numerically by performing the sum, giving $s(M)\approx\log(2)$, if the full system is at half-filling. For $M=2$ it can be checked explicitly that $\lim_{L\to\infty}s(2)=\log(2)$. The departures can be calculated exactly, as listed in Table 6.1.

M	$s(M)-\log(2)$
2	-0.000400107
4	-0.00127077
6	-0.00225232
8	-0.00337116
10	-0.00466372
12	-0.00618211

Table 6.1: Deviations for $L=26, N=13$, from the perfect scaling of the entropy density $s-\log(2)$, as the dimension of the subsystem M increases.

In the publication, we calculated the series expansion in L^{-1} of $s(M)$ to the order L^{-k}, which terminates for every term at the $O(N^k)$ order. Using computer algebra to perform the expansion over L and sum over N_S, we obtained the following simplified formula valid at half-filling:

$$s_\infty \approx \log(2) - \frac{M-1}{4L^2} - \frac{M^2-1}{6L^3} \tag{6.34}$$

which lends itself to extrapolation for higher orders

$$s_\infty \xrightarrow{\text{Extrapolation}} \log(2) + \frac{M\log\left(\frac{L}{L-1}\right)+\log\left(1-\frac{M}{L}\right)}{2M}, \tag{6.35}$$

in perfect agreement with the numerical results of Table 6.1.

In order to further improve the results for the subsystem entropy in thermal equilibrium, a much more accurate relation between energy density and temperature can be obtained using the methods outlined in Section 2.3.5, together with the exact infinite-temperature entropy density given in Eq. (6.33). We have found the usefulness of the analytical first-order result in Eq. (6.30) to be more appealing for a comparison in the sections to follow.

6.3 Quasi equilibrium

The initial equilibrium state is prepared corresponding to a well-defined temperature β. The microcanonical approach at an average energy $E=E(\beta)$ gives equivalent results. All observables calculated in the initial state agree with their equilibrium expectation values.

What about later times? We posited that after we switch on the electrical field $F>0$ at $t=0$, after a nonequilibrium transient, we reach a quasi-equilibrium state, where the expectation value of local observables depend only on the effective temperature, set by the local energy density $\varepsilon(t)=\langle\psi(t)\,|H(t)|\,\psi(t)\rangle/L$, from which an effective temperature $\beta_{\text{eff}}(t)=\beta_{\text{eff}}[\varepsilon(t)]$ is inferred, as explained in Section 5.3, Eq. (5.39).

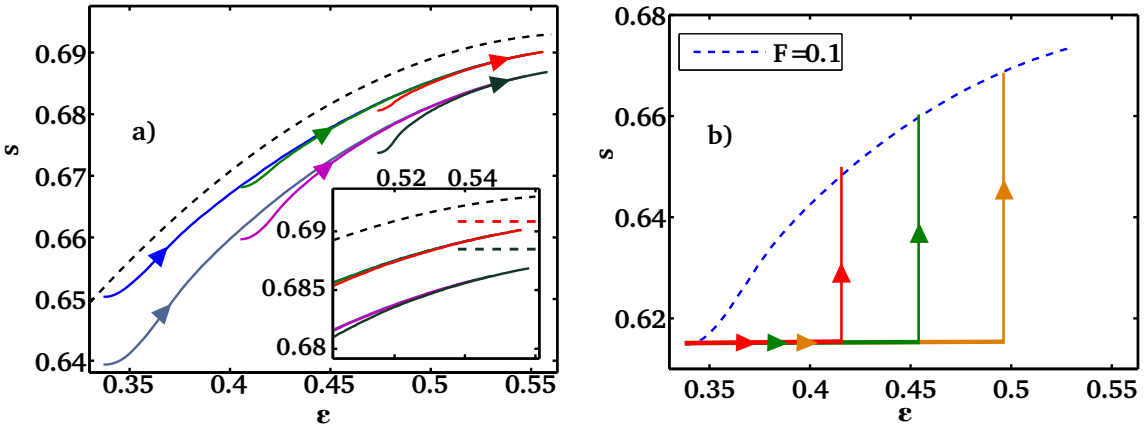

Figure 6.4: Instantaneous entropy density $s(t)$ vs. energy density $\varepsilon(t)$ for generic metals. (a) Results for systems driven by a field $F = 0.1$ and $M = 6, 10$ subsystems. Dashed curves represent high–T analytic results, Eq. (6.30) for $L \to \infty$. In the insets the high-ε regime is magnified and the corrections from Eq. (6.33) to s_∞ are included and marked as horizontal lines. (b) Relaxation after flux quenching for a $M = 12$ subsystem. Here, dashed curves show quasi-equilibrium results for the same systems driven with $F = 0.1$. Arrows mark the direction of the processes.

If that is the case, then driving a system slowly increases its energy density due to the Joule effect, and the effective local temperature rises, as reflected by $s(\varepsilon)$ in Eq. (6.30).

To test the prediction using the results from the subsystem entropy, we prepared many different initial states, for generic and integrable systems with $L = 24, N = 12$ (half filling). The system was chosen in a metallic phase (see Section 1.1.3), with $V = 1.4$ and $W = 0$ ($W = 1$) if integrable (resp. generic). The distinct initial states correspond to different initial conditions: $\beta = 0.3, 0.2, 0.1$, as it can be seen from the different values of the initial energy density (higher for lower β). The RDM was calculated on $M = 6, 10$ in Fig. 6.4(a) and Fig. 6.5(a) in order to have a better convergence to the thermodynamical limit ($M \to 0$). In Fig. 6.4(b) and Fig. 6.5(b) we used $M = 12$ subsystems to have better statistics in the RDM to compute the entropy. The systems were either:

1. Driven with $F = 0.1$: the weak driving should slowly increase the temperatures of the system allowing them to reach a quasi-equilibrium after an initial transient, as shown in Section 3.1.1 and 3.1.4.

2. Quenched by an instantaneous phase change: in this case the evolution proceeded according to a constant Hamiltonian for $t > 0$, as explained in Section 5.2. The expectation is thermalization for generic systems, and a nonthermal equilibrium state for the integrable case (see sections 3.1.2 and 3.1.5)

As a strong indication of the thermal (or quasi-equilibrium) nature of the state $|\psi(t)\rangle$ we can use the relation (6.30) of the subsystem entropy density (defined in Eq. 6.8) and the energy density (6.6) of the subsystem. Hence, we present in Fig. 6.4 the time-evolution of $s(t)$ plotted versus $\varepsilon(t)$ for a generic system: driven by a constant electric field $F = 0.1$ in Fig. 6.4(a) and after a sudden flux quench in Fig. 6.4(b).

We note that $s(t)$ only weakly depends on M, confirming its macroscopic relevance [SPR12]. This is in contrast with a specific case of the ground state, where we have found $s(0) \propto M^{-1}$ in agreement with area laws for the entanglement entropy [ECP10].

The relation defined in Eq. (6.30) allows specifying regimes which are clearly nonequilibrium or steady but non–thermal. The former case occurs after turning on the electric field, when $s = s(\varepsilon)$ is convex

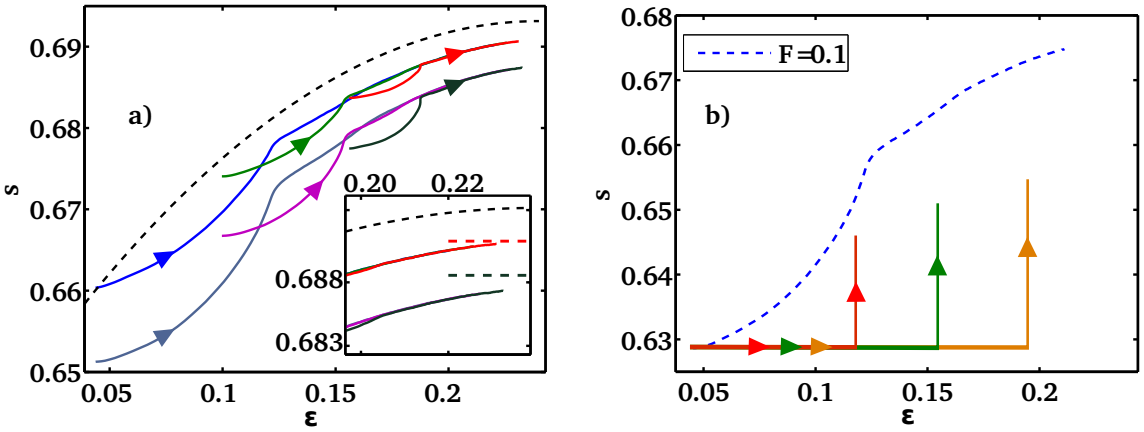

Figure 6.5: Same plot as in Fig. 6.4, only for the integrable system with $V = 1.4, W = 0$. Instantaneous entropy density $s(t)$ vs. energy density $\varepsilon(t)$ for (a) Driven system with $F = 0.1$, with data taken on $M = 6$ and $M = 10$ subsystems. (b) Relaxation after flux quenching for a $M = 12$ subsystem. Here, dashed curves show quasi-equilibrium results for the same systems driven with $F = 0.1$. Arrows mark the direction of the processes.

contrary to the concave dependence which according to the aforementioned equation should characterize the quasi–equilibrium evolution. More interesting is the observation in Fig. 6.5(b), that the stationary, non–thermal state emerges when integrable systems relax after a sudden quench [RDYO07b, KWE11] but $s(t)$ remains evidently smaller than expected after the thermal relaxation. This result nicely complies with the hypothesis of the generalized Gibbs ensemble (GGE) since ρ_{GGE} maximizes the entropy but only subject to constraints imposed by the integrals of motion [RDYO07b, CCR11].

One of the nonlocal conserved operators is the time-averaged value of the current J^N, as mentioned in Section 1.4.1. The current does not decay after the quench, holding energy into motional degrees of freedom. When the system is not integrable, this energy is transformed into heat by resistive interactions, so the system can reach its equilibrium state via the *entropy production*. This mechanism is forbidden in integrable state, which in the GGE equilibrium state have lower entropy, as shown in Ref. [SPR11, SPR12].

The results shown in Figures 6.4 and 6.5 hint at regimes when the system reaches a quasi-equilibrium thermal state. In this case $s(\varepsilon)$ should become independent of the initial state and close to the prediction of HTE. Different starting temperatures were selected, but the observables of the system depend only on the instantaneous energy density, after the initial transient regime. This indeed happens for integrable or non–integrable systems driven long enough by a moderate steady F (remember that F breaks integrability of an integrable system) or when non–integrable system relaxes after the flux quench as in Fig. 6.4(b). It should be noted that after the quench the energy does not increase, since $F = 0$, however the system slowly reaches the equilibrium manifold following unitary microscopical dynamics and the entropy density rises. As mentioned in Section 1.5, the LR entropy production in a nonequilibrium state is always positive and vanishes when the system finally attains the thermodynamical equilibrium. In the driven systems, so much entropy has been produced by heating, that the equilibrium is achieved even with a nonzero electrical field, by raising the temperature effectively to $T = \infty$.

6.4 Canonicality of subsystems

A more stringent criterion for a thermal state is the requirement that the RDM obeys the canonical distribution

$$\rho_S(t) = \frac{1}{Z_{\rm eff}} \exp[-\beta(t) H_{\rm eff}], \tag{6.36}$$

whereby $H_{\rm eff}$ plays the role of an effective subsystem Hamiltonian. In the literature, it is also called the *entanglement Hamiltonian* [LR14, AAN13, VJ09, CH09, AHL12, WKPV13, PC11]

The effective inverse temperature $\beta_{\rm eff}(t)$ can be determined by the instantaneous energy density, using relation (6.26), or inverting the numerically exact Eq. (2.40) derived in Section 2.3. The main open problem concerns the meaning of $H_{\rm eff}$ when the subsystem is strongly coupled to its surroundings or it is subject to external driving. However, we avoid this problem by testing the thermalization hypothesis without specifying the explicit form of $H_{\rm eff}$.

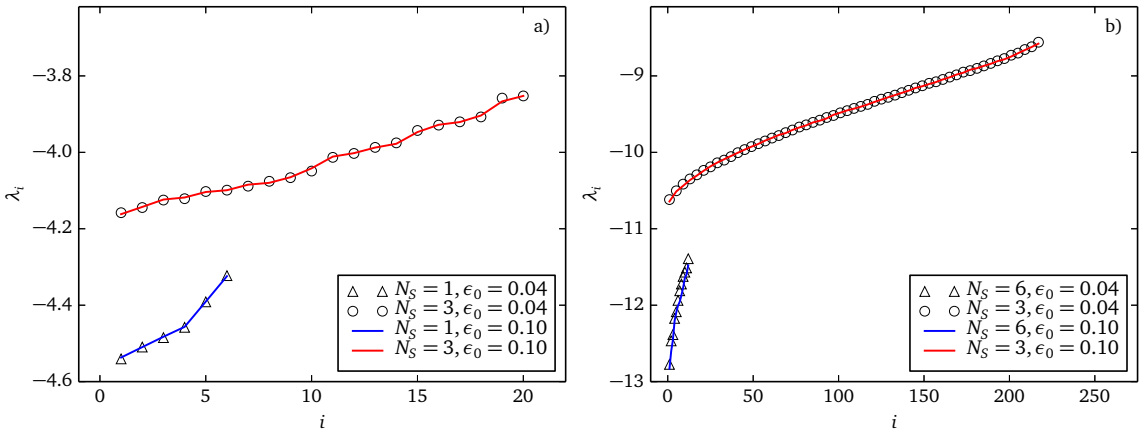

Figure 6.6: Eigenvalues λ_i of $\log[\rho(t)]$ for the integrable system driven by field $F = 0.1$ determined at time t such that $\varepsilon(t) = 0.21$ but evolved from different initial energy densities $\varepsilon_0 = 0.04, 0.1$ and different particle subsectors n. (a) Subsystem with $M = 6$ sites, and 1 or 3 fermions (b) $M = 12$ sites with 3 or 6 fermions.

In order to verify that the quasi–thermal state is determined solely by the energy density, we have computed the reduced dynamics of two identical subsystems (labeled by subscripts 1 and 2) driven by the same field $F = 0.1$ but starting from different initial energies. We compare $\rho_1(t_1)$ and $\rho_2(t_2)$ for such times t_1 and t_2 that both systems have the same instantaneous energies (temperatures) $E(t_1) = E(t_2)$. Then, one expects

$$\log[\rho_1(t_1)] = -\beta(t_1) H_{\rm eff}[\phi(t_1)] + \Delta_1 \quad \text{and} \quad \log[\rho_2(t_2)] = -\beta(t_2) H_{\rm eff}[\phi(t_2)] + \Delta_2. \tag{6.37}$$

In other words, for the quasi–thermal state operators $\log[\rho_1(t_1)]$ and $\log[\rho_2(t_2)]$ should give Hamiltonians of the same system but possibly sensitive to different fluxes. Since the times were selected to match the energy densities, the local temperatures β cancel out from the equation. The effective Hamiltonians may have different eigenfunctions due to the flux dependence, but the energy spectrum should be the same. The additional constants $\Delta_{1,2}$ depend only on the respective $Z_{\rm eff}$, but since the latter are only functions of the temperature and Hamiltonian which are equal, the constants also cancel. The above hypothesis was tested in Fig. 6.6 by comparing systems with the instantaneous temperature (energy) but evolving from different initial conditions, for two different subsystems $M = 6, 12$ and two sectors N_S, respectively. It is quite evident that the spectra are independent of the initial microcanonical

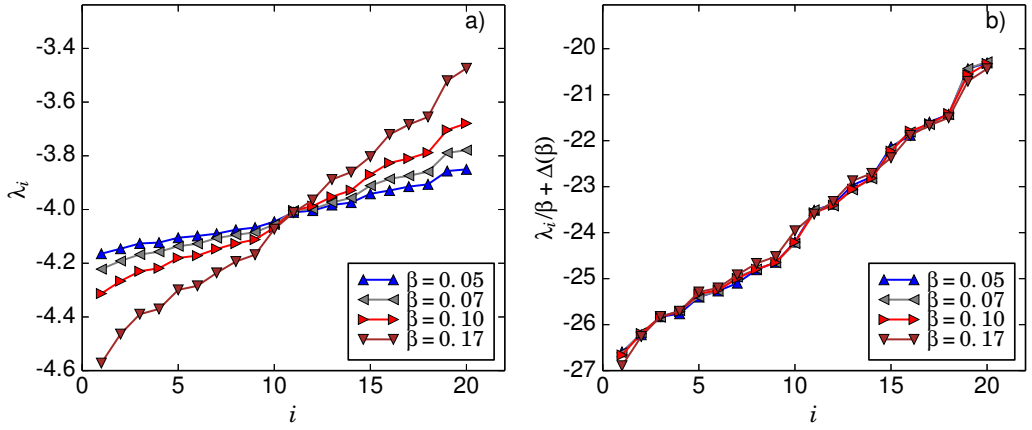

Figure 6.7: Spectra of $\log[\rho]$ for the integrable system ($N = 6, n = 3$) driven by $F = 0.1$ determined for t corresponding to different $\beta(t)$ obtained from HTE. Panels (a) and (b) show eigenvalues of $\log[\rho]$ and normalized (and shifted) $\log[\rho]/\beta$, respectively.

energy density ε_0, at least for the states for which the previous results on the entropy density already pointed towards thermalization.

One can also compare systems with different energies and check the exponential dependence between ρ_S and β. Fig. 6.7(a) finally shows spectra of $\log[\rho(t)]$ for driven integrable system (only the largest sector with $n = 3$ is presented). Various curves are obtained for successive times, when the system has different instantaneous energies $\varepsilon(t)$. For a quasi–thermal evolution the spectra of

$$\log[\rho(t)]/\beta(t) = -H_{\text{eff}}[\phi(t)] + \Delta(\beta) \tag{6.38}$$

should be equal up to a constant value $\Delta(\beta)$. As shown in Fig. 6.7(b), even the driven integrable system perfectly fulfills this requirement. The results for generic systems are just as well defined, expected a fortiori since the canonicality of RDM of integrable systems holds so well.

6.5 Temperature from the eigenvalue distribution

So far we have only mentioned the determination of the instantaneous effective temperature $\beta_{\text{eff}}(t)$ based on observables such as the energy density $\varepsilon(t)$. However, knowing that the RDM of any subsystem is locally described by an effective Gibbs distribution, allows us to estimate a temperature from its eigenvalues. In Fig. 6.8(a), we plot the observables needed for the determination of the temperature by the methods described so far. The initial nonequilibrium transient needs to be identified, and to this end we plot also the expectation value of the particle current $j^N(t)$. As argued in section 5.3, the current has a monotonous value depending only on the temperature: we can identify the quasi-equilibrium regime by choosing the time t_0 after which the current has a slowly varying profile. Only after t_0 the quasi-equilibrium relations can be trusted. The times $t < t_0$ are marked by a gray area on the plots.

A more stringent test has been employed in Section 6.3, using the concavity of the entropy density as a function of ε. Fig. 6.8(b) shows $s(\varepsilon)$ with the area corresponding to $\varepsilon(t) < \varepsilon(t_0)$ grayed out. Indeed before t_0 the entropy displays a nonthermodynamical convexity.

Fig. 6.8(c) shows the profile of the effective temperature $\beta_{\text{eff}}[\varepsilon(t)]$ determined using the energy density, and the estimate $\beta_{\text{RDM}}(t)$ obtained from the distribution of the eigenvalues of H_{eff} in Eq. (6.38). Since H_{eff} is not known a priory, the temperature can not be inferred directly. However, the ratio of the

temperatures $\beta(t_1)/\beta(t_2)$ can be obtained by comparing the eigenvalues λ_i of $\log \rho_S(t)$ at different times. In order to get rid of the unknown constant $\Delta(t)$ which equally shifts all the eigenvalues in the same sector of the density matrix, we subtract the lowest eigenvalue λ_1 from the remaining

$$\tilde{\lambda}_i = \lambda_i - \lambda_1 \qquad \text{for } i \in [2, \ldots, D_S]. \tag{6.39}$$

After this necessary normalization, the ratio of the eigenvalues gives directly the ratio of the temperatures

$$\frac{\tilde{\lambda}_i(t_2)}{\tilde{\lambda}_i(t_1)} = \frac{\beta(t_2)}{\beta(t_1)} \qquad \text{for all } \tilde{\lambda}_i. \tag{6.40}$$

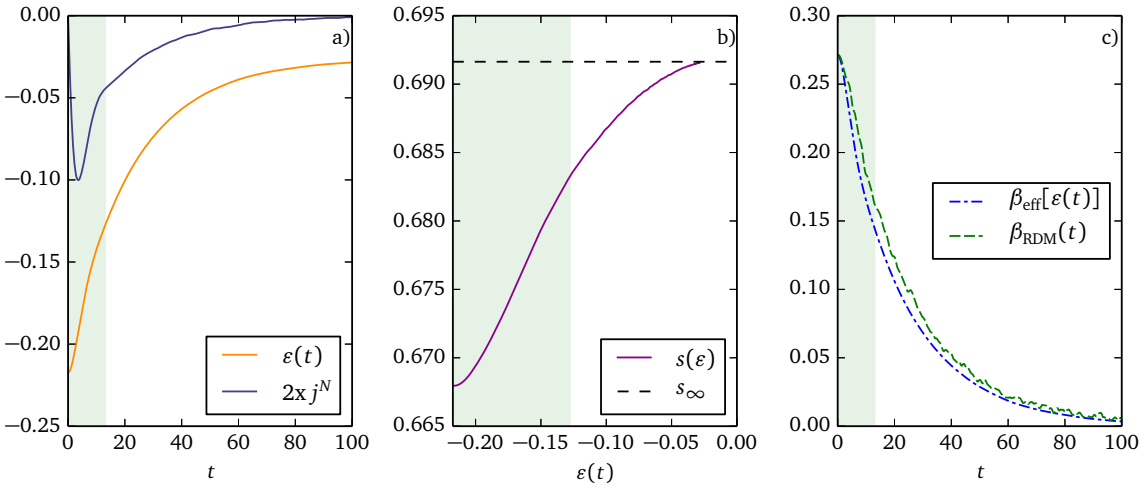

Figure 6.8: Determination of the temperature in a driven generic system with $N = 24, L = 12, V = 1.4, W = 1$, using the RDM eigenvalue distribution on a $M = 4$ subsystem. The system is driven by a $F = 0.2$ field from an initial equilibrium temperature $\beta \approx 0.3$. (a) The expectation values for the (rescaled by a factor of 2x) particle current j^N and instantaneous energy $\varepsilon(t)$ are plotted. (b) The density entropy used to check that the transient has been correctly identified (c) The local temperature determined in two different ways, leading to comparable results, up to a time delay in the quasi-equilibrium regime due to the initial transient.

The ratio is then averaged over all eigenvalues of $\log \rho_S(t)$ in the largest subsector of the density matrix, in order to obtain the best statistics. This determination of β relies on two assumptions:

1. The effective Hamiltonian H_{eff} has a time-independent spectrum in the quasi-equilibrium regime
2. One temperature $\beta(t = 0)$ is known exactly

The second assumption is needed in order to recover an instantaneous temperature

$$\beta_{\text{RDM}}(t) = \frac{\beta(t)}{\beta(t_0)} \times \beta(t_0), \tag{6.41}$$

where the ratio is determined using Eq. (6.40). But it has been shown that the initial microcanonical state has a well defined temperature $\beta(t = 0)$, used as a meter. The initial distribution of the RDM eigenvalues $\lambda_i(t = 0)$ is saved for the ratio computation (6.40) at later times.

The small variation between the two ways to determine the temperature is due to finite-size effects. The initial nonequilibrium transient causes a delayed response of the subsystem with respect to the parent state. Considering bigger system sizes the difference can be reduced.

6.6 Random Matrix Theory analysis of the RDM

In Section 1.2, we introduced RMT as a powerful tool to analyze the global properties of a Hamiltonian, in particular as a parameter-free estimator of complexity or integrability. However, never before had RMT been turned to the study of the entanglement Hamiltonian of a strongly interacting subsystem. This was partly due to the lack of access to the exact dynamics of the RDM with any method other than ours.

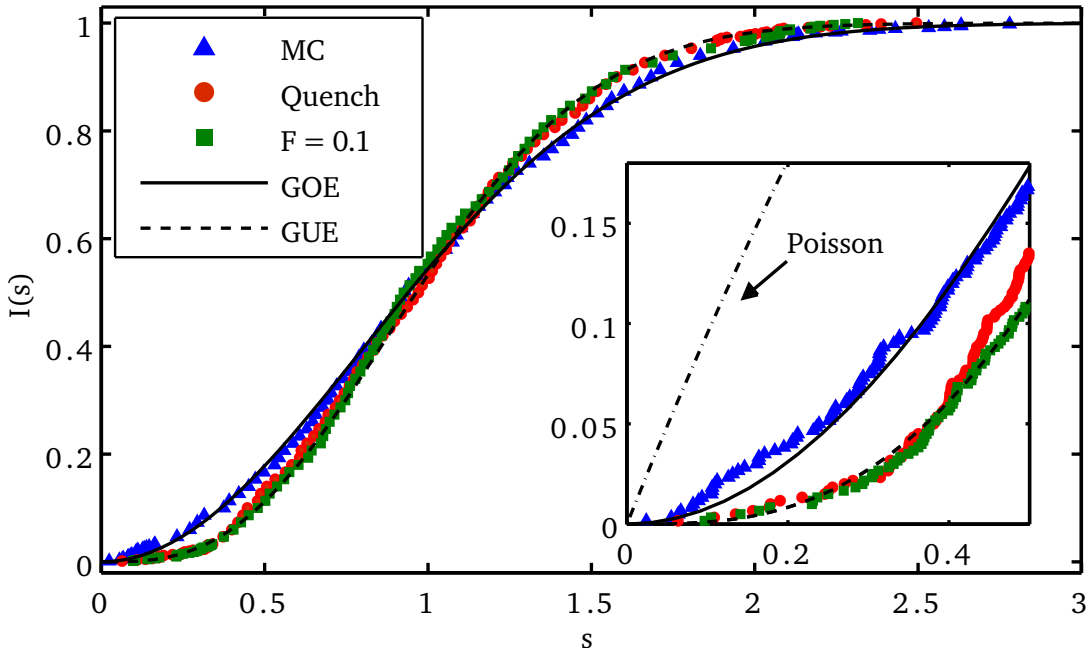

Figure 6.9: Integrated spacing distribution $I(s)$ of the unfolded spectrum of $\log(\rho)$ of an integrable system: in the initial microcanonical state $|\psi\rangle_E$, in the quasi-equilibrium evolution during driving ($F = 0.1$), and in the non–thermal steady state after quenching the flux (Quench). The inset is a zoom in the low–gap regime.

For the quasi–thermal states of the subsystem, $\rho_S(\beta) \propto \exp(-\beta H_{\text{eff}})$ and the statistics of the eigenvalues λ_i of $\log(\rho)$ should match the level statistics of the effective Hamiltonian. We selected a half-filled configuration of the total system in order to have access to better eigenvalue statistics, due to the larger global Hilbert space. The eigenvalue statistics is determined for the largest accessible subsystems of $M = 12$ sites and $N = 6$ fermions, containing 924 levels. As stressed in Section 1.2.2, it is important to select irreducible operators to perform the statistical analysis. Mixing two independent matrices trivially leads to Poissonian distribution, characteristic of uncorrelated subspaces, without providing any information.

The spectrum $\{\lambda_i\}$ of $\log(\rho)$ is unfolded according to the procedure outlined in Section 1.2.1 on page 13, mapping the eigenvalues to an ordered set with uniform average density x_i. The size of the largest sector of the RDM is smaller than the Hamiltonians typically used in RMT, so more care is needed to prevent artifacts from spoiling the results, and to this end 15% on either end of the spectrum was discarded.

We study in the following two standard quantities characterizing the statistics:

a) Level-spacing distribution $P(s)$, the probability of having difference $s = x_{i+1} - x_i$ between two unfolded eigenvalues

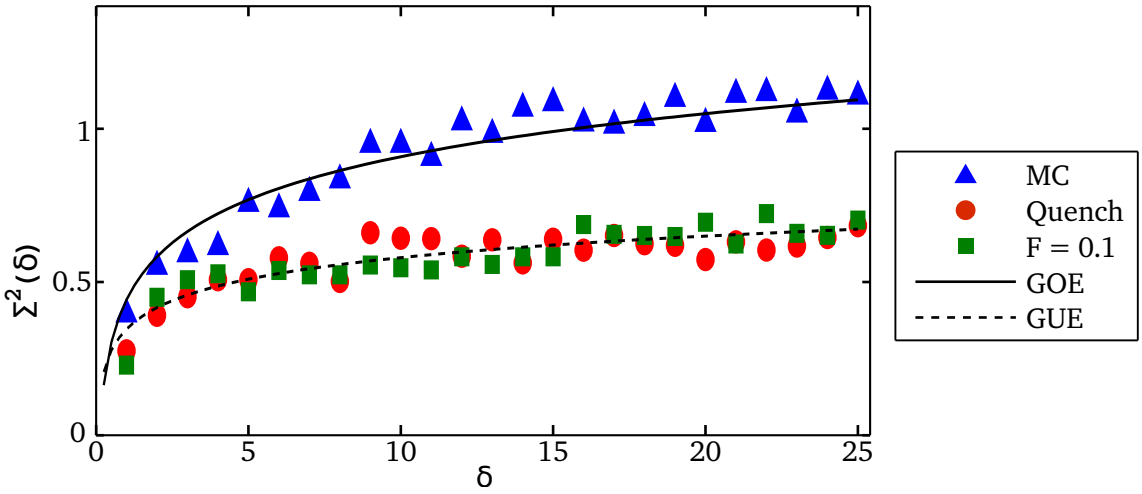

Figure 6.10: Level number variance $\Sigma_2(\delta)$ of the unfolded spectrum of $\log(\rho)$ of an integrable system. The RDM is analyzed in the same conditions as in the previous Fig. 6.9, with lines showing the expected RMT results.

b) Level number variance $\Sigma^2(\delta)$ defined as the variance of the number of unfolded eigenvalues in an integer interval of length δ

$$\Sigma^2(\delta) = \left\langle (x_{i+\delta} - x_i - \delta)^2 \right\rangle_{x_i} \tag{6.42}$$

averaged over all possible intervals starting at each x_i.

$P(s)$ and $\Sigma^2(\delta)$ characterize local correlation properties of the spectrum and long-range level correlations, respectively. The numerical results for $\log(\rho)$ can be compared with the results of the RMT for the GOE or GUE ensembles [BFF+81, GMW98]. In order to reduce the effect of random fluctuations on the spectrum distribution, instead of comparing the spacing probability density $P(s)$ (given for all distributions on page 13), we use the spacing cumulative distribution function $I(s)$. It is the probability of an unfolded spacing $x_{i+1} - x_i$ being less than s. The analytical form of the distributions is approximated by the Wigner's surmise [Haa01, Meh04]

$$I_{\mathrm{GOE}}(s) \simeq 1 - \exp\left[-\frac{\pi s^2}{4}\right] \tag{6.43}$$

$$\Sigma^2_{\mathrm{GOE}}(\delta) \simeq \frac{2}{\pi^2}\left(\log(2\pi\delta) + \gamma + 1 - \frac{\pi^2}{8}\right) \tag{6.44}$$

$$I_{\mathrm{GUE}}(s) \simeq -\frac{4s}{\pi}\exp\left[-\frac{4s^2}{\pi}\right] + \mathrm{Erf}\left[\frac{2s}{\sqrt{\pi}}\right] \tag{6.45}$$

$$\Sigma^2_{\mathrm{GUE}}(\delta) \simeq \frac{1}{\pi^2}\left(\log(2\pi\delta) + \gamma + 1\right), \tag{6.46}$$

where $\gamma \simeq 0.577$ is Euler's constant and Erf is the error function. Note that Hamiltonians of many–body integrable systems have the Poisson distribution with $I_{\mathrm{P}}(s) = 1 - \exp(-s)$ and $\Sigma^2_{\mathrm{P}}(\delta) = \delta$, while generic non–integrable systems with the time–reversal symmetry are expected to follow GOE statistics. Only cases breaking the time–reversal symmetry should result in the GUE statistics.

We have shown in the previous sections that for generic, non-integrable systems in (quasi-)equilibrium, ρ_S of any subsystem is well described by a Gibbs distribution. The spectrum of $\log(\rho)$ for the initial microcanonical thus trivially follows the predictions of the GOE in both the $I(s)$ and $\Sigma^2(\delta)$ statistics. It was expected, since without a flux the time-reversal symmetry is preserved and ρ_S can be chosen as a real symmetric matrix.

In Fig. 6.9 we present numerical data for the integrable system in the initial equilibrium state, together with the prediction of RMT. Surprisingly, the eigenvalue statistics of the RDM of a subsystem turns out to be independent of the integrability of the total system. It can be reconciled with intuition knowing that in a subsystem the conservation laws connected to integrability are broken: particles can move in and out of the subsystem, energy flows, and higher order operators are all the more not conserved. Even though the conservation laws are connected with local operators, the result is not Poissonian, but GOE as supported by a GGE distribution on the subsystem.

On the other hand, under a constant (but modest) field $F > 0$ or after a sudden flux quench we find that the statistics turn into GUE. This is the case for the non–integrable systems as well as for the integrable one, as clearly confirmed in figures 6.9 and 6.10. The GUE statistics at $F > 0$ is consistent with the time–symmetry breaking by a finite current within the subsystem. In the case of quenching the decay of the current is not complete, at least not within an integrable system where the absence of the current relaxation is a hallmark of a finite Drude weight D^N. The integrable systems after a quench relax into the GGE nonthermal equilibrium state, which in presence of persistent currents is compatible with the GUE expectations.

Chapter 7

Thermoelectrical phenomena beyond linear response

We present the realization of the first fully quantum model of a Thermo-Electric Couple (TEC), which we can drive for long times and at strong fields while following its evolution accurately, uncovering nonequilibrium phenomena that have not been previously reported in the literature.

In this chapter, we focus on the thermoelectrical response of a closed system, decoupled from any thermal or particle external reservoir, where the flow of current is generated by induction. The flow of charged fermions, as argued in Section 1.5, leads to a coupled flow of energy and heat, which is clearly seen in an inhomogeneous setup such as a thermocouple. The evolution of the system can be followed at high temperatures using the computational microcanonical pure-state ensemble, solving the time-dependent Schrödinger equation to numerical precision, with the methods following those of the previous chapters.

To investigate local thermal phenomena, we use the Reduced Density Matrix (RDM) introduced in Chapter 6. This allows us to study the local values for the entropy density, which can be connected to genuine heating effects for regimes close to the Local Quasi Equilibrium (LQE). The time-dependent quasi-equilibrium concept introduced in the previous chapter is extended to the case where the local distribution of observables is governed by a space- and time-dependent local effective temperature, consistent with a canonical ensemble of any RDM.

The LQE persists beyond the limits of LR, below the strong field regime however. The latter is marked by the appearance of Bloch Oscillations (BO) of the particle and energy currents, which in this inhomogeneous setup lead to potentially observable oscillations in the particle and energy densities.

7.1 Thermocouple setup

The thermoelectric couple we model is built out of two correlated metallic nanowires with opposite doping. We chose the spinless fermion ring already studied in detail in the previous chapter, with an additional site-dependent potentials ϵ_i to model the doping of the two arms of the TEC. The Hamiltonian is the one shown in Eq. (5.9), and repeated below:

$$
\begin{aligned}
H(\phi) &= \sum_l H_l(\phi) \\
H_i(\phi) &= \left(-t_h\, \mathrm{e}^{i\phi}\, c^\dagger_{i+1} c_i + \mathrm{H.c.}\right) + V\, \tilde{n}_i \tilde{n}_{i+1} + \frac{1}{2} W \left(\tilde{n}_{i-1}\tilde{n}_{i+1} + \tilde{n}_i \tilde{n}_{i+2}\right) + \frac{1}{2}\left(\epsilon_i\, \tilde{\mathrm{n}}_i + \epsilon_{i+1}\, \tilde{\mathrm{n}}_{i+1}\right), \qquad (7.1)
\end{aligned}
$$

with constant repulsion coefficients V and W, hopping constant t_h and PH-symmetrized number operators $\tilde{n}_i = c_i^\dagger c_i - \frac{1}{2}$. Due to the inhomogeneity of the doping, it is crucial to use a correctly defined support for the nearest-neighbor interactions (see Fig. 5.1) and a consistent definition for the energy current J^E, which we take to be Eq. (5.16). The particle current is unaffected by the additional local potentials and it is given by Eq. (5.5).

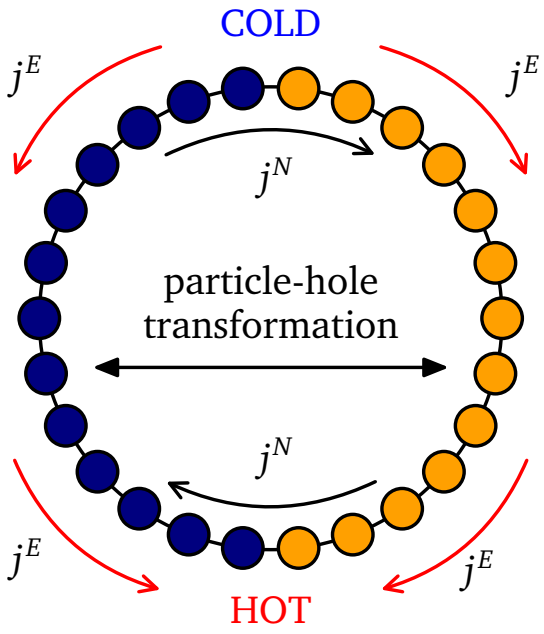

Figure 7.1: Sketch of a TEC: the two colors represent different dopings, respectively positive and negative, with the directions of the currents marked on the drawing.

The TEC is modeled in a way to maintain maximum reflection symmetry between the two components: the system is at half-filling with $N = L/2$, with the antisymmetric local potentials $\epsilon_i = -\epsilon_0$ for $i \leq L/2$ and $\epsilon_i = \epsilon_0$ for $L/2 < i \leq L$, respectively. The first half is thus negatively doped and has an average occupation above half-filling, and vice versa. Such a choice means that the carriers in the wires are of opposite character, i.e. they are electrons and holes. The statement is proven by demonstrating a particular particle–hole transformation PHZ, which specularly maps the two-halves into each other, as shown in Fig. 7.1. It is a mixture of the PH and Z operations introduced in Section 1.1.1,

$$c_i \xrightarrow{\text{PHZ}} (-1)^i c_{L+1-i}^\dagger . \tag{7.2}$$

The symmetry is exact for all times and values of the field ϕ, if it holds for the initial state $|\psi(0)\rangle$[1]. This means that the concentration of fermions on one side of each junction is the same as the concentration of holes on the other

$$\langle n_i \rangle = \left\langle c_i^\dagger c_i \right\rangle = \left\langle c_{L+1-i}\, c_{L+i-1}^\dagger \right\rangle = 1 - \langle n_{L+i-1} \rangle . \tag{7.3}$$

The other symmetry is the inversion with respect to the middle of TEC: $c_i \to c_{L/2+1-i}, \quad \phi \to -\phi$. This explains how the polarity of the TEC can be inverted by reversing the driving field $F(t) = -\frac{d\phi(t)}{dt}$, which leads to a swap of the hot and cold junctions. We will drive the TEC with a *dc* field $F(t) = const > 0$ unless stated otherwise, and the quench protocol will not be employed.

[1] It holds for the Hamiltonian and the transformations generated by it, such as the infinitesimal $e^{-i\,\delta t\, H(t)}$.

The expectation values of J^N are symmetric with respect to the PHZ transformation (7.2)

$$j_i^N = j_{L+1-i}^N, \tag{7.4}$$

but the values of the energy current J^E change sign at the junctions

$$j_i^E = -j_{L+i-1}^E \tag{7.5}$$

This means that if any energy current flows, at one junction it will be directed inwards, while at the other it will be necessarily flowing out. The actual signs are determined by the doping and the direction of the current at the level of LR response, but it can be dynamically reversed by strong fields in the Mott insulating regime, as seen in Section 7.5.

Using the RDM of all of the subsystems of the TEC, scanned sequentially using the algorithm detailed in Section 6.1.2, a map of local properties of the operating TEC can be obtained for arbitrary fields and times. From the RDM the local densities of energy $\varepsilon_i(t)$, entropy $s_i(t)$, and particles $n_i(t)$ can be obtained, and linked to the local effective temperature $\beta_i(t)$ in the LQE regime.

Due to the balance of $\langle n_i \rangle = 0.5$ of the occupation–number at the junctions following from Eq. (7.3), the density of fermions cannot increase in time. Any increase in the entropy density $s_i(t)$ cannot be thus attributed to an influx of particles, but to genuine heating effects. The antisymmetry (7.5) of j_i^E implies that the divergence ∇j_i^E is largest in magnitude at the junctions, which together with the energy continuity equation

$$\frac{d}{dt}\langle H_i \rangle + \nabla j_i^E = F\, j_i^N, \tag{7.6}$$

imply a maximum increase in the local energy at the junctions, which is the main effect behind the operation of the TEC. The right-hand side of the equation represents a local source of heat due to the Joule effect and it is homogeneous across the system. For weak fields however, the Joule heating is proportional to F^2 (since in LR $j^N \propto F$), but the inhomogeneous term ∇j_i^E is linear in F (since $j_i^E \propto F$).

7.2 Weak field and LR

After preparing the equilibrium state $|\psi(0)\rangle = |\psi_E\rangle$ with the microcanonical method, corresponding to an initial inverse temperature $\beta = 0.3$, we drive the system. For the moment we construct the arms of the TEC by chains in the metallic generic (non-integrable) phase, with $L = 26$, $N = 13$, $V = 1.4$, $W = 1.0$ and $\epsilon_0 = 1.4$. To see the effects of the operation of the TEC, we map the density entropy s_i using the RDM of subsystems of size $M = 4$. The RDM for such a subsystem is the partial trace over the remaining sites B of the ring

$$\rho_i(t) = \mathrm{Tr}_B\, |\psi(t)\rangle\langle\psi(t)|, \tag{7.7}$$

with the entropy density given by $s_i(t) = S_i(t)/M$, where $S_i(t)$ is the entanglement entropy of the $M-$site subsystem $\rho_i(t)$, $S_i(t) = \mathrm{Tr}[\rho(t)\log\rho_i(t)]$. The entropy $S_i(t)$ is calculated using all the fermion–number subsectors of $\rho_i(t)$.

The effects of the TEC are clearly visible at the junctions in Fig. 7.2, the cold junction (c) at $i = L/2 = 13$ where the entropy is decreasing, and the junction (h) we dubbed hot at $i = 26$ due to the additional heating.

Support for the interpretation as due to genuine heating/cooling comes from Fig. 7.3, showing the difference ΔS^{hc} between the total entropies for subsystems covering the junctions. Initially, the results

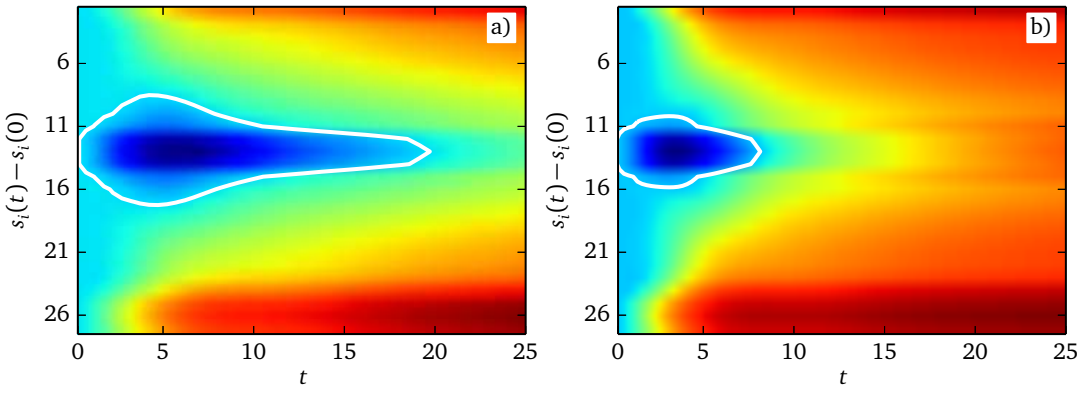

Figure 7.2: Increase of the entropy density $s_i(t)$ from the initial value $s_i(0)$ due to the operation of the TEC. The white contour denotes the region where the value is equal to the starting density. The junctions around $L/2 = 13$ and $L = 26$ are clearly visible. (a) $F = 0.2$ (b) $F = 0.4$. For higher fields, the time scale is reduced.

are independent of M, showing that the effect is completely local, consistently with the Peltier heating. The entropy production at each junction is proportional to the generated heat:

$$\dot{S}_{\text{junction}} = \frac{\dot{Q}}{T} = \beta\,\dot{Q} = -\beta\nabla j^Q_{\text{junction}} = 2\beta\, j^Q_{\text{junction}}, \tag{7.8}$$

where the divergence at the junction $\nabla j^Q_j = j^Q_{j+1} - j^Q_j = 2j^Q_{j+1}$ simplifies to due to $j^Q_{j+1} = -j^Q_j$. The heat production is due to the heat current, and consequently proportional to the particle current via $j^Q = \Pi\, j^N$. The Peltier coefficient at high temperatures can be approximated by *Heikes' formula*, since the chemical potential[2] satisfies $\mu \propto T$, when $T \to \infty$:

$$\Pi = \frac{j^Q}{j^N} = \frac{j^E}{j^N} - \mu \quad \xrightarrow{\mu\to\infty} \quad -\mu. \tag{7.9}$$

A rough local estimate is $\mu_i \simeq \epsilon_i = \pm\epsilon_0$. Both junctions at $t = 0$ are at the same temperature $\beta(0)$ and the effects are symmetrical, thus the difference between the entropies at the hot and cold junctions is

$$\Delta S^{hc} = S_h(t) - S_c(t) \approx 4\beta(0)\int_0^t \epsilon_0\, j^N(t')\, dt', \tag{7.10}$$

in perfect agreement at initial times with the results of Fig. 7.3.

7.2.1 Local Equilibrium regime

The evolution of the TEC for weak fields is consistent with a local quasi equilibrium, where the local density matrix ρ_i is found in a canonical Gibbs distribution set by the local inverse temperature $\beta_i(t)$, which varies in time and space. At every point of the system

$$\rho_i(t) \propto \exp[-\beta_i(t) H_{\text{eff}}(i)], \tag{7.11}$$

where the density matrix further decomposes into blocks with fixed particle number. The spectrum $\{\lambda_i\}$ of the effective Hamiltonian H_{eff} is independent of β, and the details of the driving of the system only affect the macroscopic thermodynamical constraints through $\beta_i(t)$.

Although for small subsystems H_{eff} may significantly differ [KGK$^+$14, HSRH$^+$15] from H, one may still estimate $\beta_i(t)$ without specifying explicit form of $H_{\text{eff}}(i)$. The algorithm was detailed in Section 6.5:

[2] Using the Maxwell relations, $\frac{\mu}{T} = \left(\frac{\partial S}{\partial N}\right)_{V,T}$, so the ratio must be finite at all temperatures

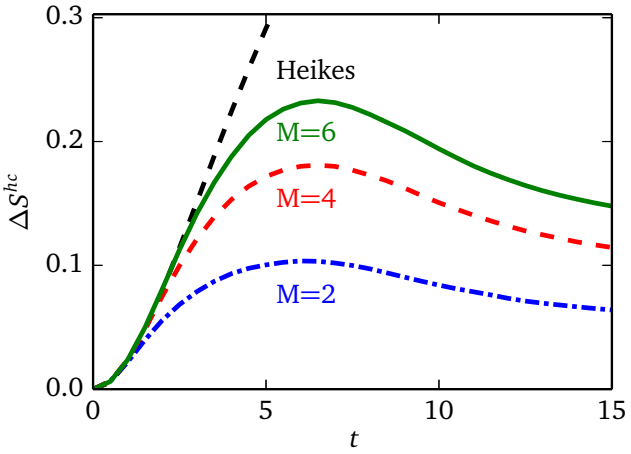

Figure 7.3: Growth of the entropy difference ΔS^{hc} between the junctions, driven with $F = 0.2$, over subsystems with $M = 2, 4, 6$ respectively. The entropy difference is compared with the LR estimation using Heikes' formula (7.10).

the eigenvalue distribution of the RDM is sampled at the initial uniform temperature $\beta_i(0) = \beta(0)$ to determine the eigenvalue distribution $\lambda_{m,i}(0)$ of $\log \rho_i(0)$. The eigenvalues at later times $\lambda_{m,i}(t)$ are used to determine $\beta_i(t)$, knowing that

$$\frac{\beta_i(t)}{\beta_i(0)} = \frac{\lambda_{m,i}(t) - \lambda_{1,i}(t)}{\lambda_{m,i}(0) - \lambda_{1,i}(0)}. \tag{7.12}$$

The results are averaged over all eigenvalues $m \geq 2$ on each site to provide a better estimate.

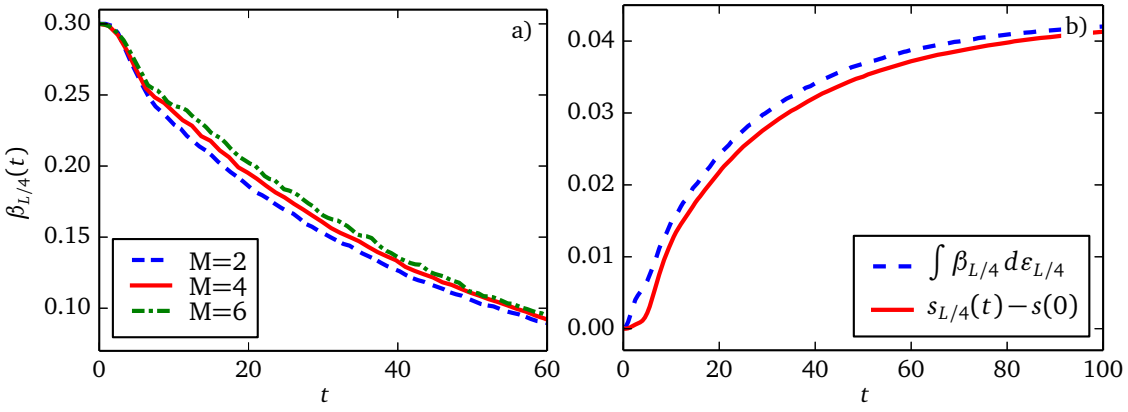

Figure 7.4: Effective temperature away from the junctions, at the point $L/4 = 6$, for a system driven with $F = 0.2$ and $\epsilon_0 = 1.2$. (a) The effective inverse temperature as a function of the subsystem size M (b) The entropy determined by the direct measure on the subsystem $\rho_i(t)$ (solid) compared with the second law estimate (7.13) using the local density of energy and the temperature defined in Eq. (7.12).

Fig. 7.4(a) shows the resulting $\beta_i(t)$ for the subsystem in the middle between hot and cold junctions. Being almost independent of M, β is a well defined intensive quantity.

Furthermore, the consistency of the our local definition of the temperature is strengthened by demonstrating that β is consistent with the 2nd law of thermodynamics. In Fig. 7.4(b) we compare $s_i(t) - s_i(0)$ determined directly from ρ with the integral

$$s_i(t) - s_i(0) = \int_{\varepsilon(0)}^{\varepsilon(t)} d\varepsilon_i\, \beta_i(\varepsilon), \tag{7.13}$$

where $\varepsilon_i(t) = \langle H_i(t) \rangle$ is the energy density in the subsystem. Both quantities are very close to each other, with the same small shift observed for homogeneous systems in Section 6.8 on page 102.

This consistency of the LQE approach breaks down only for subsystems covering one of the junctions, where the details of the average over the sites becomes significant. The snapshots of the temperatures $T_i(t) = \beta_i^{-1}(t)$, across the whole system at three different times, are plotted in Fig. 7.5. Clearly visible is the *temperature gradient*, however an asymmetry in the change of T_i is present at the junctions. The asymmetry gradually decreases for smaller fields, so we attribute it to heating effects. The effect of the passage of time is a gradual overall raise in the effective temperature due to the Joule heating.

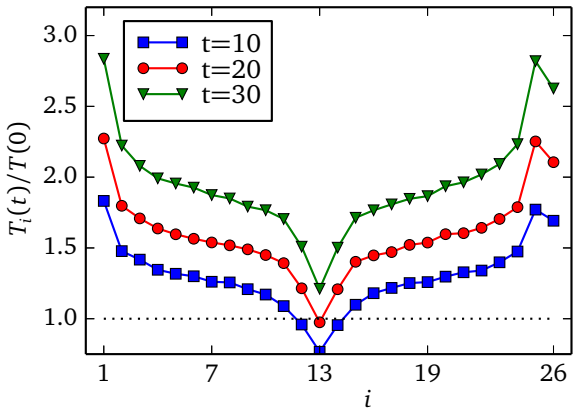

Figure 7.5: Normalized temperature profiles across the TEC over subsystems $M = 4$ wide, driven with a field $F = 0.2$ and $\epsilon_0 = 1.2$.

7.2.2 HTE for the particle number

Position-dependent observables can also be compared with the HTE expectation values, in order to validate the LQE hypothesis. Using the Hamiltonian (7.1), we employ the HTE for the expectation value of the particle density $\langle \tilde{n}_i \rangle$. According to the HTE,

$$\langle \tilde{n}_i \rangle = \langle \tilde{n}_i \rangle_\infty - \beta(\langle \tilde{n}_i H \rangle_\infty - \langle H \rangle_\infty \langle \tilde{n}_i \rangle_\infty) \tag{7.14}$$

but $\langle \tilde{n}_i \rangle_\infty = 0$ at half-filling (HF). The only surviving term of the above equation, is the local-potential term of the Hamiltonian contracted with $\tilde{n}_i$:

$$\left\langle \tilde{n}_i \sum_j \epsilon_j \tilde{n}_j \right\rangle_\infty = \langle \tilde{n}_1 \tilde{n}_2 \rangle_\infty \sum_{j \neq i} \epsilon_j + \epsilon_i \left\langle \tilde{n}_1^2 \right\rangle_\infty = \epsilon_i \left\langle \tilde{n}_1 \tilde{n}_2 - \frac{1}{4} \right\rangle_\infty . \tag{7.15}$$

To simplify the expression above, we used that the sum $\sum_i \epsilon_i = 0$, so $\sum_{j \neq i} \epsilon_j = -\epsilon_i$. Even powers of $\tilde{n}$ on the same site yield a constant expectation value, e.g. $\left\langle \tilde{n}_i^2 \right\rangle_\infty = \frac{1}{4}$. All odd powers of $\tilde{n}$ on different sites vanish ($\langle \tilde{n}_1 \tilde{n}_2 \tilde{n}_3 \rangle_\infty = 0$), whereas $\langle \tilde{n}_1 \tilde{n}_2 \rangle_\infty = -\frac{1}{4} \frac{1}{L-1}$ at half-filling. Finally, the particle occupation number is

$$\langle \tilde{n}_i \rangle = -\beta \left(\langle \tilde{n}_1 \tilde{n}_2 \rangle_\infty - \frac{1}{4} \right) \epsilon_i = \frac{\epsilon_i \beta_i}{4} \frac{1}{1 + 1/L}, \tag{7.16}$$

in perfect agreement with the results shown in Fig. 7.6 for $n_i(t) = \tilde{n}_i(t) + 0.5$, where we averaged ϵ_i over all M sites of the subsystem to generate the prediction.

Strong particle currents flowing in inhomogeneous systems can cause a redistribution of the carriers in the TEC. However, the strong PHZ symmetry from Eq. (7.2) implemented throughout the operation

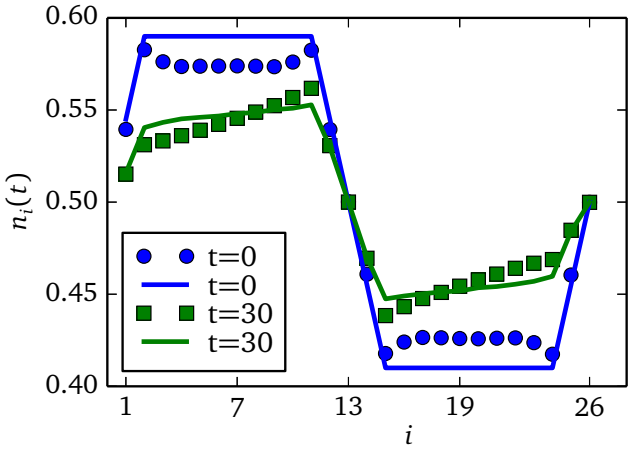

Figure 7.6: Particle occupation profile (points) over a subsystem with $M = 4$, together with the HTE prediction (lines), for the whole TEC at two different times. Field $F = 0.2$ and $\epsilon_0 = 1.2$.

of the system prevents this from happening. The particle density is determined solely by $\beta_i(t)$ and the time-independent ϵ_i, playing the role of the chemical potential in the HTE expansion.

The constraints on the fermion density prevent a flow of particles to the junctions which would increase the entropy density, without being a contribution to the heating. The nonequilibrium density of particles could serve as an additional thermodynamical force, which can oppose the operation of the TEC, as seen in the following section.

7.3 Long time operation of the TEC

In the short-time regime, all curves for the entropy difference at the junctions Δs^{hc} merge if plotted as a function of Ft for various drivings, as shown in Fig. 7.7(a). Due to the closeness of the system, the heat accumulated by the Joule effect uniformly raises the temperature, leveling the differences induced by thermoelectrical effects and stopping the flow of the currents for $t > 0$. The entropy difference is

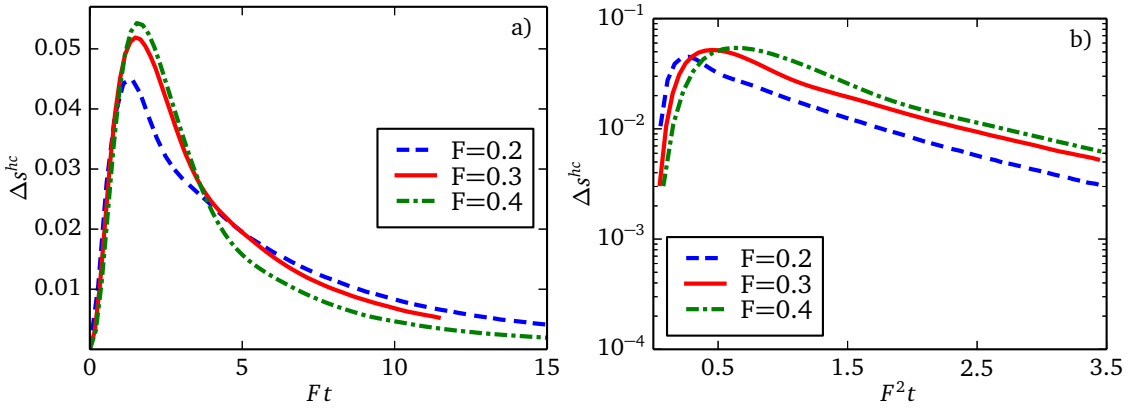

Figure 7.7: Joule heating seen as a leveling of the entropy difference at the junctions in time. The system is driven with different fields $F = 0.2, F = 0.3, F = 0.4$. (a) The overall temperature increase (b) The exponential decrease in Δs^{hc} with a time constant proportional to F^2 seen on the semilogarithmic scale.

exponentially decaying for longer times proportionally to $e^{-a F^2 t}$, with a decay constant 'a' independent of the field, as seen in Fig. 7.7(b). The decay of the particle current j^N in time is identical.

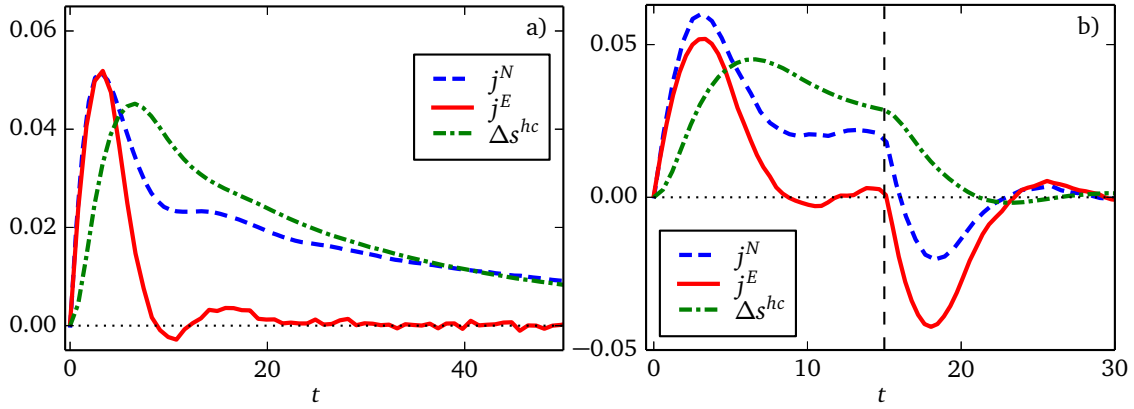

Figure 7.8: Results for $M = 4$, $F = 0.2$ and $\epsilon_0 = 1.2$. (a) The system is driven continuously (b) The electric field is switched off at $t = 15$. The plots show the time profile of j^N and j^E between the junctions (at $i = \frac{3}{4}L$), and the entropy difference Δs^{hc}.

The heating effects are consistent with the picture of a temperature rising uniformly due to the Joule effect, as analyzed by means of the RDM in Chapter 6 and by the estimate of a temperature-dependent *dc* conductivity $\sigma^N(\beta)$ in Chapter 5 (see Fig. 5.4).

Another surprising property of the long time regime can be inferred from Fig. 7.8(a) that shows j^N and j^E in the middle of the left part of TEC, far from the junctions. Initially, both currents show similar time–dependence, however j^E vanishes for $t > 10$ while j^N remains large. In order to explain this nonlinear effect we recall that in the linear-response local-equilibrium regime the currents can be driven by two independent forces: F and $\nabla\beta$. A particular combination of these forces may cause the vanishing of j^N (Seebeck effect) or j^E (present case). In order to explicitly show that the vanishing of j^E originates from compensation of two forces we instantaneously switch off one of them: the electric field, the only we have complete control over. As shown in Fig. 7.8(b), the remaining force drives j^E in the opposite direction.

The particle–hole symmetry implies that either j^E vanishes or $\nabla j^E \propto F$ is large at the junctions. As follows from Eq. (7.6), the latter possibility would preclude the quasi-stationary evolution of an *isolated* TEC. In case of open systems we expect only partial compensation of driving forces in a stationary state which diminishes the efficiency of heat pumping under a strong driving. The cancellation of the energy current is unexpected, but not contradictory with the phenomenology of the Peltier effect: the latter is typically derived under the uniform-temperature boundary condition $\nabla\beta = 0$, which precludes the thermodynamical flux from interfering and the effects of the Joule heating to hinder the transport efficiency.

7.4 Strong field Bloch oscillations

Strong fields have been shown to destroy the quasi-equilibrium regime in homogeneous systems and produce Bloch oscillations.

The operation of the TEC is similarly disrupted under strong F. The first nonequilibrium effect concerns the magnitude of F which destroys the LQE. Since the TEC is spatially inhomogeneous, different conditions can lead to the persistence of the local equilibrium in certain parts of TEC while being destroyed in others, as it is the case of the hot and cold junctions. We have tested the equilibrium relations by comparing observables calculated in the canonical ensemble with local observable densities

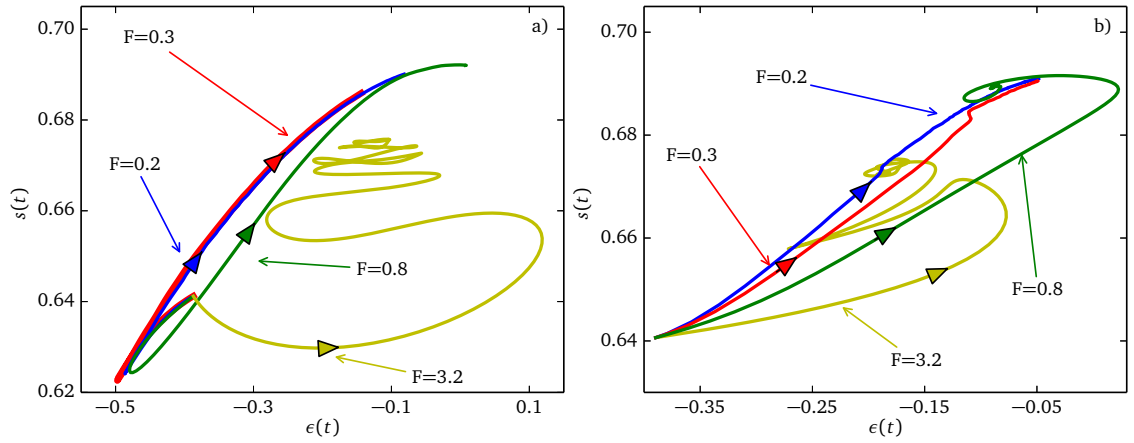

Figure 7.9: Results for $M = 4$, $F = 0.2$ and $\epsilon_0 = 1.2$. (a) The system is driven continuously (b) The electric field is switched off at $t = 15$. The plots show the time profile of j^N and j^E between the junctions (at $i = L/4$), and the entropy difference Δs^{hc}

and checked that the same relations are satisfied, following the procedure outlined in Section 6.3. In the LQE regime, intensive quantities including $s_i(t)$ and $\varepsilon_i(t)$, are uniquely determined by $\beta_i(t)$, establishing a monotonic relation between the three.

The universal relation, analogous to Eq. (6.30), is confirmed for $F \leq 0.4$ for the cold and hot junctions, in figures 7.9(a) and 7.9(b) respectively. In the former case the curves for weak F merge during the entire evolutions, while in the latter case it happens only in the long–time regime after the nonequilibrium transient. It can be observed that the local equilibrium relations are broken first at the hot junction, where the thermal effects play a greater role, as seen in Fig. 7.5. For large F, $\varepsilon_i(t)$ starts to oscillate, while oscillations of $s_i(t)$ are rather limited. Therefore, the equilibrium relation between ε_i and s_i is broken as early as when the energy current $j_i^E(t)$ begins to undergo the Bloch oscillations. Conversely in homogeneous half-filled systems the limits of nonequilibrium evolution are signaled by the Bloch oscillations of the particle current $j_i^N(t)$ [Fre08, EW11, ECP14].

Although in homogeneous systems j_i^N and j_i^E may Bloch oscillate, the densities of particles and energy still do not show any oscillatory behavior. The oscillations of the density are connected by the continuity equations to the gradient of the currents

$$\frac{d}{dt}\langle H_i \rangle + \nabla j_i^E = F\, j_i^N \quad \text{and} \quad \frac{d}{dt}\langle N_i \rangle + \nabla j_i^N = 0. \tag{7.17}$$

In homogeneous systems the currents are translationally symmetric and $\nabla \left\langle J_j^{N(E)} \right\rangle = 0$. Conversely in the TEC, large gradients of the currents are present at the junctions, thus leading to oscillations in $n_i(t)$ and $h_i(t)$ shown in Fig. 7.10. The oscillations are particularly strong at the cold and less visible at the hot junctions, due to thermal effects. The energy density oscillations in panel (b) are only positive across the cold junction due to the symmetry requirement, whereas the particle number oscillations in panel (a) are antisymmetric and display both signs.

The presence of Bloch oscillations of the currents is a phenomenon expected in all tight-binding models driven by strong fields, as already shown in Section 5.5. The density Bloch oscillations have not been previously observed, due to the necessary homogeneity of systems needed for the experimental and numerical realizations. Given the derivation above, grounded in the continuity equations and the bandwidth limitation of tight-binding Hamiltonians, the density oscillations are expected at the junctions of composite realistic systems in the quantum regime.

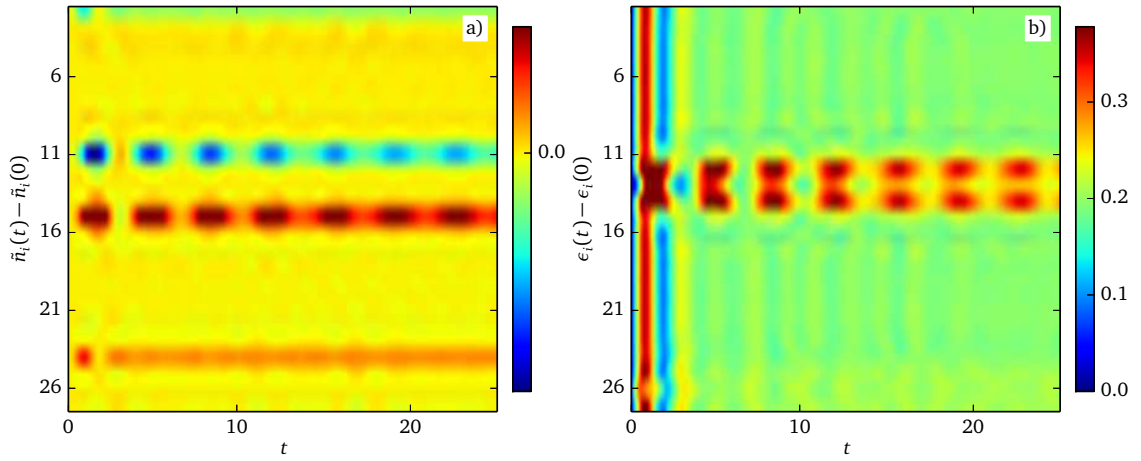

Figure 7.10: Results for $M = 4$, and $\epsilon_0 = 1.2$, driven with a strong field $F = 3.2$. (a) Particle density variation relative to the initial state (b) Local energy density with respect to the initial value.

7.5 Dynamical reversal of the Peltier response in strong fields

After investigating models of the TEC built out of two differently doped featureless metals, we turn to the case of two doped Mott insulators. At half-filling, when $W < V$, for interaction strengths $V > 2$ the ground state of the system is an insulator, as mentioned in Section 1.1.3.

We tune the interaction constant from $V < 2$ to $V > 2$ in Fig. 7.11(a). At short times, the LR Peltier response is visible, and the entropy difference at the junctions Δs^{hc} is independent of the interaction strength V as per Eq. (7.10). For longer times $t > 5$, tuning V reverses the *dc* flow of the entropy and interchanges the role of the junctions. The effect is expected, being due to switching the charge carriers from electrons in the metallic regime, to holes in the Mott-insulating phase. Unexpected results are

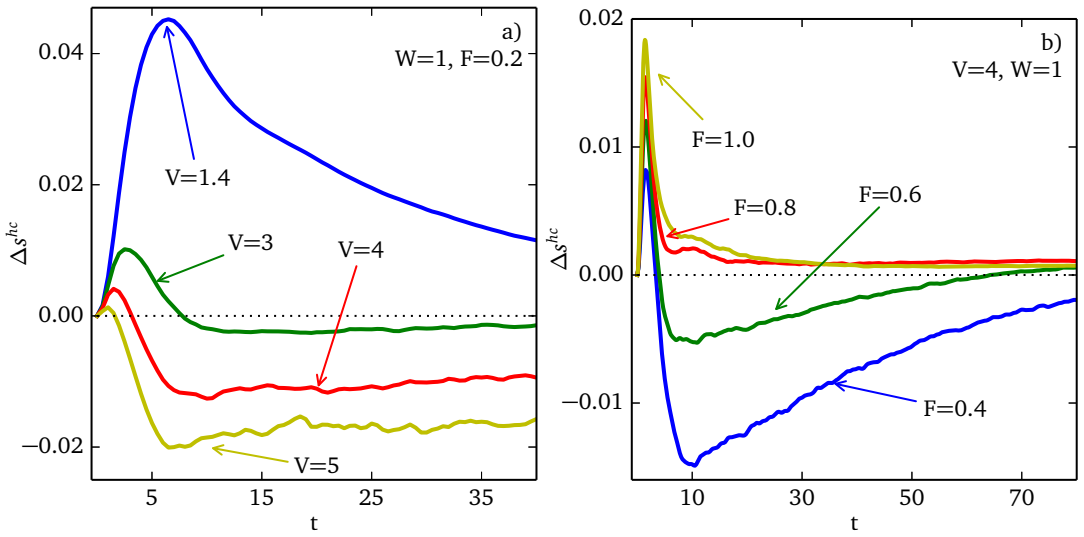

Figure 7.11: Difference Δs^{hc} in the entropy density between the two junctions $h = 26, c = 13$. (a) TEC driven with a constant field $F = 0.2$, as V is varied from the metallic ($V = 1.4$) to the insulating phase ($V > 2$) (b) Strong Mott insulating phase with $V = 4, W = 1$, driven with fields from $F = 0.4$ to $F = 1.0$.

obtained in the insulating phase, seen in Fig. 7.11(b). Under strong driving, the TEC operates in the same way as seen for generic metals, i.e. the current is carried again by electrons. The breaking of

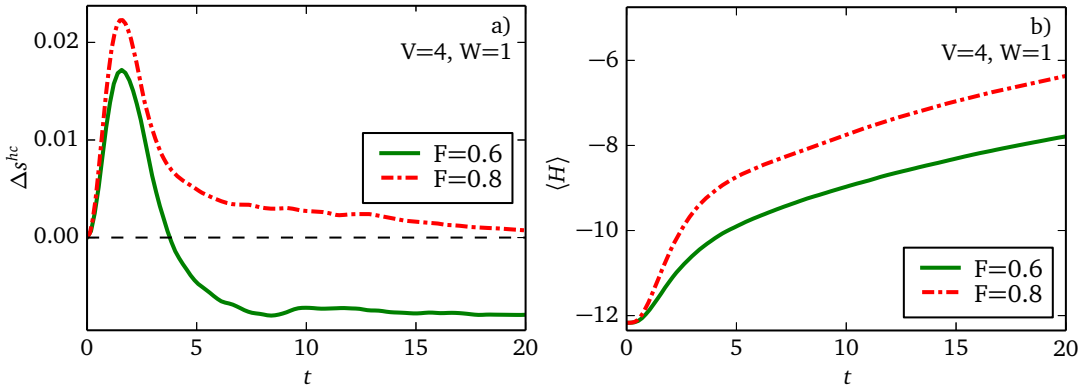

Figure 7.12: Difference Δs^{hc} in the entropy density between the two junctions $h = 26, c = 13$. (a) TEC driven with a constant field $F = 0.2$, as V is varied from the metallic ($V = 1.4$) to the insulating phase ($V > 2$) (b) Strong Mott insulating phase with $V = 4, W = 1$, driven with fields from $F = 0.4$ to $F = 1.0$.

the insulating *ground state* by strong fields has been investigated in the framework of Landau-Zener transitions from a dispersionless ground state to a dispersionful excited state. However, the present case involves highly energetic states of a doped Mott insulator, where the energy density is finite and a continuum of states exists.

The objection that this is due to heating effects has been raised, explaining away the inversion as being the result of a faster increase in the energy at higher F. We have explicitly ruled out this scenario, by comparing the average energy of the system to the entropy difference at the junctions Δs^{hc}, in Fig. 7.12. A Mott insulator with $V = 4$ is driven with two different fields, $F = 0.6$ and $F = 0.8$. Waiting a sufficient time for the systems to reach the same energy $\langle H \rangle \approx -8$, the Peltier response is still reversed for the two fields. It is thus possible to control the direction of the flow of heat by changing F alone, which is a truly nonequilibrium phenomenon, with a probable entropic origin still eluding a complete explanation.

7.5.1 Finite-size scaling

Finally, we provide support in Fig. 7.13, that the nonequilibrium phenomena treated in this Chapter are well defined quantities in the $L \gg 1$ limit. The scaling of $\beta_i(t)$ away from the junctions in panel (a) shows differences of similar magnitude as the scaling by M, confirming the significant of the temperature measurable we have defined. The time necessary for zeroing of the energy current in panel (b) does not scale with L, proving that the effect can be seen in systems in the thermodynamical limit. The Bloch oscillations at the junctions in panels (c) and (d) do not show any dependence on the system size, as the oscillations merely follow the external field and the microscopical details have limited effects. The Peltier effect reversal due to strong fields in panels (e) and (f), on the other hand shows even-odd effects, due to the parity of the site $c = L/2$.

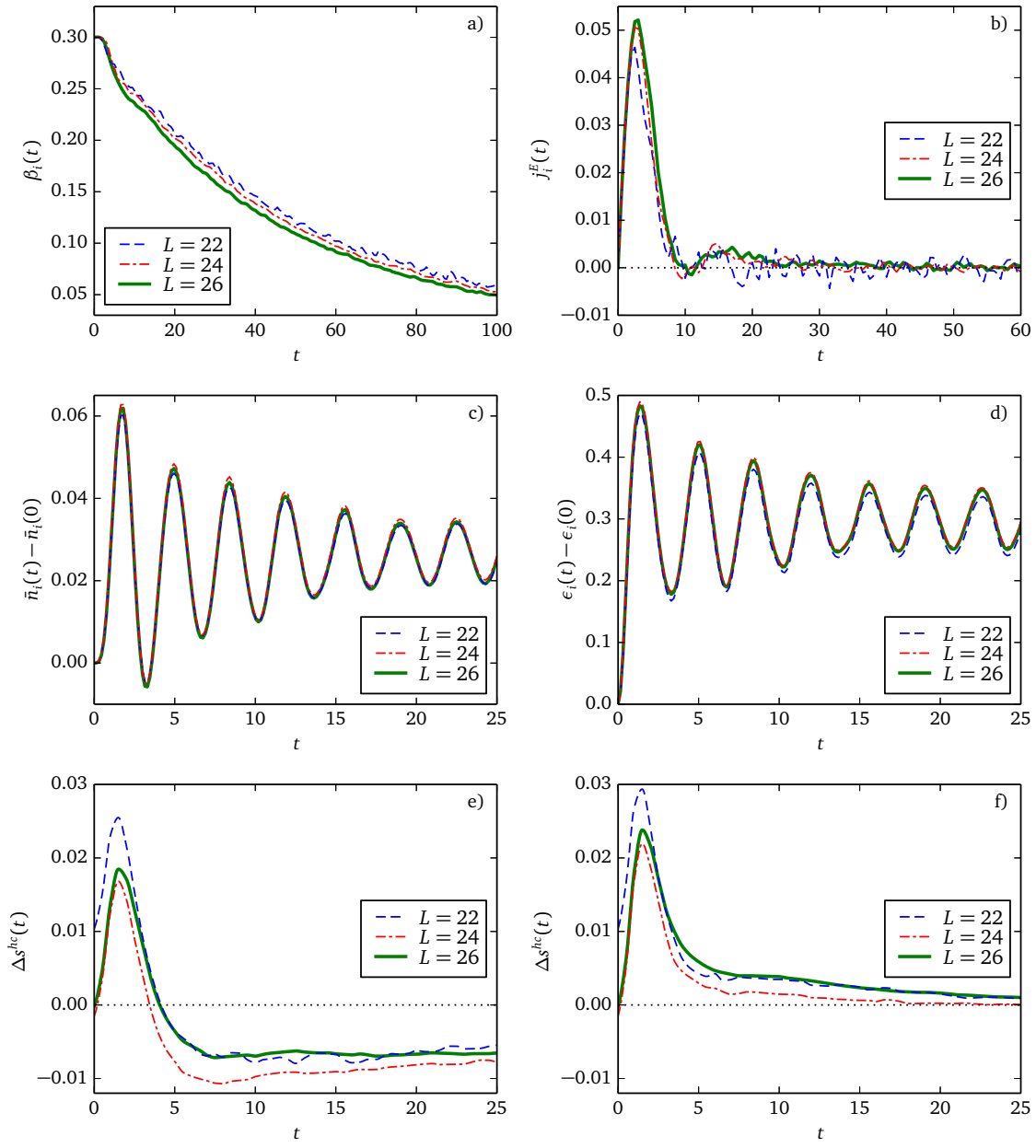

Figure 7.13: (a) Scaling of $\beta_{L/4}(t)$ with respect to L with data from Fig. 7.4 (b) Interruption of the flow of $j^E_{L/4}$ due to balancing of thermodynamical fluxes from Fig. 7.8 (c) and (d) Particle and energy density oscillations at the junctions driven by strong fields, as in Fig. 7.10 (e) and (f) Reversal of the Peltier response Δs^{hc} in a $V = 4, W = 1$ Mott insulator between the driving with $F = 0.6$ and $F = 0.8$ respectively, using the setup of figures 7.11 and 7.12

Chapter 8

Results

Over the course of this Dissertation, a one–dimensional ring of interacting spinless fermions has been presented in its static and dynamical properties under driving, in the integrable and generic regime, in the metallic or insulating phase. The system was studied starting with its equilibrium, by introducing computational ensembles for the calculation of observables in thermal equilibrium, to the extreme nonequilibrium regimes where the quantum Bloch oscillations disrupt the ordered transport. In between, the quasi–equilibrium regime, where the local observables can be described by an effective temperature, is observed and compared to the linear response framework.

The original results are summarized below, divided by the corresponding Chapter.

Chapter 5.

The equilibrium thermodynamics of the system was established by presenting all the necessary computational methods to calculate arbitrarily complicated observables at any temperature in the range $T \in [0, \infty]$. This was preliminary in order to determine the frequency–dependent conductivities $\sigma^{N(E)}(\omega)$, which control the system response to a vanishing externally–applied electrical field. Known as the Linear Response (LR) regime, it provides a benchmark for the finite–field response. The imaginary part of the off–diagonal correlation function $\mathrm{Im}\, C_E^{>}(\omega)$ required the development of a new projection method in Krylov space in Section 2.4 to calculate accurately the response directly in the spectral domain.

The time–dependent external magnetic field inductively generates a flow of currents in the system, leading to the transport of charge and energy throughout the system. The expression for the energy current operator J^E, fully respecting the combined system symmetry PHZ, was derived in the general case when the interaction parameters vary arbitrarily between sites, allowing precise site–wise measurement of the observable in Section 5.1.

The flow of the current in presence of a nonzero external field is countered by an electrical resistance growing with the temperature, and the dissipation increases the energy of the system even in integrable cases. The Joule effect is the source for the energy dependence of the *dc* response, which is the leading effect beyond LR, and the energy–dependent response of the energy current is shown in Section 5.3.

Under *dc* driving by a nonzero electric field F, the long–time ratio of the energy current (j^E) and the particle current (j^N) values was shown to recover the LR results in the weak–field limit of driven nonintegrable systems, validating the more versatile real–time approach in Section 5.4. Going beyond the linear regime is needed for ballistic systems, as the equilibrium LR theory predicts singular responses of both currents, quantified by the stiffnesses D^E and D^N, respectively. Since j^E is a conserved quantity

(at $F = 0$), D^E represents simply the stress coefficient. However, j^N is not conserved and the physical origin of a finite D^N is more complex.

We have first considered a system (doped insulator) where the local conserved quantities saturate the Mazur bound on D^N. In this case the long–time results for $R(t) = j^E(t)/j^N(t)$ agree with the LR ratio D^E/D^N, despite the currents themselves are steady or oscillating in contrast to the LR prediction $j^{N(E)} \propto Ft$, in Sections 5.5 and 5.6.

We have then studied a metal close to half–filling in Section 5.7, where the large D^N cannot be explained by the Mazur bound formulated in terms of local conserved quantities. On the one hand, the ratio $j^E(t)/j^N(t)$ obtained for a system which relaxes after a flux–quench (δ–like pulse of electric field) nicely agrees with the LR theory. On the other hand, $j^E(t)/j^N(t)$ obtained for a steady driving becomes much larger than the LR value D^E/D^N, reaching the value predicted using the Mazur bound. The driving by a field reduces the coupling of j^N to conserved currents other than j^E, enhancing the ratio $R(t)$ greatly beyond the LR bound.

Chapter 6.

Using the Reduced Density Matrix (RDM), detailed in Section 6.1, of the subsystem offers the possibility to study the case at the foundations of statistical mechanics, in a nonequilibrium setting: the dynamics of a small system interacting (albeit strongly) with a much larger, in the number of degrees of freedom, bath. The dynamics is projected directly from the accurate evolution of the whole state of the system, thus it is not constrained to the Markovian second-order perturbative approximation that hinders the Lindblad equation. Systems strongly interacting with their environment cannot be modeled by the latter approach, as the subsystem and the environment have similar correlation times, and the secular approximation[1] fails.

The RDM evolution is a useful tool to investigate nonequilibrium properties of any system, and our results concern mostly the unknown behavior of a metallic integrable ring. The thermalization of integrable system is prevented by the existence of local conserved operators. However, when the system is driven, those conservation laws are broken. As shown in Section 6.3, the observables defined on the subsystems finally attain their thermodynamical values.

Subsystems of an integrable systems have been shown in Section 6.4 to approach a locally thermal state, according to the hypothesis of *canonical typicality*: the local state is constrained to $\rho_S \propto \mathrm{e}^{-\beta(t)H_{\mathrm{eff}}}$, with an a priori unspecified local H_{eff}. The spectrum of $\log(\rho_S)$ thus contains information useful for identifying the quasi–thermal, steady non–thermal, and the non–equilibrium regimes. For the case of quasi–thermal states, which are realized also for finite but modest driving, we have demonstrated that the effective inverse temperature β (see Section 6.5) as the only relevant parameter determines the state of ρ_S, for states evolved from thermal states. This result sets straightforward limits on the relaxation of integrable systems, but more importantly, it confirms the nontrivial concept of the subsystem effective Hamiltonian H_{eff}, which is shown to be independent of the temperature and initial conditions.

The *entropy density* introduced on the RDM in Section 6.1.1 is an invaluable tool to monitor the approach to the thermal state, which is defined as the maximum entropy state under the constraint of conservation of energy. Integrable systems after a quench do not thermalize, resulting in an entropy deficit compared to canonical state. The convexity of the entropy density sets the threshold of the quasi–equilibrium evolution after the initial nonequilibrium transient. The density is a quantity directly related to the heating of the system, which we have shown to follow the second law of thermodynamics

[1] Infinitely short coherence time of the bath.

for systems not performing any work.

For the first time, the *RMT analysis* was applied to the *RDM spectrum* instead of the global energy operator. The results from Section 6.6 based on the spectral statistics of the RDM reveal a universal conclusion: subsystems of a system in equilibrium obey the GOE eigenvalue statistics. This is the case regardless of integrability of the whole system, even when the global Hamiltonian operator obeys Poisson statistics. The subsystems of the driven system and systems quenched with a field pulse follow the GUE universality, although the model by itself does not break the time–reversal symmetry. For the quenched integrable system, the state reached is the *GGE*, or maximum entropy state with the finite-current constraint, towards which the relaxation is effectively irreversible as shown by the transition from Poissonian to GUE statistics.

Chapter 7.

Thermoelectrical effects are more evident in inhomogeneous systems, where they were historically observed for the first time. The typicality approach can be easily extended to a quantum thermo-electric couple, where the arms are modeled (Section 7.1) by two inversely doped materials at high temperatures. The intensive thermodynamical potentials can vary in such a system, so we have introduced the concept of *local quasi-equilibrium*, parametrized by a spatially varying effective temperature $\beta_i(t)$, defined from the local Gibbs state of the RDM.

The reflection and particle-hole symmetry relate the two halves of the system, guaranteeing that the particles do not accumulate at the junctions, and that the energy flows from one junction to the other under the driving field, giving rise to the Peltier effect.

When the system is slowly driven from a uniform–temperature state, as shown in Section 7.2, the gradient of the energy current ∇j^E at the junctions is maximal, leading to a time–dependent energy density, which increases at the hot (h), and decreases at the cold (c) junction. For $t \to 0$, the difference in the entropy density between the junctions $\Delta s^{hc} \propto F$ follows the LR relation for the Peltier effect at high temperatures, independently of the analyzed junction size M. Using the effective local temperature $T_i(t) = \beta_i^{-1}(t)$ we can show that a gradient forms between the junctions, where discontinuities arise. For short times, all observables in the TEC follow the local equilibrium values, albeit with an exponential time dependence in $\beta_i(t)$ due to the Joule effect which is beyond the LR regime.

In a driven closed system, we have shown that the energy increase opposes the flow of the currents. The uniform Joule heating thus blurs the response of the TEC, which exponentially vanishes as e^{-aF^2t}. Moreover, the continuity equations imply the nonstationarity of the energy whenever the gradient ∇j^E is nonzero. Already at short times, the system reaches a stationary state by producing a balancing nonzero thermodynamical flux (i.e. the temperature gradient), which opposes the flow of the energy current, which abruptly vanishes away from the junctions. We have been able to show this explicitly in Section 7.3, by zeroing the other thermodynamical flux: the electrical field. The remaining gradient is released in the form of a flow of energy with opposite sign.

Strong fields in homogeneous systems produce Bloch oscillations of the currents, which are however translationally invariant. In the TEC, the Bloch oscillations in ∇j^N and ∇j^E, strongest at the junctions, couple to oscillations in the density of energy and charge, seen in Section 7.4. The strong variations in the densities at the junctions are then directly observable, an effect that was not previously visible in the classical description of a thermocouple.

We have observed another intriguing novel effect at strong fields, below the level needed for the Bloch oscillations, in Section 7.5. The external driving field can dynamically reverse the sign of the

carriers in a TEC made out of two Mott insulating arms. The effect is a high–temperature dynamical transition between the insulating state and a metallic behavior, induced by sufficiently strong driving after a universal transient.

Appendix A

List of Own Publications

Articles regarding the topic of the dissertation

1. Dawid Crivelli, Marcin Mierzejewski, and Peter Prelovšek, *Energy and particle currents in a driven integrable system*, Physical Review B **90** (2014), 195119.

2. Dawid Crivelli, Marcin Mierzejewski, and Peter Prelovšek, *Energy Current and Energy Fluctuations in Driven Quantum Wires*, NATO Science for Peace and Security Series C: Environmental Security, Springer Netherlands, Dordrecht, 2015.

3. Marcin Mierzejewski, Dawid Crivelli, and Peter Prelovšek, *Peltier effect in strongly driven quantum wires*, Physical Review B **90** (2014), 075124.

4. Marcin Mierzejewski, Tomaž Prosen, Dawid Crivelli, and Peter Prelovšek, *Eigenvalue Statistics of Reduced Density Matrix during Driving and Relaxation*, Physical Review Letters **110** (2013), no. 20, 200602.

Nonconventional Superconductivity and Computational Physics

1. Dawid Crivelli and Andrzej Ptok, *Unconventional Superconductivity in Iron-Based Superconductors in a Three-Band Model*, Acta Physica Polonica A **126** (2014), no. 4A, 16–20.

2. Andrzej Ptok and Dawid Crivelli, *The Fulde–Ferrell–Larkin–Ovchinnikov State in Pnictides*, Journal of Low Temperature Physics **172** (2013), no. 3-4, 226–233.

3. Andrzej Ptok, Dawid Crivelli, and Konrad Jerzy Kapcia, *Change of the sign of superconducting intraband order parameters induced by interband pair hopping interaction in iron-based high-temperature superconductors*, Superconductor Science and Technology **28** (2015), no. 4, 045010.

4. Michał Januszewski, Andrzej Ptok, Dawid Crivelli, and Bartłomiej Gardas, *GPU-based acceleration of free energy calculations in solid state physics*, Computer Physics Communications **192** (2015), 220–227.

Bibliography

[AAN13] Mohsen Alishahiha, Davood Allahbakhshi, and Ali Naseh, *Entanglement thermodynamics*, Journal of High Energy Physics **2013** (2013), no. 8, 102.

[AES14] Felix Andraschko, Tilman Enss, and Jesko Sirker, *Purification and Many-Body Localization in Cold Atomic Gases*, Physical Review Letters **113** (2014), no. 21, 217201.

[AF08] Andreas Alvermann and Holger Fehske, *Chebyshev approach to quantum systems coupled to a bath*, Physical Review B **77** (2008), no. 4, 045125.

[AF11] Andreas Alvermann and H. Fehske, *High-order commutator-free exponential time-propagation of driven quantum systems*, Journal of Computational Physics **230** (2011), no. 15, 5930–5956.

[AFL12] Andreas Alvermann, H. Fehske, and P. B. Littlewood, *Numerical time propagation of quantum systems in radiation fields*, New Journal of Physics **14** (2012), no. 10, 105008.

[AFP09] Gennaro Auletta, Mauro Fortunato, and Giorgio Parisi, *Quantum Mechanics*, no. 9781107665897, Cambridge University Press, 2009.

[AG02] J. V. Alvarez and Claudius Gros, *Low-Temperature Transport in Heisenberg Chains*, Physical Review Letters **88** (2002), no. 7, 077203.

[AHL12] Vincenzo Alba, Masudul Haque, and Andreas M. Läuchli, *Boundary-Locality and Perturbative Structure of Entanglement Spectra in Gapped Systems*, Physical Review Letters **108** (2012), no. 22, 227201.

[AKT14] Anthony P Austin, Peter Kravanja, and Lloyd N Trefethen, *Numerical Algorithms Based on Analytic Function Values at Roots of Unity*, SIAM Journal on Numerical Analysis **52** (2014), no. 4, 1795–1821.

[AL06] R Alicki and K Lendi, *Quantum Dynamical Semigroups*, Springer-Verlag Berlin Heidelberg, 2006.

[Arb12] Peter Arbenz, *Lecture Notes on Solving Large Scale Eigenvalue Problems*, D-MATH, EHT Zurich 2 (2012).

[BBW04] J. Berges, Sz. Borsányi, and C. Wetterich, *Prethermalization*, Physical Review Letters **93** (2004), no. 14, 142002.

[BC15] Fernando G. S. L. Brandao and Marcus Cramer, *Equivalence of Statistical Mechanical Ensembles for Non-Critical Quantum Systems*, ArXiv (2015), 1502.03263.

[BCH11] Mari Carmen Bañuls, J. Ignacio Cirac, and Matthew B. Hastings, *Strong and Weak Thermalization of Infinite Nonintegrable Quantum Systems*, Physical Review Letters **106** (2011), no. 5, 050405.

[BCMM14] Giuliano Benenti, Giulio Casati, and Carlos Mejía-Monasterio, *Thermoelectric efficiency in momentum-conserving systems*, New Journal of Physics **16** (2014), no. 1, 015014.

[BCMMP15] Giuliano Benenti, Giulio Casati, Carlos Mejia-Monasterio, and Michel Peyrard, *From thermal rectifiers to thermoelectric devices*, ArXiv (2015), 1512.06889.

[BCW13] Giuliano Benenti, Giulio Casati, and Jiao Wang, *Conservation Laws and Thermodynamic Efficiencies*, Physical Review Letters **110** (2013), no. 7, 070604.

[BDD+00] Zhaojun Bai, James Demmel, Jack Dongarra, Axel Ruhe, and Henk van der Vorst, *Templates for the Solution of Algebraic Eigenvalue Problems: A Practical Guide*, SIAM, Philadelphia, PA (2000), 316.

[Bee15] C. W. J. Beenakker, *Random-matrix theory of Majorana fermions and topological superconductors*, Reviews of Modern Physics **87** (2015), no. 3, 1037–1066.

[BEL14] Lars Bonnes, Fabian H.L. Essler, and Andreas M. Läuchli, *"Light-Cone" Dynamics After Quantum Quenches in Spin Chains*, Physical Review Letters **113** (2014), no. 18, 187203.

[BFF+81] T. Brody, J Flores, J. French, P. Mello, A Pandey, and S. Wong, *Random-matrix physics: spectrum and strength fluctuations*, Reviews of Modern Physics **53** (1981), no. 3, 385–479.

[BG09] Christian Bartsch and Jochen Gemmer, *Dynamical typicality of quantum expectation values*, Physical Review Letters **102** (2009), no. 11, 8–11.

[BH12] Thomas Barthel and Robert Hübener, *Solving Condensed-Matter Ground-State Problems by Semidefinite Relaxations*, Physical Review Letters **108** (2012), no. 20, 200404.

[BHVC09] M. C. Bañuls, M. B. Hastings, F. Verstraete, and J. I. Cirac, *Matrix Product States for Dynamical Simulation of Infinite Chains*, Physical Review Letters **102** (2009), no. 24, 240603.

[BIL83] M Büttiker, Y Imry, and R Landauer, *Josephson behavior in small normal one-dimensional rings*, Physics Letters A **96** (1983), no. 7, 365–367.

[BK03] Andreas Buchleitner and Andrey R. Kolovsky, *Interaction-Induced Decoherence of Atomic Bloch Oscillations*, Physical Review Letters **91** (2003), no. 25, 253002.

[BKL10] Giulio Biroli, Corinna Kollath, and Andreas M. Läuchli, *Effect of Rare Fluctuations on the Thermalization of Isolated Quantum Systems*, Physical Review Letters **105** (2010), no. 25, 250401.

[Boy00] John P Boyd, *Chebyshev and Fourier Spectral Methods*, New York (2000), 688.

[BP03] J. Bonča and P. Prelovšek, *Thermodynamics of the planar Hubbard model*, Physical Review B **67** (2003), no. 8, 085103.

[BP07] Heinz-Peter Breuer and Francesco Petruccione, *The Theory of Open Quantum Systems*, Oxford University Press, 2007.

[BPR+96] Maxime Ben Dahan, Ekkehard Peik, Jakob Reichel, Yvan Castin, and Christophe Salomon, *Bloch Oscillations of Atoms in an Optical Potential*, Physical Review Letters **76** (1996), no. 24, 4508–4511.

[Bra06] Paolo Brandimarte, *Numerical Methods in Finance and Economics*, John Wiley & Sons, Inc., Hoboken, NJ, USA, sep 2006.

[BS14] Alexander Braun and Peter Schmitteckert, *Numerical evaluation of Green's functions based on the Chebyshev expansion*, Physical Review B **90** (2014), no. 16, 165112.

[BSS12] Thomas Barthel, Ulrich Schollwöck, and Subir Sachdev, *Scaling of the thermal spectral function for quantum critical bosons in one dimension*, ArXiv (2012), 1212.3570.

[BSW09] Thomas Barthel, Ulrich Schollwöck, and Steven White, *Spectral functions in one-dimensional quantum systems at finite temperature using the density matrix renormalization group*, Phys. Rev. B **79** (2009), no. 24, 245101.

[BT04] Jean-Paul Berrut and Lloyd N. Trefethen, *Barycentric Lagrange Interpolation*, SIAM Review **46** (2004), no. 3, 501–517.

[BV04] Stephen Boyd and Lieven Vandenberghe, *Convex Optimization*, Cambridge University Press, New York, NY, USA, 2004.

[Cal48] Herbert B. Callen, *The application of onsager's reciprocal relations to thermoelectric, thermomagnetic, and galvanomagnetic effects*, Physical Review **73** (1948), no. 11, 1349–1358.

[Cal57] ———, *Principle of Minimum Entropy Production*, Physical Review **105** (1957), no. 2, 360–365.

[Cas45] H. B. G. Casimir, *On Onsager's Principle of Microscopic Reversibility*, Reviews of Modern Physics **17** (1945), no. 2-3, 343–350.

[CBPS13] Yunfeng Cai, Zhaojun Bai, John E. Pask, and N. Sukumar, *Hybrid preconditioning for iterative diagonalization of ill-conditioned generalized eigenvalue problems in electronic structure calculations*, Journal of Computational Physics **255** (2013), 16 – 30.

[CCR11] Amy C Cassidy, Charles W Clark, and Marcos Rigol, *Generalized Thermalization in an Integrable Lattice System*, Phys. Rev. Lett. **106** (2011), no. 14, 140405.

[CE13] Jean-Sébastien Caux and Fabian H. L. Essler, *Time Evolution of Local Observables After Quenching to an Integrable Model*, Physical Review Letters **110** (2013), no. 25, 257203.

[CET01] D. Controzzi, F. Essler, and a. Tsvelik, *Optical Conductivity of One-Dimensional Mott Insulators*, Physical Review Letters **86** (2001), no. 4, 680–683.

[CH09] Siew-Ann Cheong and Christopher Henley, *Correlation density matrix: An unbiased analysis of exact diagonalizations*, Physical Review B **79** (2009), no. 21, 212402.

[CHQZ06] C. Canuto, M. Y. Hussaini, a. Quarteroni, and T. a. Zang, *Spectral Methods Fundamentals in Single Domains*, 2006.

[CM11] Jean-Sébastien Caux and Jorn Mossel, *Remarks on the notion of quantum integrability*, Journal of Statistical Mechanics: Theory and Experiment **2011** (2011), no. 02, P02023.

[CMP14] Dawid Crivelli, M Mierzejewski, and Peter Prelovšek, *Energy and particle currents in a driven integrable system*, Physical Review B **90** (2014), 195119.

[CMP15] Dawid Crivelli, Marcin Mierzejewski, and Peter Prelovšek, *Energy Current and Energy Fluctuations in Driven QuantumWires*, NATO Science for Peace and Security Series C: Environmental Security, Springer Netherlands, Dordrecht, 2015.

[CP10] Zuojing Chen and Eric Polizzi, *Spectral-based propagation schemes for time-dependent quantum systems with application to carbon nanotubes*, Physical Review B **82** (2010), no. 20, 205410.

[CZP95] H Castella, X. Zotos, and Peter Prelovšek, *Integrability and ideal conductance at finite temperatures*, Physical review letters **74** (1995), no. 6, 972–975.

[Dag94] Elbio Dagotto, *Correlated electrons in high-temperature superconductors*, Reviews of Modern Physics **66** (1994), no. 3, 763–840.

[Dal14] Andrew J. Daley, *Quantum trajectories and open many-body quantum systems*, Advances in Physics **63** (2014), no. 2, 77–149.

[Deg04] A Nishino T Deguchi, *Completeness of Bethe ansatz for 1D Hubbard model with AB-flux through combinatorial formulas and exact enumeration of eigenstates*, Nucl. Phys. B **688** (2004), 266.

[Deu10] J. M. Deutsch, *Thermodynamic entropy of a many-body energy eigenstate*, New Journal of Physics **12** (2010), no. 7, 075021.

[DKPR15] Luca D'Alessio, Yariv Kafri, Anatoli Polkovnikov, and Marcos Rigol, *From Quantum Chaos and Eigenstate Thermalization to Statistical Mechanics and Thermodynamics*, ArXiv (2015), 1509.06411.

[DLS13] J. M. Deutsch, Haibin Li, and Auditya Sharma, *Microscopic origin of thermodynamic entropy in isolated systems*, Physical Review E **87** (2013), no. 4, 042135.

[Dol06] Andreas Dolfen, *Massively parallel exact diagonalization of strongly correlated systems*, Ph.D. thesis, 2006.

[Dom54] Charles A. Domenicali, *Stationary temperature distribution in an electrically heated conductor*, Journal of Applied Physics **25** (1954), 1310–1311.

[DP13] Luca D'Alessio and Anatoli Polkovnikov, *Many-body energy localization transition in periodically driven systems*, Annals of Physics **333** (2013), 19–33.

[DPS13] Edoardo Di Napoli, Eric Polizzi, and Yousef Saad, *Efficient estimation of eigenvalue counts in an interval*, ArXiv (2013), 1308.4275.

[DR14] Luca D'Alessio and Marcos Rigol, *Long-time Behavior of Isolated Periodically Driven Interacting Lattice Systems*, Physical Review X **4** (2014), no. 4, 041048.

[DS03] Abhishek Dhar and B. Sriram Shastry, *Quantum transport using the Ford-Kac-Mazur formalism*, Physical Review B **67** (2003), no. 19, 195405.

[DWH+12] P. E. Dargel, a. Wöllert, a. Honecker, I. P. McCulloch, U. Schollwöck, and T. Pruschke, *Lanczos algorithm with matrix product states for dynamical correlation functions*, Physical Review B **85** (2012), no. 20, 205119.

[ECJ12] M Einhellinger, A Cojuhovschi, and E Jeckelmann, *Numerical method for nonlinear steady-state transport in one-dimensional correlated conductors*, Physical Review B **85** (2012), no. 23, 235141.

[ECP10] J Eisert, M Cramer, and M B Plenio, *Colloquium: Area laws for the entanglement entropy*, Rev. Mod. Phys. **82** (2010), no. 1, 277–306.

[ECP14] D. Nasr Esfahani, L. Covaci, and F. M. Peeters, *Nonlinear response to electric field in extended Hubbard models*, Physical Review B **90** (2014), no. 20, 205121.

[EF13] Tarek a. Elsayed and Boris V. Fine, *Regression Relation for Pure Quantum States and Its Implications for Efficient Computing*, Physical Review Letters **110** (2013), no. 7, 070404.

[EFG15] Jens Eisert, M Friesdorf, and Christian Gogolin, *Quantum many-body systems out of equilibrium*, Nature Physics **11** (2015), no. 2, 124–130.

[EK08] Martin Eckstein and Marcus Kollar, *Theory of time-resolved optical spectroscopy on correlated electron systems*, Physical Review B **78** (2008), no. 20, 205119.

[EKW09] Martin Eckstein, Marcus Kollar, and Philipp Werner, *Thermalization after an Interaction Quench in the Hubbard Model*, Physical Review Letters **103** (2009), no. 5, 056403.

[EOG15] Massimiliano Esposito, Maicol a. Ochoa, and Michael Galperin, *Efficiency fluctuations in quantum thermoelectric devices*, Physical Review B **91** (2015), no. 11, 115417.

[ES12] Tilman Enss and Jesko Sirker, *Light cone renormalization and quantum quenches in one-dimensional Hubbard models*, New Journal of Physics **14** (2012), no. 2, 023008.

[EW11] Martin Eckstein and Philipp Werner, *Damping of Bloch Oscillations in the Hubbard Model*, Physical Review Letters **107** (2011), no. 18, 186406.

[FA14] Johannes Floß and Ilya Sh. Averbukh, *Anderson Wall and Bloch Oscillations in Molecular Rotation*, Physical Review Letters **113** (2014), no. 4, 043002.

[FKAB15] Johannes Floß, Andrei Kamalov, Ilya Sh. Averbukh, and Philip H. Bucksbaum, *Observation of Bloch Oscillations in Molecular Rotation*, Phys. Rev. Lett. **115** (2015), 203002.

[FLS+92] J. Feldmann, K. Leo, J. Shah, D. A. B. Miller, J. E. Cunningham, T. Meier, G. von Plessen, A. Schulze, P. Thomas, and S. Schmitt-Rink, *Optical investigation of Bloch oscillations in a semiconductor superlattice*, Physical Review B **46** (1992), no. 11, 7252–7255.

[FM13] Barbara Fresch and Giorgio J Moro, *Typical response of quantum pure states*, The European Physical Journal B **86** (2013), no. 5, 233.

[Fre08] J. Freericks, *Quenching Bloch oscillations in a strongly correlated material: Nonequilibrium dynamical mean-field theory*, Physical Review B **77** (2008), no. 7, 075109.

[FS12] H Fang and Y Saad, *A filtered Lanczos procedure for extreme and interior eigenvalue problems*, Siam J. Sci. Comput. **34** (2012), no. 4, 2220–2246.

[GBM08] P. Gosselin, H. Boumrar, and H. Mohrbach, *Semiclassical quantization of electrons in magnetic fields: The generalized Peierls substitution*, EPL (Europhysics Letters) **84** (2008), no. 5, 50002.

[GE15] Christian Gogolin and Jens Eisert, *Equilibration, thermalisation, and the emergence of statistical mechanics in closed quantum systems*, ArXiv (2015), 1503.07538.

[Geo95] H.-O. Georgii, *The equivalence of ensembles for classical systems of particles*, J. Stat. Phys. **80** (1995), no. 5, 1341–1378.

[GHT13] Sheldon Goldstein, Takashi Hara, and Hal Tasaki, *Time Scales in the Approach to Equilibrium of Macroscopic Quantum Systems*, Physical Review Letters **111** (2013), no. 14, 140401.

[GKK+13] Theodoros Gkountouvas, Vasileios Karakasis, Kornilios Kourtis, Georgios Goumas, and Nectarios Koziris, *Improving the Performance of the Symmetric Sparse Matrix-Vector Multiplication in Multicore*, 2013 IEEE 27th International Symposium on Parallel and Distributed Processing, IEEE, may 2013, pp. 273–283.

[GKL+12] Michael Gring, Maximilian Kuhnert, Tim Langen, Takuya Kitagawa, Bernhard Rauer, Matthias Schreitl, Igor Mazets, David a. Smith, Eugene Demler, and Jörg Schmiedmayer, *Relaxation and Prethermalization in an Isolated Quantum System*, Science **337** (2012), no. 6100, 1318–1322.

[Gla66] M.Lawrence Glasser, *Thermodynamic properties of bloch electrons in a magnetic field*, Journal of Physics and Chemistry of Solids **27** (1966), no. 9, 1459–1467.

[GLTZ10] S. Goldstein, J. L. Lebowitz, R. Tumulka, and N. Zanghì, *Long-time behavior of macroscopic quantum systems: Commentary accompanying the English translation of John von Neumann's 1929 article on the quantum ergodic theorem*, European Physical Journal H **35** (2010), no. 2, 173–200.

[GM94] M. P. Grabowski and P. Mathieu, *Structure of the conservation laws in integrable spin chains with short range interactions*, Annals of Physics **243** (1994), 79.

[GME11] Christian Gogolin, Markus P. Müller, and Jens Eisert, *Absence of thermalization in nonintegrable systems*, Physical Review Letters **106** (2011), no. January, 1–4.

[GMM04] J. Gemmer, M. Michel, and G. Mahler, *Quantum Thermodynamics*, Lecture Notes in Physics, vol. 657, Springer Berlin Heidelberg, Berlin, Heidelberg, 2004.

[GMW98] Thomas Guhr, Axel Müller–Groeling, and Hans A. Weidenmüller, *Random-matrix theories in quantum physics: common concepts*, Physics Reports **299** (1998), no. 4-6, 189–425.

[GOM01] Jochen Gemmer, Alexander Otte, and Günter Mahler, *Quantum Approach to a Derivation of the Second Law of Thermodynamics*, Physical Review Letters **86** (2001), no. 10, 1927–1930.

[GR06] Juan José García-Ripoll, *Time evolution of Matrix Product States*, New Journal of Physics **8** (2006), no. 12, 305–305.

[Gra08] Walter T. Grandy, Jr., *Entropy and the Time Evolution of Macroscopic Systems*, vol. 62, Oxford University Press, jun 2008.

[GSZ+11] Christophe Goupil, Wolfgang Seifert, Knud Zabrocki, Eckhart Müller, and G. Jeffrey Snyder, *Thermodynamics of Thermoelectric Phenomena and Applications*, Entropy **13** (2011), no. 12, 1481–1517.

[Gut92] Martin H Gutknecht, *A Completed Theory of the Unsymmetric Lanczos Process and Related Algorithms, Part I*, SIAM Journal on Matrix Analysis and Applications **13** (1992), no. 2, 594–639.

[Haa01] F Haake, *Quantum Signatures of Chaos*, Springer Series in Synergetics, Springer, 2001.

[Haw09] Michael Stuart Hawkins, *Local conservation laws in quantum integrable systems*, July 2009.

[HFG+05] F H L Essler, H Frahm, F Gohmann, a Klumper, and V E Korepin, *The One-dimensional Hubbard Model*, 2005.

[HHK72] R Haydock, V Heine, and MJ Kelly, *Electronic structure based on the local atomic environment for tight-binding bands*, Journal of Physics C: Solid State **5** (1972), no. 20, 2845–2858.

[HHK75] ———, *Electronic structure based on the local atomic environment for tight-binding bands. II*, Journal of Physics C: Solid State **2591** (1975).

[HHW67] R. Haag, N. M. Hugenholtz, and M. Winnink, *On the equilibrium states in quantum statistical mechanics*, Communications in Mathematical Physics **5** (1967), no. 3, 215–236.

[HMHCB03] F. Heidrich-Meisner, A. Honecker, D. C. Cabra, and W. Brenig, *Zero-frequency transport properties of one-dimensional spin-12 systems*, Physical Review B **68** (2003), no. 13, 134436.

[HMT11] Nathan Halko, P. G. Martinsson, and Joel a. Tropp, *Finding Structure with Randomness: Probabilistic Algorithms for Constructing Approximate Matrix Decompositions*, SIAM Review **53** (2011), no. 2, 217–288.

[HNO14] David A. Huse, Rahul Nandkishore, and Vadim Oganesyan, *Phenomenology of fully many-body-localized systems*, Physical Review B **90** (2014), no. 17, 174202.

[HPK13] Markus Heyl, Anatoli Polkovnikov, and Stefan Kehrein, *Dynamical Quantum Phase Transitions in the Transverse-Field Ising Model*, Physical Review Letters **110** (2013), no. 13, 135704.

[HPZ11] J. Herbrych, P. Prelovšek, and X. Zotos, *Finite-temperature Drude weight within the anisotropic Heisenberg chain*, Physical Review B **84** (2011), no. 15, 155125.

[HS05] Naomichi Hatano and Masuo Suzuki, *Finding Exponential Product Formulas of Higher Orders*, Quantum Annealing and Other Optimization **679** (2005), no. 3, 1–22.

[HSRH+15] Senaida Hernández-Santana, Arnau Riera, Karen V Hovhannisyan, Martí Perarnau-Llobet, Luca Tagliacozzo, and Antonio Acín, *Locality of temperature in spin chains*, New Journal of Physics **17** (2015), no. 8, 085007.

[HT12] Nicholas Hale and Lloyd N. Trefethen, *Chebfun and numerical quadrature*, Science China Mathematics **55** (2012), no. 9, 1749–1760.

[HWM+11] Andreas Holzner, Andreas Weichselbaum, Ian P. McCulloch, Ulrich Schollwöck, and Jan von Delft, *Chebyshev matrix product state approach for spectral functions*, Physical Review B **83** (2011), no. 19, 195115.

[JF07] Eric Jeckelmann and Holger Fehske, *Exact numerical methods for electron-phonon problems*, Rivista del Nuovo Cimento **30** (2007), 259.

[JHR06] P. Jung, R. W. Helmes, and a. Rosch, *Transport in Almost Integrable Models: Perturbed Heisenberg Chains*, Physical Review Letters **96** (2006), no. 6, 067202.

[JP94] J. Jaklič and P. Prelovšek, *Lanczos method for the calculation of finite-temperature quantities in correlated systems*, Physical Review B **49** (1994), no. 7, 5065–5068.

[JP96] ———, *Thermodynamic Properties of the Planar t-J Model*, Physical Review Letters **77** (1996), no. 5, 892–895.

[JP00] ———, *Finite-temperature properties of doped antiferromagnets*, Advances in Physics **49** (2000), no. 1, 1–92.

[JR07] Peter Jung and Achim Rosch, *Spin conductivity in almost integrable spin chains*, Physical Review B **76** (2007), no. 24, 245108.

[JŽ11a] Simon Jesenko and Marko Žnidarič, *Finite-temperature magnetization transport of the one-dimensional anisotropic Heisenberg model*, Physical Review B **84** (2011), no. 17, 174438.

[JŽ11b] ———, *Finite-temperature magnetization transport of the one-dimensional anisotropic Heisenberg model*, Physical Review B **84** (2011), no. 17, 174438.

[Kas10] Michael Kastner, *Nonequivalence of Ensembles for Long-Range Quantum Spin Systems in Optical Lattices*, Physical Review Letters **104** (2010), no. 24, 240403.

[Kas15] ———, *Entanglement-enhanced spreading of correlations*, ArXiv (2015), 1507.00529.

[KBM12] Christoph Karrasch, J. H. Bardarson, and J. E. Moore, *Finite-Temperature Dynamical Density Matrix Renormalization Group and the Drude Weight of Spin-1/2 Chains*, Physical Review Letters **108** (2012), no. 22, 227206.

[KF13] Mehdi Kargarian and Gregory a. Fiete, *Multiorbital effects on thermoelectric properties of strongly correlated materials*, Physical Review B **88** (2013), no. 20, 205141.

[KGE14] Martin Kliesch, Christian Gogolin, and Jens Eisert, *Many-Electron Approaches in Physics, Chemistry and Mathematics: A Multidisciplinary View*, Springer International Publishing, Cham, 2014, pp. 301–318.

[KGK+14] Martin Kliesch, Christian Gogolin, M. J. Kastoryano, a. Riera, and J. Eisert, *Locality of Temperature*, Physical Review X **4** (2014), no. 3, 1–19.

[KIM13] C. Karrasch, R. Ilan, and J. E. Moore, *Nonequilibrium thermal transport and its relation to linear response*, Physical Review B **88** (2013), no. 19, 195129.

[KK14] D. M. Kennes and C. Karrasch, *Extending the range of real time density matrix renormalization group simulations*, ArXiv (2014), 1404.3704.

[KKHM15] C. Karrasch, D. M. Kennes, and F. Heidrich-Meisner, *Thermal conductivity of the one-dimensional Fermi-Hubbard model*, ArXiv (2015), 1506.05788.

[KKM14] C. Karrasch, D. M. Kennes, and J. E. Moore, *Transport properties of the one-dimensional Hubbard model at finite temperature*, Physical Review B **90** (2014), no. 15, 155104.

[KM01] W. Koshibae and S. Maekawa, *Effects of Spin and Orbital Degeneracy on the Thermopower of Strongly Correlated Systems*, Physical Review Letters **87** (2001), no. 23, 236603.

[KMHM14] C. Karrasch, J. E. Moore, and F. Heidrich-Meisner, *Real-time and real-space spin and energy dynamics in one-dimensional spin-1/2 systems induced by local quantum quenches at finite temperatures*, Physical Review B **89** (2014), no. 7, 075139.

[Koc11] E Koch, *The Lanczos Method*, The LDA+DMFT approach to strongly correlated materials (2011), Section 8.1 – 8.30.

[Kub57] Ryogo Kubo, *Statistical-Mechanical Theory of Irreversible Processes. I. General Theory and Simple Applications to Magnetic and Conduction Problems*, Journal of the Physical Society of Japan **12** (1957), no. 6, 570–586.

[KWE11] Marcus Kollar, F Alexander Wolf, and Martin Eckstein, *Generalized Gibbs ensemble prediction of prethermalization plateaus and their relation to nonthermal steady states in integrable systems*, Phys. Rev. B **84** (2011), no. 5, 54304.

[Lan87] R. Landauer, *Electrical transport in open and closed systems*, Z. Phys. B: Condens. Matter **68** (1987), 217–228.

[LDZ12] Mateusz Lacki, Dominique Delande, and Jakub Zakrzewski, *Numerical computation of dynamically important excited states of many-body systems*, Physical Review A **86** (2012), no. 1, 013602.

[LG03] Kim Louis and C. Gros, *Diverging magnetothermal response in the one-dimensional Heisenberg chain*, Physical Review B **67** (2003), no. 22, 224410.

[LGBP14] Zala Lenarčič, Denis Golež, Janez Bonča, and Peter Prelovšek, *Optical response of highly excited particles in a strongly correlated system*, Physical Review B **89** (2014), no. 12, 125123.

[LGK+13] Tim Langen, Remi Geiger, Maximilian Kuhnert, Bernhard Rauer, and Joerg Schmiedmayer, *Local emergence of thermal correlations in an isolated quantum many-body system*, Nature Physics **9** (2013), no. 10, 640–643.

[LJV08] Georgy Lebon, David Jou, and Jose Casas Vazquez, *Understanding non-equilibrium thermodynamics: foundations, applications, frontiers*, Springer, 2008.

[LL69] J. L. Lebowitz and Elliott H. Lieb, *Existence of Thermodynamics for Real Matter with Coulomb Forces*, Physical Review Letters **22** (1969), no. 13, 631.

[LL77] L D Landau and E M Lifshitz, *Quantum mechanics. Non-relativistic theory* , vol. 3, 1977.

[LPE+03] M. Long, P. Prelovšek, S. El Shawish, J. Karadamoglou, and X. Zotos, *Finite-temperature dynamical correlations using the microcanonical ensemble and the Lanczos algorithm*, Physical Review B **68** (2003), no. 23, 235106.

[LPSW09] Noah Linden, Sandu Popescu, Anthony J Short, and Andreas Winter, *Quantum mechanical evolution towards thermal equilibrium*, Phys. Rev. E **79** (2009), no. 6, 61103.

[LPSW10] Noah Linden, Sandu Popescu, Anthony J. Short, and Andreas Winter, *On the speed of fluctuations around thermodynamic equilibrium*, New Journal of Physics **12** (2010), 2–5.

[LR72] Elliott H. Lieb and Derek W. Robinson, *The finite group velocity of quantum spin systems*, Communications in Mathematical Physics **28** (1972), no. 3, 251–257.

[LR14] Nicolas Laflorencie and Stephan Rachel, *Spin-resolved entanglement spectroscopy of critical spin chains and Luttinger liquids*, Journal of Statistical Mechanics: Theory and Experiment **2014** (2014), no. 11, P11013.

[LZMG01] Jon Links, Huan-Qiang Zhou, Ross McKenzie, and Mark Gould, *Ladder Operator for the One-Dimensional Hubbard Model*, Physical Review Letters **86** (2001), no. 22, 5096–5099.

[MA06] N. Mohankumar and Scott M. Auerbach, *On time-step bounds in unitary quantum evolution using the Lanczos method*, Computer Physics Communications **175** (2006), no. 7, 473–481.

[MAAACJ13] J J Mendoza-Arenas, S Al-Assam, S R Clark, and D Jaksch, *Heat transport in the X X Z spin chain: from ballistic to diffusive regimes and dephasing enhancement*, Journal of Statistical Mechanics: Theory and Experiment **2013** (2013), no. 07, P07007.

[Mah00] Gerald D. Mahan, *Many-Particle Physics*, Springer US, Boston, MA, 2000.

[Mar13] Leonid Martyushev, *Entropy and Entropy Production: Old Misconceptions and New Breakthroughs*, Entropy **15** (2013), no. 4, 1152–1170.

[Maz69] P. Mazur, *Non-ergodicity of phase functions in certain systems*, Physica **43** (1969), no. 4, 533–545.

[Maz10] Giacomo Mazzi, *Numerical treatment of the Liouville-von Neumann equation for quantum spin dynamics*.

[MBP11] Marcin Mierzejewski, Janez Bonča, and Peter Prelovšek, *Integrable Mott Insulators Driven by a Finite Electric Field*, Physical Review Letters **107** (2011), no. 12, 126601.

[MCP14] Marcin Mierzejewski, Dawid Crivelli, and Peter Prelovšek, *Peltier effect in strongly driven quantum wires*, Physical Review B **90** (2014), 075124.

[MCR11] Tapan Mishra, Juan Carrasquilla, and Marcos Rigol, *Phase diagram of the half-filled one-dimensional t-V-W model*, Physical Review B **84** (2011), no. 11, 115135.

[Meh04] M L Mehta, *Random Matrices*, Pure and Applied Mathematics, Elsevier Science, 2004.

[MH03] John C. Mason and David Cristopher Handscomb, *Chebychev Polynomials*, Chapman and Hall, 2003.

[MH14] Daniel Manzano and Pablo I Hurtado, *Symmetry and the thermodynamics of currents in open quantum systems*, Physical Review B **125138** (2014), no. 90, 1–10.

[MHWG08] Mathias Michel, Ortwin Hess, Hannu Wichterich, and Jochen Gemmer, *Transport in open spin chains: A Monte Carlo wave-function approach*, Physical Review B **77** (2008), no. 10, 104303.

[Mir00] A Mirlin, *Statistics of energy levels and eigenfunctions in disordered systems*, Physics Reports **326** (2000), no. 5-6, 259–382.

[MK10] Michael Moeckel and Stefan Kehrein, *Crossover from adiabatic to sudden interaction quenches in the Hubbard model: prethermalization and non-equilibrium dynamics*, New Journal of Physics **12** (2010), no. 5, 055016.

[MP10] Marcin Mierzejewski and Peter Prelovšek, *Nonlinear Current Response of an Isolated System of Interacting Fermions*, Physical Review Letters **105** (2010), no. 18, 186405.

[MPCP13] Marcin Mierzejewski, Tomaž Prosen, Dawid Crivelli, and Peter Prelovšek, *Eigenvalue Statistics of Reduced Density Matrix during Driving and Relaxation*, Physical Review Letters **110** (2013), no. 20, 200602.

[MPP14] Marcin Mierzejewski, Peter Prelovšek, and Tomaž Prosen, *Breakdown of the Generalized Gibbs Ensemble for Current-Generating Quenches*, Physical review letters **113** (2014), no. 2, 20602.

[MPP15a] ———, *Identifying Local and Quasilocal Conserved Quantities in Integrable Systems*, Physical Review Letters **114** (2015), no. 14, 140601.

[MPP15b] Marcin Mierzejewski, Tomaž Prosen, and Peter Prelovšek, *Approximate conservation laws in perturbed integrable lattice models*, Physical Review B **92** (2015), no. 19, 195121.

[MR98] M. J. Martins and P. B. Ramos, *The Quantum Inverse Scattering Method for Hubbard-like Models*, Nuclear Physics B **00** (1998), 71.

[MS59] Paul C. Martin and Julian Schwinger, *Theory of Many-Particle Systems. I*, Physical Review **115** (1959), no. 6, 1342–1373.

[MS08] Subroto Mukerjee and B. Shastry, *Signatures of diffusion and ballistic transport in the stiffness, dynamical correlation functions, and statistics of one-dimensional systems*, Physical Review B **77** (2008), no. 24, 245131.

[MSLL12] Jason Matthews, David Sánchez, Marcus Larsson, and Heiner Linke, *Thermally driven ballistic rectifier*, Physical Review B **85** (2012), no. 20, 205309.

[MV03] Cleve Moler and Charles Van Loan, *Nineteen Dubious Ways to Compute the Exponential of a Matrix, Twenty-Five Years Later*, SIAM Review **45** (2003), no. 1, 3–49.

[MWH+10a] W Münder, a Weichselbaum, a Holzner, Jan Von Delft, and C L Henley, *Correlation density matrices for one-dimensional quantum chains based on the density matrix renormalization group*, New Journal of Physics **12** (2010), no. 7, 075027.

[MWH+10b] W. Münder, A. Weichselbaum, A. Holzner, Jan von Delft, and C. L. Henley, *Correlation density matrices for one-dimensional quantum chains based on the density matrix renormalization group*, New Journal of Physics **12** (2010), no. 7, 075027.

[ND03] Akinori Nishino and Tetsuo Deguchi, *Bethe-ansatz studies of energy-level crossings in the one-dimensional Hubbard model*, Physical Review B **68** (2003), no. 7, 075114.

[NMA98] BN Narozhny, AJ Millis, and N Andrei, *Transport in the XXZ model*, Physical Review B **58** (1998), no. 6, 2921–2924.

[NTEKK10] Mamadou Ndong, Hillel Tal-Ezer, Ronnie Kosloff, and Christiane P. Koch, *A Chebychev propagator with iterative time ordering for explicitly time-dependent Hamiltonians*, The Journal of Chemical Physics **132** (2010), no. 6, 064105.

[OCC03] E. Orignac, R. Chitra, and R. Citro, *Thermal transport in one-dimensional spin gap systems*, Physical Review B **67** (2003), no. 13, 134426.

[Ols15] Maxim Olshanii, *Geometry of quantum observables and thermodynamics of small systems*, Physical Review Letters **114** (2015), no. February, 060401.

[Ons31] Lars Onsager, *Reciprocal Relations in Irreversible Processes. I.*, Physical Review **37** (1931), no. 4, 405–426.

[PC11] Ingo Peschel and Ming-Chiang Chung, *On the relation between entanglement and subsystem Hamiltonians*, Europhysics Letters **96** (2011), no. 5, 50006.

[Per84] Asher Peres, *Ergodicity and mixing in quantum theory. I*, Physical Review A **30** (1984), no. 1, 504–508.

[PHT85] Eric M. Pearson, Timur Halicioglu, and William A. Tiller, *Laplace-transform technique for deriving thermodynamic equations from the classical microcanonical ensemble*, Physical Review A **32** (1985), no. 5, 3030–3039.

[PK03] Indranil Paul and Gabriel Kotliar, *Thermal transport for many-body tight-binding models*, Physical Review B **67** (2003), no. 11, 115131.

[PKCS15] Frank Pollmann, Vedika Khemani, J. Ignacio Cirac, and S. L. Sondhi, *Efficient variational diagonalization of fully many-body localized Hamiltonians*, ArXiv (2015), 1506.07179.

[PL86] Tae Jun Park and J. C. Light, *Unitary quantum time evolution by iterative Lanczos reduction*, The Journal of Chemical Physics **85** (1986), no. 10, 5870.

[Pol08] Anatoli Polkovnikov, *Microscopic Expression for Heat in the Adiabatic Basis*, Physical Review Letters **101** (2008), no. 22, 220402.

[Pol09] Eric Polizzi, *Density-matrix-based algorithm for solving eigenvalue problems*, Physical Review B **79** (2009), no. 11, 115112.

[Pol11] Anatoli Polkovnikov, *Microscopic diagonal entropy and its connection to basic thermodynamic relations*, Annals of Physics **326** (2011), no. 2, 486–499.

[Poz13] Balázs Pozsgay, *The generalized Gibbs ensemble for Heisenberg spin chains*, Journal of Statistical Mechanics: Theory and Experiment **2013** (2013), no. 07, P07003.

[PPHA15] Pedro Ponte, Z. Papić, François Huveneers, and Dmitry A. Abanin, *Many-Body Localization in Periodically Driven Systems*, Physical Review Letters **114** (2015), no. 14, 140401.

[PPSA14] R. G. Pereira, V. Pasquier, J. Sirker, and I. Affleck, *Exactly conserved quasilocal operators for the XXZ spin chain*, Journal of Statistical Mechanics: Theory and Experiment **2014** (2014), no. 9, P09037.

[Pro11] Tomaž Prosen, *Exact Nonequilibrium Steady State of a Strongly Driven Open XXZ Chain*, Physical Review Letters **107** (2011), no. 13, 137201.

[Pro15] ———, *Matrix product solutions of boundary driven quantum chains*, Journal of Physics A: Mathematical and Theoretical **48** (2015), no. 37, 373001.

[PSH07] Michael Peterson, B. Shastry, and Jan Haerter, *Thermoelectric effects in a strongly correlated model for NaxCoO2*, Physical Review B **76** (2007), no. 16, 165118.

[PSW06] Sandu Popescu, Anthony J. Short, and Andreas Winter, *Entanglement and the foundations of statistical mechanics*, Nature Physics **2** (2006), no. 11, 754–758.

[PT07] Andrew J. Pounds and David Joshua Tannor, *Introduction to Quantum Mechanics: A Time-Dependent Perspective (David J. Tannor)*, Journal of Chemical Education **85** (2007), no. 7, 919.

[PVM13] Ho N. Phien, Guifré Vidal, and Ian P. McCulloch, *Dynamical windows for real-time evolution with matrix product states*, Physical Review B **88** (2013), no. 3, 035103.

[PWA09] Rodrigo G. Pereira, Steven R. White, and Ian Affleck, *Spectral function of spinless fermions on a one-dimensional lattice*, Physical Review B **79** (2009), no. 16, 165113.

[PŽ13] Tomaž Prosen and Marko Žnidarič, *Eigenvalue statistics as an indicator of integrability of nonequilibrium density operators*, Physical Review Letters **111** (2013), no. 12, 1–5.

[PZB+93] D Poilblanc, T Ziman, J Bellissard, F Mila, and G Montambaux, *Poisson vs. GOE Statistics in Integrable and Non-Integrable Quantum Hamiltonians*, EPL (Europhysics Letters) **22** (1993), no. 7, 537.

[RDYO07a] Marcos Rigol, Vanja Dunjko, Vladimir Yurovsky, and Maxim Olshanii, *Relaxation in a Completely Integrable Many-Body Quantum System: An Ab Initio Study of the Dynamics of the Highly Excited States of 1D Lattice Hard-Core Bosons*, Physical Review Letters **98** (2007), no. 5, 050405.

[RDYO07b] ———, *Relaxation in a Completely Integrable Many-Body Quantum System: An Ab Initio Study of the Dynamics of the Highly Excited States of 1D Lattice Hard-Core Bosons*, Physical Review Letters **98** (2007), no. 5, 050405.

[Rei07] Peter Reimann, *Typicality for Generalized Microcanonical Ensembles*, Physical Review Letters **99** (2007), no. 16, 160404.

[Rei08] ———, *Foundation of statistical mechanics under experimentally realistic conditions*, Physical Review Letters **101** (2008), no. 19, 1–4.

[Rei10] ———, *Canonical thermalization*, New Journal of Physics **12** (2010), no. 5, 055027.

[Rei15a] ———, *Eigenstate thermalization: Deutsch's approach and beyond*, New Journal of Physics **17** (2015), no. 5, 55025.

[Rei15b] ———, *Generalization of von Neumann's Approach to Thermalization*, Physical Review Letters **115** (2015), no. 1, 010403.

[RGSB08] Dario Rocca, Ralph Gebauer, Yousef Saad, and Stefano Baroni, *Turbo charging time-dependent density-functional theory with Lanczos chains*, The Journal of Chemical Physics **128** (2008), no. 15, 154105.

[RNM04] D. A. Rabson, B. N. Narozhny, and A. J. Millis, *Crossover from Poisson to Wigner-Dyson level statistics in spin chains with integrability breaking*, Phys. Rev. B **69** (2004), 054403.

[RS08] Marcos Rigol and B. Shastry, *Drude weight in systems with open boundary conditions*, Physical Review B **77** (2008), no. 16, 161101.

[RS12] Marcos Rigol and Mark Srednicki, *Alternatives to Eigenstate Thermalization*, Physical Review Letters **108** (2012), no. 11, 110601.

[RSS13] Angelo Russomanno, Alessandro Silva, and Giuseppe E. Santoro, *Linear response as a singular limit for a periodically driven closed quantum system*, Journal of Statistical Mechanics: Theory and Experiment **2013** (2013), no. 09, P09012.

[Rug97] Hans Henrik Rugh, *A Dynamical Approach to Temperature*, Physical review letters **78** (1997), no. 4, 772–774.

[Saa03] Yousef Saad, *Iterative Methods for Sparse Linear Systems*, Society for Industrial and Applied Mathematics, Zuerich, Switzerland, jan 2003.

[San10] Anders W Sandvik, *Computational Studies of Quantum Spin Systems*, AIP Conf. Proc. 1297 (Adolfo Avella and Ferdinando Mancini, eds.), vol. 135, jan 2010, pp. 135–338.

[SBR06] Olaf Schenk, Matthias Bollhöfer, and Rudolf A. Römer, *On Large-Scale Diagonalization Techniques for the Anderson Model of Localization*, SIAM Journal on Scientific Computing **28** (2006), no. 3, 963–983.

[Sch04] Peter Schmitteckert, *Nonequilibrium electron transport using the density matrix renormalization group method*, Physical Review B **70** (2004), no. 12, 121302.

[SF12] Anthony J. Short and Terence C. Farrelly, *Quantum equilibration in finite time*, New Journal of Physics **14** (2012), 0–13.

[SG09] Robin Steinigeweg and Jochen Gemmer, *Density dynamics in translationally invariant spin-12 chains at high temperatures: A current-autocorrelation approach to finite time and length scales*, Physical Review B **80** (2009), no. 18, 184402.

[SGB14] Robin Steinigeweg, Jochen Gemmer, and Wolfram Brenig, *Spin-Current Autocorrelations from Single Pure-State Propagation*, Physical Review Letters **112** (2014), no. 12, 120601.

[SGB15] ———, *Spin and energy currents in integrable and nonintegrable spin- 1/2: A typicality approach to real-time autocorrelations*, Physical Review B **91** (2015), no. 10, 104404.

[SGO+00] A. V. Sologubenko, K. Giannó, H. R. Ott, U. Ammerahl, and A. Revcolevschi, *Thermal Conductivity of the Hole-Doped Spin Ladder System*, Physical Review Letters **84** (2000), no. 12, 2714–2717.

[SGO+01] A. V. Sologubenko, K. Giannò, H. R. Ott, A. Vietkine, and A. Revcolevschi, *Heat transport by lattice and spin excitations in the spin-chain compounds SrCuO2*, Physical Review B **64** (2001), no. 5, 054412.

[Sha86] B Sriram Shastry, *Exact Integrability of the One-Dimensional Hubbard Model*, Physical Review Letters **56** (1986), no. 23, 2453–2455.

[Sha09] ———, *Electrothermal transport coefficients at finite frequencies*, Reports on Progress in Physics **72** (2009), no. 1, 016501.

[She94] Jonathan Richard Shewchuk, *An Introduction to the Conjugate Gradient Method Without the Agonizing Pain*, Science **49** (1994), no. CS-94-125, 64.

[Sho11] Anthony J. Short, *Equilibration of quantum systems and subsystems*, New Journal of Physics **13** (2011).

[SHP13] Robin Steinigeweg, J. Herbrych, and P. Prelovšek, *Eigenstate thermalization within isolated spin-chain systems*, Physical Review E **87** (2013), no. 1, 012118.

[Sim13] V Simoncini, *Computational methods for linear matrix equations*, SIAM Review (2013), 1–58.

[SJ09] Tomonori Shirakawa and Eric Jeckelmann, *Charge and spin Drude weight of the one-dimensional extended Hubbard model at quarter filling*, Physical Review B **79** (2009), no. 19, 195121.

[SKAS14] J. Sirker, N. P. Konstantinidis, F. Andraschko, and N. Sedlmayr, *Locality and thermalization in closed quantum systems*, Physical Review A **89** (2014), no. 4, 042104.

[SKN+14] Robin Steinigeweg, A. Khodja, H. Niemeyer, Christian Gogolin, and Jochen Gemmer, *Pushing the limits of the eigenstate thermalization hypothesis towards mesoscopic quantum systems*, Physical Review Letters **112** (2014), no. 13, 1–5.

[SL78] Herbert Spohn and Joel L. Lebowitz, *Irreversible Thermodynamics for Quantum Systems Weakly Coupled to Thermal Reservoirs*, Advances in Chemical Physics, vol. 38, 1978, pp. 109–142.

[SPR11] Lea F Santos, Anatoli Polkovnikov, and Marcos Rigol, *Entropy of Isolated Quantum Systems after a Quench*, Physical Review Letters **107** (2011), no. 4, 040601.

[SPR12] ———, *Weak and strong typicality in quantum systems*, Phys. Rev. E **86** (2012), no. 1, 10102.

[SRH14] Yulia E. Shchadilova, Pedro Ribeiro, and Masudul Haque, *Quantum Quenches and Work Distributions in Ultralow-Density Systems*, Physical Review Letters **112** (2014), no. 7, 070601.

[SRU13] Daniel Stanek, Carsten Raas, and Götz S. Uhrig, *Dynamics and decoherence in the central spin model in the low-field limit*, Physical Review B **88** (2013), no. 15, 155305.

[SRVK96] R. N. Silver, H Röder, a. F. Voter, and J. D. Kress, *Kernel Polynomial Approximations for Densities of States and Spectral Functions*, Journal of Computational Physics **124** (1996), no. 1, 115–130.

[SS11] Robert H. Shumway and David S. Stoffer, *Time Series Analysis and Its Applications*, vol. 64, Springer Texts in Statistics, no. 9-12, Springer New York, New York, NY, oct 2011.

[SS12] Sho Sugiura and Akira Shimizu, *Thermal pure quantum states at finite temperature*, Physical Review Letters **108** (2012), no. 24, 4–7.

[SS13] ———, *Canonical thermal pure quantum state*, Physical Review Letters **111** (2013), no. 1, 1–5.

[SSB+10] Gerald Schubert, Jens Schleede, Krzysztof Byczuk, Holger Fehske, and Dieter Vollhardt, *Distribution of the local density of states as a criterion for Anderson localization: Numerically exact results for various lattices in two and three dimensions*, Physical Review B **81** (2010), no. 15, 155106.

[SSZT12] M Siahatgar, B Schmidt, G Zwicknagl, and P Thalmeier, *Moment screening in the correlated Kondo lattice model*, New Journal of Physics **14** (2012), no. 10, 103005.

[ST07] T Schmelzer and L N Trefethen, *Evaluating matrix functions for exponential integrators via Caratheodory-Fejer approximation*, Electronic Transactions on Numerical Analysis (2007), 1–19.

[Sta93] C. A. Stafford, *Unusual low-temperature thermopower in the one-dimensional Hubbard model*, Physical Review B **48** (1993), no. 11, 8430–8433.

[SW04] Peter Schmitteckert and Ralph Werner, *Charge-density-wave instabilities driven by multiple umklapp scattering*, Physical Review B - Condensed Matter and Materials Physics **69** (2004), no. 19, 1–5.

[SW10] E.M. Stoudenmire and SR White, *Minimally entangled typical thermal state algorithms*, New Journal of Physics (2010), 1–18.

[SWZ93] DJ Douglas Scalapino, Steven SR White, and Shoucheng Zhang, *Insulator, metal, or superconductor: The criteria*, Physical Review B **47** (1993), no. 13, 7995–8007.

[TB97] Lloyd N. Trefethen and D Bau III, *Numerical linear algebra*, vol. 12, SIAM, 1997.

[TEKS12] Hillel Tal-Ezer, Ronnie Kosloff, and Ido Schaefer, *New, Highly Accurate Propagator for the Linear and Nonlinear Schrödinger Equation*, Journal of Scientific Computing **53** (2012), no. 1, 211–221.

[TMEU96] M. Takigawa, N. Motoyama, H. Eisaki, and S. Uchida, *Dynamics in the SrCuO2 One-Dimensional Antiferromagnet*, Physical Review Letters **76** (1996), no. 24, 4612–4615.

[Tre00] Lloyd N Trefethen, *Spectral Methods in MATLAB*, Society for Industrial and Applied Mathematics, jan 2000.

[Tre13] Lloyd N. Trefethen, *Approximation theory and approximation practice*, SIAM, 2013.

[Tsc00] Nicholas W Tschoegl, *Fundamentals of Equilibrium and Steady-State Thermodynamics*, 280 pages, Elsevier Science, 2000.

[UWE13] Cozmin Ududec, Nathan Wiebe, and Joseph Emerson, *Information-theoretic equilibration: The appearance of irreversibility under complex quantum dynamics*, Physical Review Letters **111** (2013), no. 8, 1–5.

[VJ09] Suriyanarayanan Vaikuntanathan and Christopher Jarzynski, *Dissipation and lag in irreversible processes*, Epl-Europhys Lett **87** (2009), no. 6, 60005.

[VR01] J M Vilar and J M Rubi, *Thermodynamics "beyond" local equilibrium.*, Proceedings of the National Academy of Sciences of the United States of America **98** (2001), no. 20, 11081–11084.

[vSG14] Michael von Spakovsky and Jochen Gemmer, *Some Trends in Quantum Thermodynamics*, Entropy **16** (2014), no. 6, 3434–3470.

[VWB99] Amrendra Vijay, Robert E. Wyatt, and Gert D. Billing, *Time propagation and spectral filters in quantum dynamics: A Hermite polynomial perspective*, The Journal of Chemical Physics **111** (1999), no. 24, 10794.

[WC12] M L Wall and Lincoln D Carr, *Out-of-equilibrium dynamics with matrix product states*, New Journal of Physics **14** (2012), no. 12, 125015.

[WKPV13] Gabriel Wong, Israel Klich, Leopoldo a. Pando Zayas, and Diana Vaman, *Entanglement temperature and entanglement entropy of excited states*, Journal of High Energy Physics **2013** (2013), 1–17.

[WMPS14] F. Alexander Wolf, Ian P. McCulloch, Olivier Parcollet, and Ulrich Schollwöck, *Chebyshev matrix product state impurity solver for dynamical mean-field theory*, Physical Review B **90** (2014), no. 11, 115124.

[WN95] Michael R. Wall and Daniel Neuhauser, *Extraction, through filter-diagonalization, of general quantum eigenvalues or classical normal mode frequencies from a small number of residues or a short-time segment of a signal. I. Theory and application to a quantum-dynamics model*, The Journal of Chemical Physics **102** (1995), no. 20, 8011–8022.

[WWAF06] Alexander Weiße, Gerhard Wellein, Andreas Alvermann, and Holger Fehske, *The kernel polynomial method*, Reviews of Modern Physics **78** (2006), no. 1, 275–306.

[Wya95] Robert E Wyatt, *Matrix spectroscopy: Computation of interior eigenstates of large matrices using layered iteration*, Physical Review E **51** (1995), no. 4, 3643–3658.

[YS13] Emil A. Yuzbashyan and B. Sriram Shastry, *Quantum Integrability in Systems with Finite Number of Levels*, Journal of Statistical Physics **150** (2013), no. 4, 704–721.

[ZBF14] V. Zlatić, G. R. Boyd, and J. K. Freericks, *Universal thermopower of bad metals*, Physical Review B **89** (2014), no. 15, 155101.

[ZF12] V. Zlatić and J. K. Freericks, *Strongly Enhanced Thermal Transport in a Lightly Doped Mott Insulator at Low Temperature*, Physical Review Letters **109** (2012), no. 26, 266601.

[ZKAHD07] Wenxian Zhang, N Konstantinidis, K a Al-Hassanieh, and V V Dobrovitski, *Modelling decoherence in quantum spin systems*, Journal of Physics: Condensed Matter **19** (2007), no. 8, 083202.

[ZMK+15] Michael P. Zaletel, Roger S. K. Mong, Christoph Karrasch, Joel E. Moore, and Frank Pollmann, *Time-evolving a matrix product state with long-ranged interactions*, Physical Review B **91** (2015), no. 16, 165112.

[Žni11] Marko Žnidarič, *Spin Transport in a One-Dimensional Anisotropic Heisenberg Model*, Phys. Rev. Lett. **106** (2011), no. 22, 220601.

[ZNP97] X. Zotos, F Naef, and P Prelovsek, *Transport and conservation laws*, Physical Review B **55** (1997), no. 17, 29–32.

[Zot99] X. Zotos, *Finite Temperature Drude Weight of the One-Dimensional Spin-1/2 Heisenberg Model*, Physical Review Letters **82** (1999), no. 8, 1764–1767.

[ZP03] X. Zotos and Peter Prelovšek, *Transport in one dimensional quantum systems*, ArXiv (2003), cond–mat/0304630.

[ZP05] M. Zemljič and P. Prelovšek, *Thermoelectric power in one-dimensional Hubbard model*, Physical Review B **71** (2005), no. 8, 085110.

[Zur03] Wojciech Hubert Zurek, *Decoherence, einselection, and the quantum origins of the classical*, Reviews of Modern Physics **75** (2003), no. 3, 715–775.